Fundamentals of Renewable and Alternative Energy

Sandip Das
Javad Khazaii
Turaj Ashuri
Yousef Mahmoud
Valmiki Sooklal

A Textbook On

Fundamentals of Renewable Energy

Table of Contents

Chapter 1

Energy Efficiency

Javad Khazaii

1.1 Introduction to Energy Efficiency

The general definition of energy is the ability to do work. Our current state of living was not possible without learning how to change one form of energy to another and then use that to do some kind of work to improve our life. Using energy to do work is a major part of our lives. We use energy to walk, to drive the car, to freeze the food to keep it fresh, to manufacture things, and to light up our homes. [1]

There are many forms of energy such as heat, light, motion, electrical, chemical, gravitational, etc. EIA (U.S. energy information administration) categorizes all energies to two main groups of potential (stored) and kinetic (working) energy, and two different sources of energy renewable, and non-renewable sources.

The stored energy has different sub-categories such as chemical, mechanical, nuclear, and gravitational energy, while the kinetic energy has different sub-categories of radiant, thermal, motion, sound, and electrical energy.

Chemical energy is the energy stored in the bonds and molecules. Chemical energy is stored in batteries, biomass, petroleum, coal, etc. An example is when one burns the coal in a powerplant to convert chemical energy to thermal energy. The stored energy in a spring and energy stored in the nucleus of an atom are examples of mechanical and nuclear energy, and energy stored in an object's height like water in a hydropower plant is an example of gravitational energy. Radiant energy is the electromagnetic energy that travels in transverse waves such as sunshine radiant energy. Thermal energy is the energy that comes from the movement of atoms and molecules, and motion energy is the energy stored in moving objects that increases with the increase of the speed of the object. Sound is the energy moving through substances in waves, and electrical energy is delivered by charged particles (electrons) moving through a wire. [1]

"Energy efficiency (EE) and energy conservation (EC) are related and often complimentary or overlapping ways to avoid or reduce energy consumption. Energy efficiency generally pertains to the technical performance of energy conversion and consuming devices and building materials. Energy conservation generally includes actions to reduce the amount of energy end use. For example, installing energy-efficient lights is an EE measure, whereas turning them off when not needed, either manually or with timers or motion sensor switches, is an EC measure." [2]

As it was noted earlier a common definition of energy is the capability of doing something, and a common definition for efficiency is to utilize less of your resources to achieve your goal. It is useful to talk about the rate at which energy is transferred from one system to another (energy per time). This rate is called power. One joule of energy transferred in one second is called one Watt (i.e., 1 joule/second = 1 Watt).

The general definition of energy efficiency can be formulated to the ratio of what we desire to what does it costs for us to achieve that. Even though EIA has categorized all the energies to potential and kinetic energy, the classical (macroscopic) thermodynamics that is the specialized science looking at work and heat as the main forms of energies governing state of the current industry has a slightly different categorization. This is to make one able to analyze the laws of energy for any type of thermal systems. There are other types of energy such as different types of non-thermal methods (ultrasound, pulse light, etc.) for processing food, etc., but our focus here will be on thermal energy that has been the main responsible field of energy at least for the past two centuries. Classical thermodynamics categorizes energies as potential energy (subject to the elevation of a system regarding a selected base elevation), kinetic energy (subject to the velocity of a system regarding a selected base velocity) and every other type is categorized as internal energy.

Before being able to really understand energy and energy efficiency in a technical/ engineering environment there are a few basic thermodynamic (i.e., science of movement of heat) concepts that need to be understood. Concepts such as different forms of energy, definition of efficiency, and the limitations to improving energy efficiency. Therefore, in the following paragraphs, we are going to point out some of these concepts that will help the readers to make a better sense of what is energy and what is energy efficiency from the point of view of engineers in general and mechanical/ thermal engineers specifically.

Thermal systems are divided into three categories. These categories are closed, open, and isolated systems. An isolated system, that in fact is only a theoretical system, is a system that does not allow any mass, heat, or work to cross the boundaries of it. In practice such a system is rare if it is not impossible. A closed system is one that does not allow mass to cross its boundaries, but heat and work can cross its boundaries. Finally, an open system is a system where mass, heat and work can cross its boundaries. The substance that composes the system can go through a process (change of at least one of its characteristics, such as pressure, temperature, etc.) or a cycle. A cycle is made of a succession of processes, that at the end brings the substance in the system to its original conditions.

The most common definition of energy (E) is the capability to produce an effect. Energy can be stored inside a system and can be transferred from one system to another system. Two main forms of energy are heat (Q) and work (W). From the thermodynamics point of view, work is the high-value (ordered) energy, and heat is the low-value (disordered) energy. According to the law of conservation of energy, energy cannot be created or destroyed, but can be changed from one form of energy to the other. This law can be formulated for a closed system that goes through a cycle, or a process as it is presented in equations 1 and 2 accordingly as follows:

$$\oint \partial Q = \oint \partial W \qquad Equ\ (1.1)$$

$$E_2 - E_1 = U_2 - U_1 + 0.5 \times m \times (V_2^2 - V_1^2) + m \times g \times (Z_2 - Z_1) = Q_{12} - W_{12} \qquad Equ\ (1.2)$$

In these equations E represents the total energy, U represents the internal energy and "$0.5mV^2$" and "mgz" represents kinetic and potential energy all in Kilo-Joules (kJ) units. As noted earlier, Q and W also represent heat and work and are in kJ units. Internal energy is the sum of all other energies (such as chemical energy or microscopic kinetic and potential energy between molecules, etc.) except macroscopic potential and kinetic energy. It is measured as the quantity of energy that is required to bring the system from its standard internal state to the current internal state. It is also considered when the system is free from magnetic, electric, and surface tension effects.

The law of conversion of energy for a process in an open system structure can be defined by equation 3 as follows:

$$\frac{dE_{C.V.}}{dt} = \dot{Q}_{c.v.} - \dot{W}_{c.v.} + \sum \dot{m}_i \times (h_i + 0.5 \times V_i^2 + g \times Z_i) - \sum \dot{m}_e \times (h_e + 0.5 \times V_e^2 + g \times Z_e) \qquad Equ\ (1.3)$$

The lefthand side of the above equation represents the change of total energy in the open system (control volume) per unit of time and it has units of kJ/s (kilojoules per second), or kW. The accented $\dot{Q}_{c.v.}$ and $\dot{W}_{c.v.}$ represent the rate of heat and mechanical work exchange crossing the boundaries of the system also have units of kJ/s. The subscriptions of "i" and "e" stand for "into" the system and "exiting" from the system. Therefore, $\dot{m}_i$, h_i , V_i^2, and Z_i represent rate of mass into the system (mass entering the system per unit of time, kg/s (kilogram per second)), enthalpy per unit of mass (kJ/kg) of the mass entering the system, square of the velocity of the mass entering the system and elevation at which the mass entering to the system respectively. Similarly, $\dot{m}_e$, h_e , V_e^2, and Z_e represent rate of mass leaving the system (mass exiting the system per unit of time, kg/s (kilogram per second)), enthalpy per unit of mass (kJ/kg) of the mass exiting the system, square of the velocity of the mass exiting the system and elevation at which the mass exiting the system respectively. In this equation "g" is the gravitational acceleration and it is in units of "meter per square second (m/s^2)). It is good to have a simple definition of enthalpy at this point as well. Enthalpy is simply can be defined as the heat content of a system. The magnitude of enthalpy is equal to the sum of the internal energy with the product of the pressure and volume. It is used as total energy (except kinetic and potential energies) of mass entering or leaving the open system. You can find a detail discussion of the first law of thermodynamics (law of conservation of energy) under two specific assumptions of steady state and transient modes in different thermodynamic books.

As one can see the law of conservation of energy that is also known as the first law of thermodynamics, does not discriminate between the forms of energy (i.e., heat and work). In fact, it only describes the balance of energy in its different forms. Based on this law these forms of energy can change to each other freely and without any limitations. Of course, this does not reduce anything from the legitimacy of this law, but as everybody can also see, it is not the complete fact regarding phenomenon that happens in the real world. It is obvious that there are limitations for the phenomenon that happens in the real world that cannot be explained by the law of conservation of energy alone. Because of that scientists have developed another complementary law for explaining these limitations. This is the second law of thermodynamics that in its core tries to help explain the real-life phenomena, and as the second law tries to do so, the concept of energy efficiency surfaces as well.

Before beginning to focus on energy efficiency let's discuss the background that led to such discussions. There are two improbable phenomena in nature that naturally will not happen. The first one is the fact that we cannot find occasions when heat (disordered energy) is fully converted to work (ordered energy) in nature. The other one is the fact that the movement of heat from a colder environment to a hotter environment does not happen on its own. Even though these two phenomena would not happen naturally, we can clearly see that there are situations where scientists have interest to convert as much as possible heat to work or move heat from a colder environment to a hotter environment. Such interests have led the scientists to develop two types of mechanical system in attempt to perform these functions. As the industrial revolution was unfolding in the past couple of hundreds of years, the scientists developed two machines that each attempted to perform one of the improbable functions in nature to its best capability.

The first of these two machines are called ***heat engines***. A heat engine is a machine that operates between two different heat reservoirs, one at higher temperature, and the other one at lower temperature. Heat from the higher temperature reservoir is input to the heat engine, perform some work, and then a residue of the heat is transferred to the lower temperature reservoir. An example of a heat engine in the industry is the power generation cycles used to create electricity. In these cycles the heat from higher temperature reservoir (heat generated in the boiler by the means of burning fuel) is used to increase the temperature of the circulating agent (water) to a level (steam) that is suitable to be discharged into a power generating turbine. As the steam passes through the turbine, causes the turbine to generate a rotating movement in the turbine shaft (in the form of mechanical work). This rotation of the turbine shaft then will be engaged with an electricity generator that will produce electricity. As the steam generates power in turbine shaft, it loses its energy and becomes colder water vapor with lower pressure at exit from the turbine. This will then pass through a condenser where will exchange heat to the environment (lower temperature reservoir) to become colder liquid, and ready to be pumped back to the boiler for the next cycle. One statement of the second law of thermodynamics (Kelvin-Plank statement) targets the heat engines and states that it is impossible to make a machine that creates mechanical work and only exchange heat with one reservoir with one level of temperature. In other words, there is always need for a second reservoir with lower temperature for releasing some of the input heat to this lower temperature reservoir, which represents some kind of energy waste.

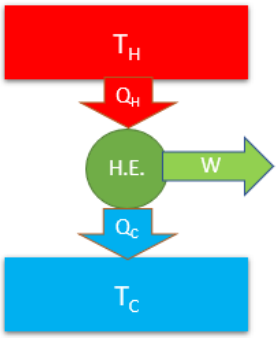

Figure 1.1 - heat engine cycle

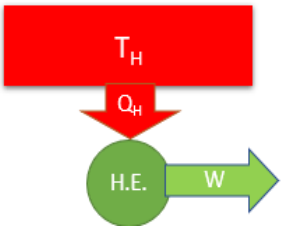

Figure 1.2 - **Impossible** heat engine as per second law of thermodynamics

The thermal efficiency of a heat engine has been defined as the ratio of the desired output to the used energy and can be represented as follows:

$$\eta = Heat\ Engine\ Thermal\ Efficiency = \frac{Desired\ Output}{Used\ Energy} = \frac{W}{Q_H} = (Q_H - Q_L)/\ Q_H \qquad Equ(1.4)$$

The second of these two machines are called refrigeration cycles/ heat pumps. A refrigeration cycle is made of a machine that operates between two different heat reservoirs, one at higher temperature, and the other one at lower temperature. Heat from the lower temperature reservoir is absorbed and is transferred to the higher temperature reservoir. To perform this act, there is a need for input of work into the system.

A vapor-compression refrigeration cycle is made of four main components. (a) A compressor that increase the pressure and temperature of the refrigerant from a state near dry vapor to a super heat vapor state, (b) a condenser that provides means of heat exchange with an environment with high temperature to allow the super heat refrigerant vapor to cool down to a state near saturated liquid, (c) an expansion valve that causes a drop of temperature and pressure to allow the refrigerant to be in state of mixture of liquid and vapor, and finally (d) an evaporator in which the heat is absorbed from the cold environment. This heat makes the mixture of refrigerant liquid and vapor in evaporator to boil to a near saturated (dry) vapor state. Refrigerant cycles inside this system and helps to remove the heat from a colder space and discharge it to an environment with higher temperature. Of course, this

process is possible because of the work that is input to the compressor. It is possible to add a three-way switching valve, an extra expansion valve and two check valves parallel to each expansion valve and convert this same cooling generating refrigeration cycle into a heating generation refrigerant cycle as well. The machines with the ability to work in both cooling and heating modes (reversed) cycle is known as a heat pump and therefore it can produce cooling and heating with the same structure. Therefore, this same refrigeration cycle can produce cooling in summer by removing the heat from the colder area that is required to be cooled (at evaporator) and produce heating in wintertime by discharging the heat that was removed from the colder outdoor environment and will be introduced to the space that is required to be heated (at condenser). It is important to notice that both evaporator and condenser are two simple coils that do different duties when operating in cooling and heating mode. Of course, this achievement is possible due to the change of the direction of the movement of the refrigerant in the cycle as it switches from cooling to heating mode or vice versa. Therefore, a heat pump operates exactly like a refrigeration cycle, but the difference is that in heat pump the amount of heat used for heating the space is the desired outcome, but in refrigeration cycle the amount of heat removed from the colder space is the desirable outcome. The second and final statement of the second law of thermodynamics (Clasius statement) targets the refrigeration/ heat pump machines and states that it is impossible to make a machine that moves heat from lower-level temperature reservoir to higher level temperature reservoir without consuming mechanical work. In other words, there is always a need to input work (waste of energy) to move heat from a lower-level temperature reservoir into a higher-level temperature reservoir.

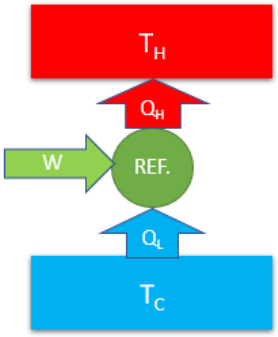

Figure 1.3 - Refrigeration cycle

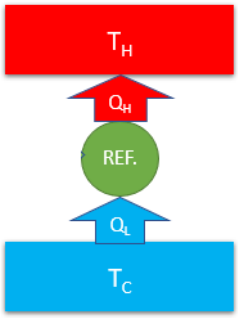

Figure 1.4 - **Impossible** refrigeration cycle as per second law of thermodynamics

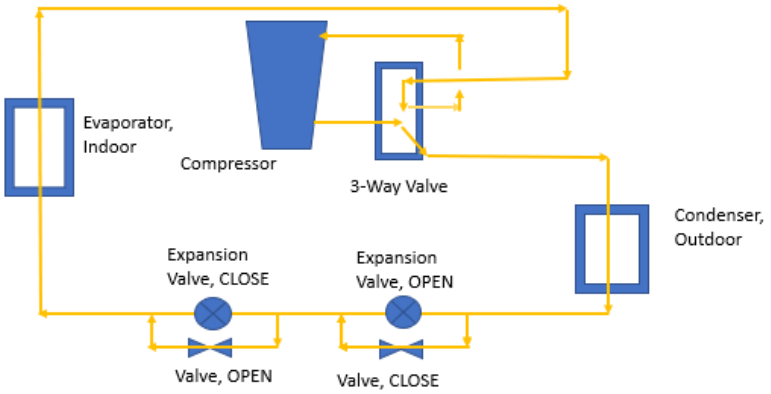

Figure 1.5 - heat pump cooling cycle

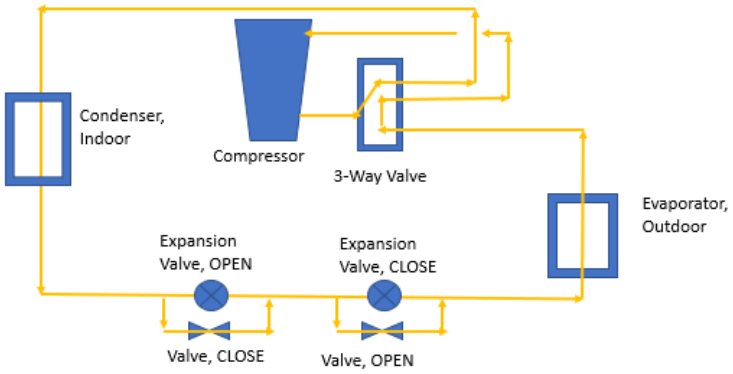

Figure 1.6 - heat pump heating cycle

The efficiency of refrigeration cycle / heat pump is defined with coefficient of performance (COP). The COP of refrigeration cycle and heat pumps can be calculated as follows:

$$COP = Ref.\ Cycle\ Coefficient\ of\ Performance = \frac{Desired\ Output}{Used\ Energy} = \frac{Q_L}{W} = Q_L / (Q_H - Q_L)$$

Equ (1.5)

$$COP = Heat\ Pump\ Coefficient\ of\ Performance = \frac{Desired\ Output}{Used\ Energy} = \frac{Q_H}{W} = Q_H / (Q_H - Q_L)$$

Equ (1.6)

It is also customary to use another measure for refrigeration/ heat pump efficiency that is energy efficiency ratio (EER). The energy efficiency ratio of a cooling system is defined as the ratio of the

delivered cooling/ heating to the electrical input (Watts). Therefore, a 24,000-BTU (British Thermal Unit) air conditioner that uses 2,400 watts to operate has a (24,000/2,400) EER of 10. The higher the COP or EER are the higher the efficiency of the system is. Sometimes seasonal energy efficiency (SEER) is used in place of EER. The difference is the fact that SEER measures how good the system works throughout the season, but EER is just the standardized measurement method.

As it can be seen from the discussion made in the above paragraphs, based on both statements of second law of thermodynamics, when operating either one of the heat engines, or refrigeration/ heat pump machines there is a loss either in form of heat loss, or need for extra work. This means that hundred percent conversion of heat to work, or moving heat from colder environment to hotter environment without spending energy is not possible. In other words, a hundred percent energy efficiency is not possible.

The next questions arising from this discussion are, "What does contribute to these inefficiencies?" and, "If we cannot have hundred percent energy efficiency, then what is the maximum efficiency that can be achieved?"

To answer the first question, we need to investigate the concepts of reversibility/irreversibility and entropy. A process or a cycle can be called reversible, if at any point it can be brought back (reversed) to its previous condition without affecting either the system or the environment surrounding the system. Throughout an entire reversible process, the assumption is that the system stays in complete equilibrium with the surroundings, from the point of view of physical state, chemical state, pressure, temperature, etc. To achieve and maintain reversibility, the processes should undergo extremely slowly, the surfaces of heat exchange should be extremely large, and temperature difference where heat exchange happens, should be extremely small. There should be no friction loss, or sudden change of state, etc. Such conditions are normally not completely achievable, and therefore lack of presence of such conditions will contribute to irreversibility, and as a result inefficiency in the system. On the other hand, entropy is generally defined as the level of disorder, or the tendency of energy to be distributed instead of staying in concentrated form. Change of entropy generally is shown by the equation "$dS = dQ/T$". The entropy of a system can be increased through addition of heat, or existence of irreversibility, but can be decreased only by removing heat from it. As the energy become more and more distributed, resulting in loss of opportunities for performing useful work, the overall entropy of the system plus its surroundings increases.

To answer the second question, scientists have imagined reversible cycles, and combination of adiabatic (completely isolated) and reversible processes. Such cycles and processes if exist in real world, they would be loss-free processes or cycles. If this happens, then we have the maximum theoretical efficiencies, and of course it is obvious that any actual system will have lower efficiency than such cycles, and processes.

Carnot cycle is the reversible model depicted for heat engines and refrigeration cycles/ heat pumps. Such cycle has four processes. Two reversible, constant temperature processes in which heat is added

or removed from the system, and two reversible, adiabatic (completely isolated) processes that during these processes the temperature level of the substance in the cycle changes. The efficiency of such cycle has been shown to be as follows:

$$\eta = Carnot\ Heat\ Engine\ Thermal\ Efficiency = \frac{Desired\ Output}{Used\ Energy} = \frac{W}{Q_H} = (Q_H - Q_L)/\ Q_H = (T_H - T_L)/\ T_H \quad \text{Equ (1.7)}$$

$$COP = Carnot\ Ref.\ Cycle\ Coefficient\ of\ Performance = \frac{Desired\ Output}{Used\ Energy} = \frac{Q_L}{W} = Q_L/\ (Q_H - Q_L) = T_L/\ (T_H - T_L) \quad \text{Equ (1.8)}$$

$$COP = Carnot\ Heat\ Pump\ Coefficient\ of\ Performance = \frac{Desired\ Output}{Used\ Energy} = \frac{Q_H}{W} = Q_H/\ (Q_H - Q_L) = T_H/\ (T_H - T_L) \quad \text{Equ (1.9)}$$

Also, for a process the maximum efficiency can be achieved if the process can happen adiabatically (no heat exchange) and reversible (no losses). Such a process is also called isentropic (constant entropy) process. Entropy is a measure of disorder in a substance, and as it can be seen from its definition can be changed due to addition or removing heat from the system, and of course by irreversibility that occur during the process. Therefore, the entropy of a system as it goes through a process can increase by adding heat to it, or due to irreversibility, but it only can decrease by removing heat from the system, since irreversibility at best is zero and cannot be a negative value. The entropy of the system and its surroundings together, however, always increases. The efficiency of an isentropic process can be shown by equation 10 below:

$$Isentropic\ Process\ Efficiency = (h_{2s} - h_1)/(h_{2a} - h_1) \qquad Equ\ (1.10)$$

In this equation h_1 is the enthalpy of the system at the beginning of the process, h_{2a} is the enthalpy of the system at end of the actual process, and h_{2s} is the enthalpy at the end of the process if the process is an isentropic one.

After this discussion, one can realize what is the meaning of energy, energy efficiency and the burdens preventing achieving high efficiency levels. This is a heads-up for making the reader aware of the current state of energy efficiency, which is not very high if we look at the reports given by the department of energy. A report from department of energy in 2018 shows out of 19,663 Tera-Btu (trillion British thermal unit) total primary energy use in all manufacturing industries in United States, 12,048 Tera-Btu or close to 62% of it is wasted through energy inefficiencies. Even though these efficiencies look low, at the same time it shows a big opportunity for improving the energy efficiency of engineering systems.

Chapter 2

Solar Power

Sandip Das

2.1 Introduction to Solar Energy

Solar energy is an abundant source of renewable and sustainable energy. There are two fundamental mechanisms by which solar energy is harvested – (i) **Solar Photovoltaic** and (ii) **Solar Thermal** energy harvesting. Solar Photovoltaic technologies use photovoltaic devices (popularly known as solar cells) which perform direct conversion of sunlight into electrical energy. On the other hand, Solar Thermal energy harvesting technologies employ various types of devices to capture the heat energy from the sunlight which can be subsequently used for water heating, space heating, and electricity generation.

2.1.1 Plank's Law of Blackbody Emission

The surface temperature of the sun is approximately 5,777 Kelvin (K). The radiation emitted by the sun closely resembles the emission from a blackbody having the above-mentioned temperature. **Planck's law** describes the spectral power density of electromagnetic radiation emitted by a blackbody under thermal equilibrium at a given temperature. Equation 2.1 presents the mathematical formula to calculate spectral power density which is derived from Plank's function.

$$E(\lambda, T) = \frac{2\pi hc^2}{\lambda^5(e^{hc/\lambda kT} - 1)} \quad \ldots\ldots\ldots\ldots\ldots (2.1)$$

Where, h is the Planck's constant (6.626×10^{-34} J·s), c is the speed of light in vacuum (3×10^{8} m/s), k is the Boltzmann constant (1.38×10^{-23} J/K), and T is the temperature of the blackbody. Using this equation, one can calculate E, the spectral power density for a given wavelength (λ) and temperature.

Figure 2.1 shows the ideal blackbody radiation curves for various temperatures including one for sun's temperature (T = 5777 K). These curves are plotted using Equation 2.1. Wien's displacement law presented in Equation 2.2 allows to find the wavelength at which the peak emission occurs in a blackbody spectrum.

$$\lambda_{max} = \frac{b}{T} \quad \ldots\ldots\ldots\ldots\ldots (2.2)$$

Where, λ_{max} is the wavelength at which the emission of a blackbody spectrum is at its maximum, and b is Wien's constant (2.9×10^{-3} m·K). By substituting T = 5777K in Equation 2.2, we obtain $\lambda_{max} = 5.02\times10^{-7}$m = 502 nm. We can visually see from Figure 2.1 that the peak of the ideal blackbody spectrum for 5777K is located at ~500 nm. In addition, it is evident that the peak shifts toward higher wavelength as temperature of the blackbody drops.

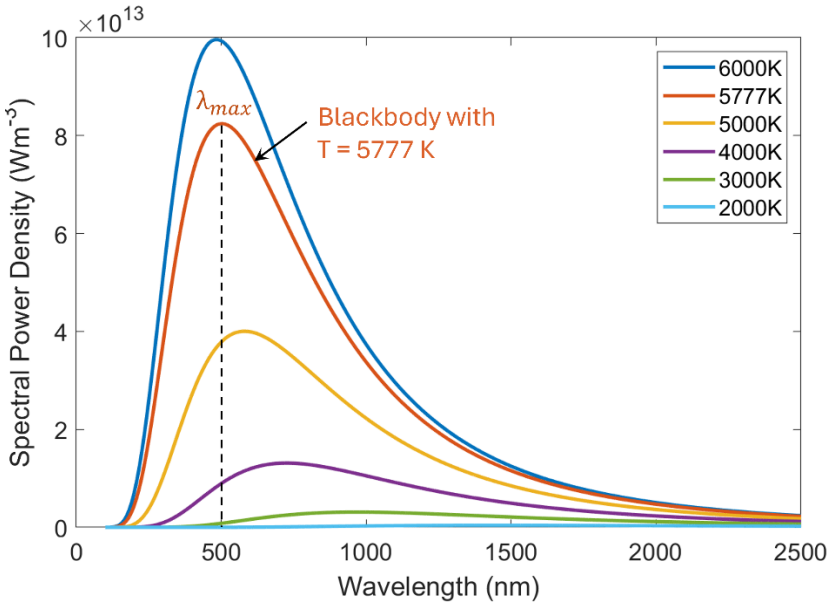

Figure 2.1. Spectral emission curves of an ideal blackbody having different temperatures.

2.1.2 The Sun and The Solar Spectrum

The solar spectrum refers to the distribution of electromagnetic radiation emitted by the sun at different wavelengths. The sun emits a broad range of radiation, which includes visible light, ultraviolet (UV) radiation, and infrared (IR) radiation. Visible light is the portion of the solar spectrum that can be seen by the human eye. The visible part of the solar spectrum has a wavelength range from approximately 400 to 700 nanometers (nm). Different wavelengths of light within this range appear as different colors to the human eye. It includes the colors of the rainbow (violet, indigo, blue, green, yellow, orange, and red) with violet having the shortest wavelength and red light having the longest wavelength. The UV portion of the solar spectrum has shorter wavelengths than visible light, ranging from approximately 100 to 400 nm. The IR radiation has longer wavelengths (>700 nm) than the visible light. The **spectral irradiance** of the sun refers to the amount of power per unit area per unit wavelength received from the Sun. Therefore, it is expressed in watts per square meter per nanometer ($W/m^2/nm$). The spectral irradiance varies with wavelength, and it provides information on how sun's emitted energy is distributed over different wavelengths. When we plot the spectral irradiance data vs. wavelength, the plot graphically represents the nature of the sunlight (or solar) spectrum.

AM0 and AM1.5: The spectral irradiance profile of the sunlight just outside of the earth's atmosphere is known as **Air Mass 0** or **AM0** spectrum. It signifies that the sunlight has not passed through any atmosphere, that means it has passed through zero atmosphere, hence referred as Air Mass **Zero**. It is also known as the extraterrestrial solar spectrum. This spectrum includes all wavelengths of solar radiation and is not affected by atmospheric absorption or scattering. As the sunlight passes through the earth's atmosphere, certain wavelengths of light get absorbed or scattered by various types of gas molecules present in the atmosphere, clouds and aerosols. As a result, the solar spectrum changes as it travels through the earth's atmosphere. The most common terrestrial spectrum used for solar energy applications is the **Air Mass 1.5** or **AM1.5** spectrum. AM1.5 represents the spectral irradiance received at the seal level after the sunlight has passed through the atmosphere at a 48° angle. Figure 2.2 shows the AM0 and AM1.5 spectrum with regions colored corresponding to ultraviolet, visible, and infrared wavelengths. In the AM1.5 radiation, the UV wavelengths carry approximately 5% of the total energy, while the visible region (400-700 nm)

accounts for ~43%, and the infrared region accounts for ~52% of the total energy. Note that the AM0 curve in Figure 2.2 resembles the shape of the blackbody radiation curve (for 5777K) shown in Figure 2.1.

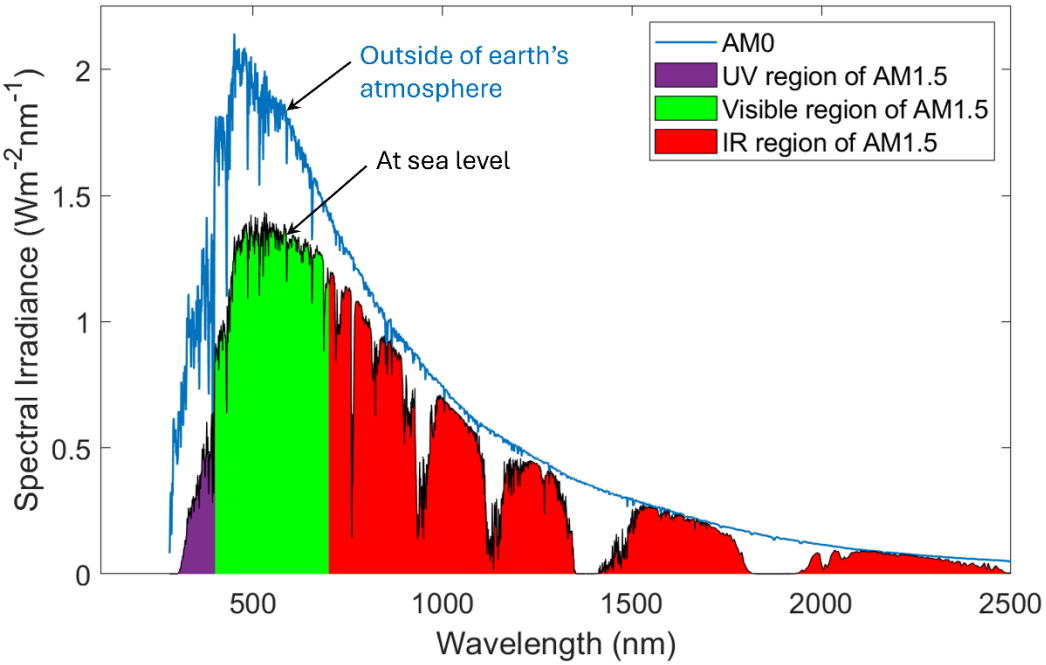

Figure 2.2. Extraterrestrial (AM0) and Terrestrial (AM1.5) Solar Spectra.

2.2 Solar Irradiance and Insolation

Solar irradiance is the amount of solar radiation (or solar power) received on a surface per unit area. It is measured in watts per square meter (W/m^2). Hence, we can also refer to it as power density. The average solar irradiance just outside of the Earth's atmosphere is approximately 1,368 W/m^2, which is known as the **Solar Constant**. This value is based on one astronomical unit from the Sun, which is the average distance of the Earth from the Sun. The actual irradiance value slightly changes throughout the year due to the slightly non-circular orbit of the earth. Some of this incoming radiation is absorbed and scattered by the atmosphere and the remaining portion reaches the earth's surface. The Global Horizontal Irradiance (GHI) is the total irradiance available on a horizontal surface. GHI is commonly used for solar power calculations. GHI has two components – (i) direct light and (ii) diffused light. Direct Normal Irradiance (DNI) is the component of the sunlight that travels directly from the sun without being scattered. Diffused Horizontal Irradiance (DHI) is the component of the sunlight that has been scattered by the atmosphere. The GHI can be calculated using Equation 2.3 given below.

$$GHI = DHI + DNI \cdot \cos\theta \ldots\ldots\ldots\ldots\ldots (2.3)$$

Where, θ is the Zenith angle. There are several methods for measuring solar irradiance, including ground-based instruments and satellites. Ground-based instruments include pyranometers, which are typically used for the measurement of GHI. Pyrheliometers, on the other hand, are used to measure the DNI, i.e. the direct solar radiation received by a surface perpendicular to the sun's rays. DHI is also measured using a pyranometer, often in conjunction with shading devices to block the direct component of the sunlight.

Solar Insolation is the total amount of solar energy received per unit area during a given period of time. It is typically measured in kilowatt-hours per square meter (kWh/m²) per day or per year. Hence, insolation can be calculated by integrating the solar irradiance over a specified time period (e.g., daily, monthly, yearly) and mathematically it can be represented using Equation 2.4 or Equation 2.5.

$$\text{Insolation} = \int_{t_1}^{t_2} \text{Irradiance}\ dt \ \ldots\ldots\ldots\ldots\ldots\ldots\ldots\ldots (2.4)$$

$$\text{Insolation} = \text{Irradiance} \times \Delta t \ \ldots\ldots\ldots\ldots\ldots\ldots\ldots\ldots (2.5)$$

The amount of insolation received by a particular location depends on several factors, including latitude, altitude, and local weather conditions. Typically, areas closer to the equator (having low latitude value) receive more insolation than areas at higher latitudes. Also, areas at higher altitudes will receive more insolation due to the thinner atmosphere.

2.2.1 Calculation of Solar Irradiance

We can calculate the solar irradiance at any location on earth at a given time using a set of equations. The steps to calculate solar irradiance involve the calculation of – (i) Hour Angle, (ii) Solar Declination Angle, (iii) Zenith Angle, and finally calculation of the (iv) Irradiance, by taking atmospheric loss into account. Each of these steps are described below.

(i) Hour Angle (H): The hour angle represents the angular displacement of the sun from the local meridian at a given time. It tells us how far the sun is east or west of the **solar noon** position. **Solar noon** refers to the moment when the sun is at its highest point in the sky, and it corresponds to 12:00 PM LST. The hour angle (H) can be calculated using Equation 2.6.

$$H = (LST - 12) \times 15^{\circ} \ldots\ldots\ldots\ldots\ldots\ldots (2.6)$$

Where, **LST** is the Local Solar Time. It is important to note that the **solar noon** does not necessarily occur at 12:00 PM on a clock, i.e. **LST** can be different from the local time (**LT**). The exact local time at which solar noon occurs (that means the sun is found at its highest elevation in the sky) depends on multiple factors including the day of the year, the time zone, longitude of the location, and the status of the daylight-saving time. Therefore, the exact local time when solar noon occurs at a location varies daily.

From Equation 2.6, it is evident that at solar noon (LST = 12:00), the hour angle is 0°, meaning the Sun is directly on the local meridian. The local meridian of a location is the imaginary line that runs from the north pole to the south pole of earth passing through the location. Before solar noon, the LST is less than 12:00 and therefore the hour angle is negative, indicating that the sun is on the east side of the local meridian. Similarly, after the solar noon, the hour angle would be positive, that means the sun would be on the west of the local meridian. The earth makes a complete rotation (360°) in 24 hours. Hence, it rotates on its axis at a rate of 15° per hour. Therefore, 1 hour of difference in Equation 2.6 translates to 15° of angular displacement. For example, if the hour angle (H) is -15°, that means it is one hour before solar noon, and if H is +30°, it is two hours after solar noon at the given location. To calculate the hour angle (H) using Equation 2.6, we must first find out the local solar time (LST). The **LST** can be calculated using Equation 2.7.

$$LST = LT + \left(\frac{TC}{60}\right) \ldots\ldots\ldots\ldots\ldots\ldots (2.7)$$

Where, **TC** is the total Time Correction factor (in minutes) and is given by Equation 2.8.

$$TC = 4 \times (\text{Longitude} - LSTM) + EOT - DST \ldots\ldots\ldots\ldots\ldots\ldots (2.8)$$

Where, **LSTM** is the Local Standard Time Meridian, **EOT** is the Equation of Time, and **DST** accounts for the status of daylight saving. The value of the DST in Equation 2.8 is 0 if daylight saving is off and is 60 min when daylight saving is on. Daylight saving in the U.S. starts on the second Sunday of March and ends on the first Sunday of November.

The earth is divided into 360° of longitude. For standardized timekeeping, we have created 24 time zones, where each time zone typically spans over 15° of longitude. LSTM is usually located at the central meridian (midpoint) of a given time zone. It represents the longitude value which is used to set the standard time for that time zone. Since the location for our solar power (or solar irradiance) calculation may have a different longitude, we need to make a longitude correction for accurate calculations. This is done by the first part of Equation 2.8, where **Longitude** refers to the exact longitude value for the location where we want to calculate the solar irradiance. For West longitudes the value must be entered with a negative sign, and for East longitudes, the value will be positive. For example, the longitude of Chicago, IL is 97.74°W. Hence, we must input it as: Longitude = −97.74° when using Equation 2.8. LSTM for a location can be found using Equation 2.9.

$$\text{LSTM} = 15° \times \Delta T \ \ldots\ldots\ldots\ldots\ldots\ldots (2.9)$$

Where, ΔT is the time zone offset. Local times at different time zones are set based on the Coordinated Universal Time (**UTC**), formerly known as Greenwich Mean Time (GMT). Therefore, each time zone has a specific offset from UTC. This offset (ΔT) is positive for a location that is situated on the east side of the standard meridian (UTC) and is negative for a location that is situated on the west side of the standard meridian. For example, the city of Atlanta falls within the Eastern Standard Time (EST) zone, which is located on the west and is 5 hours behind the Coordinated Universal Time (UTC−05:00). Hence, for Atlanta, the time zone offset (ΔT) would be equals to −5.0 and consequently the LSTM would be $-75°$. An important note here is that we must input the ΔT value considering the local standard time (**EST**), not the daylight time (hence, **do not use EDT**).

The **Equation of Time** (**EOT**) is an empirical equation that accounts for the earth's elliptical shaped orbit and axial tilt. It is presented in Equation 2.10.

$$\text{EOT} = 0.0172 + 0.4282\cos B - 7.352\sin B - 3.3498\cos 2B - 9.372\sin 2B \ldots\ldots (2.10)$$

$$\text{Where,}\ \ B = (d-1) \times \frac{360^{\circ}}{365} \ldots\ldots\ldots\ldots\ldots\ldots (2.11)$$

Where, d is the day of the year. For example, if you are calculating the solar irradiance on January 20, then d would be 20. Equation 2.11 provides the value of $\boldsymbol{B}$ in degrees and Equation 2.10 provides the value of **EOT** in minutes.

(ii) Solar Declination Angle (δ): The earth's axis is tilted at an angle of 23.45° relative to the normal to the plane of revolution (orbital plane) around the sun. This is depicted in Figure 2.3 (a). This axial tilt or obliquity changes very slowly in the range between 22.1°−24.5° over an extremely long cycle of ~41,000 years, and therefore for all practical solar power calculations, the tilt angle can be considered constant at its current value of 23.45°. Due to this axial tilt of the earth, the incoming sunlight strikes the earth's equator at a certain angle, which is known as the solar declination angle. Since the direction of earth's tilt is fixed in space, the solar declination angle gradually varies between +23.45° and −23.45° over the course of a year as the earth orbits around the sun. As a result, the intensity of sunlight and the length of daytime at a specific location change throughout the year which gives rise to the seasons.

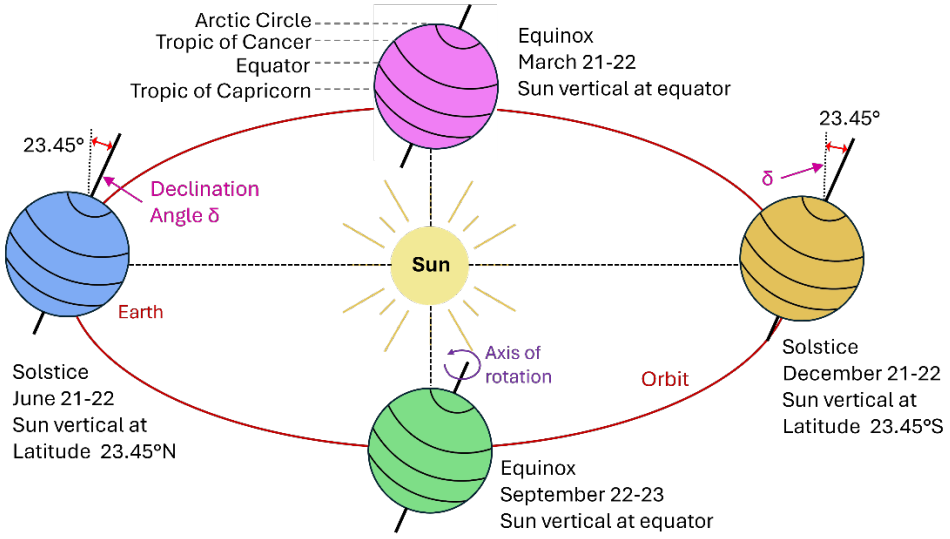

Figure 2.3. Schematic showing the concept of declination angle and the variation of declination angle due to earth's rotation around the sun.

On June 21, the solar declination angle (δ) reaches its maximum value of +23.45° in the northern hemisphere, resulting in the longest day of the year. At the same time, δ reaches its minimum value of −23.45° in the southern hemisphere, resulting in the shortest day of the year. Hence, June 21 is designated as the Summer Solstice in the northern hemisphere, and Winter Solstice in the southern hemisphere. The opposite occurs on December 21 when δ becomes −23.5° in the northern and +23.45° in the southern hemisphere, respectively. Thus, December 21 is referred to as the winter solstice in the northern hemisphere, and summer solstice in the southern hemisphere. These positions are graphically depicted in Figure 2.3. During the Spring Equinox (March 21) and Fall Equinox (September 23), the declination angle becomes 0°, resulting in nearly equal length of day and night. The Declination Angle (δ) can be calculated using Equation 2.12 given below.

$$\delta = 23.45° \cdot \sin\left[\frac{360}{365}(284 + d)\right] \ldots\ldots\ldots\ldots\ldots\ldots (2.12)$$

Where, d is the day of the year. Note that the solar Declination Angle is not dependent on the location.

(iii) Zenith Angle (Z): The Zenith Angle refers to the angle between the direction of the sun and the vertical line from the observer to the zenith point. It measures the angular distance of the sun from the zenith point, where zenith point refers to an imaginary point located directly overhead in the vertical

direction, above the observer. When the sun is directly overhead, the Zenith Angle is 0°. As the sun moves lower in the sky, the Zenith Angle increases, reaching 90° when the sun is at the horizon during sunrise or sunset. On the other hand, the angle that the sun makes with the horizontal plane is called the **Elevation Angle** (or altitude angle). During sunrise and sunset, the elevation angle (α) is 0°. After sunrise, as the sun's position climbs up in the sky, the elevation angle gradually increases, attaining the maximum value at solar noon when the sun is at its highest point in the sky. Hence, Zenith Angle (Z) and Elevation Angle (α) are complementary to each other, and mathematically we can represent their relationship as: $Z = 90° - \alpha$. The Zenith Angle (Z) can be calculated using Equation 2.13.

$$Z = \cos^{-1}(\sin\delta \cdot \sin\varphi + \cos\delta \cdot \cos\varphi \cdot \cos H) \dots\dots\dots\dots (2.13)$$

Where, φ is the latitude of the location, H is the hour angle (calculated using Equation 2.6), and δ is the solar declination angle (calculated using Equation 2.12).

The solar **Elevation Angle** (α) can be easily calculated if the Zenith Angle (Z) is known. Alternatively, α can be directly calculated using Equation 2.14 given below.

$$\alpha = \sin^{-1}(\sin\delta \cdot \sin\varphi + \cos\delta \cdot \cos\varphi \cdot \cos H) \dots\dots\dots\dots (2.14)$$

(iv) Solar Irradiance (I): The Solar Irradiance (I) can be calculated using Equation 2.14.

$$I = (S \cdot \cos Z) \times T \dots\dots\dots\dots (2.15)$$

Where, S is the Solar Constant as discussed in section 2.1.2, Z is the Zenith Angle (calculated using Equation 2.13), and T is the transmittance which takes the atmospheric absorption (or atmospheric loss) into account. For example, if the atmospheric loss is 20%, then T would be = (1−0.2) = 0.8.

Example Problem (2.1): Calculate the Solar Irradiance at Marietta, GA on October 5 at 2:00 pm local time. Consider 25% atmospheric loss.

Solution:

Step 1: Note the latitude and longitude from google maps.

Lattitude (φ) = $\mathbf{33.95°N}$, Longitude = 84.55°W = $\mathbf{-84.55°}$

Step 2: Calculate the Local Standard Time Meridian (LSTM).

LSTM = $15° \times \Delta T = 15° \times (-5) = \mathbf{-75°}$

[Note: Marietta is in Easten time zone (EST) which is 5 hours behind UTC]

Step 3: Calculate EOT.

$$\text{EOT} = 0.0172 + 0.4282\cos B - 7.352\sin B - 3.3498\cos 2B - 9.372\sin 2B$$

Where, $B = (d-1) \times \frac{360}{365} = (278-1) \times \frac{360}{365} = \mathbf{273.2°}$

[Note: October 5 is the 278th day of the year]

$\therefore \text{EOT} = 0.0172 + 0.4282\cos(273.2°) - 7.352\sin(273.2°) - 3.3498\cos(546.4°) - 9.372\sin(546.4°)$

$\Rightarrow \text{EOT} = \mathbf{11.76\ minute}$

Step 4: Calculate the total Time Correction (TC).

$TC = 4 \times (\text{Longitude} - LSTM) + EOT - DST$

$= 4 \times \left(-84.55° - (-75°)\right) + 11.76 - 60 = \mathbf{-86.44\ minute}$

[Note: On Oct 5, Daylight Savings Time is ON in the U. S. Hence, DST = 60 min]

Step 5: Calculate the Local Solar Time (LST).

$\boldsymbol{LST} = LT + \left(\frac{TC}{60}\right) = 14 + \left(\frac{-86.44}{60}\right)\ \text{hours} = \mathbf{12.56\ hours}$

[Note: Local time should be written in 24h format. Hence 2: 00 pm = 14]

Step 6: Calculate the Hour Angle (H).

$\boldsymbol{H} = 15° \times (LST - 12) = 15° \times (12.56 - 12) = \mathbf{8.4}°$

Step 7: Calculate the Solar Declination Angle (δ).

$\delta = 23.45° \sin\left[\frac{360}{365}(284 + d)\right] = 23.45° \sin\left[\frac{360}{365}(284 + 278)\right] = \mathbf{-5.8}°$

Step 8: Calculate the Zenith Angle (Z).

$Z = \cos^{-1}(\sin\delta \sin\varphi + \cos\delta \cos\varphi \cos H)$

$= \cos^{-1}(\sin 5.8° \sin 33.95° + \cos 5.8° \cos 33.95° \cos(8.4°)) = \mathbf{40.53}°$

Step 9: Calculate the Solar Irradiance (I).

$I = \text{S} \times cos\, Z \times T = 1368 \times \cos(40.53°) \times (1 - 0.25) = \mathbf{780\ Wm^{-2}}$

Example Problem (2.2): Repeat the calculations done in problem 2.1 for every 15 min interval and plot the resulting Solar Irradiance Profile (with Irradiance on the y-axis and Local Time on the x-axis). You may use a computer program for the repeated calculations and plotting the Irradiance profile. Limit the y-axis to start from zero, so that only the positive irradiances are visible within the plotted graph.

Solution:

By repeating the calculations as shown in the step-by-step solution of problem 2.1, irradiance values were calculated at every 15 min interval. Following is the resulting Irradiance plot with the Local Time (LT) on the x-axis. Note that the peak irradiance does not occur at 12:00 o'clock local time. The peak irradiance value is found around 1:30 pm local time. This is because there is about −87 minutes time correction as per the calculations. Therefore, the solar noon at Marietta on Oct 5 has an offset of

about 87 minutes from the 12:00 noon local time (clock time). Remember that solar noon is the time when the sun is at its highest elevation in the sky on a specific day. As a result, the maximum irradiance is received at solar noon.

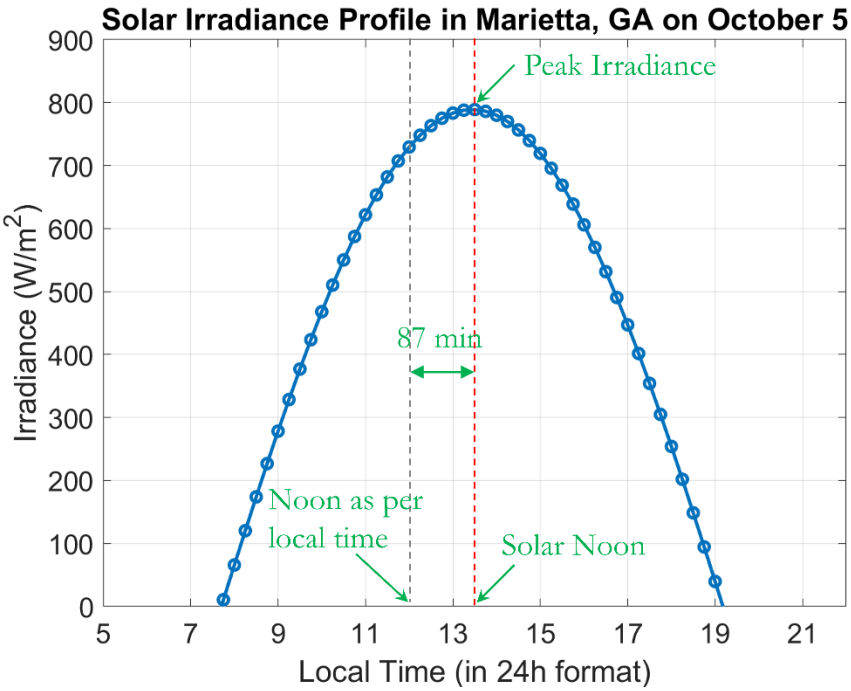

2.3 Sun Path Chart

The sun path chart, also referred to as solar path diagram or sun chart is a graphical representation that depict how the sun moves across the sky at a given location throughout the year. This chart is a useful tool for solar energy site surveying, designing energy-efficient buildings, and assessing the solar insolation at the installation location for solar power generation. The following section describes the details of sun path charts, their construction, and how to read these charts.

2.3.1 Construction of a Sun Path Chart:

Two angles are used to define the exact position of the sun in the sky – (i) the **Altitude Angle** and (ii) the **Azimuth Angle**. The Altitude or **Elevation Angle** can be calculated using Equation 2.14 as discussed in section 2.1.3. The **Solar Azimuth Angle** can be estimated using Equation 2.16.

$$\gamma_s = \begin{cases} \cos^{-1}\left(\dfrac{\sin\delta \cdot \cos\varphi - \cos\delta \cdot \sin\varphi \cdot \cos H}{\cos\alpha}\right), & \text{if } H \leq 0 \\ 360° - \cos^{-1}\left(\dfrac{\sin\delta \cdot \cos\varphi - \cos\delta \cdot \sin\varphi \cdot \cos H}{\cos\alpha}\right), & \text{if } H > 0 \end{cases} \quad \ldots\ldots\ldots\ldots\ldots (2.16)$$

Where, φ is the latitude of the location, α is the Elevation Angle (calculated using Equation 2.14), and δ is the solar declination angle (calculated using Equation 2.12).

To plot a sun path chart, these two angles are used. There are different ways to draw a sun path chart. The two most widely used techniques are – Cartesian Sun Path Chart and Polar Sun Path Chart. Both use the

same information (Altitude and Azimuth angles) but differ in the method of plotting the data, and consequently have different appearances. In the Cartesian style Sun Path Chart, there are two cartesian axis, where x-axis is used for the Azimuth angle, and the y-axis is used for the Elevation angle.

The solar **Azimuth Angle** describes the angular displacement of the sun from the true north, measured on the horizontal plane. It is measured clockwise from the north. Therefore, when the sun is directly east, the azimuth angle is 90°, when it is directly south, the azimuth angle is 180°, and when it is directly west, the azimuth angle is 270°. The sun's path changes daily, and sun path charts graphically illustrate these variations by drawing the sun's trajectory through the sky.

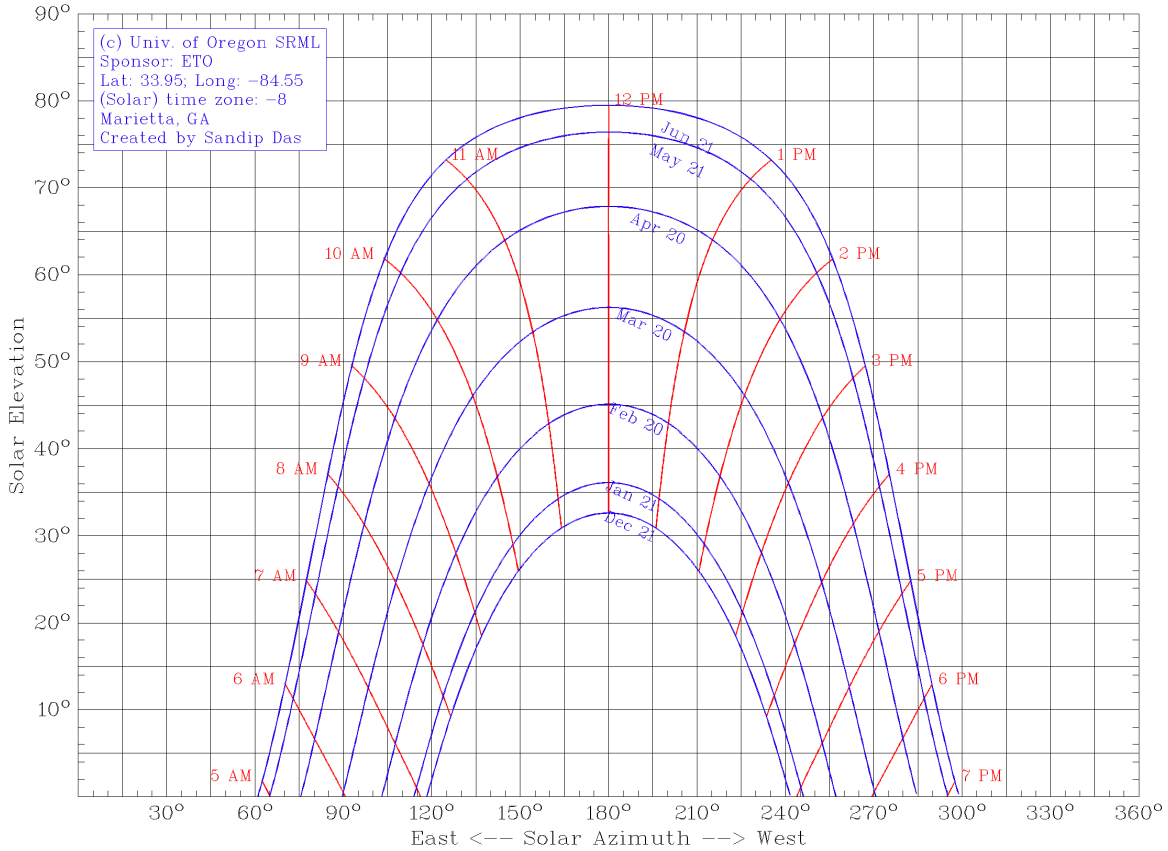

Figure 2.4. Sun Path Diagram for Marietta, GA

The sun path chart is constructed using polar coordinates, where the Elevation and Azimuth angles of the sun are used to plot the sun's trajectory taken in the sky for different days of the year. The two most important elements of a typical sun path chart are the date lines and hour lines which are explained below.

Date Lines: These curves represent the sun's trajectory on the sky on specific dates. Commonly, charts include sun paths for summer solstice, winter solstice, spring and fall equinoxes, and for few more intermediate dates, typically one month apart. An example sun part chart (created using Univ. of Oregon's SRML sun path chart creator website) for Marietta, GA (latitude = 33.95° N, longitude: 84.55° W) is shown in Figure 2.4. The blue lines in this diagram are the date lines. To find the sun's trajectory on any other day, a day line for that specific day can be drawn by within this diagram manually by extrapolation with reasonable accuracy. The sun path chart also graphically shows the seasonal variations of the sun's trajectory and the variations of sunrise and sunset times at a location.

Hour Lines: These curves indicate the position of the sun at different hours of the day throughout the year. The red lines in Figure 2.4 are the hour lines. The intersection point of an hour line and a date line will provide the exact position of the sun at that specific date and time.

Example Problem (2.3): Sun path chart for Philadelphia, PA is given below. Find the following information by analyzing the chart. Do not use any equations.

(a) The Sun's position in the sky on April 20 at 4:00 pm solar time.

(b) The Sun's position in the sky on May 6 at 10:30 am solar time.

(c) The total duration of the daytime on February 20.

Solution:

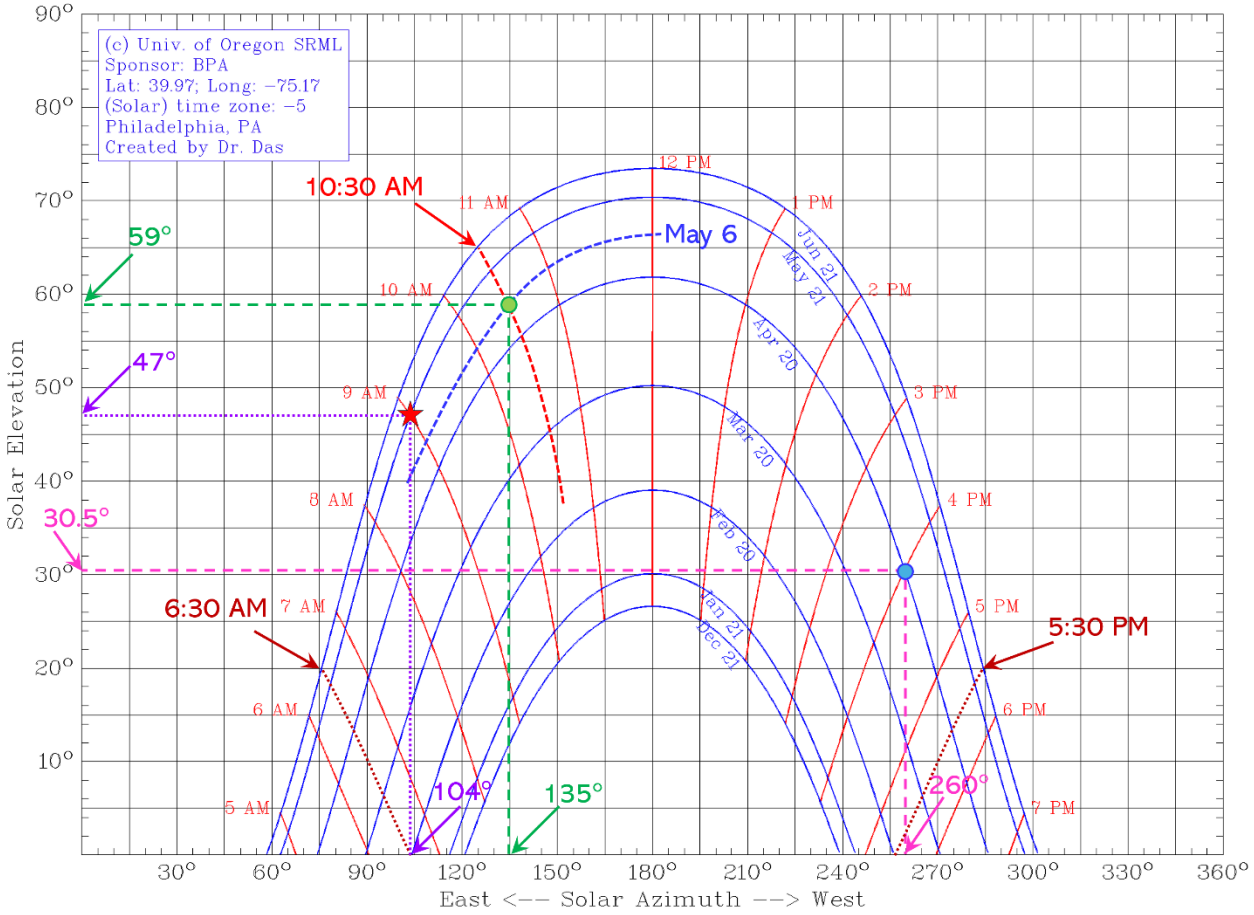

(a) The intersection point of the April 20 line and 4 PM line is circled (blue). The coordinate of this point indicate the Sun's position in the sky. The coordinates are found as follows:

Azimuth Angle = 260° and **Elevation Angle = 30.5°** (shown using pink dashed lines on the chart).

(b) The day line for May 6 did not exist in the given graph. Hence, an approximate line for May 6 is drawn (red dashed line on the chart). Also, the hour line for 10:30 AM did not exist in the given graph. Hence, an approximate line for 10:30 AM is drawn (shown with red arrow on the chart). The intersection point of these two lines (circled in green) gives the position of the Sun. The coordinate for this position is read from the chart as follows:

Azimuth Angle = 135° and **Elevation Angle = 59°** (shown using green dashed lines on the chart).

(c) To find the duration of the daytime, we need to find the apparent sunrise and sunset times. At the time of sunrise and sunset, the sun is on the horizon and the solar elevation angle is zero. Hence, two lines, one for sunrise and one for sunset, (shown using brown dashed lines) are extrapolated from the points where the February 20 day line touches the x-axis (points where the elevation angle is zero). It is evident that the left line, corresponding to sunrise, is about halfway between the 6 AM and 7 AM hour lines. Hence, the sunrise time is 6:30 AM. Similarly, we can see that the right line, corresponding to sunset, is approximately halfway between the 5 PM and 6 PM hour lines. Hence, the estimated sunset time is 5:30 PM. Therefore, the total daytime is = **11 hours**.

Example Problem (2.4): Latitude and longitude for Philadelphia, PA are 39.97°N and 75.17°W, respectively.

(a) Using analytical calculations, find the solar Elevation Angle (α) and the solar Azimuth Angle (γ_s) on May 21 at 10:00 am local time.

(b) Find the position of the sun on the same day and time by analyzing the sun path chart given in Example Problem (2.3) above, and then compare the result with the analytically obtained values in part (a).

Solution:

(a) Lattitude $(\varphi) = \mathbf{39.97°}$, Longitude $= \mathbf{-75.17°}$

$\text{LSTM} = 15° \times \Delta T = 15° \times (-5) = \mathbf{-75°}$

[Note: Philadelphia is in Easten time zone (EST) which is 5 hours behind UTC]

$\text{EOT} = 0.0172 + 0.4282\cos B - 7.352\sin B - 3.3498\cos 2B - 9.372\sin 2B$

$$\text{Where, } B = (d-1) \times \frac{360}{365} = (141-1) \times \frac{360}{365} = \mathbf{138.1°}$$

[Note: May 21 is the 141 day of the year]

$\therefore \text{EOT} = 0.0172 + 0.4282\cos(138.1°) - 7.352\sin(138.1.2°) - 3.3498\cos(276.2°) - 9.372\sin(276.2°)$

$\Rightarrow \text{EOT} = \mathbf{3.75\ minute}$

$TC = 4 \times (\text{Longitude} - LSTM) + EOT - DST$

$= 4 \times \left(-75.17° - (-75°)\right) + 3.75 - 60 = \mathbf{-56.93\ minute}$

[Note: On May 21, Daylight Savings Time is ON in the U. S. Hence, DST = 60 min]

$$\boldsymbol{LST} = LT + \left(\frac{TC}{60}\right) = 10 + \left(\frac{-56.93}{60}\right) \text{ hours} = \mathbf{9.05\ hours}$$

$$\boldsymbol{H} = 15° \times (LST - 12) = 15° \times (9.05 - 12) = \mathbf{-44.2°}$$

$$\delta = 23.45° \sin\left[\frac{360}{365}(284 + d)\right] = 23.45° \sin\left[\frac{360}{365}(284 + 141)\right] = \mathbf{20.1°}$$

$$\text{Elevation Angle, } \alpha = \sin^{-1}(\sin\delta \cdot \sin\varphi + \cos\delta \cdot \cos\varphi \cdot \cos H)$$

$$\Rightarrow \alpha = \sin^{-1}(\sin 20.1° \cdot \sin 39.97° + \cos 20.1° \cdot \cos 39.97° \cdot \cos(-44.2°)) = \mathbf{47.5°}$$

$$\text{Azimuth Angle, } \gamma_s = \cos^{-1}\left(\frac{\sin\delta \cdot \cos\varphi - \cos\delta \cdot \sin\varphi \cdot \cos H}{\cos\alpha}\right)$$

$$[\text{Note: H} < 0]$$

$$\Rightarrow \gamma_s = \cos^{-1}\left(\frac{\sin 20.1° \cdot \cos 39.97° - \cos 20.1° \cdot \sin 39.97° \cdot \cos(-44.2°)}{\cos 47.5°}\right) = \mathbf{104.4°}$$

(b) It is to note that the times in the given sun path chart are the local solar time (not local clock time). From the calculation done in part (a), we find that the local solar time (LST) corresponding to 10:00 am local time is 9.05 hours or approximately 9:00 am solar time. The sun's position for this day/time is marked on the chart using a red star marker. The coordinates are read from the chart which gives us:

Azimuth Angle = 104° and **Elevation Angle = 47°** (shown using purple dotted lines on the chart).

It is evident that the values obtained from the sun path chart match very close to the analytically calculated values obtained in part (a).

2.4 Angle of Incidence

The solar Angle of Incidence refers to the angle at which sunlight strikes a surface, such as a solar panel or a solar thermal collector. This angle is measured between the direction of the incoming sunlight and the normal (perpendicular line) on the surface of interest. The Incidence Angle (θ_i) for a tilted surface can be calculated via Equation 2.17.

$$\theta_i = \cos^{-1}[(\sin\alpha \cdot \cos\beta) + (\cos\alpha \cdot \sin\beta \cdot \cos(\gamma_s - \gamma_{PV}))] \dots\dots\dots\dots\dots\dots \quad (2.17)$$

Where, β is the tilt angle of the solar energy receiving surface (let's say a PV array) measured with respect to the horizontal plane, α is the solar Elevation Angle, γ_s is the Solar Azimuth Angle (for the sun), and γ_{PV} is the Azimuth Angle of the PV array (measured clockwise from the north).

For a perfectly horizontal surface, $\beta = 0°$, and the expression for Incidence Angle (θ_i) can be reduced as follows: $\theta_i = \cos^{-1}[\sin\alpha] = \cos^{-1}[\sin(90° - Z)] = Z$

Hence, for a perfectly horizontal surface, the Angle of Incidence (θ_i) becomes equal to the Zenith Angle (Z), and can be written as:

$$\theta_i = \cos^{-1}(\sin\delta \cdot \sin\varphi + \cos\delta \cdot \cos\varphi \cdot \cos H) \dots\dots\dots\dots (2.18)$$

Where, φ is the latitude of the location, δ is the solar declination angle, and H is hour angle. Note that this Equation is same as the Zenith Angle equation (2.13).

A schematic is depicted in Figure 2.5 which shows all the angles involved in the calculation of the Incidence Angle. The performance of a solar energy receiver, such as a Photovoltaic panel or a Flat Plate Solar Thermal Collector strongly depend on the Angle of Incidence (θ_i), which affects the amount of solar radiation received by the receiver and consequently its output power.

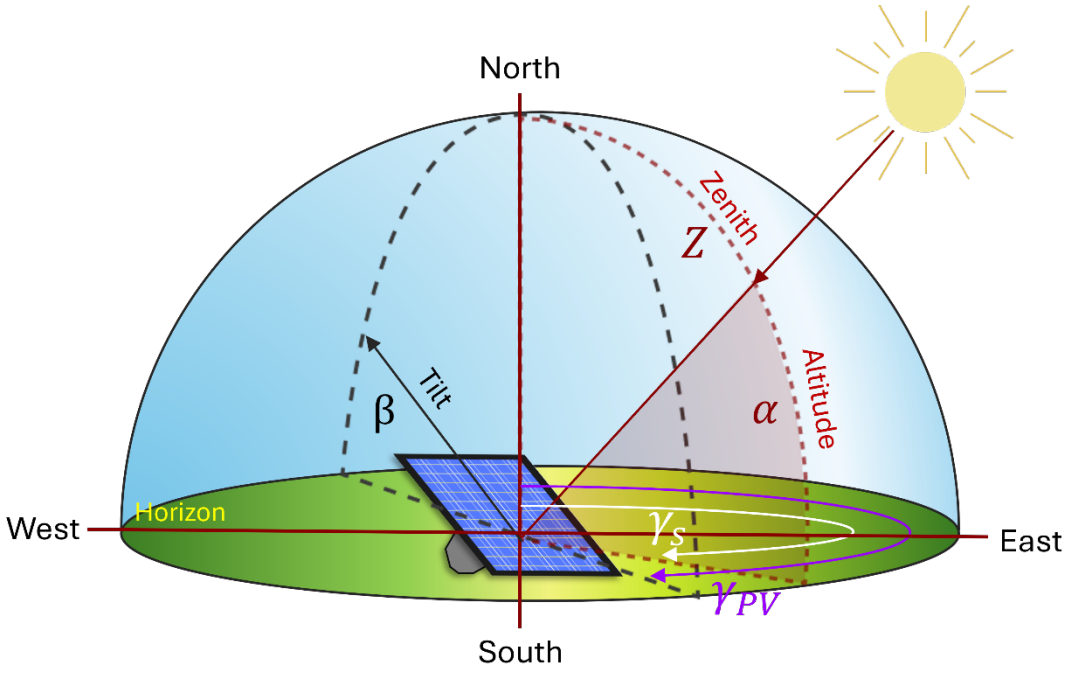

Figure 2.5. Important angles associated with incidence angle and solar power calculations.

Example Problem (2.5): Calculate the Angle of Incidence on a solar panel with the following specifics. Latitude of the location: 40°N; Day of the year: April 9; Time of the Day (Local Solar Time): 15:00 (pm); tilt angle: 30° from the horizontal plane; and facing southeast.

Solution:

$$H = 15° \times (LST - 12) = 15° \times (15 - 12) = \mathbf{45°}$$

$$\delta = 23.45° \sin\left[\frac{360}{365}(284 + d)\right] = 23.45° \sin\left[\frac{360}{365}(284 + 99)\right] = \mathbf{7.15°}$$

Elevation Angle, $\alpha = \sin^{-1}(\sin\delta \cdot \sin\varphi + \cos\delta \cdot \cos\varphi \cdot \cos H)$

$$\Rightarrow \alpha = \sin^{-1}(\sin 7.15° \cdot \sin 40° + \cos 7.15° \cdot \cos 40° \cdot \cos(45°)) = \mathbf{38.13°}$$

Azimuth Angle, $\gamma_s = 360° - \cos^{-1}\left(\frac{\sin\delta \cdot \cos\varphi - \cos\delta \cdot \sin\varphi \cdot \cos H}{\cos\alpha}\right)$

[Note: H > 0]

$$\Rightarrow \gamma_s = 360° - \cos^{-1}\left(\frac{\sin 7.15° \cdot \cos 40° - \cos 7.15° \cdot \sin 40° \cdot \cos(45°)}{\cos 38.13°}\right) = \mathbf{243.12°}$$

$$\theta_i = \cos^{-1}[(\sin\alpha \cdot \cos\beta) + (\cos\alpha \cdot \sin\beta \cdot \cos(\gamma_s - \gamma_{PV}))]$$

$$\Rightarrow \theta_i = \cos^{-1}[(\sin 38.13° \cdot \cos 30°) + (\cos 38.13° \cdot \sin 30° \cdot \cos(243.12° - 135°))] = \mathbf{65.6°}$$

Example Problem (2.6): A solar panel is installed at an angle of 45° from horizontal and pointed 10° west of due south. It is located at 35°N latitude. Calculate the incident angle at 1 h before solar noon on June 15.

Solution:

$H = 15° \times (LST - 12) = 15° \times (11 - 12) = \mathbf{-15°}$

$\delta = 23.45° \sin\left[\frac{360}{365}(284 + d)\right] = 23.45° \sin\left[\frac{360}{365}(284 + 166)\right] = \mathbf{23.3°}$

Elevation Angle, $\alpha = \sin^{-1}(\sin\delta \cdot \sin\varphi + \cos\delta \cdot \cos\varphi \cdot \cos H)$

$\Rightarrow \alpha = \sin^{-1}(\sin 23.3° \cdot \sin 35° + \cos 23.3° \cdot \cos 35° \cdot \cos(-15°)) = \mathbf{72.5°}$

Azimuth Angle, $\gamma_s = \cos^{-1}\left(\frac{\sin\delta \cdot \cos\varphi - \cos\delta \cdot \sin\varphi \cdot \cos H}{\cos\alpha}\right)$

[Note: H < 0]

$\Rightarrow \gamma_s = \cos^{-1}\left(\frac{\sin 23.3° \cdot \cos 35° - \cos 23.3° \cdot \sin 35° \cdot \cos(-15°)}{\cos 72.5°}\right) = \mathbf{127.83°}$

$\theta_i = \cos^{-1}[(\sin\alpha \cdot \cos\beta) + (\cos\alpha \cdot \sin\beta \cdot \cos(\gamma_s - \gamma_{PV}))]$

$\Rightarrow \theta_i = \cos^{-1}[(\sin 72.5° \cdot \cos 45°) + (\cos 72.5° \cdot \sin 45° \cdot \cos(127.83° - 190°))] = \mathbf{39.3°}$

2.5 Solar Photovoltaics

Solar photovoltaics (PV) refers to the technology that directly converts sunlight into electricity using photovoltaic devices, which are commonly known as solar cells. Solar PV provides a clean and sustainable source of energy. Solar cells work based on the photovoltaic effect – a physical process in which certain materials produce an electric current when exposed to light. The photovoltaic effect was first observed in 1839 by a French physicist, Alexandre Becquerel. Becquerel's experimental setup involved an electrolytic cell that comprised of two electrodes immersed in a liquid electrolyte solution. He observed that when the electrodes were exposed to light, a small electric current was generated by the cell which was proportional to the light intensity. Although Becquerel did not fully understand the underlying mechanisms, his discovery was pivotal, and it laid the foundation for future research and development of solar photovoltaic technology. Later, in 1905, Albert Einstein provided the theoretical framework for the photoelectric effect which explained the mechanism behind the emission of electrons from a material when exposed to light.

2.5.1 Evolution of Photovoltaic Technologies

The first practical photovoltaic solar cell was invented in 1954 by three researchers — Daryl Chapin, Calvin Fuller, and Gerald Pearson at Bell Laboratories. Their developed silicon-based solar cell demonstrated conversion of sunlight into electricity with a power conversion efficiency of 6%. This groundbreaking work marked the beginning of modern solar cell technology using semiconductor materials. The early PV cells were highly expensive, and their applications were limited to space exploration missions. In the 1970s, the first commercial PV modules were introduced in the market, and they were primarily used for remote power

applications such as lighthouses, telephone lines, and weather stations. In the following decades, significant research and development in the field of photovoltaics has created more efficient and cost-effective solar cells through innovations in new materials, device structures, and manufacturing processes. As a result, solar photovoltaic technology has now emerged as a competitive option for affordable and renewable source of electricity.

The evolution of efficiency over time for various solar cell technologies can be visualized in Figure 2.6. An interactive version of this chart is available at the NREL website. This Research Cell Efficiency Chart marks major efficiency breakthroughs made by different institutions around the world over the past five decades. In this chapter, we will primarily discuss the monocrystalline Silicon solar cells (non-concentrator). As of 2023, the highest efficiency of single junction monocrystalline Silicon solar cell has reached 26.1% in the laboratory. Also, notably, a team of researchers at the Fraunhofer Institute for Solar Energy Systems in Germany has developed the most efficient solar cell to date using four junctions made of III-V compound semiconductor materials that has achieved an astounding efficiency of 47.6% under 665X concentration of the sunlight.

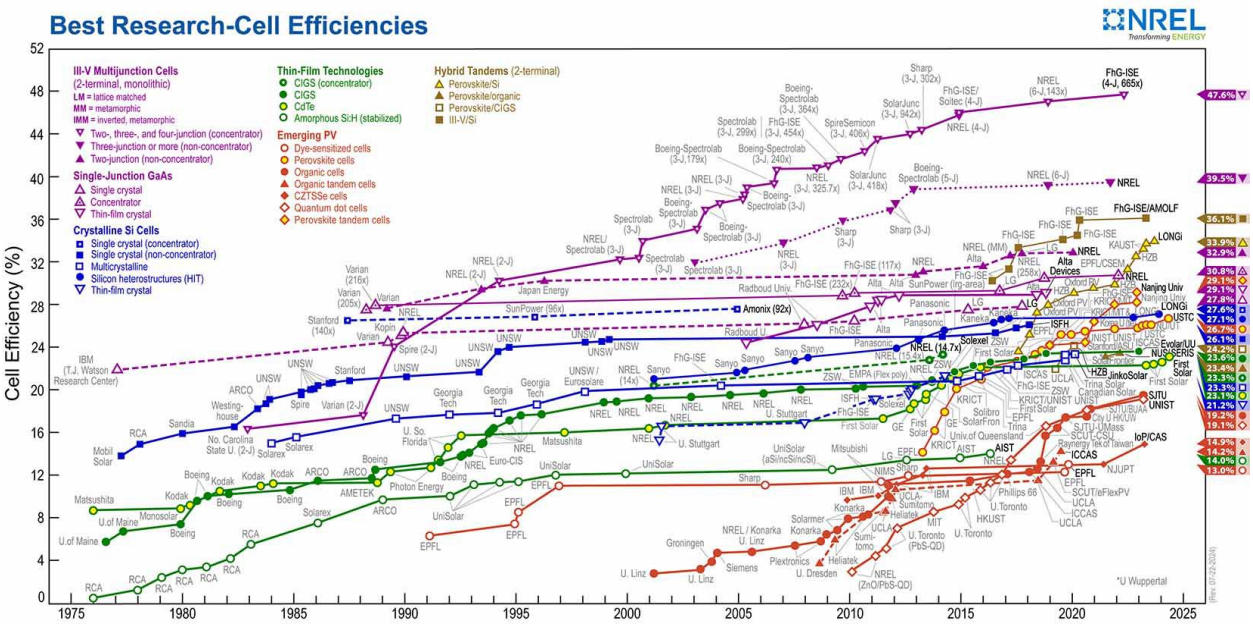

Figure. 2.6. Evolution of solar cell efficiency over time (source: NREL).

Today, crystalline Silicon (Si) photovoltaic cells are the most widely used type of solar cell, accounting for more than 80% share of the global solar cell market. They are used in a variety of applications, including rooftop solar for residential and commercial installations, large utility-scale solar power plants, small rechargeable electronic devices etc.

2.5.2 PV Technology Generations

After the invention of the Si-based solar cell in 1954, Silicon, the most widely used semiconductor in the electronics industry, also became the primary material of choice for photovoltaic cells. The theoretical maximum possible efficiency of a single junction crystalline Silicon solar cell under one sun irradiance is about 32%.

First Generation Solar Cells (Si-based Photovoltaics): Solar cells made of mono-crystalline Silicon and multi-crystalline (or Polycrystalline) Silicon are referred to as the first-generation solar cells. c-Si cells are made using c-Si wafers having a highly oriented atomic arrangement of Si atoms. These wafers, typically about 160 – 200 μm thick, are produced by slicing a solid cylindrical Si ingot, grown using a highly controlled and expensive crystal growth process. Such controlled growth of high-purity Si takes huge amount of time and energy, and as a result they are expensive to produce. On the other hand, polycrystalline or multi-crystalline Silicon (mc-Si) cells use mc-Si wafers which contain large number of grains, each grain having a different atomic arrangement. This causes inferior electrical properties than c-Si and as a result mc-Si solar cells have lower efficiency compared to c-Si cells. However, mc-Si solar cells are cheaper than c-Si cells since mc-Si wafers are obtained by slicing a rectangular shaped mc-Si ingot which are produced by a simpler and cost-effective manufacturing process of casting molten Si into large bricks. Another variation of mc-Si cells use Ribbon Silicon, where a large thin Si sheet is directly produced by pulling a thin ribbon of Silicon from a molten Si bath. This process eliminates the step of ingot production, reduces material waste, and is more cost-effective. The first-generation PV technology is well matured reaching an efficiency (η) of ~26% for c-Si cells and ~23% for mc-Si solar cells in the laboratory. The first-generation Si-based photovoltaic technology is widely deployed and currently dominates the commercial market for terrestrial solar power generation.

Second Generation Solar Cells (Thin-Film Photovoltaics): In the 1970s, researchers started exploring alternative materials for solar cells, which led to the development of thin film solar cell technologies, which is referred to as the second-generation solar cells. Second generation solar cells typically use various compound semiconductor materials. Unlike Si, these materials have direct bandgaps. As a result, they are much more efficient in absorbing the incident sunlight and consequently require a very thin layer of light absorbing semiconductor material. Hence, these solar cells are known as Thin Film Solar Cells (TFSC). There are various TFSC technologies developed over the past few decades. The most prominent ones include Cadmium Telluride (CdTe), Copper Indium Gallium Selenide (CIGS), Amorphous Silicon (a-Si), and very recently Perovskite Solar cells. TFSCs typically use only a few micrometers thick light absorbing semiconductor layer which is about 50-100 times less than the thickness of a c-Si solar cell. The semiconductor films in TFSCs are typically polycrystalline in nature, and they are deposited on a substrate material, such as a piece of glass or a metal foil. Use of flexible substrate allows flexible solar cells which is not possible for first-generation solar cells. Among the above mentioned TFSCs, CdTe, CIGS and a-Si solar cells are commercially available; however, their market share is much less compared to the first-generation solar cells.

Third Generation Solar Cells: There are various PV technologies that fall under this classification, typically more advanced and emerging technologies, most of which are still under research and have not reached the commercialization stage yet. Some examples of third generation solar cells include dye-sensitized solar cells (DSSC), Organic photovoltaic devices, Quantum Dot solar cells, Perovskite solar cells etc. Among these, Perovskite solar cells have demonstrated a very competitive efficiency of ~27% and is being considered as a possible candidate to replace Si in the near future.

2.5.3 Photons: The Light Particles

Photons are the particles of light, each carrying a 'quanta' of energy. Photons have no mass, but they do have energy and momentum. They were proposed by Albert Einstein in 1905 in his groundbreaking paper which explained the photoelectric effect and created the foundation of our understanding of the operation of solar cells.

Photon Energy: The energy of a photon is directly proportional to its frequency, and inversely proportional to its wavelength. This relationship is described by Equation 2.19, where E_{ph} is the energy of the photon, h is Planck's constant (6.626×10^{-34} J.s), and ν is the frequency. The frequency (ν) is inversely proportional to the wavelength (λ), and it is related to the speed of light as: $\nu = c/\lambda$. Equation 2.19 provides photon energy in Joules. However, photon energies are typically expressed in electron-Volts or eV, where 1 eV = 1.602×10^{-19} Joules. Hence, Equation 2.20 can be conveniently used to calculate the photon energy directly in eV when the wavelength of the light is input in micrometers.

$$E_{ph} = h\nu = \frac{hc}{\lambda} \quad \ldots\ldots\ldots\ldots\ldots\ldots\ldots\ldots\ldots\ldots\ldots\ldots\ldots\ldots (2.19)$$

$$E_{ph}[eV] = \frac{1.24}{\lambda\,[\mu m]} \ldots\ldots\ldots\ldots\ldots\ldots\ldots\ldots\ldots\ldots\ldots\ldots\ldots\ldots (2.20)$$

Different wavelengths of light (in the visible region) appear as different colors to the human eye. In other words, photons with different energies have different colors. Photons with higher frequencies have shorter wavelengths and appear as blue or violet light, while photons with lower frequencies have longer wavelengths and appear as red or orange light. Photons having intermediate wavelengths appear as green and yellow light.

Example Problem (2.7): The light emitted from the red laser pointers (used in the classroom for presentations) typically has a wavelength of 650 nm. Calculate the energy of the photons [in eV] emitted from this red laser source.

Solution:

$$E_{ph} = \frac{hc}{\lambda} = \frac{6.626\times10^{-34}\ \text{Js} \times 3\times10^{8}\ \text{ms}^{-1}}{650\times10^{-9}\ \text{m}} = 3.06\times10^{19}\ \text{J} = \frac{3.06\times10^{19}}{1.6\times10^{19}}\text{eV} = \mathbf{1.91\ eV}$$

Alternatively, using Equation 2.20, we get: $E_{ph}\ [\text{in eV}] = \frac{1.24}{\lambda\ [\text{in } \mu m]} = \frac{1.24}{0.65} = \mathbf{1.91\ eV}$

2.5.4 Solar Cell: Structure and Operating Principle

Solar cells are the devices which perform conversion of light to electricity. In this chapter, we discuss the operating principle of first-generation Si-based solar cells. First, let's look at the basic structure of c-Si solar cell depicted in Figure 2.7, where different parts of the solar cell are marked. The cell comprises of a c-Si wafer which is typically about 200 μm thick. The Si on the top side of the wafer is made n-type and on the bottom side, it is of p-type. This is achieved by doping the silicon with donor (typically Phosphorous) and acceptor type (typically Boron) impurities, respectively. This forms a **p-n junction** and results in a **depletion region** near the interface of the p- and n-type Si.

A cross-sectional view of the solar cell is shown in Figure 2.8. Within the depletion region, an electric field, known as the **built-in electric field**, is created within the device which is marked as **E** in Figure 2.7 and 2.8. A bottom electrode (typically aluminum) is deposited on the rear surface, and front electrodes (typically silver or silver alloys) in the form of grid lines are deposited on the top surface, which facilitate electrical connection to the solar cell.

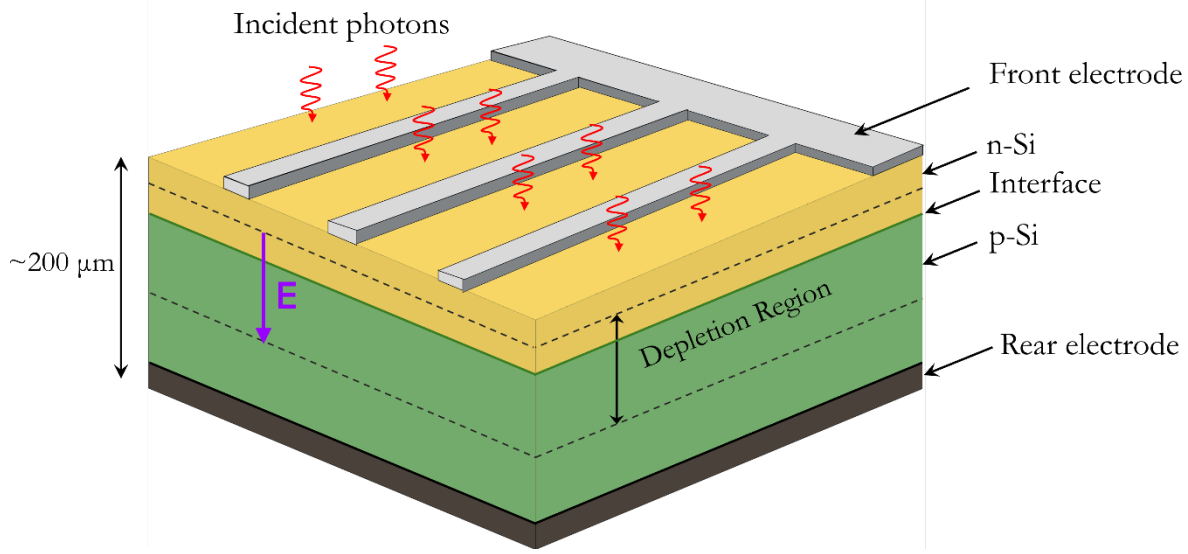

Figure. 2.7. 3D schematic of a c-Si solar cell showing the basic structure.

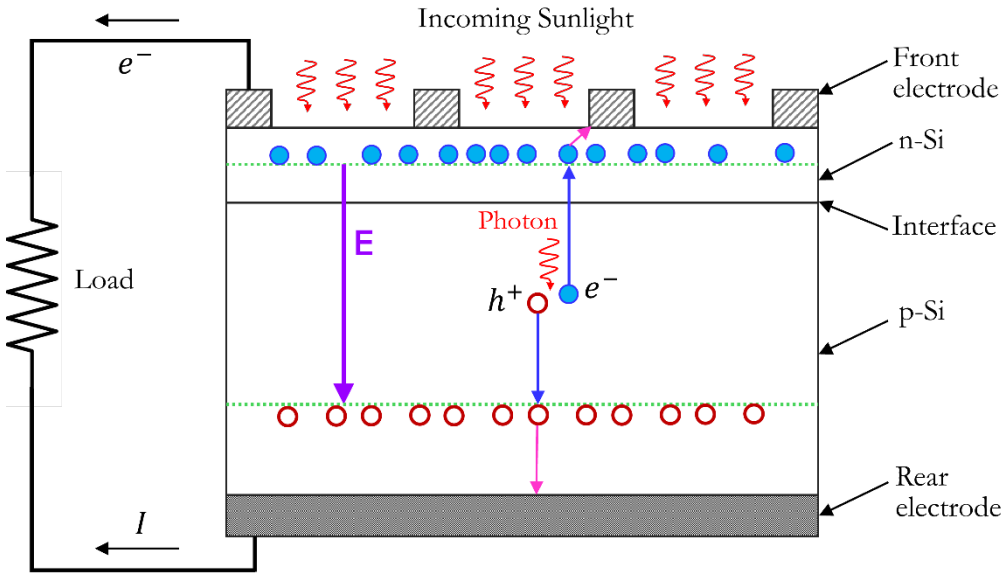

Figure. 2.8. Cross-sectional view of a c-Si cell structure and its operation.

The operation of a solar cell can be divided in three parts (a-c) as described below –

(a) **Light absorption and generation of free electron-hole pairs:** When light strikes a solar cell, some of the incident photons get absorbed by the semiconductor material (Silicon). If a photon has sufficient energy, then it knocks off a valence electron from a Silicon atom within the cell. As a result, a free electron and a hole are produced. This phenomenon is schematically presented in Figure 2.8, which shows the process of generating a negatively charged electron (e^-) and a positively charged hole (h^+) by photon absorption. The criterion for this electron-hole pair (EHP) generation is that the energy of the phonon must be at least the bandgap energy (or more) of the semiconductor material. Mathematically, this requirement it can be written as: $E_{ph} \geq E_g$; where, E_{ph} is the photon energy

and E_g is the semiconductor's bandgap energy. Different semiconductor materials have different bandgap energies. For Si, E_g = 1.1 eV.

(b) **Separation of EHPs:** As shown in Figure 2.8, the photo-generated electron and hole falls under the influence of the built-in electric field (**E**) that is present within the depletion region of the device. This electric field causes the electron to accelerate toward the top of the cell (opposite to the direction of the field), while the hole is accelerated toward the bottom (along the direction of the field). This process results in spatial separation of the free electron and the hole. The built-in electric field plays a critical role in separating them. The movement of the free electrons and holes under the influence of the built-in electric field is known as drift. The drifted electrons are then accumulated at the edge of the depletion region of the n-side, and the drifted holes are accumulated at the edge of the depletion region of the p-side, respectively.

(c) **Carrier collection and current generation:** In Figure 2.8, the edges of the depletion region are marked by dashed green lines. The accumulated free electrons on the n-side's depletion edge diffuse through the n-layer and finally reach the top metal electrodes. Similarly, the accumulated holes on the p-side's depletion edge diffuse through the p-layer to reach the rear metal electrode. When a load connected between the top and the bottom metal contacts, an electric current flows out of the cell, thus delivering electric power to the load. As electrons flow out of the top electrode, it serves as the negative terminal, and consequently the rear electrode serves as the positive terminal of the solar cell. bottom of the solar cell.

The second-generation thin film solar cells also operate in a similar fashion; however, instead of Si they use different other semiconductor materials.

2.5.5 Testing of Solar Cells and Modules

Terrestrial solar cells and solar modules are tested under a specific test environment, known as Standard Test Condition or **STC**. The STC serves as the standard reference for testing which allows easy comparison of the performance of different types of solar cells and modules. By adhering to the STC for measurements, manufacturers, researchers, and consumers can conveniently evaluate and compare the voltage, current, power, efficiency, and other PV performance metrics of different photovoltaic technologies. **STC** is defined by the following conditions under which the current-voltage characteristics of terrestrial solar cells must be measured:

- **Irradiance**: 1000 W/m^2
- **Cell Temperature**: 25°C
- **Air Mass**: 1.5

In the testing facility, an artificial light source, such as a calibrated Solar Simulator is used to produce AM1.5 spectrum with an output optical power density of 1000 W/m^2 (also known as **1-sun**). Controlled environmental chambers or testbeds with temperature sensors are used to maintain the temperature at 25°C. All commercially available solar cells and modules for outdoor terrestrial applications are tested under STC and their specifications are given at STC. This not only ensures quality assurance, STC also plays a key role in the design of photovoltaic systems. Specifications obtained under STC are used by engineers to design system components, simulate and predict real-world performance, and estimate energy yields.

2.5.6 Electrical Characteristics and Photovoltaic Parameters

Current-voltage (I-V) and Power-Voltage (P-V) curves are the most important electrical characteristics of a solar cell (or a module or a solar array). By analyzing these curves, one can estimate various important photovoltaic performance parameters. A typical Current-Voltage curve and the corresponding Power-Voltage curve of a solar cell are presented in Figure 2.9. Important electrical parameters of a solar cell and the method to find them are explained below.

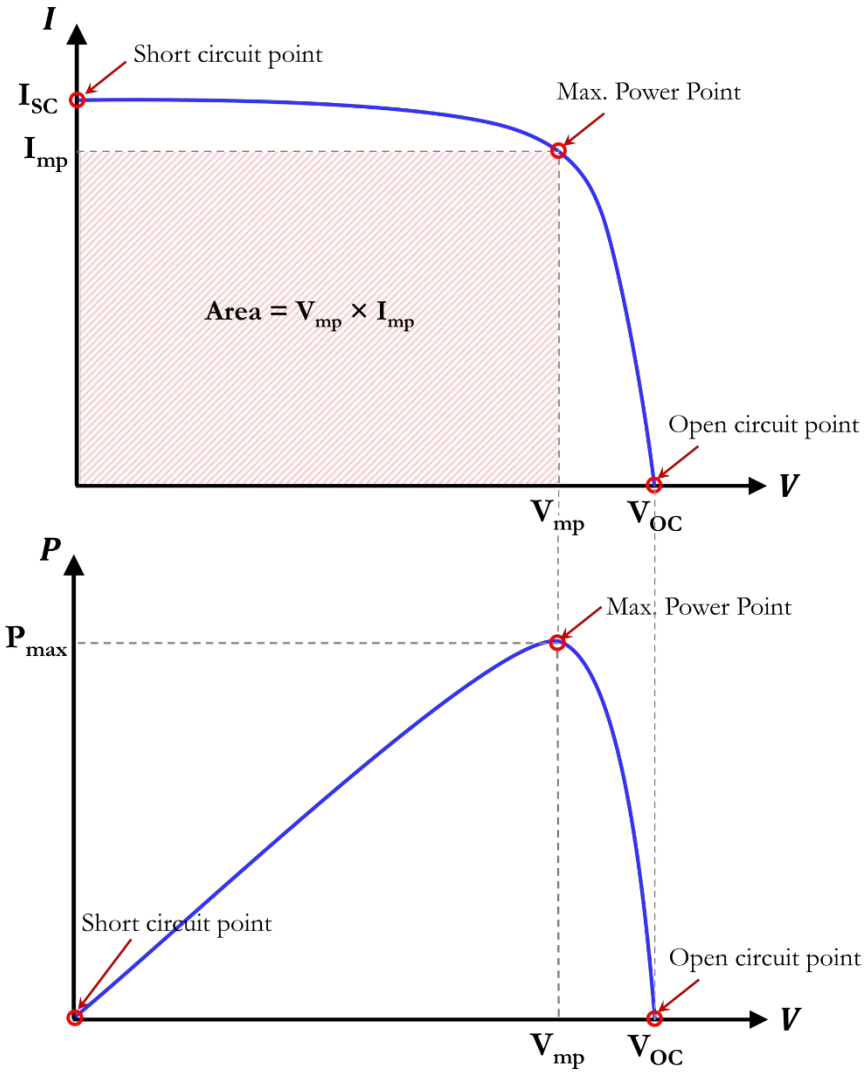

Figure. 2.9. I-V and P-V Characteristics of a Solar Cell.

Open Circuit Voltage (V_{OC}): The open circuit voltage (V_{OC}) is the maximum voltage that a solar cell can produce. The maximum voltage value at the solar cell terminals is measured when no load is connected to it, i.e. $R_L = \infty$. The V_{OC} can be measured by directly connecting a voltmeter (which has high input impedance) across the solar cell terminals. For high quality monocrystalline Si solar cells, the V_{OC} value typically ranges around 0.6V under 1-sun illumination (STC). The open-circuit point on the I-V and P-V curves are marked in Figure 2.9. V_{OC} is the voltage value where the I-V curve meets the x-axis.

Short Circuit Current (I_{SC}): The short circuit current (I_{SC}) is the maximum current that a solar cell can produce at a given irradiance. The cell outputs the maximum current when its terminals are shorted, i.e. $R_L = 0$. I_{SC} can be measured by directly connecting an ammeter (which has very low series resistance) at the solar cell's output terminals without any additional circuitry. The short-circuit point on the I-V and P-V curves are marked in Figure 2.9. I_{SC} is the current value where the I-V curve meets the y-axis.

The short circuit current (I_{SC}) is directly proportional to the intensity of the incident light. Therefore, if the irradiance level is doubled, the I_{SC} value will also double; if the irradiance is halved, the I_{SC} value will also decrease by one-half, provided that all other ambient conditions remain unchanged.

Maximum Power (P_{max}): The maximum power point (MPP) refers to a specific point on the I-V curve of a solar cell where the product of current and voltage results in the maximum value. This value represents the maximum power (P_{max}) that the cell can deliver. Graphically, this point represents a peak on the Power-Voltage curve. Also, it can be represented by the shaded rectangle area shown on the Current-Voltage curve of Figure 2.9. Mathematically, it can be represented by Equation 2.21.

$$P_{max} = V_m \times I_m \quad \ldots\ldots\ldots\ldots\ldots\ldots\ldots\ldots\ldots\ldots\ldots\ldots\ldots\ldots\ldots\ldots (2.21)$$

Optimum Voltage and Current (V_{mp}, Imp): The voltage corresponding to the maximum power point (MPP) is known as the optimum voltage or the voltage at maximum power (V_{mp}), while the current corresponding to the MPP is called the optimum current or the current at maximum power (I_{mp}). A solar cell or module must be operated at V_{mp} to extract the maximum power out of it.

Fill Factor (FF): The fill factor (FF) is the ratio of the maximum power that a solar cell or module can produce to the product of the open circuit voltage and the short circuit current. It represents how much power the solar cell can deliver in comparison to the theoretical maximum. It can be calculated using Equation 2.22.

$$FF = \frac{V_m \times I_m}{V_{OC} \times I_{SC}} = \frac{P_{max}}{V_{OC} \times I_{SC}} \quad \ldots\ldots\ldots\ldots\ldots\ldots\ldots\ldots\ldots\ldots\ldots\ldots\ldots\ldots\ldots\ldots (2.22)$$

For high quality Si solar cells, the FF values is typically between 0.8 – 0.9.

Power Conversion Efficiency (η): The efficiency (η) of a solar cell (or module) is the ratio of the output power (P_{max}) that it can produce to the input power (power of the incident sunlight). It can be calculated using Equation 2.23.

$$\eta = \frac{P_{out}}{P_{in}} = \frac{P_{max}}{P_{in}} \quad \ldots\ldots\ldots\ldots\ldots\ldots\ldots\ldots\ldots\ldots\ldots\ldots\ldots\ldots\ldots\ldots (2.23)$$

$$\text{Where,} \quad P_{in} = \text{Irradiance} \times \text{Area} \quad \ldots\ldots\ldots\ldots\ldots\ldots\ldots\ldots\ldots\ldots\ldots\ldots\ldots\ldots\ldots\ldots (2.24)$$

Example Problem (2.6): I-V and P-V characteristics of a polycrystalline Si solar cell tested at STC is given below. The cell has a dimension of 6.0 in × 4.0 in. By analyzing these curves, find the following parameters:

(a) V_{OC}, (b) I_{SC}, (c) J_{SC}, (d) P_{max}, (e) V_{mp}, (f) I_{mp}, (g) FF, and (h) power conversion efficiency, η.

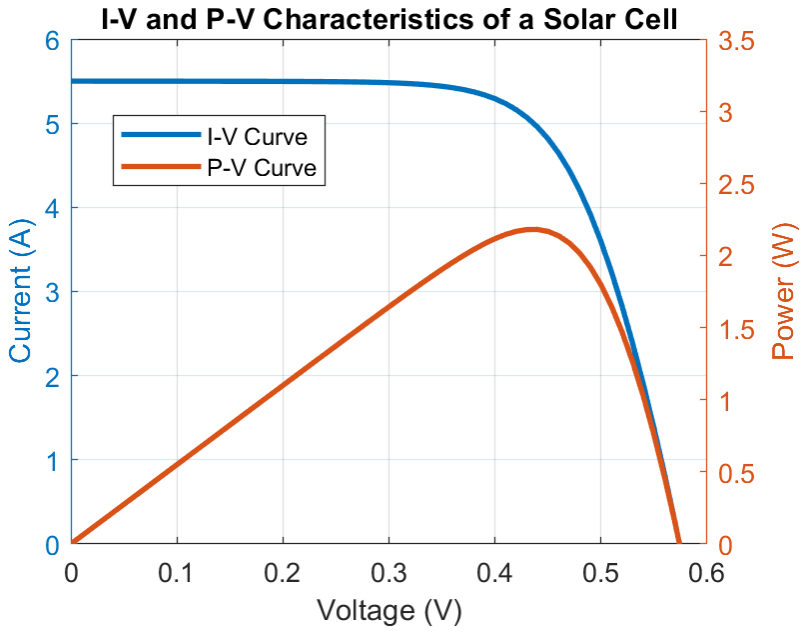

Solution:

First the open circuit, short circuit, and maximum power points are identified. These points are circled on the graph with different colors as shown below. Calculations and the estimated values of the requested parameters are given below.

Area of the solar cell = 6 in × 4 in = 24 in^2 = 24 × 6.4516 cm^2 = 154.84 cm^2 ≈ 0.0155 m^2.

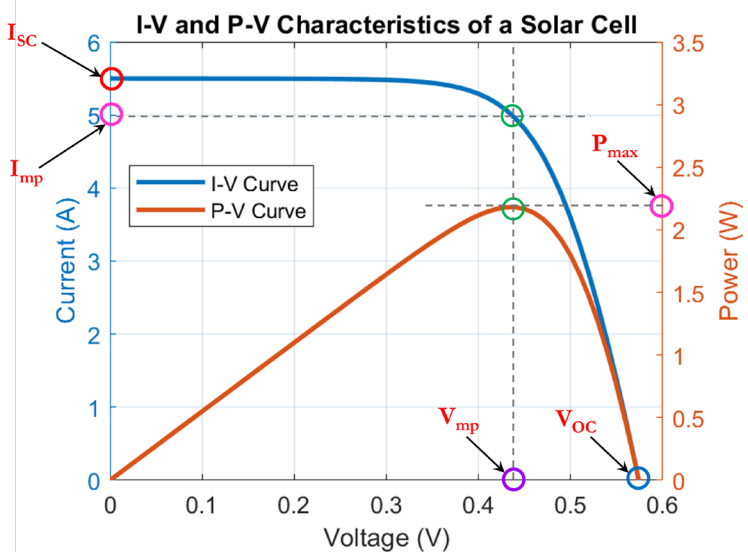

(a) $V_{OC} = \mathbf{0.58\ V}$

(b) $I_{SC} = \mathbf{5.5\ A}$

(c) $J_{SC} = \dfrac{I_{SC}}{A} = \dfrac{5.5\text{ A}}{154.84}$

$= \mathbf{35.52\ mA/cm^2}$

(d) $P_{max} = \mathbf{2.2\ W}$

(e) $V_{mp} = \mathbf{0.44\ V}$

(f) $I_{mp} = \mathbf{5\ A}$

(g) $FF = \dfrac{P_{max}}{V_{OC} \times I_{SC}} = \dfrac{2.2}{0.58 \times 5.5}$

$= \mathbf{68.97\%}$

(h) $\eta = \dfrac{P_{max}}{P_{in}} = \dfrac{P_{max}}{\text{Irradiance} \times \text{Area}} = \dfrac{2.2\text{ W}}{1000\text{ Wm}^{-2} \times 0.0155\text{ m}^2} = \mathbf{14.2\%}$

Example Problem (2.7): A snapshot of a solar cell's datasheet containing important electrical parameters at STC are given below.

ELECTRICAL DATA (AT STC)

		ND-R250A5	ND-R245A5	
Maximum power	P_{max}	250	245	W_p
Open-circuit voltage	V_{oc}	37.6	37.3	V
Short-circuit current	I_{sc}	8.68	8.62	A
Voltage at point of maximum power	V_{mpp}	30.9	30.7	V
Current at point of maximum power	I_{mpp}	8.10	7.99	A
Module efficiency	η_m	15.2	14.9	%

STC = Standard Test Conditions: irradiance 1,000 W/m², AM 1.5, cell temperature 25 °C.

(a) Sketch the approximate I-V and P-V characteristic curves for the solar module ND-R250A5 in two separate graphs.

(b) Circle and label the open-circuit, short-circuit, and maximum power points on the I-V and P-V curves. Write the values corresponding to these points on both curves.

Solution:

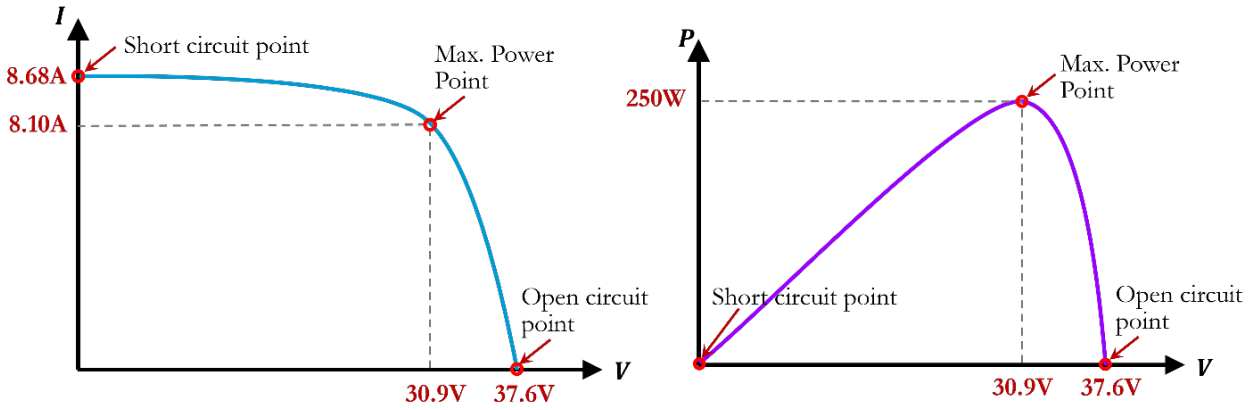

2.5.7 PV Modules and Arrays

A single solar cell produces about 0.6V which is not sufficient for practical applications. Hence, solar cells are packed in a module form in which several cells are connected together in series. Modules with 36 cells, 60 cells, and 72 cells are commonly available in the market. To complete the installation of a PV system, usually one module is not sufficient to meet the necessary power demand, and therefore multiple modules are placed side by side to form a solar PV array. Modules in an array can be connected in series and parallel combinations depending on the inverter's input voltage and current specifications. Figure 2.10 presents the concepts of solar module and array.

The PV module protects the solar cells from the environment, such as moisture, dust, snow, rain, hails, and other types of mechanical impacts. Figure 2.11 illustrates different components of a typical Si solar PV module. The module consists of a front glass cover (tempered), encapsulation layers, a backsheet, a metal frame, and a junction box.

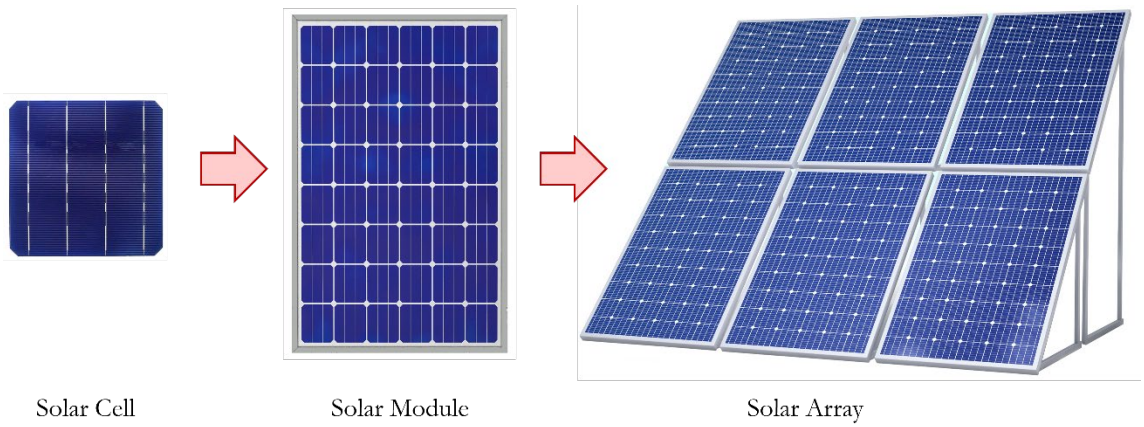

Figure. 2.10. Illustration of a solar cell, a solar module, and a solar array (image source: Freepik).

To assemble solar cells in a module, the cells are first soldered using tabbing wires to interconnect them in series configuration which forms a 'string'. The strings of cells are then sandwiched between two EVA (Ethylene Vinyl Acetate) sheets, which is then heated to permanently bond the layers together, thus laminating the cells. PVB (Polyvinyl Butyral) can also be used as an encapsulant. A backsheet layer is then added which provides mechanical protection on the back side of the module. The backsheet also provides electrical insulation which prevents leakage currents and ensures electrical safety of the modules. High-quality backsheets have high thermal stability and maintain excellent dielectric properties over the module's lifespan. Backsheets are typically made of Polyvinyl Fluoride (also known as Tedlar), which is a fluoropolymer material offering excellent durability. Polyester films can also be used as a more affordable alternative; however, its long-term durability and performance is inferior compared to Tedlar. A metal frame, typically made of aluminum alloys or anodized aluminum is used to provide structural support to the module. Stainless steel can also be used if higher mechanical strength is required, however it is more expensive. Aluminum alloys are common frame choices for most applications due to their strength, light weight, and corrosion resistance properties. The metal frame edges with the top glass cover and bottom backsheet are sealed using industrial sealants and gaskets. Finally, the module is fitted with a junction box attached on the backsheet at the rear, which allows electrical connections to the external world.

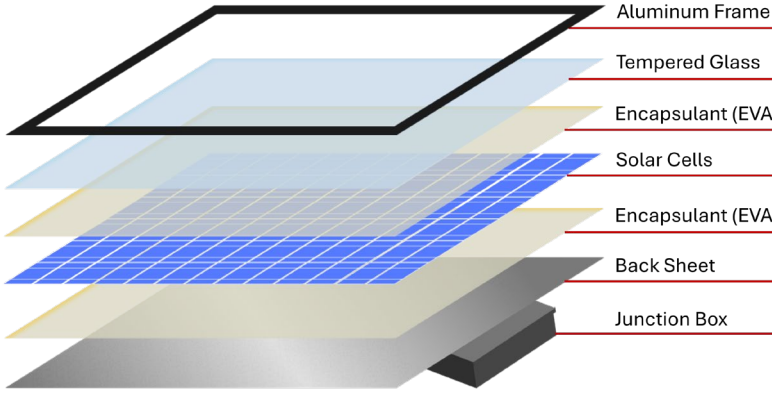

Figure. 2.11. Components of a Solar Module.

2.5.8 Operation and Components of PV System

Grid-tied and off-grid systems: PV arrays can be operated as grid-tied or off-grid system. For a **grid-tied** array the output of the PV system is connected to the utility grid. When the PV system generates more power than needed by the household, it feeds the excess power into the grid, and draws power from the grid at night or other times when the PV system is not generating adequate power to run the electrical loads.

A local storage system, such as batteries are not necessary for grid-tied system since the grid serves as the backup. Usually, utility companies offer net metering where the homeowner received credit for the amount of electrical energy delivered to the grid and is billed for the net energy usage. The exact mechanism for such a billing process greatly varies between utility companies. On the other hand, an **off-grid (or stand-alone)** system is not connected to the utility grid. Such systems are typically deployed in remote locations where electric grid is not available nearby. Off-grid systems must include a battery storage unit to ensure availability of power at night or during overcast weather conditions.

Components of a PV System: A typical solar PV system consists of the following components:

(a) Solar Modules: PV modules (or Panels) are the main component of a PV system, which contain the photovoltaic cells that generate direct current (DC) electricity. The most common type of PV modules contain crystalline or polycrystalline Si solar cells.

(b) Mounting System: The mounting system is required to secure the solar modules to a building rooftop, the ground, or other structures. Broadly, there are two main types of mounting systems – (i) fixed mounts, and (ii) tracking mounts. Fixed mounts fasten the modules in a stationary position, usually at an optimum tilt angle and direction chosen based on the location. They are easy to install and are cost-effective. Tracking mounts on the other hand allows adjustment of the angle of the modules to better match with the sun's path throughout the year, which increases the amount of energy production. However, these are more complex mounting systems requiring additional components and comes at a higher cost.

(c) Inverter: All of our household electrical appliances need alternating current (AC) electricity, whereas solar modules generate DC electricity. Therefore, DC to AC conversion is required to utilize the electrical energy produced by a PV array. An inverter is a power electronic device that converts the DC electricity generated by the solar modules into alternating current (AC) electricity. There are different types of inverters, such as string inverters, microinverters etc. Depending on the system design and budget, an appropriate type of inverter is chosen by the installer.

(d) Battery Storage: A local energy storage system, such as battery storage may be required depending on the system design. For grid-tied system, batteries are optional, whereas for stand-alone systems batteries are required for reliable power.

(e) Charge Controller or BMS: PV systems containing a battery storage unit must include a charge controller or a battery management system (BMS) which is an electronic device that manages the charging and discharging of the battery bank to prevent overcharging, over discharging, and ensures safe operation of the battery and extends the battery life.

(f) Electrical Wiring and Safety Components: This includes electric cables, junction boxes, fuses, and circuit breakers to ensure proper electrical connections and safe operation of a PV system.

2.5.9 Equivalent Circuit Model

Mathematical models of solar cells or PV modules are very useful to simulate their behavior and performance under different ambient conditions. In addition, these models allow better understanding of their electrical characteristics and help us to optimize the performance of a solar PV system. The most widely used model is the single diode equivalent circuit model shown in Figure 2.10. This model represents the physical processes within a solar cell using an electrical circuit that can be easily analyzed and simulated using a circuit simulator or a computer program.

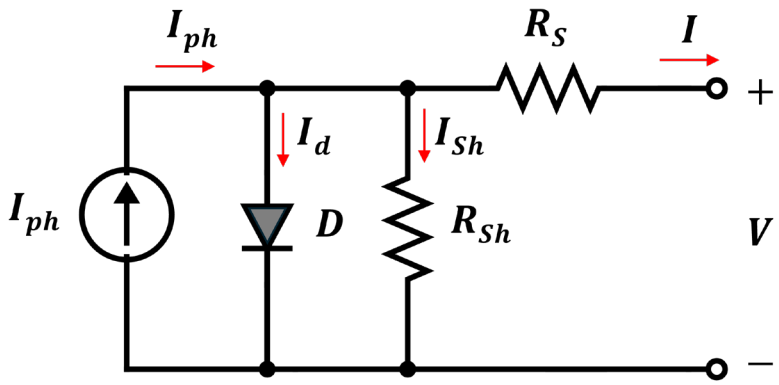

Figure. 2.10. One-diode equivalent circuit of a solar cell.

Different components of this model represent different physical processes in a solar cell. Components of the single diode model and their significance are detailed below.

DC Current Source (I_{ph}): This component represents the photocurrent generated due to the absorption of photons in the solar cell. Magnitude of I_{ph} is directly proportional to the intensity of the incident light.

Diode (D): The diode represents the existence of the p-n junction within the solar cell structure. A component of the photogenerated current, I_d flows through it. Under dark condition no I_{ph} is generated, and a solar cell's electrical characteristic looks like that of a p-n junction diode.

Series Resistance (R_S): This component accounts for the ohmic losses in the cell, which includes the resistance of the p- and n-type semiconductor layers and the metal contacts.

Shunt Resistance (R_{Sh}): This component accounts for the leakage current paths within the solar cell. Manufacturing defects is a dominant origin of shunt resistance. R_{Sh} provides an alternate (shunt) current path for the photo-generated current to flow within the solar cell, representing that some of the photogenerated electrons and holes recombine within the cell, leading to reduced power output.

For a high-efficiency solar cell, R_S should be very small, and R_{Sh} should be very high. Low shunt resistance reduces the open circuit voltage, whereas high series resistance reduces the short circuit current.

Applying simple circuit analysis techniques on the model of Figure 2.10, we can derive a relationship between the solar cells' output current (I) and the output voltage (V), which is given in Equation 2.24.

$$I = I_{ph} - I_s\left[\exp\left\{\frac{q(V+IR_s)}{nkT}\right\} - 1\right] - \left(\frac{V+IR_s}{R_{sh}}\right) \ldots\ldots\ldots\ldots\ldots\ldots\ldots\ldots\ldots (2.24)$$

Where, I_{ph} is the photocurrent (or light-generated current), q is the charge of an electron (1.602×10^{-19} C), I_s is the reverse saturation current (also known as the dark current) of the diode, n is the ideality factor of the diode, k is the Boltzmann's constant (1.380649×10^{-23} J/K), T is the temperature in Kelvin, V is the voltage at the solar cell's output terminals, and I is the output current of the solar cell.

2.5.10 Modeling and Simulation of Solar Cell and PV Module

Accurate modeling and simulation of solar cells and modules are important to study their performance under different operational conditions (such as different light intensities and temperatures), design a PV

system, and optimize performance and power output. This section details the basics of modeling and simulation of solar cells and PV modules using MATLAB and Simulink.

Simulation using MATLAB: MATLAB is a popular computational software used by engineers. In this section, we discuss how to implement the governing mathematical equations of a solar cell in MATLAB. These steps can also be implemented using any other computer program to achieve similar results.

The goal for the simulation is to produce the current-voltage and power-voltage characteristics of a solar cell (or module). To achieve this, the main task is to implement the governing mathematical equations. First, a MATLAB script file is created by clicking "New Script" under the 'HOME' menu on top of the MATLAB window.

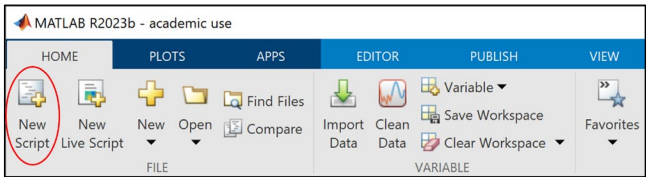

The current-voltage relationship of a solar cell is given by equation 2.24 which we need to implement (write) within the MATLAB script file. Equation 2.24 requires dark current (I_S) which is usually not available from a manufacturer's datasheet. To estimate the approximate value of I_S, first we simplify the equivalent circuit of Figure 2.10 by ignoring the parasitic resistances as shown in Figure 2.11(a), which contains only the DC current source and the diode. By applying circuit analysis techniques, we can obtain the relationship between the output voltage and current of the cell for this simplified model, which is given by Equation 2.25 below.

$$I = I_{ph} - I_s\left[\exp\left(\frac{qV}{nkT}\right) - 1\right] \ldots\ldots\ldots\ldots\ldots\ldots\ldots\ldots\ldots\ldots\ldots\ldots (2.25)$$

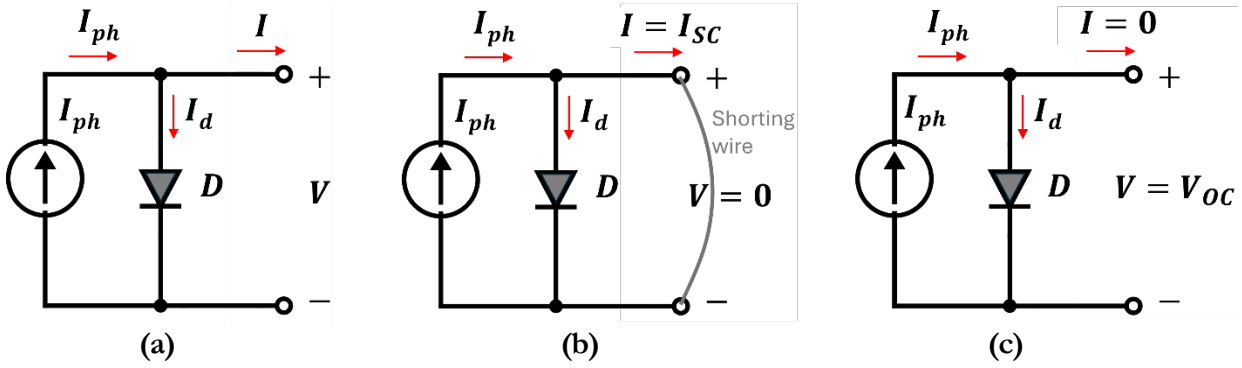

Figure. 2.11. (a) The simplified one diode circuit model, (b) under open circuit condition, and (c) under short-circuit condition.

Now we can find I_S by analyzing this simplified model under short circuit and open circuit conditions. As shown in Figure 2.11(b), under short circuit condition, the output voltage, V becomes zero and the output current I becomes equal to I_{SC}. By applying these boundary conditions to Equation 2.24, we get:

$$I_{SC} = I_{ph} - I_s\left[\exp\left(\frac{q \times 0}{nkT}\right) - 1\right] \quad \Rightarrow \quad I_{ph} = I_{SC} \ldots\ldots\ldots\ldots\ldots\ldots\ldots (2.26)$$

As shown in Figure 2.11(b), under open circuit condition, the output current, I becomes zero and the output voltage V becomes equal to V_{OC}. By applying these boundary conditions to Equation 2.25, we get:

$$0 = I_{ph} - I_s\left[\exp\left(\frac{qV_{OC}}{nkT}\right) - 1\right] \qquad \Rightarrow \; I_{ph} = I_s\left[\exp\left(\frac{qV_{OC}}{nkT}\right) - 1\right]$$

Now replacing I_{ph} with I_{SC} (as found in Equation 2.26) in the above equation, we get:

$$\Rightarrow I_{SC} = I_s\left[\exp\left(\frac{qV_{OC}}{nkT}\right) - 1\right] \qquad \Rightarrow \; I_s = \frac{I_{SC}}{\exp\left(\frac{qV_{OC}}{nkT}\right) - 1} \ldots\ldots\ldots\ldots\ldots\ldots\ldots\ldots\ldots\ldots (2.27)$$

Equation 2.27 allows us to estimate the value of the reverse saturation current (or dark current) of the solar cell from the known V_{OC} and I_{SC} values from a manufacturer's datasheet. By implementing Equations (2.27) and 2.24, we can simulate a solar cell's electrical characteristics. An example simulation exercise with solution is provided below.

Example Problem (2.8): Write a MATLAB script to model and simulate a Si solar cell's I-V and P-V characteristics under STC given the following parameters:

Short circuit current = 2.84 A; open circuit voltage = 0.631 V; series resistance = 0.005 Ω; shunt resistance = 1000 Ω, ideality factor = 1.5.

Solution:

MATLAB code this simulation exercise is provided within the Appendix section which includes detailed annotations. The code is divided in three major segments – (i) defining the values of the required constants, (ii) calculating I_S and then calculating the output current by sweeping (incrementing) the voltage using a 'for loop', and (iii) plotting the simulated I-V and P-V curves using the saved current, voltage and power arrays calculated in step (ii). After the script file is saved with the code, clock on the 'Run' button under the 'EDITOR' menu to run the simulation which shall produce the output curves after successful run.

The resulting current-voltage and power-voltage curves of the solar cell is shown below.

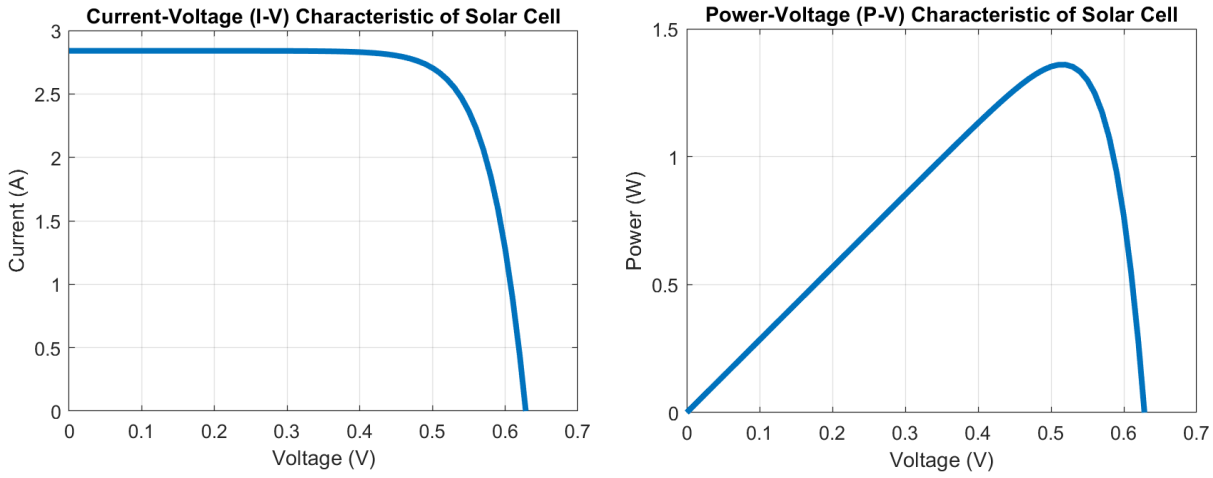

2.5.11 Advantages and Disadvantages of PV Systems

Solar photovoltaic system offer various advantages compared to using fossil fuels and some other renewable energy technologies. It also has some limitations or disadvantages as listed below.

Advantages of Solar PV:

- Renewable Energy Source: PV systems harness the energy from the sunlight, which is virtually limitless and a renewable resource.
- Reduction of Greenhouse Gas Emissions: Unlike fossil fuels, during the process of solar electricity generation, it does not emit CO_2 or other greenhouse gases. Therefore, widespread deployment of solar PV can help reduce carbon footprint and mitigate the associated adverse effects CO_2 emission on the climate.
- Environmentally Friendly: Solar modules produce clean energy without releasing any toxic gases, pollutants or harmful particulate matter (such as PM2.5) into the atmosphere. Thus, solar PV-based electricity generation can help to improve the air quality.
- Low Operating Costs: There are no moving parts in a solar PV system. Only routine inspection and cleaning are sufficient to keep them operational. As a result, PV systems require very low maintenance.
- Energy Independence: Solar PV systems enhance energy security by reducing energy imports from outside of the country.
- Reduction of Utility Bills: By generating their own electricity at home, homeowners can offset the charges for the amount of electricity fed into the grid and therefore can reduce (or even eliminate) monthly electricity bills. Having solar PV can result in substantial savings in the long-term.
- New Job Creation: The solar industry has high potential to create new jobs related to the research & development, manufacturing, design, installation, and maintenance of PV systems. The solar PV sector offers diverse employment opportunities and economic growth.

Disadvantages of PV Systems:

- High Initial Costs: The upfront investment for a PV system installation can be substantial. The high initial cost is a challenge in many places and remains a barrier for the adoption of solar power. However, various incentives and financing options can help to mitigate this issue.
- Intermittent and Unpredictable: Solar power generation can be inconsistent due to local weather conditions. Clouds cause fluctuations in the output power. Also, snowfall and rainy seasons can impact the power generation capacity of a solar PV system unpredictably.
- Space Requirements: To generate the necessary amount of power, PV systems require adequate space for the solar array installation. For residential and commercial applications, this requires a large unobstructed roof area, which is not always available.
- Energy Storage Requirements: The sun is not available at night. Also, its output greatly varies during the day depending on the local climate. Therefore, storing energy for use during non-sunny periods require storage systems such as batteries, which can be expensive resulting in an increase of the overall operational cost.
- Environmental Impact of Manufacturing: Although solar PV systems are environmentally friendly as they have zero emission during operation, the production of solar cells and module components involve mining. Also, the cell and module manufacturing processes often involve toxic chemicals. Another aspect is safe recycling of discarded solar panels after their lifetime which requires careful consideration to avoid any negative impacts to the environment.

2.6 Solar Thermal Energy Harvesting

Solar thermal energy is a renewable energy source that harnesses the heat from the sun to produce electricity or heat for residential, commercial, and industrial applications. The technology used in solar thermal energy has been around for decades, but recent advancements in materials and manufacturing techniques have made it more efficient, practical, and cost-effective.

The solar thermal energy harvesting systems captures the heat energy from the sunlight and converts it to thermal energy, which can either be used directly in various applications where thermal energy is required or can be further converted to electrical energy. The common goal for all solar thermal systems is to capture the heat to warm fluids or air. There are two main types of solar thermal energy systems – (a) solar thermal collectors, and (b) concentrating solar thermal power (CSTP). The most common types of solar thermal collectors are **Flat Plate Collectors** and **Evacuated Tube Collectors**. More details on the Flat Plate Collector and a water heating system based on this device is described in the following section.

2.6.1 Flat Plate Collector

Flat plate collectors are a type of simple solar thermal energy harvesting device used to convert sunlight into heat energy. They consist of a flat, insulated box with a dark absorber plate inside and a transparent cover on top, typically made of glass. A cross-sectional schematic of a typical Flat Plate Collector depicted in Figure 2.12. The absorber plate is painted using a special coating designed to absorb broadband sunlight and heat up, and the heat energy is then transferred to a fluid that circulates through tubes attached to the collector plate. The fluid is usually water or a mixture of water and an anti-freeze solution. The glass cover allows sunlight to pass through while reducing emission of captured heat from inside. The box is properly insulated around the edges and the back side to minimize heat loss from the sides and bottom of the collector. The fluid circulating through the collector absorbs the heat and it is circulated to a heat exchanger or a storage tank. A complete water heating system based on flat plate collector is shown in Figure 2.13. The hot water can be used for various applications, including domestic hot water, space heating, or industrial processes.

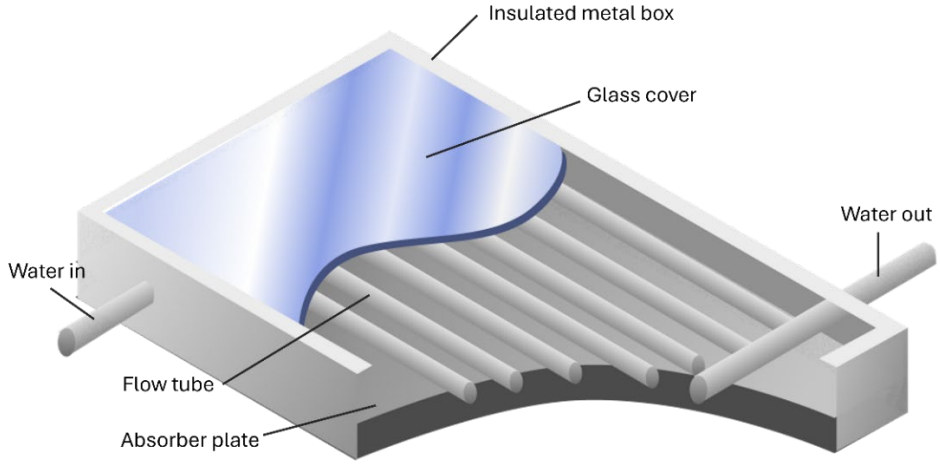

Figure. 2.12. Schematic of a Flat Plate Collector.

The performance and efficiency of flat plate collectors is measured based on their thermal efficiency, which is the ratio of the heat output of the collector to the incident solar radiation. The thermal efficiency of flat plate collectors greatly varies and can range between 30-80%, depending on the design and operating conditions. Plates made of copper can achieve higher fluid temperature and higher efficiency. Aluminum

(or certain plastics) can also be used as a more cost-effective material; however, they exhibit lower efficiencies. To mitigate heat loss through the front glass cover, a double panel glass arrangement can be used which results in improved efficiency.

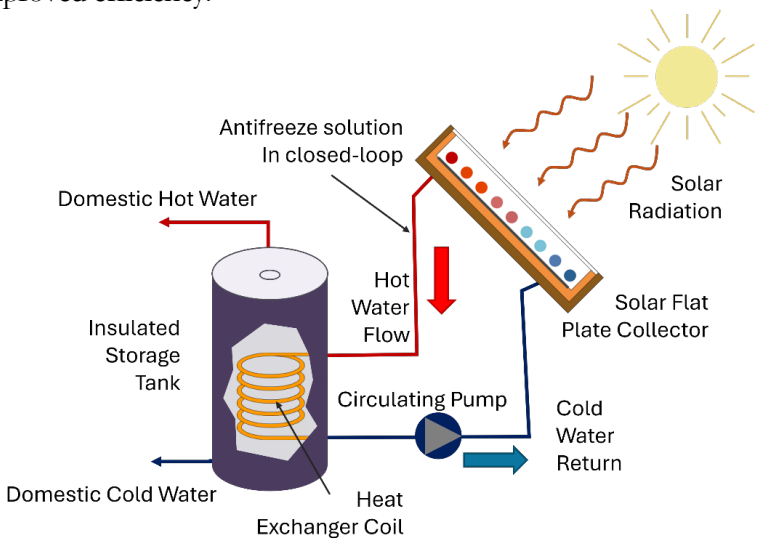

Figure. 2.13. Flat plate collector-based solar water heating system.

Advantages and Limitations: A key advantage of flat plate collectors is their simplicity and reliability. They have no moving parts and require very minimal maintenance. Flat plate collectors can be used in a wide range of applications, from hot water to heating swimming pools and industrial processes.

Flat plate collectors also have some disadvantages. One of the main limitations is their lower efficiency compared to other technologies, such as concentrating solar thermal power (CSTP) systems. Also, flat plate collectors require a large area to achieve high output, which can be challenging in urban areas.

2.6.2 Concentrating Solar Thermal Power (CSTP)

Concentrating Solar Thermal Power (CSTP) is a promising renewable energy technology that harnesses the power of the sun to produce electricity. CSTP systems use optical reflectors (mirrors) or lenses to concentrate sunlight into a receiver, which heats up a fluid to high temperature that can be used to produce steam and drive a steam turbine to generate electricity.

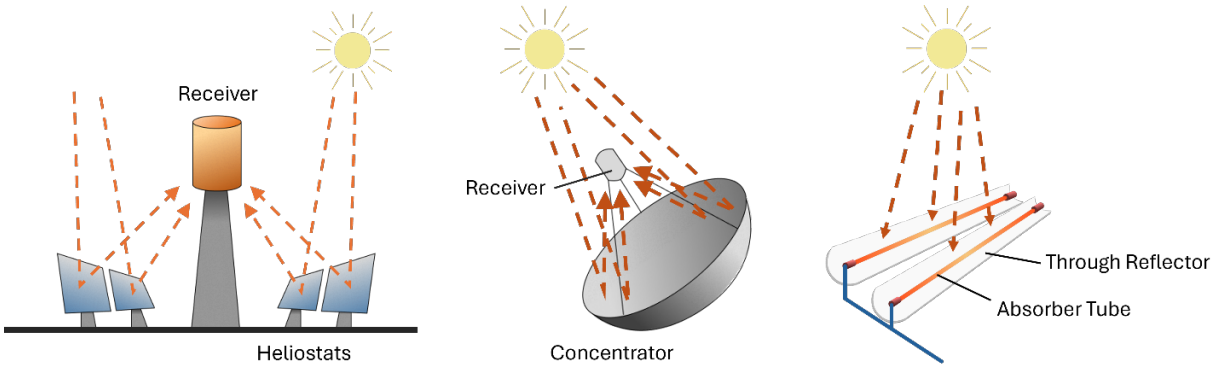

Figure. 2.14. Different CSTP technologies.

There are various types of CSTP systems. Common CSTP configurations include Power Tower, Dish Stirling Systems, and Parabolic Trough as depicted in Figure 2.14.

Power Tower: These systems use a large number of adjustable tilt mirrors, known as heliostats, which are used to reflect and focus sunlight on a central receiver located on top of a tower. The heliostats are distributed on the field all around the tower. The angle of each heliostat is continuously and precisely adjusted throughout the day to ensure reflection of light on to the receiver. The receiver heats up a fluid that is used to produce steam and to generate electricity.

Dish Stirling Systems: These systems use a parabolic dish to concentrate sunlight onto a receiver that powers a Stirling engine to produce electricity. Sterling engine is a type of heat engine that operates on the principle of compression and expansion of air or other gases. The solar-powered Sterling engine is similar to that of a conventional Sterling engine, where the solar collector (the concentrating dish) replaces the conventional heat source. The dish focuses the sunlight onto a small receiver where a fluid (typically air) is heated to a high temperature. As a result, the heated air expands generating mechanical power that drives pistons, which are coupled to a generator to produce electricity. The cooled working fluid then flows back to the heat exchanger, where gets heated up again, and the cycle repeats.

Parabolic Trough: These systems use a set of parabolic mirrors aligned in linear fashion to focus sunlight onto a receiver tube running along the focal line of the trough. The tube is filled with a heat-transfer fluid. The heated fluid is then used to produce steam that drives a steam turbine to generate electricity. Parabolic trough technology was first developed in the 1970s and is currently the most widely deployed CSTP technology, with many commercial utility scale solar thermal power plants operating around the world. Schematic of a Parabolic Trough is shown in Figure 2.15 which illustrates different components of the system.

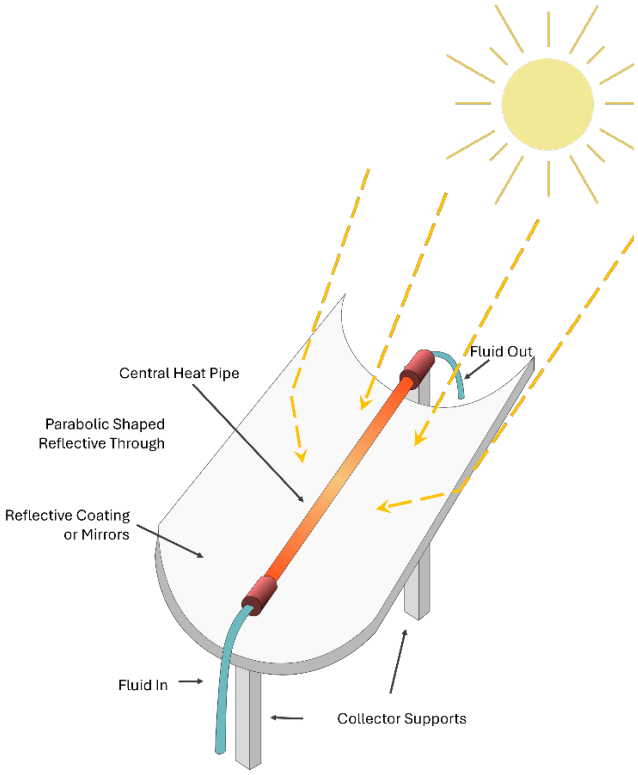

Figure. 2.15. Schematic of a Parabolic Trough.

The receiver tube is usually made of metal and is coated with a selective absorber material that is designed to absorb broadband sunlight and convert it into heat. The heat-transfer fluid is usually a synthetic oil, molten salt, or water. The fluid is pumped through the tube, which absorbs the heat and carries it away to a heat exchanger to produce steam. Parabolic trough systems can achieve efficiencies of up to 30%.

Advantages and Disadvantages of CSTP:
One of the main advantages of CSTP technology is its ability to produce electricity which is more stable and immune to sudden passage of clouds. Integrated thermal energy storage systems can drastically extend its operation beyond daytime. These advantages make CSTP very attractive for large utility-scale electric power generation. However, CSTP also has some limitations. One of the main drawbacks is its higher cost compared to other renewables, such as solar PV and wind power. CSTP systems are more complex and the

maintenance cost is higher than other competing technologies, such as solar PV. Also, these systems can't be integrated onto existing structures, such as buildings, and therefore require a large amount of dedicated land for installation.

2.6.3 Passive Solar Heating

Passive solar heating is a mechanism by which we can harness the energy from sunlight to maintain indoor temperatures to a comfortable level, thus reducing the need for supplemental heating and contributing to reduced energy consumption and environmental impacts. Engineering of passive solar heating is a viable strategy for sustainable building design. Passive solar heating of buildings are designed with large south-facing windows (in the northern hemisphere) to maximize solar gain. **Trombe Wall** is a matured passive solar heating technology designed to enhance thermal efficiency of buildings. Named after the French engineer Félix Trombe, this method utilizes a thermal mass to capture and store solar thermal energy. The Trombe Wall consists of a south-facing, insulated concrete (or brick) wall with an air gap between the wall and a transparent glazing material (typically glass). Similar to a flat plate collector, solar radiation enters through the glass and heats up the wall. The glass helps to minimize heat loss from the wall. The heat is then controllably released inward (often by controlling vents), into the building interior, contributing to temperature regulation. Warm air rises and circulates through the building and distributes the heat.

2.7 Appendix

MATLAB code for solar cell simulation:

```
%% Solar Cell Modeling and Simulation. Written by Dr. Sandip Das
clc; clear all; close all;

%% Define Constants
q = 1.602*10^(-19);
k = 1.38*10^(-23);
T = 25 + 273;
n = 1.5;
Eg = 1.1;
Isc = 2.84;
Voc = 0.631;
Rs = 0.005;
Rsh = 1000;

%% Sweep Voltage and measure Current
i =1;
I = 1;
for V = 0: 0.01:0.7
    Is = Isc/((exp((q*Voc)/(n*k*T)))-1); % Equation 2.25
    I = Isc - Is*((exp((q*(V+I*Rs))/(n*k*T)))-1)-((V+I*Rs)/Rsh); % Equation 2.24
    Vo(i) = V;
    Io(i) = I;
    Po(i) = V*I;
    i=i+1;
end
```

```
%% Plot simulated I-V and P-V Characteristics
figure(1);
plot(Vo,Io, 'Linewidth', 3); grid on;
axis([0 0.7 0 3]);
xlabel('Voltage (V)');
ylabel('Current (A)');
title('Current-Voltage (I-V) Characteristic of Solar Cell');

figure(2);
plot(Vo,Po, 'Linewidth', 3); grid on;
axis([0 0.7 0 1.5]);
xlabel('Voltage (V)');
ylabel('Power (W)');
title('Power-Voltage (P-V) Characteristic of Solar Cell');

% ----------------- End of Program -----------------
```

Chapter 3

Wind Energy

Turaj Ashuri

3.1 Introduction to Wind Energy

Wind energy has been harnessed for ages, initially for tasks like drawing water from wells and grinding grains in Persia. In recent years, it has been used for generating electricity. The wind energy sector boomed in the 1970s due to oil crises, drawing research funds in the US, Denmark, and Germany for alternative energy. While US incentives waned in the early 1980s, Europe maintained investments, taking the lead in wind technology and capacity until recent times.

As we embark on this journey into the realm of wind turbine technology, this chapter will comprehensively examine the intricacies of wind turbine configuration, power generation, aerodynamics, control systems, design loads, materials, applications, and their economic impact.

The configuration of wind turbines forms the foundation of their functionality. We will delve into the diverse designs and layouts of wind turbine systems, investigating how these configurations impact energy capture efficiency. Moreover, we will explore the fundamental concept of kinetic energy conversion from wind flow to mechanical rotation.

Betz's Limit, a fundamental principle in wind energy, dictates the maximum theoretical efficiency of a wind turbine. We will examine how this limit influences the power extraction capabilities of turbines and delve into the concept of the wind turbine power curve, which illustrates the relationship between wind speed and power output.

Understanding the available wind resources is vital for optimizing wind turbine installations. We will explore methodologies for assessing wind resources, considering factors like wind speed distribution, turbulence, and site-specific characteristics. Additionally, we will discuss how wind resource assessment informs estimations of annual energy production from wind turbines.

We will also cover how the levelized cost of energy is calculated. The Levelized Cost of Energy is a metric used to estimate the per-unit cost of generating electricity from a renewable energy source over the project's lifetime, accounting for all costs and expected energy production. It helps assess the economic viability and competitiveness of different energy generation methods.

The airfoil shape of wind turbine blades directly influences their aerodynamic performance. We will provide insight into the aerodynamic principles underlying airfoil design, lift and drag forces, and how these factors impact the efficiency of energy conversion.

Rotor blades, with their intricate shape and design, play a pivotal role in capturing wind energy effectively. This section will explore the aerodynamics governing rotor blade behavior, detailing concepts such as angle of attack, and axial and radial induction factors.

Efficient wind energy generation requires sophisticated control systems. We will explore how these systems manage pitch angles, generator torque, yaw control, and more, to optimize energy capture, ensure safety, and contribute to grid stability.

Wind turbines must endure a multitude of loads, from aerodynamic forces to extreme weather conditions. This section will discuss the design principles that safeguard wind turbines against these diverse loads. We will also investigate the materials used in turbine construction, considering their mechanical properties, sustainability, and longevity.

Beyond generating clean energy, wind turbines have far-reaching applications in various sectors. We will examine how wind energy contributes to economic growth, energy independence, job creation, and environmental benefits. By analyzing the broader impact of wind energy adoption, we can better understand its role in shaping a sustainable future.

As we embark on this comprehensive exploration of wind turbine technology and its myriad applications, we will gain insights into the intricate mechanics, engineering marvels, and economic dynamics that underpin this vital contributor to the renewable energy landscape.

3.2 Wind Turbine Configuration

The most prevalent wind turbine design, and the main subject of this chapter is the horizontal axis wind turbine (HAWT). This means the rotation axis runs parallel to the ground. HAWT can be classified based on several factors:

1. **Number of Blades:** Wind turbines typically have two or three blades, although some variations exist.

2. **Rotor Orientation:** Wind turbines can be upwind (wind hits the rotor before the tower) or downwind (wind hits the tower before the rotor).

3. **Rotor Control:** Rotor control methods include pitch control (adjusting the angle of the blades) or stall control (letting the airflow over the blades stall).

4. **Hub Design:** Hub design can be either rigid (fixed in place) or teetering (able to move).

5. **Yaw Alignment:** Wind turbines can have free yaw (able to turn freely with the wind) or active yaw (uses a mechanism to steer into the wind).

These classifications help categorize and differentiate several types of HAWTs based on their design and operational characteristics. A wind turbine consists of several key components:

1. **Rotor Blades:** These are the large, aerodynamic surfaces that capture the energy from the wind. They are connected to the hub and turn as the wind blows.

2. **Hub:** The hub connects the rotor blades to the main shaft, allowing them to spin together and transfer the captured wind energy.

3. **Main Shaft:** The main shaft transfers the rotational energy from the spinning rotor to the generator.

4. **Generator:** The generator converts the rotational energy from the main shaft into electrical energy through electromagnetic induction.

5. **Gearbox:** In some wind turbines, a gearbox is used to increase the rotational speed of the main shaft before it reaches the generator. However, some modern turbines use direct-drive systems without gearboxes.

6. **Yaw System:** This allows the turbine to turn and face the wind as it changes direction. It ensures optimal wind capture.

7. **Nacelle:** The nacelle is a housing that contains the gearbox, generator, and other critical components. It is usually located atop the tower.

8. **Tower and Foundation:** The tower supports the entire structure and raises the rotor to a height where it can access higher and more consistent wind speeds. The tower itself must be installed on a foundation to hold the entire wind turbine firmly in place.

9. **Anemometer and Wind Vane:** These instruments measure wind speed and direction, helping the turbine adjust its position for optimal wind capture.

10. **Controller and Sensors:** These components monitor various parameters like wind speed, generator speed, and other operational factors to ensure safe and efficient turbine operation.

11. Power **Cable**: The power cable in a wind turbine transmits the generated electricity from the turbine's nacelle to the ground-based power systems, ensuring efficient and safe delivery to the grid or storage systems.

These components work in harmony to capture wind energy and convert it into usable electrical power. Figure 1 shows a schematic view of the different components of a HAWT.

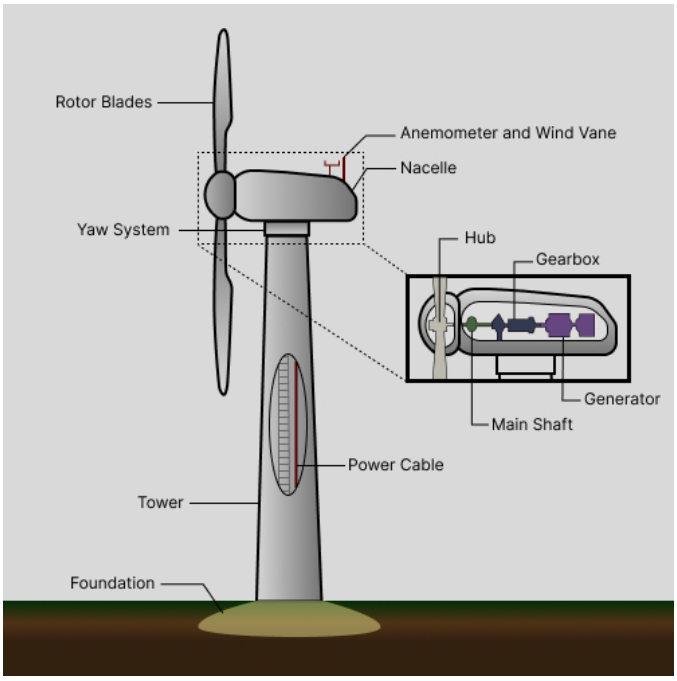

Figure 3.1: Main components of a HAWT.

3.3 Kinetic Energy and Power

Kind kinetic energy (*KE*) is a crucial factor in the operation of wind turbines. Kinetic energy is the energy possessed by a moving object due to its motion. In the context of wind turbines, it is the energy carried by the moving air particles, or wind, which strikes the turbine's rotor blades.

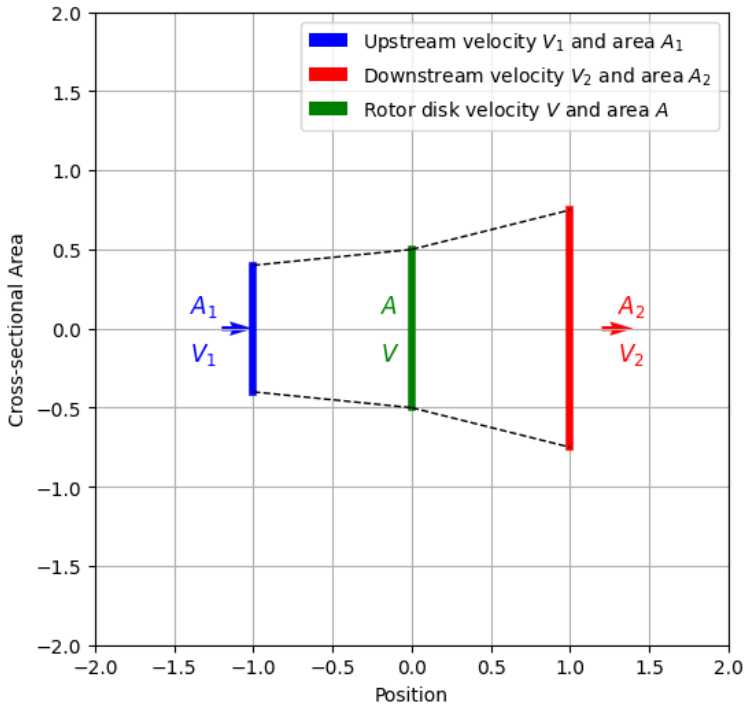

Figure 3.2: Upstream and Downstream Wind Velocities at a Wind Turbine Rotor Disk.

This kinetic energy can be calculated using the formula:

$$KE = \frac{1}{2}mv^2$$

In this case, the mass of air passing through the disk, m, with the velocity, v, in each time interval t can be determined by considering the volume of air passing through the disk. The volume is given by the surface area of the disk, A, multiplied by the wind speed (v) and the time interval (t). The mass of air (m) is then obtained by multiplying this volume by the air density (ρ):

$$m = \rho Avt$$

Substituting this mass into the kinetic energy formula:

$$KE = \frac{1}{2}mv^2 = \frac{1}{2}(\rho Avt)v^2 = \frac{1}{2}\rho Atv^3$$

This kinetic energy represents the energy carried by the moving air particles that strike the disk's surface within the time interval (t).

The power extracted, P, from the wind passing through the disk, is the rate at which this kinetic energy is being converted into usable energy. It can be calculated by dividing the kinetic energy by the time interval:

$$P = \frac{KE}{t} = \frac{1}{2}\rho A v^3$$

This equation gives the power generated by the wind passing through the disk's surface. It indicates that the power extracted is proportional to the surface area of the disk, the cube of the wind speed, and the time interval. However, this simplified calculation does not account for various inefficiencies and factors that influence actual power generation in real wind turbine systems.

Example 3.1: Suppose we have a wind turbine with a rotor diameter of 50 meters (radius, R = 25 meters) placed in an area where the air density (ϱ) is 1.2 kg/m³. The wind speed (v) is a steady 10 meters per second, and we want to calculate the kinetic energy and power generated in a time interval (t) of 1 hour.

***Solution*:**

Step 1. KE Calculation:

The surface area of the rotor's disk (A) can be calculated using the formula for the area of a circle:

$$A = \pi R^2 = \pi(25^2) = 1963.5\, m^2$$

The mass of air passing through the disk in 1 hour is given by:

$$m = \rho A\, vt = 1.2 \times 1963.5 \times 10 \times 3{,}600 = 84{,}823{,}002\, kg$$

Now, we calculate the kinetic energy (KE):

$$KE = \frac{1}{2}mv^2 = \frac{1}{2} \times 84{,}823{,}200 \times 10^2 = 4{,}241{,}150{,}082\, Joules$$

Step 2. Power Calculation:

Power (P) can be calculated using the kinetic energy divided by the time interval:

$$P = \frac{KE}{t} = \frac{4{,}241{,}150{,}082}{3600} = 1{,}178{,}097\ Watts\ (or\ 1{,}178.1\ kW)$$

So, for this wind turbine with a rotor diameter of 50 meters, operating in air with a density of 1.2kg/m³ and a steady wind speed of 10 meters per second, it would generate approximately 1,178.1 kW of power in 1 hour or 3,600 seconds, due to the kinetic energy carried by the wind passing through its rotor's surface.

3.4 Betz's Limit

Betz's Limit, also known as the Betz Limit or Betz's Law, sets the theoretical maximum efficiency of a wind turbine in converting kinetic energy from the wind into mechanical energy. It states that no wind turbine can capture more than 59.3% (or 16/27) of the kinetic energy available in the wind. The power coefficient (Cp) is a measure of how efficiently a wind turbine extracts energy from the wind. The maximum power coefficient achievable according to Betz's Limit is:

$$C_p = \frac{\text{Power Extracted by Turbine}}{\text{Power Available in Wind}} = 0.593$$

Example 3.2: Suppose you have a wind turbine with an upstream wind speed, v_1, of 10 m/s. What is the maximum downstream wind speed and the maximum power the wind turbine can extract? Let us assume the density of air (ρ) is 1.225 kg/m³ and the effective swept area (A) is 100 m².

Solution:

Step 1: Calculate the downstream velocity

By using the conversations of mass and momentum energy, the maximum possible downstream wind speed achievable due to wind energy extraction is one-third of the upstream wind speed. That is:

$$\frac{v_2}{v_1} = \frac{1}{3}$$

$$v_2 = \frac{1}{3} \cdot v_1 = 3.33\ m/s$$

Step 2: Calculate Maximum Power Production

The power extracted by a wind turbine is proportional to the cube of the wind speed ($E \propto v^3$), and it is calculated as:

$$P_{\text{turbine}} = C_p \cdot \frac{1}{2} \cdot \rho \cdot A \cdot v_1^3$$

Therefore:

$$P_{\text{turbine}} = \frac{1}{2} \cdot 0.593. 1.225\,\text{kg/m}^3 \cdot 100\,\text{m}^2 \cdot (10\,\text{m/s})^3 \;=\; 36{,}321.3\;kW$$

So, with a wind turbine operating at the Betz's Limit and given the specified conditions, you can generate approximately 36,321 kW of power from the wind. In real-world scenarios, additional factors and losses need to be considered, which typically reduce the amount of energy that can be extracted from a wind turbine to less than 50% for modern wind turbines.

3.5 Wind Turbine Power Curve

The wind turbine power characteristic, often referred to as the power curve or power performance curve, is a graphical representation that shows how the power output of a wind turbine varies with the wind speed. It is a crucial tool for assessing the performance and efficiency of a wind turbine under different wind conditions. The power curve provides insights into how much energy the wind turbine can produce at various wind speeds.

In a typical wind turbine power characteristic graph:

- The x-axis represents the wind speed, usually measured in meters per second (m/s).
- The y-axis represents the power output of the wind turbine, typically measured in kilowatts (kW) or megawatts (MW).

As Figure 2 shows, the power curve illustrates the relationship between wind speed and power output. At low wind speeds, the power output is minimal since there is not enough kinetic energy in the wind to generate significant power. As the wind speed increases, the power output of the turbine rises, following a certain pattern.

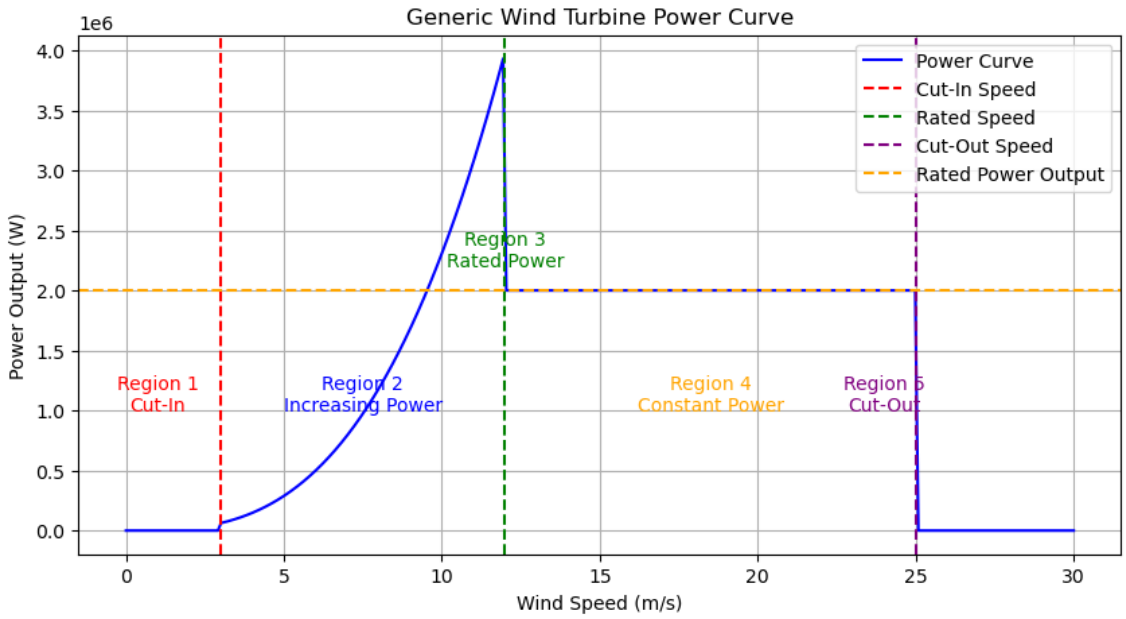

Figure 3.3: Wind Turbine Power Curve.

The curve typically has the following regions:

1. **Region 1 (Cut-In Wind Speed):** This is the minimum wind speed at which the wind turbine starts producing power. Below this speed, the turbine may not be operational.

2. **Region 2 (Increasing Power):** As the wind speed increases beyond the cut-in speed, the power output of the turbine increases. The power curve shows a gradual or steep slope, depending on the turbine design.

3. **Region 3 (Rated Power):** The wind speed at which the turbine reaches its rated power output, often represented as the nominal power rating of the turbine.

4. **Region 4 (Constant Power):** After reaching the rated wind speed, the power output remains constant. This is the optimal operating range for the turbine.

5. **Region 5 (Cut-Out Wind Speed):** This is the maximum wind speed at which the turbine operates before shutting down to prevent damage. Above this speed, the turbine's blades may be feathered, or the turbine might stop entirely.

The wind turbine power characteristic is an essential tool for wind farm planning, turbine selection, and assessing the performance of existing turbines. It helps determine the energy production potential of a turbine in different wind regimes, aiding in optimizing energy generation and ensuring the economic viability of wind energy projects.

Example 3.3: Draw the power curve for a wind turbine given the information below.

- Power Coefficient: *Cp* = 0.48
- Rotor Diameter: *D* = 100 m
- Rated Power Output: *Prated* = 2 MW
- Cut-In Wind Speed: *Vcut-in* = 3 m/s
- Cut-Out Wind Speed: *Vcut-out* = 25 m/s
- Density of air: $\rho = 1.225$ kg/m³

Solution:

We will use the power generation formula of the wind turbine as:

$$P_{\text{turbine}} = C_p \cdot \frac{1}{2} \cdot \rho \cdot A \cdot v_1^3$$

1. Below Cut-In Wind Speed:

   P=0 kW

2. Between Cut-In and Rated Wind Speeds:

$$P = C_p \cdot 0.5 \cdot \rho \cdot A \cdot v_1^3$$

$$= C_p \cdot 0.5 \cdot \rho \cdot \left(\frac{\pi}{4} \cdot D^2\right) \cdot v_1^3$$

$$= 0.48 \cdot 0.5 \cdot 1.225 \cdot \left(\frac{\pi}{4} \cdot (100\text{ m})^2\right) \cdot v_1^3$$

$$= 2{,}309.1 \cdot v_1^3 \text{ kW}$$

3. At Rated Wind Speed:

   P=Prated=2000 kW

4. Between Rated and Cut-Out Wind Speeds:

   P = Prated = 2000 kw

5. Above Cut-Out Wind Speed:

   P = 0 kW

Using these equations, the power curve of the wind turbine is shown in Figure 4.

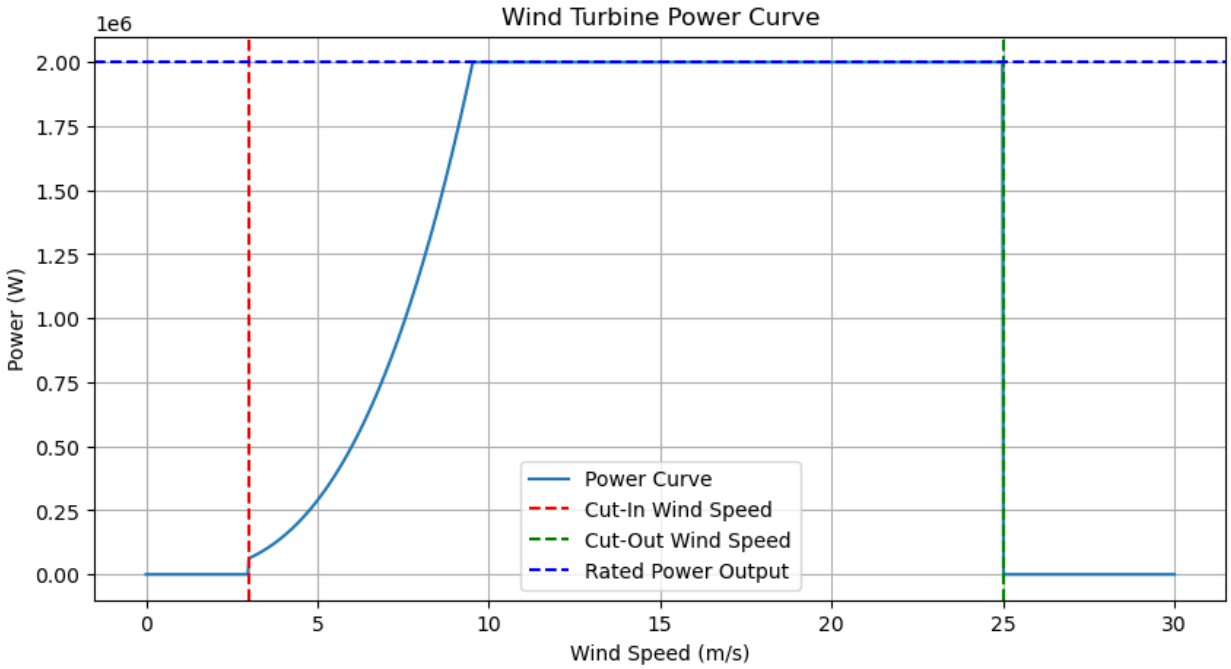

Figure 3.4: Wind Turbine Power Curve for the defined inputs.

The cut-in speed is 3 m/s, below which the turbine does not generate power. The power output increases with wind speed up to the rated wind speed, where it reaches the rated power of 2 MW at the rated wind speed of 9.533 m/s. Beyond this speed, the power output remains constant at 2 MW until the cut-out speed of 25 m/s, after which the power output drops to zero.

3.6 Wind Resource Assessment

Wind resource assessment is the systematic evaluation of the wind's potential energy at a specific geographical location. This assessment involves the collection, analysis, and interpretation of wind data over time to ascertain the wind's behavior, frequency, and variability. Successful wind energy projects hinge on precise wind resource assessments, which guide

developers in making informed decisions regarding turbine selection, project layout, and energy output projections.

Central to wind resource assessment are probability distributions that model wind speed frequency. Two widely used distributions are the Weibull distribution and the Rayleigh distribution. These distributions provide insights into the wind speed patterns and aid in predicting the likelihood of specific wind speeds occurring.

Wind resource assessment is a cornerstone of wind energy projects, guiding developers through data-driven decisions. The Weibull and Rayleigh distributions offer the mathematical frameworks to understand wind speed patterns, thus enabling the optimization of energy capture. With accurate assessments, wind energy projects stand poised to harness nature's power efficiently, contributing to a greener and more sustainable energy landscape.

3.6.1 The Weibull Distribution

The Weibull distribution is a versatile tool that accurately models wind speed variations. Its probability density function (PDF) for $v \geq 0$ is given by:

$$f(v) = \frac{k}{c}\left(\frac{v}{c}\right)^{k-1} e^{-(v/c)^k}$$

Here:

- $f(v)$ represents the probability density function for wind speed v.
- k is the shape parameter, influencing the distribution's shape and skewness.
- c is the scale parameter, determining the average wind speed.

To fit the Weibull distribution to the dataset, the method of maximum likelihood estimation is often employed. This involves finding the values of k and c that maximize the likelihood of observing the actual wind speed data. Various software tools, such as statistical packages or programming languages like Python, facilitate this process.

3.6.2 The Rayleigh Distribution

The Rayleigh distribution is a simplified version of the Weibull distribution for specific wind speed conditions ($v \geq 0$) and for when the shape parameter is set to 2. The shape parameter indicates the

distribution's shape. A k value around 2 suggests a balanced distribution, neither too skewed nor too peaked.

Its PDF is defined as:

$$f(v) = \frac{v}{c^2} e^{-\frac{v^2}{2c^2}}$$

To conduct a wind resource assessment, an extensive dataset of wind speed measurements is collected from anemometers and other meteorological instruments. Through statistical methods, such as least squares fitting, the Weibull or Rayleigh distributions are fitted to the dataset. The shape and scale parameters are determined, revealing the distribution that best matches the collected wind data.

Accurate wind resource assessment carries significant implications:

- **Optimal Turbine Siting:** Understanding wind patterns helps in strategically positioning turbines to capture maximum energy.
- **Energy Output Estimation:** Distribution parameters assist in predicting annual energy production, aiding in financial planning and feasibility analysis.
- **Risk Mitigation:** Assessing the variability of wind speeds informs decisions regarding backup power systems and grid integration.

Example 3.4: Assume we have collected wind speed data over a year at a specific site. Our goal is to fit a wind speed distribution to the data and analyze the results. Wind speed measurements (in meters per second) collected over a year are: 4.3, 5.2, 6.1, 5.8, 4.9, 6.5, 7.2, 4.6, 5.9, 6.3, 5.4, 6.8, 7.5, 5.7, 5.3, 4.8, 5.5, 6.7, 6.0, and 5.6.

Solution:

Step 1: Calculate Sample Mean and Sample Variance:

The sample mean is calculated by the following formula:

$$\bar{v} = \frac{1}{n}\sum_{i=1}^{n} v_i = \frac{1}{20}\sum_{i=1}^{20} v_i = 5.805\,\text{m/s}$$

The sample variance is obtained using the following formula:

$$s^2 = \frac{1}{n-1}\sum_{i=1}^{n}(v_i - \bar{v})^2 = \frac{1}{19}\sum_{i=1}^{20}(v_i - 5.805)^2 = 0.734\ (\text{m/s})^2$$

Step 2: Fitting the Weibull Distribution:

Using any statistical software, we find the best-fitting Weibull distribution parameters to be k = 7.464 and c = 6.172.

Step 3: Generating Wind Speed Distribution:

With k and c calculated in step 2, we generate the Weibull distribution curve. This curve represents the probability density of different wind speeds. The red dots represent the actual wind speed measurements.

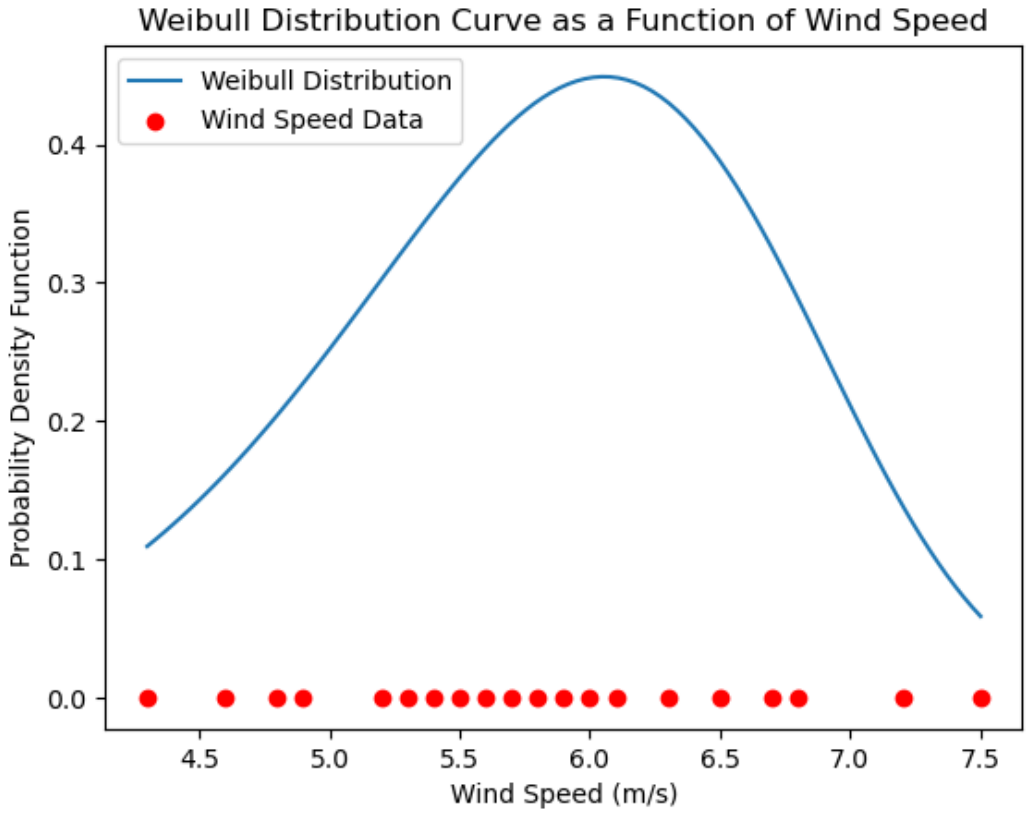

Figure 3.5: Weibull distribution based on a shape factor of 7.464 and a scale factor of 6.172.

3.7 Annual Energy Production

Among the critical metrics that govern the performance and viability of wind energy projects, the concept of Annual Energy Production (AEP) takes center stage. In this comprehensive discussion, we will delve deeper into AEP, exploring its intricacies, calculation methods, influencing factors, and the overarching significance it holds in the context of wind energy generation.

At its core, AEP encapsulates the total amount of electricity that a wind turbine generates over the span of a year. It serves as a foundational indicator, facilitating the evaluation of a wind energy project's effectiveness, economic feasibility, and contribution to the overall energy grid. AEP forms the bedrock for decision-making in project planning, financial analysis, and strategic integration into existing energy systems.

The calculation of AEP involves the harmonization of several factors, with wind speed and the turbine's power curve taking the lead. The power curve delineates the relationship between wind speed and the turbine's power output. By amalgamating the wind speed distribution specific to the project site, AEP can be calculated using a comprehensive formula that accounts for the turbine's power characteristics and wind speed distribution over a year:

$$AEP = h . \sum_{i=1}^{n} P(v_i) \cdot f(v_i)$$

In this equation:

- $P(v_i)$ signifies the power output of the turbine at wind speed v_i
- $f(v_i)$ represents the frequency of occurrence of wind speed v_i
- h denotes the total number of hours in a year that is 8760.
- n signifies the number of wind speed bins.

Numerous factors intricately influence the determination of AEP, further enhancing its complexity and significance:

1. **Wind Resource**: The primary driver, wind speed consistency, and distribution at the project site profoundly shape the AEP. Locations with higher average wind speeds typically yield more substantial energy production.

2. **Turbine Capacity**: The rated power of the wind turbine establishes the upper limit of energy generation. Higher-capacity turbines inherently generate more electricity.

3. **Hub Height**: The height at which turbines are installed affects wind speed exposure. Elevated turbines often experience faster wind speeds, elevating AEP.

4. **Rotor Diameter**: A larger rotor diameter translates to a greater area exposed to the wind, resulting in enhanced energy capture, especially at lower wind speeds.

5. **Turbine Availability**: Operational uptime is a crucial factor. Downtime due to maintenance, repairs, or other factors directly reduces the total operating hours and thereby affects AEP.

The estimation of AEP extends its influence across multiple domains:

- **Project Viability**: Accurate AEP predictions guide project developers in selecting the most suitable turbine models, optimizing layout designs, and predicting revenue streams.

- **Financial Planning**: A robust understanding of AEP aids in securing funding, evaluating return on investment, and determining the levelized cost of energy, thus impacting the financial sustainability of a project.

- **Grid Integration**: Precise AEP insights empower grid operators to effectively manage energy supply, strategically plan maintenance schedules, and ensure the stability and reliability of the grid.

- **Environmental Impact**: Higher AEP directly corresponds to increased renewable energy generation, leading to a reduction in greenhouse gas emissions and fostering environmental sustainability.

The concept of Annual Energy Production is far more than a mere numerical representation; it serves as the lynchpin upon which wind energy projects rest. With evolving technology and advanced methodologies for AEP estimation, wind energy continues its ascent towards a cleaner energy future. Through meticulous AEP analysis, wind energy projects are poised to carve an indelible path in the global energy landscape, driving sustainable progress and a resilient energy transition.

Example 3.5: Estimate the Annual Energy Production (AEP) for a wind turbine using the Weibull distribution and the following information.

- Wind turbine cut-in wind speed at 3 m/s.

- Wind turbine power curve of example 3

- Air density: ϱ=1.225 kg/m3

- Weibull distribution parameters: k=2 and c=9.47 (these values typically represent the condition of the Dutch part of the North Sea in Europe)

Solution:

We need to take 3 distinct steps as follows.

Step 1: Calculate Energy Production for Each Wind Speed Bin:

Table 1 shows the energy production for each wind speed bin using the power curve of example 4 for the wind speed bins ranging from 0 to 26.

Table 1: Power curve for the wind turbine of example 3.

Wind Speed (m/s)	Power Output, *P(v)* in *(kW)*
0	0
1	0
2	0
3 (cut-in)	62
4	148
5	289
6	499
7	792
8	1,182
9	1,683
9.533 (rated speed)	2,000

10	2,000
11	2,000
12	2,000
13	2,000
14	2,000
15	2,000
16	2,000
17	2,000
18	2,000
19	2,000
20	2,000
21	2,000
22	2,000
23	2,000
24	2,000
25 (cut-out speed)	2,000
26	0

Step 2: Calculate the probability of wind distribution for each wind speed bin:

In this step, we calculate the probability density f(v) for each wind speed bin as presented in Table 2.

Table 2: Weibull PDF for each wind speed bin.

Wind Speed (m/s)	Weibull function, *f(v)*
0	0.0000
1	0.0221
2	0.0427
3	0.0605
4	0.0746
5	0.0844
6	0.0896
7	0.0904
8	0.0874
9	0.0813
10	0.0731
11	0.0636
12	0.0537
13	0.0440
14	0.0351
15	0.0272
16	0.0205

17	0.0151
18	0.0108
19	0.0076
20	0.0052
21	0.0034
22	0.0022
23	0.0014
24	0.0009
25	0.0005
26	0.0003

Step 3: Calculate energy potential for each wind speed bin:

In step 3, we calculate the energy production contribution for each wind speed using the power curve and the probability of each bin as presented in Table 3.

Table 3: Energy potential for each wind speed bin.

Wind Speed (m/s)	*P(v) in kW*	*f(v) no unit*	*P(v). f(v) in kW*
0	0	0.0000	0.000
1	0	0.0221	0.000
2	0	0.0427	0.000
3 (cut-in speed)	62	0.0605	3.751

4	148	0.0746	11.041
5	289	0.0844	24.392
6	499	0.0896	44.710
7	792	0.0904	71.597
8	1,182	0.0874	103.307
9	1,683	0.0813	136.828
10	2,000	0.0731	146.200
11	2,000	0.0636	127.200
12	2,000	0.0537	107.400
13	2,000	0.0440	88.000
14	2,000	0.0351	70.200
15	2,000	0.0272	54.400
16	2,000	0.0205	41.000
17	2,000	0.0151	30.200
18	2,000	0.0108	21.600
19	2,000	0.0076	15.200
20	2,000	0.0052	10.400
21	2,000	0.0034	6.800
22	2,000	0.0022	4.400

23	2,000	0.0014	2.800
24	2,000	0.0009	1.800
25 (cut-out speed)	2,000	0.0005	1.000
26	0	0.0003	0.000
$\sum_{i=0}^{26} P(v_i) \cdot f(v_i)$			1,124.225

Step 4: Calculate the total AEP:

The AEP is calculated as:

$$AEP = 8760 \sum_{i=0}^{25} P(v_i) \cdot f(v_i) = 9{,}848{,}211\ kWHr\ or\ 9.848\ MWHr$$

This AEP estimation is critical for assessing the economic feasibility and energy potential of wind energy projects.

3.8 Levelized Cost of Energy

The Levelized Cost of Energy (LCOE) is a critical metric used to assess the economic feasibility of a wind turbine project over its operational lifespan. It represents the per-unit cost of generating electricity that would be required to recover all the project's costs, including initial investments, operational and maintenance expenses, financing costs, and potential decommissioning costs, while also accounting for energy produced over the project's lifetime.

The formula to calculate the LCOE for a wind turbine project involves several key components:

1. **Capital Costs:** These include the expenses associated with purchasing and installing the wind turbine, including the turbine itself, tower, foundation, and electrical infrastructure.

2. **Operational and Maintenance Costs:** These expenses cover the ongoing upkeep of the wind turbine, including regular inspections, repairs, component replacement, and other maintenance activities.

3. **Financing Costs:** This includes the cost of capital, which accounts for the interest on loans, return on equity, and other financial factors.

4. **Expected Lifetime Energy Production:** The total amount of energy that the wind turbine is expected to generate over its operational lifespan. This is usually estimated based on the wind resource at the site and the turbine's capacity factor.

5. **Discount Rate:** A discount rate is applied to account for the time value of money and the opportunity cost of capital. It reflects the rate of return that investors could earn on alternative investments with similar risks.

A simplified formula for calculating LCOE can be expressed as follows:

$$LCOE = \frac{Total\ Costs + O\&M\ Costs}{Total\ Expected\ Lifetime\ Energy\ Production}$$

Where:

- Total Costs are the sum of capital costs and discounted financing costs.
- O&M Costs are the sum of operational and maintenance costs discounted over the project's lifetime.
- Total Expected Lifetime Energy Production is the total amount of energy that the wind turbine is expected to produce over its operational lifespan.

The LCOE is usually expressed in terms of cost per unit of energy, typically in cents per kilowatt-hour (c/kWh) or dollars per megawatt-hour ($/MWh). A lower LCOE indicates a more cost-effective project.

It is important to note that calculating LCOE requires making assumptions about future costs, energy production, and financial parameters, and therefore the accuracy of the LCOE calculation depends on the accuracy of these assumptions. Additionally, LCOE does not capture all economic and environmental externalities, and other factors such as grid integration costs, regulatory incentives, and potential future technology advancements should also be considered when evaluating the overall economics of a wind turbine project.

Example 3.6: Calculate the LCOE for a hypothetical wind turbine project. In this example, we will use hypothetical values for the various parameters involved. The given parameters are:

- Capital Costs: $2,000,000
- Operational and Maintenance Costs (annual): $40,000
- Project Lifetime: 20 years
- Expected Annual Energy Production: 3,000 MWh
- Discount Rate: 7%

Solution:

Step 1: Calculate the Total Costs:

Total Costs = Capital Costs + Discounted Financing Costs

Total Costs = $2,000,000 + ($2,000,000 × 0.07) (assuming 7% discount rate)

Total Costs = $2,140,000

Step 2: Calculate Discounted O&M Costs:

To calculate discounted O&M costs, we sum up the annual O&M costs over the project's lifetime, each discounted back to the present value using the discount rate.

Discounted O&M Costs = Σ [O&M Costs / (1 + Discount Rate) ^ Year]

Discounted O&M Costs = $40,000 / (1 + 0.07) ^1 + $40,000 / (1 + 0.07) ^2 + ... + $40,000 / (1 + 0.07) ^20

Discounted O&M Costs ≈ $423,760

Step 3: Calculate Total Expected Lifetime Energy

Total Expected Lifetime Energy Production = Expected Annual Energy Production × Project Lifetime

Total Expected Lifetime Energy Production = 3,000 MWh/year × 20 years = 60,000 MWh

Step 4: Calculate LCOE:

LCOE = (Total Costs + Discounted O&M Costs) / Total Expected Lifetime Energy Production

LCOE = ($2,140,000 + $423,760) / 60,000 MWh LCOE ≈ 4.27 cents/kWh

So, in this example, the Levelized Cost of Energy (LCOE) for the wind turbine project is approximately 4.27 cents per kilowatt-hour (kWh). This value represents the cost per unit of energy that needs to be generated over the project's lifetime to cover all costs and provide a return on investment. Keep in mind that this is a simplified example, and real-world calculations might involve more complex considerations and factors.

3.9 Aerodynamics of Wind Turbines Airfoils

The aerodynamics of wind turbines is a fascinating field that involves the intricate interplay of forces and fluid dynamics. Wind turbines harness the power of the wind to generate clean and renewable energy, making understanding their aerodynamics crucial for efficient design and operation. Central to this understanding are concepts of lift and drag, which are pivotal in shaping a wind turbine's performance.

Wind turbines convert the wind kinetic energy into mechanical energy by the rotor, which is then transformed into electrical energy by the generator. This conversion process relies heavily on the aerodynamic principles governing the interaction between the turbine's rotor blades and the flowing air. The rotor blades play a pivotal role in capturing wind energy by utilizing lift and minimizing drag.

Lift and drag are fundamental forces in aerodynamics that play a vital role in the operation of wind turbines. Lift is the force perpendicular to the flow direction that arises due to pressure differences between the upper and lower surfaces of an airfoil (such as a rotor blade). Drag is the opposing force that acts parallel to the flow direction, resisting the motion of the airfoil through the air.

3.9.1 Lift Generation of Wind Turbine Blades

The lift force on an airfoil is governed by Bernoulli's principle, which states that as the speed of a fluid increases, its pressure decreases. This pressure difference between the upper and lower surfaces of the airfoil creates a net upward force, generating lift. The lift force can be calculated using the lift equation:

$$L = \frac{1}{2} \cdot C_L \cdot \rho \cdot A \cdot v^2$$

Where:

- L is the lift force,
- C_L is the coefficient of lift,
- ρ is the air density,
- A is the reference area of the airfoil,
- v is the relative velocity of the airfoil with respect to the wind.

The coefficient of lift, C_L, depends on the airfoil's shape, angle of attack, and other factors. It is determined experimentally and is a crucial factor in maximizing the lift force for a given airfoil design.

The angle of attack (AoA) is the angle between the chord line of an airfoil and the direction of the incoming wind (or incoming flow). The lift and drag coefficients are influenced by the AoA. At a certain AoA, the lift coefficient reaches its maximum value, known as the stall angle. Beyond this angle, the flow becomes turbulent, and lift decreases while drag increases. Thus, controlling the AoA is crucial for maintaining optimal performance. Figure 6 shows the relation among the incoming flow and lift and drag forces over an airfoil.

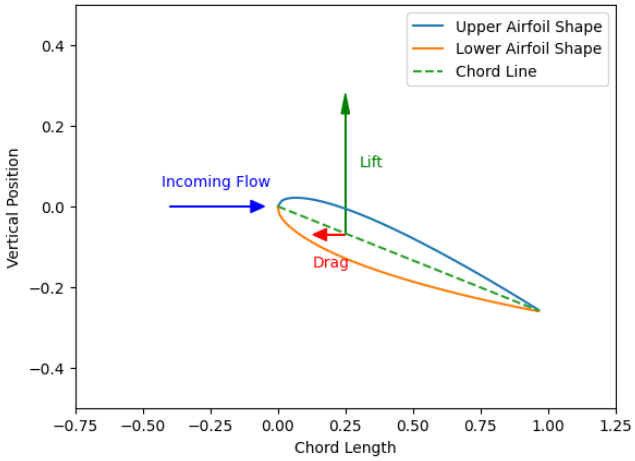

Figure 3.6: Visualizing the relation among the incoming flow, and lift and drag forces over an airfoil.

Typically, the lift coefficient increases with the angle of attack up to a certain point, beyond which it starts to decrease. This increase and subsequent decrease in lift coefficient can be attributed to the changing pressure distribution over the airfoil's surfaces. At lower angles of attack, the airfoil generates lift efficiently as the flow remains attached to the upper surface. However, as the angle of attack increases further, the flow may separate from the airfoil's surface, leading to a drop in lift and an increase in drag. Figure 7 shows the lift and drag coefficient dependency to the AoA for the NACA 0012 airfoil. The left figure (Figure 7a) with the blue curve represents the lift coefficient (C_L), which increases approximately linearly with the angle of attack until the stall angle (15 degrees), indicated by the red dashed line.

The right figure (Figure 7b) with green curve represents the drag coefficient (C_D), which increases gradually with the angle of attack and more significantly past the stall angle due to increased pressure drag from flow separation.

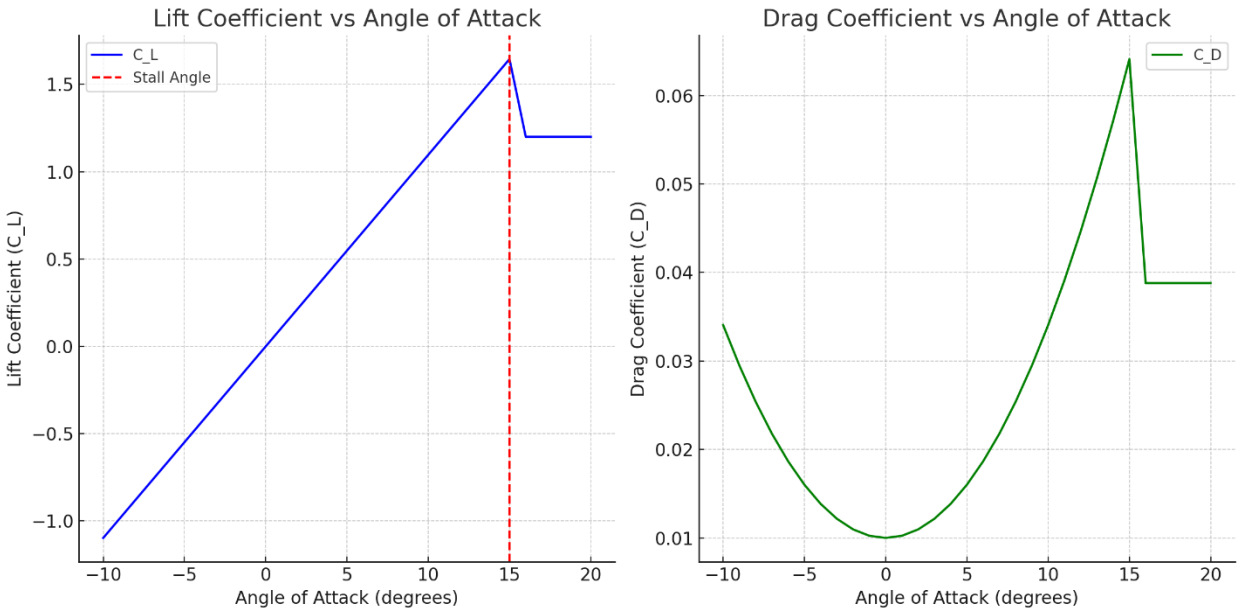

a) Lift Coefficient b) Drag Coefficient

Figure 3.7: The lift and drag coefficients as a function of Angle of Attack for NACA 0012 airfoil.

The drag coefficient also varies with the angle of attack. At small angles of attack, the drag coefficient is low as the airfoil experiences mostly pressure drag. However, as the angle of attack increases, the airfoil experiences both pressure drag and friction drag due to flow separation, leading to an increase in drag coefficient.

The angle of attack directly influences the lift and drag coefficients of an airfoil. The relationship between α, CL, and CD guides airfoil design and helps engineers optimize aerodynamic performance for various applications, including wind turbines, aircraft, and other aerodynamic systems.

3.9.2 Drag Generation of Wind Turbine Blades

Drag is the resistive force that opposes the motion of the airfoil through the air. The drag force can be calculated using the drag equation:

$$D = \frac{1}{2} \cdot C_D \cdot \rho \cdot A \cdot v^2$$

Where:

- D is the drag force acting on the airfoil or wind turbine blade.
- C_D is the coefficient of drag, representing the airfoil's drag characteristics.

The coefficient of drag is also determined experimentally and depends on factors such as the airfoil's shape and surface roughness. Minimizing drag is essential for reducing energy losses and improving the overall efficiency of the wind turbine.

Example 3.7: Calculate the lift and drag force for a wind turbine blade section that uses the NACA 0012 airfoil at an AoA of 8° degrees, and a wind speed of 7 m/s. What is the lift-over-drag ratio at this wind speed and AoA and how does it compare with the ratio shown in Table 4.

Solution:

The NACA 0012 is a symmetrical airfoil about its cord line. Figure 8 shows the cross-section of this airfoil.

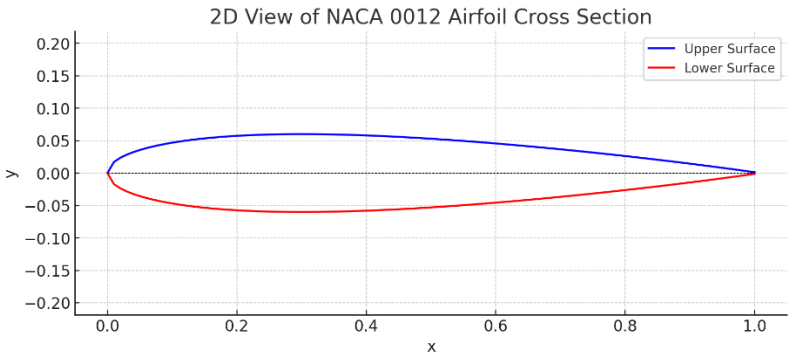

Figure 3.8: NACA 0012 airfoil profile.

The lift and drag coefficients, often referred to as polar data, for the NACA 0012 airfoil are presented in Table 4.

Table 4: Airfoil polar data for the NACA 0012.

Airfoil	NACA 0012	
Reynolds number	200,000	
Max Cl/Cd	47.4349	
Max Cl/Cd alpha	5	
Alpha	*Cl*	*Cd*
-14	-0.963	0.080
-13	-1.059	0.056
-12	-1.106	0.044
-11	-1.068	0.036
-10	-1.007	0.030
-9	-0.929	0.025
-8	-0.848	0.021
-7	-0.773	0.018
-6	-0.697	0.015
-5	-0.620	0.013
-4	-0.536	0.012
-3	-0.446	0.011
-2	-0.309	0.011
-1	-0.145	0.010
0	0.000	0.010
1	0.145	0.010
2	0.309	0.011

3	0.446	0.011
4	0.536	0.012
5	0.620	0.013
6	0.697	0.015
7	0.773	0.018
8	0.848	0.021
9	0.929	0.025
10	1.007	0.030
11	1.068	0.036
12	1.107	0.044
13	1.060	0.056
14	0.963	0.080

Using this table, we find the lift and drag coefficient of the airfoil to be:

$$C_L(at\ \propto = 8) = 0.848$$

$$C_D(at\ \propto = 8) = 0.021$$

We use an air density of 1.225 kg/m3. Since we are only analyzing a 2D section of the airfoil, we assume the cross-sectional area to be 1. Using these definitions and at a wind speed of 7 m/s the lift and drag are

$$L = \frac{1}{2} \cdot \rho \cdot C_L \cdot A \cdot v^2 = 0.5 \cdot 1.225 \cdot 0.848 \cdot 1 \cdot (7)^2 = 25.45\ N$$

$$D = \frac{1}{2} \cdot \rho \cdot C_D \cdot A \cdot v^2 = 0.5 \cdot 1.225 \cdot 0.021 \cdot 1 \cdot (7)^2 = 0.63\ N$$

At these conditions, the lift-over-drag ratio is:

$$\frac{L}{D} = \frac{25.45\ N}{0.63\ N} = 40.39$$

According to Table 5, the maximum lift-over-drag ratio happens at an AoA of 5° degrees. This comparison indicates that the airfoil is not operating at its optimal condition.

Keep in mind that this is a simplified example, and in actual wind turbine airfoil design, there are more factors to consider, such as Reynolds number effects, turbulence, and other aerodynamic considerations. Additionally, the lift and drag coefficients might vary with the angle of attack due to the non-linear structural behavior of the rotor and tower and its interaction with aerodynamic forces known as aeroelasticity and control loads. Therefore, more complex models might be used to capture this behavior accurately.

3.10 Aerodynamics of Wind Turbine Rotor Blades

The aerodynamics of wind turbine blades is characterized by lift and drag forces acting on the blades due to the airflow. These forces are influenced by factors such as the angle of attack, airfoil shape, wind speed, and blade geometry.

As discussed earlier, airfoil profiles are essential components of wind turbine blades. They are designed to generate lift while minimizing drag. The lift and drag coefficients of an airfoil change with the angle of attack. Polar curves illustrate this relationship and provide vital data for aerodynamic analysis.

Blade Element Momentum Theory (BEMT) is a theoretical approach used to analyze wind turbine blade aerodynamics. It divides the blade into small segments, or "elements," and calculates the aerodynamic forces on each element. BEMT considers both axial and tangential components of the wind velocity and relates them to the local inflow conditions. The key equations are:

- **Axial Induction Factor (a):** Relates the axial velocity of the rotor to the free-stream velocity.
- **Tangential Induction Factor (a'):** Relates the tangential velocity of the rotor to the free-stream velocity.
- **Thrust Coefficient (Ct):** Relates the axial force to the pressure difference across the rotor.
- **Power Coefficient (Cp):** Relates the power extracted from the wind to the available power in the wind.

The BEMT process involves:

1. Dividing the blade into sections.
2. Calculating the local angle of attack and chord length for each section.
3. Estimating the lift and drag coefficients from airfoil data.
4. Calculating axial and tangential velocities for each section.
5. Using BEMT equations to compute thrust and power coefficients.
6. Integrating coefficients along the blade span to determine overall performance.

BEMT is a simplified model that assumes steady-state flow and neglects three-dimensional effects, turbulence, and structural dynamics. However, it provides valuable insights into wind turbine performance. Advanced models, like Computational Fluid Dynamics (CFD), incorporate these complexities for more accurate analyses.

3.11 Wind Turbine Control Systems

The objective of a wind turbine's control system is to oversee the secure and automated functioning of the turbine. This serves to lower operational expenses, ensure consistent dynamic responses and enhanced product quality, and contribute to overall safety. The primary aim is to optimize the turbine's yearly energy extraction from the wind while minimizing the stress on the turbine's components.

In terms of functionality, wind turbine control systems are typically categorized into three distinct segments, even if not physically separate: (1) a central controller responsible for managing multiple wind turbines within a wind farm, (2) a supervisory controller dedicated to each individual turbine, and (3) a dedicated dynamic controllers assigned to the various subsystems of each turbine. These three tiers of control interact in a hierarchical manner, with interconnected control loops ensuring effective coordination.

The supervisory controller for each wind turbine can be classified based on its operating speed, specifically whether it operates at a constant speed or a variable speed. This classification is significant because it impacts the efficiency of energy conversion and the ability to capture energy across a range of wind speeds. Here are two primary categories:

1. **Constant Speed Wind Turbines:**

- **Operation:** Constant-speed wind turbines operate at a fixed rotational speed regardless of the wind conditions. The generator connected to the rotor spins at a consistent speed, typically synchronized with the grid frequency.

- **Advantages:** These turbines are simple in design and well-suited for regions with consistent wind conditions. They are also cost-effective and have a longer operational history.

- **Disadvantages:** Constant-speed turbines are less efficient in capturing energy under varying wind speeds. They may have limited control over the generated power output, which could lead to energy wastage during low wind conditions or excess strain on the system during high winds.

2. **Variable Speed Wind Turbines:**

- **Operation:** Variable-speed wind turbines adjust their rotational speed based on the wind conditions. The generator speed can be optimized to match the wind speed, allowing for more efficient energy capture.

- **Advantages:** Variable-speed turbines can capture energy over a broader range of wind speeds, making them more adaptable to varying wind conditions. They can generate higher energy outputs compared to constant-speed turbines.

- **Disadvantages:** These turbines are more complex in design, often requiring advanced control systems and power electronics to manage variable speeds. The increased complexity can lead to higher maintenance requirements and costs.

It is important to note that advancements in technology, such as the development of direct drive turbines and improved control strategies, have enabled variable speed turbines to become more common due to their ability to maximize energy capture and overall efficiency. Additionally, variable speed turbines are often paired with pitch angle control and generator torque control mechanisms to optimize their performance across different wind speeds and conditions.

The choice between constant-speed and variable-speed turbines depends on factors such as the wind regime of the location, grid integration requirements, and the specific goals of the wind energy project. In recent years, variable-speed turbines have gained popularity due to their ability to enhance energy capture and contribute to the overall efficiency of wind energy conversion.

The dedicated dynamic controller uses sensors, actuators, algorithms, and real-time data analysis to make informed decisions and adjustments. This dynamic controller is used at the component level, and it can be classified into the following categories:

1. Pitch Control System:

- **Function:** The pitch control system adjusts the pitch angle of the rotor blades to optimize energy capture and ensure safe operation.
- **Working:** In low wind speeds, increasing the pitch angle enhances lift and maintains a constant rotor speed, allowing efficient energy generation. During high wind speeds, decreasing the pitch angle reduces lift to prevent overloading and potential damage.
- **Components:** Pitch actuators, blade position sensors, controller.

2. Generator Torque Control System:

- **Function:** The generator torque control system manages the load on the generator to ensure optimal power output and energy conversion.
- **Working:** In variable-speed turbines, the generator torque is adjusted to match wind conditions, optimizing energy capture across varying wind speeds.
- **Components:** Torque sensors, power electronics, controller.

3. Yaw Control System:

- **Function:** The yaw control system aligns the turbine with the prevailing wind direction to maximize energy capture.
- **Working:** Yaw motors turn the nacelle (housing the rotor and generator) to face the wind. Yawing prevents the rotor from operating at an angle that reduces efficiency and creates unnecessary mechanical stress.
- **Components:** Yaw motors, wind direction sensors, controller.

4. Active Power Control System:

- **Function:** The active power control system adjusts the turbine's power output to match grid demand and maintain grid stability.
- **Working:** The controller regulates generator torque and pitch angle based on grid signals, contributing to stable energy supply to the grid.

- **Components:** Grid interface, power control algorithms, controller.

5. Reactive Power Control System:

- **Function:** The reactive power control system manages the generation of reactive power to maintain voltage stability on the grid.

- **Working:** Wind turbines can support grid voltage stability by injecting or absorbing reactive power as needed.

- **Components:** Power electronics, voltage regulation algorithms, controller.

6. Emergency Shutdown System:

- **Function:** The emergency shutdown system stops the turbine in case of severe weather conditions or mechanical failures.

- **Working:** Sensors monitor factors like wind speed, vibration, and system anomalies. If critical conditions are detected, the system initiates a safe shutdown procedure.

- **Components:** Sensors, shutdown procedures, safety mechanisms.

7. Condition Monitoring and Predictive Maintenance:

- **Function:** These systems monitor the turbine's health, detect anomalies, and predict potential failures.

- **Working:** Data from sensors and operational parameters are analyzed to identify trends and anomalies. Predictive algorithms help schedule maintenance to prevent unplanned downtime.

- **Components:** Sensors, data analysis algorithms, maintenance scheduling tools.

8. SCADA (Supervisory Control and Data Acquisition):

- **Function:** SCADA systems provide a centralized platform to monitor and control multiple wind turbines within a wind farm.

- **Working:** SCADA systems collect data in real-time from turbines, enabling operators to monitor performance, diagnose issues, and remotely control turbines.

- **Components:** Sensors, communication networks, control center.

Wind turbine control systems play a pivotal role in optimizing energy generation, ensuring turbine safety, and contributing to grid stability. The complexity of these systems continues to increase as technology advances, leading to more sophisticated control strategies that enhance efficiency and reliability in wind energy production.

3.12 Wind Turbine Design Loads and Materials

Wind turbines are pivotal in the renewable energy landscape, but their efficient and reliable operation hinges on the careful selection of materials and the understanding of design loads. To harness this resource effectively, wind turbines require durable materials and the ability to withstand complex design loads.

3.12.1 Wind Turbine Loads

Wind turbines are exposed to a diverse spectrum of loadings during their operation, a consequence of the intricate interplay between the turbine's components and the dynamic wind environment. These loadings significantly influence the turbine's structural integrity, overall performance, and operational longevity. Here is a description of the different loadings that act on a wind turbine during its operational phases:

Aerodynamic Loads: Aerodynamic loads represent the dominant forces exerted on wind turbines because of the interaction between the rotor blades and the flowing wind. These loads are intricately influenced by factors such as wind speed, direction, turbulence, and blade profiles. Aerodynamic loads give rise to various forces:

- **Lift:** Formed when wind passes over the curved surfaces of the rotor blades, leading to differing pressures on either side of the blade. Lift is responsible for harnessing wind energy and driving the rotation of the blades.

- **Drag:** Arises due to air resistance opposing the blade's forward motion. Minimizing drag is pivotal for optimizing the turbine's energy efficiency.

- **Thrust:** Generated as a reaction to the drag force and the angle of attack of the blades. Thrust force acts in the direction of the wind flow, exerting axial loads on the turbine's components.

- **Torsion:** Variation in wind pressure across the blade span triggers torsional moments, which induce twisting deformations along the length of the blades.

Gravity Loads: Gravity loads encompass the gravitational forces acting on various components of the wind turbine, primarily due to their weight. These include:

- **Dead Load:** The unchanging weight of stationary components such as the tower, nacelle, and rotor, manifesting as constant vertical forces.

- **Live Load:** Represents the dynamic weight of moving elements like rotating blades and the nacelle during operational maneuvers.

Centrifugal Loads: The rotation of the blades and the rotor induces centrifugal loads that can result in bending, tensile stresses, and deformations within the rotating components.

Dynamic Loads: Dynamic loads are transient forces that emerge from the complex interplay between the wind turbine and the ever-changing wind conditions. These encompass:

- **Rotor Imbalance:** Asymmetry in blade mass or aerodynamic characteristics can give rise to imbalances that trigger dynamic vibrations.

- **Yaw Loads:** When the nacelle is oriented to face the wind, lateral loads are exerted on the tower and the yaw bearing.

- **Tower Shadow Effects:** The turbulence generated by the tower can lead to varying loads on the blades as they transition through different wind zones.

- **Wind Gusts:** Sudden fluctuations in wind speed can induce rapid changes in loads on the blades, tower, and other critical components.

Environmental Loads: Environmental conditions significantly impact turbine performance and structural resilience:

- **Temperature Variations:** Thermal expansion and contraction caused by temperature changes result in dimensional alterations and stress variations in materials.

- **Corrosion:** Exposure to moisture, salt, and other corrosive agents can lead to material deterioration and reduced lifespan.

Extreme Loads: Wind turbines must be engineered to withstand extreme conditions without compromising safety or functionality:

- **Lightning Strikes:** Lightning events can induce electrical surges and structural damage, necessitating proper protection measures.

- **Ice Loading:** Accumulated ice on the blades can augment their weight and disturb aerodynamics, leading to imbalanced loads.

Start-Up and Shut-Down Loads: Turbines experience transient loads when commencing or discontinuing operation, as the blades accelerate or decelerate. Managing these loads is essential to prevent excessive stress on components and ensure a smooth transition.

A meticulous understanding and analysis of these diverse loadings are pivotal in devising wind turbines that exhibit efficiency, resilience, and a prolonged operational lifespan. Wind turbine designers rely on advanced simulation techniques and rigorous real-world testing to ascertain that components are adequately equipped to endure the intricate and ever-shifting loading conditions they encounter throughout their operational existence.

3.12.2 Wind Turbine Materials

Material selection is a critical aspect of wind turbine design, balancing factors like strength, durability, and cost. Engineering challenges include ensuring blade aerodynamics, tower stability, and component fatigue resistance under cyclic loading. This section provides an insight into the essential aspects of wind turbine materials, including their properties, applications, advancements, and considerations.

Blade Materials: Blades are pivotal components of a wind turbine, responsible for capturing and converting wind energy into rotational motion. Common materials include:

- **Fiberglass:** Lightweight and corrosion-resistant, fiberglass composites offer excellent strength-to-weight ratios, making them ideal for blade construction.

- **Carbon Fiber-Reinforced Polymers (CFRP):** CFRP materials enhance stiffness and strength, allowing for longer and more efficient blade designs.

- **Hybrid Materials:** Combining different composite materials can optimize specific blade characteristics, such as strength and flexibility.

Tower Materials: Towers provide structural support and elevate the nacelle to capture higher wind speeds at elevated heights. Steel is used due to its high tensile strength, cost-effectiveness, and adaptability to various tower designs.

Nacelle and Hub Materials: The nacelle houses critical components like the generator, gearbox, and control systems. Materials for nacelles and hubs include:

- **Aluminum Alloys:** Offering lightweight yet sturdy properties, aluminum alloys contribute to efficient nacelle design.

- **Steel Alloys:** High-strength steel alloys withstand dynamic loads and ensure durability in nacelle and hub structures.

Generator and Gearbox Materials: Generators and gearboxes require materials that can withstand rotational forces and mechanical stresses:

- **High-Strength Steels:** Gearboxes and generator housings are often constructed using high-strength steels to manage the demands of rotational motion.

- **Specialized Alloys:** Advanced alloys offer increased durability, efficiency, and resistance to wear and fatigue.

Foundation Materials: Wind turbine foundations bear the load of the entire structure and must withstand various environmental conditions:

- **Concrete:** Used in onshore wind turbines, concrete provides stability and support to the tower, ensuring its structural integrity.

- **Steel Reinforcement:** Incorporating steel reinforcement enhances the tensile strength and durability of concrete foundations.

Advancements in Wind Turbine Materials: As technology progresses, the wind energy industry continues to explore innovative materials and manufacturing processes:

- **Smart Materials:** Self-monitoring and self-healing materials could enhance turbine resilience and reduce maintenance requirements.

- **Nanostructured Materials:** Nanotechnology offers the potential to enhance material properties, such as strength and corrosion resistance.

- **Advanced Coatings:** Corrosion-resistant coatings can extend the lifespan of turbine components and reduce maintenance costs.

Material Considerations: When selecting materials for wind turbines, engineers consider a range of factors:

- **Mechanical Properties:** Materials must possess the required strength, stiffness, and fatigue resistance for the intended application.

- **Corrosion Resistance:** Wind turbines are exposed to environmental elements, necessitating materials that can withstand corrosion.

- **Weight and Durability:** Lightweight materials reduce loads on components, while durability ensures a longer operational lifespan.

- **Manufacturability:** Materials should be conducive to cost-effective manufacturing processes, such as molding or casting.

Sustainable Materials: As sustainability gains prominence, the wind energy sector is exploring eco-friendly materials and recycling practices to reduce environmental impact.

Wind turbine materials play a crucial role in determining the efficiency, reliability, and lifespan of these renewable energy systems. An informed selection of materials, considering mechanical, environmental, and economic factors, is essential for optimizing the performance of wind turbines and driving the transition to a cleaner energy future.

3.13 Wind Turbine Applications

Wind turbines have found diverse applications across various sectors due to their ability to harness renewable wind energy and contribute to sustainable power generation. These versatile machines are used for a wide range of purposes, each displaying the potential of wind energy in different fields.

Utility-Scale Power Generation: Large-scale wind farms consist of multiple wind turbines strategically positioned to capture wind energy efficiently. These utility-scale installations generate significant amounts of electricity, feeding clean energy into the power grid and contributing to reducing carbon emissions. Wind farms are increasingly integrated into national energy strategies to meet renewable energy targets.

Distributed Generation: Wind turbines are also used for distributed power generation. Smaller turbines, often installed on rooftops, in remote locations, or even on residential properties, can produce energy locally. These installations are particularly beneficial in areas with limited grid access or as supplemental power sources.

Hybrid Energy Systems: Wind turbines can be integrated into hybrid energy systems that combine multiple renewable sources, such as solar and energy storage. These systems ensure a continuous

power supply by utilizing wind energy when solar energy production is reduced, enhancing grid stability and resilience.

Microgrids and Remote Areas: Wind turbines are employed in microgrids, and remote areas were connecting to a centralized grid is challenging. These turbines generate electricity for local communities, improving energy access in remote regions.

Agricultural Applications: Wind turbines can be installed on farmlands to generate electricity for on-site use or to supplement income through selling excess power to the grid. This diversification of income supports rural economies.

Residential and Commercial Buildings: Small-scale wind turbines can be installed on residential and commercial buildings to generate clean energy on-site. They contribute to reducing electricity bills and reliance on traditional power sources.

Pumping Water: Wind turbines have been historically used for water pumping in remote areas. Wind pumps lift water from wells or reservoirs for agricultural irrigation, livestock watering, and domestic use. These applications provide sustainable water ***Solution***s in regions with limited access to traditional energy sources.

Water Desalination: In coastal areas facing water scarcity, wind turbines can power desalination processes, converting seawater into freshwater. This application addresses both energy and water challenge and contributes to sustainable water resources.

Telecommunication Towers: Wind turbines are integrated into telecommunication towers to provide power for remote cellular stations, radio transmitters, and other communication equipment. This ensures connectivity even in areas without access to reliable grid electricity.

Research and Education: Small-scale wind turbines are often used as educational tools for renewable energy and engineering programs. They provide direct learning experiences, helping students understand the principles of energy conversion and sustainable technology.

Disaster Relief and Humanitarian Aid: Wind turbines can be rapidly deployed in disaster-stricken areas to provide immediate power for emergency operations, medical facilities, and temporary shelters. Their mobility and ability to operate independently of existing infrastructure make them valuable tools in relief efforts.

Wind turbines have evolved beyond electricity generation, infiltrating various sectors, and addressing multifaceted challenges. As technology continues to advance, their applications are likely to expand further, contributing to a cleaner and more sustainable future.

3.14 The Economic Landscape of Wind Turbines

The economy of wind turbines extends beyond their ability to harness wind's kinetic energy; it encompasses a spectrum of socio-economic and environmental dimensions that intertwine to shape a sustainable future. Wind turbines have emerged as iconic symbols of clean energy generation, offering multifaceted economic benefits that span local communities, industries, and global markets.

Job Creation and Economic Growth: Wind energy projects catalyze job creation across the value chain. From manufacturing and construction to operation and maintenance, wind turbines stimulate employment opportunities in both rural and urban areas. Skilled technicians, engineers, researchers, and administrative personnel contribute to a growing job market, fostering economic growth and stability.

Energy Independence and Security: Investing in wind turbines enhances energy independence, reducing reliance on fossil fuels and imported energy sources. Nations can bolster their energy security by diversifying their energy mix, mitigating the impacts of global energy price fluctuations and geopolitical tensions.

Industry Innovation and Technological Advancement: The wind energy sector drives innovation, spurring advancements in turbine design, materials, control systems, and grid integration. Pioneering technologies refine the efficiency and reliability of wind turbines, subsequently influencing other industries and fostering a culture of research and development.

Environmental Stewardship: Wind turbines align with environmental preservation by producing clean energy without greenhouse gas emissions or air pollutants. This aligns with global efforts to combat climate change, reducing health costs associated with pollution-related illnesses and bolstering public health.

Regional Development and Community Benefits: Wind energy projects invigorate local economies, providing communities with a source of revenue through land lease payments, property taxes, and community benefit agreements. These funds support infrastructure development, education, healthcare, and other public services.

Export and Trade Opportunities: Countries with robust wind energy industries can leverage their expertise to export wind turbines, components, and services to international markets. This enhances trade balances and fosters international collaboration in pursuit of sustainable energy *Solution*s.

Grid Stability and Energy Market Diversity: Wind energy diversifies the energy mix, reducing the reliance on conventional power sources. As wind turbines contribute power to the grid, they enhance grid stability by supplementing baseload generation and meeting peak demand periods.

Long-Term Cost Savings: While initial investments in wind energy infrastructure may be substantial, the long-term operational and maintenance costs are lower compared to fossil fuel-based power plants. As technology advances, the cost per megawatt-hour of wind energy continues to decline.

Attracting Investment and Capital Inflow: The wind energy sector attracts private investments and venture capital, fostering innovation and growth. Institutional investors are increasingly drawn to wind energy projects due to their stable, long-term returns and alignment with sustainable development goals.

In conclusion, wind turbines drive an economy that transcends the generation of clean energy. Their impact reverberates through job creation, technological progress, environmental conservation, and community development. As nations and industries transition towards sustainable energy sources, wind turbines stand as pivotal instruments that not only propel us towards a greener future but also enrich economies on local, regional, and global scales.

3.15 Wind Energy Cost Considerations

However, understanding the cost dynamics associated with wind energy production is crucial for informed decision-making. This discourse delves into the multifaceted aspects of wind energy costs, considering factors that influence upfront investments, operational expenses, and long-term financial viability.

Initial Capital Investment: Establishing wind energy infrastructure necessitates a substantial upfront capital investment. This includes costs associated with turbine procurement, foundation construction, electrical infrastructure, and site preparation. The specific costs vary depending on turbine capacity, tower height, site location, and local regulatory requirements.

LCOE: The LCOE is a key metric used to assess the cost-effectiveness of wind energy projects over their operational lifespan. It accounts for all costs incurred, including initial investment, ongoing maintenance, operational expenses, and potential decommissioning costs, and divides this sum by the total energy generated over the project's lifetime.

Economies of Scale: Larger wind farms benefit from economies of scale, wherein the cost per unit of energy decreases as the project size increases. This phenomenon is driven by optimized logistics, efficient maintenance practices, and streamlined operations, resulting in enhanced cost efficiency.

Ongoing Operations and Maintenance: While wind turbines have lower operational and maintenance costs compared to fossil fuel-based power plants, they still require regular inspections, repairs, and occasional component replacement. Predictive maintenance strategies, enabled by advanced sensors and data analytics, minimize downtime, and optimize operational efficiency.

Technological Advancements: Advancements in turbine design, materials, and manufacturing processes continue to drive down costs. Improved aerodynamics, more efficient components, and advanced control systems contribute to enhanced energy capture and reduced operational expenditures.

Financing and Incentives: The availability of favorable financing options, government incentives, tax credits, and renewable energy certificates can significantly impact the overall cost of wind energy projects. These mechanisms incentivize private investment and aid in reducing the financial burden on project developers.

Grid Integration and Transmission Costs: Wind farms require integration with the existing power grid, which may involve additional costs for electrical infrastructure upgrades and transmission lines to deliver the generated energy to consumers. These costs are influenced by the proximity of the wind farm to existing transmission networks.

Environmental Considerations: While not a direct monetary cost, the environmental benefits of wind energy, including reduced carbon emissions and improved air quality, contribute to societal and public health cost savings.

Price Stability and Long-Term Returns: Wind energy offers price stability due to its immunity to fuel price fluctuations. With fixed costs for operation and maintenance, wind energy projects provide long-term predictable returns, making them attractive to investors seeking stable income streams.

In conclusion, the cost landscape of wind energy is intricate and dynamic, influenced by an array of factors that span initial investments, operational efficiency, technological progress, policy incentives, and environmental considerations. As the global energy landscape continues to evolve, understanding these cost dynamics is integral to harnessing wind energy's full potential while making prudent and sustainable investment decisions.

3.16 The Future of Wind Energy

This section explores the promising horizons that lie ahead, driven by the convergence of technological advancements, policy incentives, and a growing global consciousness of environmental stewardship.

Technological Advancements: Innovations in turbine design, materials, and manufacturing processes continue to redefine the landscape of wind energy. Enhanced aerodynamics, intelligent control systems, and modular components are set to amplify efficiency, augment energy capture, and increase overall reliability. Moreover, breakthroughs in energy storage technologies promise to mitigate the intermittent challenge, ensuring a more consistent and reliable power supply.

Offshore Wind Farms: The boundless potential of offshore wind farms is emerging as a notable change in wind energy's trajectory. As technological barriers are overcome, vast expanses of open water become viable platforms for energy generation. Offshore wind farms offer higher wind speeds, reduced visual impact, and the potential to tap into previously untapped wind resources.

Hybrid Energy Systems: Hybridization, the marriage of wind energy with complementary sources like solar and energy storage, holds the key to stable, 24/7 clean power supply. These systems not only enhance grid stability but also maximize energy utilization, making renewables an integral part of the global energy matrix.

Smart Grid Integration: The future of wind energy envisions a smart grid that seamlessly integrates diverse energy sources, allowing for dynamic energy flow management and real-time adjustments based on demand and supply. This integration enhances grid stability, mitigates transmission losses, and empowers consumers to play an active role in energy management.

Digitalization and AI: The fusion of digitalization and artificial intelligence (AI) is poised to revolutionize wind energy operations. Predictive maintenance, advanced data analytics, and AI-driven optimization algorithms will enhance the performance of wind farms, reduce downtime, and facilitate real-time decision-making.

Energy Equity and Access: As wind energy becomes more accessible and affordable, its potential to bridge energy disparities across the globe becomes evident. Remote communities, developing nations, and regions lacking conventional energy infrastructure can harness wind power to unlock economic opportunities and improve quality of life.

Policy and Investment: Strategic policy initiatives and increased investments are propelling wind energy towards unprecedented growth. Governments are recognizing wind energy's capacity to drive economic development, job creation, and emissions reduction, leading to favorable regulatory environments and incentives for further expansion.

Environmental Resilience: The future of wind energy dovetails with a commitment to environmental resilience. Reduced carbon emissions, improved air quality, and diminished reliance on finite resources paint a picture of a world where energy and ecology coexist harmoniously.

Global Collaborative Efforts: The future of wind energy transcends borders, fostering international cooperation and collaboration. Shared research, knowledge exchange, and cross-border transmission projects pave the way for a global network of sustainable energy interconnectivity.

In closing, the future of wind energy holds the promise of an empowered, sustainable world. It is a future where wind turbines stand not only as iconic symbols of progress but as vital contributors to a planet that thrives on clean, resilient, and abundant energy. As the wind continues to carry us forward, the future of wind energy unveils a horizon where our energy needs are met harmoniously with the rhythms of nature.

Chapter 4

Geothermal & Bioenergy

Javad Khazaii

4.1 Introduction to Geothermal Energy

Geothermal energy is the heat energy (thermal) from the earth (Geo). The source of geothermal energy is reservoirs that exist underground in different depths. The depth of these reservoirs can range from a few feet to several miles. The technology for accessing these sources of energy generally is drilling long wells into these reservoirs to tap into steam or very hot water. The hot water or steam is brought up to the earth's surface and is utilized for several types of geothermal applications. The main types of geothermal applications are electricity generation, direct use, and heating and cooling. There are many benefits that can be achieved by using geothermal energy. The first and maybe the most important is the fact that geothermal energy is a type of renewable and clean source of energy. This partly is because the heat generated inside the earth due to decay of radioactive elements can last for a very long time, and the fact that the newer closed-loop geothermal power plants emit close to zero greenhouse gases. Based on the department of energy web site, "Modern closed-loop geothermal power plants have life cycle emissions four times lower than solar PV, and six to 20 times lower than natural gas" [1]. The other benefit of geothermal energy is that by providing a constant baseload, the need for producing electricity from the other sources will be decreased, specifically during the pick demand loads. Also based on the department of energy web site "Geothermal power plants are compact. They use less land per gigawatt-hour (404 m^2) than comparable-capacity coal (3,642 m^2), wind (1,335 m^2), and solar photovoltaic (PV) power stations (3,237 m^2)" [1]

Earth layer near the surface is a large source of energy. This energy is partly because of conductive and convective heat transfer through internal layers of the earth that are moving from the hot core towards the earth's surface, as well as energy received by the surface of the earth through sun radiation. But almost half of the heat in the crust is due to radioactive decay within the earth, from isotopic of uranium-238, uranium-235, thorium-252, and potassium-40. [2] "The heat of Earth is replenished by radioactive decay at a rate of 860 EJ/yr. The global geothermal flow rates are close to more than twice the rate of human energy consumption from all primary sources." [3]

Heat from the core is transferred through the different layers of the earth until it reaches the earth's surface. On its path, this moving heat heats up the water reservoirs and rocks inside the earth between the core and the surface of the earth. As water reservoirs heat up, they may remain as hot water or change state and convert to steam. Tapping to these reservoirs allows us to use hot water or steam as

sources of energy for electricity generation or heating and cooling purposes. Also, in areas under the surface of the earth where water does not naturally exist, engineered (enhanced) methods can be utilized to benefit from the earth's heat. In this condition high pressure water is injected inside the earth to break the rocks. This allows creating a path when running the water close to these hot rocks. Water passing through the created crushed rocks absorbs the heat and creates hot water or steam that is recovered from the other end of the crushed rocks.

Different layers of earth from center upward are (a) solid inner core with a depth of 5,100 to 6,378 (center of the earth) km, followed by (b) liquid outer core from 2,900 to 5,100 km in depth. The final 2,900 km outer layer of the earth consists of (c) mantle, asthenosphere, and lithosphere that consists of upper mantle, oceanic and continental crust. The horizontal layers making the lithosphere are called tectonic plates. During plate tectonic process these plates drift away or pushed together which creates cracks allowing the magma from the core of the earth to move towards the crust. Magma can reach the surface that is known as volcanoes or stays under the surface as source of geothermal heat. [2] Geothermal resources can be categorized into three types based on their temperature level. High-temperature resources are generally higher than 180 degrees centigrade (356 F) which are associated with recent volcanic activities. Intermediate temperature (100 to 180 degrees centigrade (212 F to 356 F)) and low temperature (<100 degrees centigrade) (212 F) sources are found in continental settings, where above-normal heat production exists due to radioactive isotope decay. [4]

"Earth's estimated heat loss is about 44.2 TW (Terawatts) (4.42×10^{13} Watts). The heat that is transferred from the interior of the earth towards the surface of the continents on average is about 65 milliwatts (mW) per square meter and through the ocean floors is about 101 mW per square meter. This is 0.087 watts/ square meter on average (0.03 percent of solar power absorbed by Earth)." [2] The result is a global terrestrial flow of about 1400 exa-joules (each exa-joule is equal to one quintillion (10^{18}) joules) per year (EJ/year) heat. The continent part is estimated at about 30% of this flow or about 315 EJ/yr. [2]

The current use of geothermal resources is mostly limited to the followings:

a) High-temperature electric power production

b) Intermediate and low temperature direct use applications

c) Enhanced (engineered) Geothermal systems (EGS)

d) Ground source heat pump applications

The industry generally uses high temperature geothermal steam (at least 300 F) for electricity generation since lower temperatures are not efficient for such purposes, except the Organic Rankine Cycle that can generate electricity economically with at least 230 F. Direct use of geothermal hot water and mixed water and steam is used for intermediate and low temperature applications, that usually are between 90 F to 300 F. Ground source heat pumps generally use temperatures below 90 F. [1]

In the following paragraphs we will discuss some of these different methods of geothermal energy use briefly. Our focus will be on power generation and ground source heat pump applications, due to its variety of applications and importance of the applications.

4.2 High-Temperature Electric Power Production

There are three main types of electricity generation power plant that use geothermal resources. These systems are flash steam, dry steam, and binary cycle. Based on a 2012 [7] worldwide analysis report based on 94 geothermal plants (6-dry-steam, 34 single flash, 18 double flash, 31 binary, 2 hybrid steam-binary and 1 triple flash plants) the highest reported efficiency is approximately 21%, with the average only at 12%. This is almost less than one third of the other conventional systems coal (33%), natural fired gas (40%), oil fired (37%), and nuclear (32%).

The most common type of these three geothermal power generation systems is flash steam technology. In this system underground hot water at temperatures above 360°F and high pressure is directed to a flash tank that is kept in a much lower pressure. Due to this sudden change of pressure, high pressure steam will flash to a mixture of vapor and liquid. Systems with double and triple flashing also exist. The liquid will be removed from the bottom of the flash tank, and the saturated steam will be released from the top of the flash tank and will be directed to a steam turbine, where it generates electricity in conjunction with a generator. The generated liquid in the bottom of the flash tank we be returned to the discharge well. The weak mixture of liquid and vapor discharged from the turbine will then be circulated in setting on condenser, cooling tower with the use of a water pump. These units can generate up to 110 MW of electricity. Other than the first type, which is known as condensing turbines, there is another type called back-pressure turbines. In back-pressure turbines, the discharge of the turbine will be directly into the atmosphere, and therefore, they do not need condenser, pump, and cooling tower setting. The efficiency of back-pressure turbines is almost half the efficiency of condensing turbines. Their cost is less, and they can be utilized as small plants to start development of new larger fields in a location. [1]

Dry steam reservoirs are also available that produce the steam directly to the turbine. The control of such systems is simpler than flash type systems. Of course, such systems do not require flash tanks. Conventional flash and dry steam plants generally use 150 to 300°C geothermal fluid.

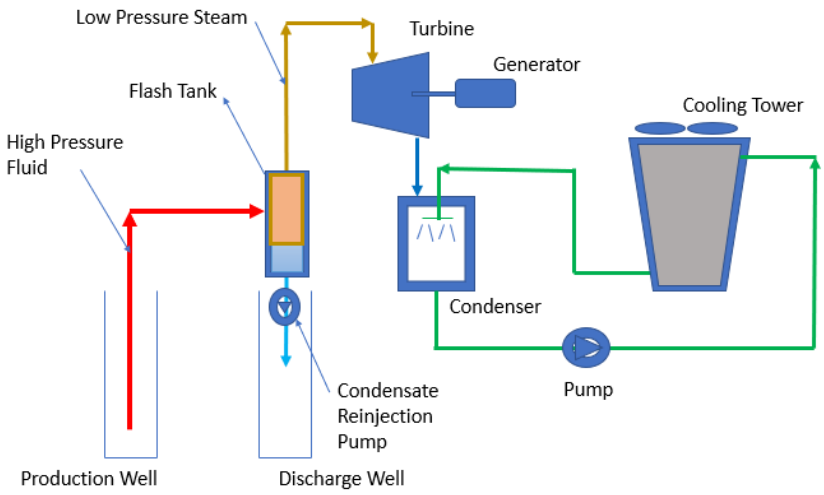

Figure 4.1: Flash Steam Geothermal Power Generation System

The binary cycle plants using an Organic Rankin Cycle are operating with lower temperatures ranging from 70 to 170°C. These systems require a heat exchanger that operates between the geothermal fluid and another separate fluid such as isobutane, R134a, or other fluids that have low boiling point. Heat from the geothermal fluid, then is transferred to the other fluid and converts it to vapor. The vapor is then used to operate a turbine and generate electricity. A second heat exchanger is also used to exchange heat between the heat rejection side of the Rankine cycle and a cooling tower.

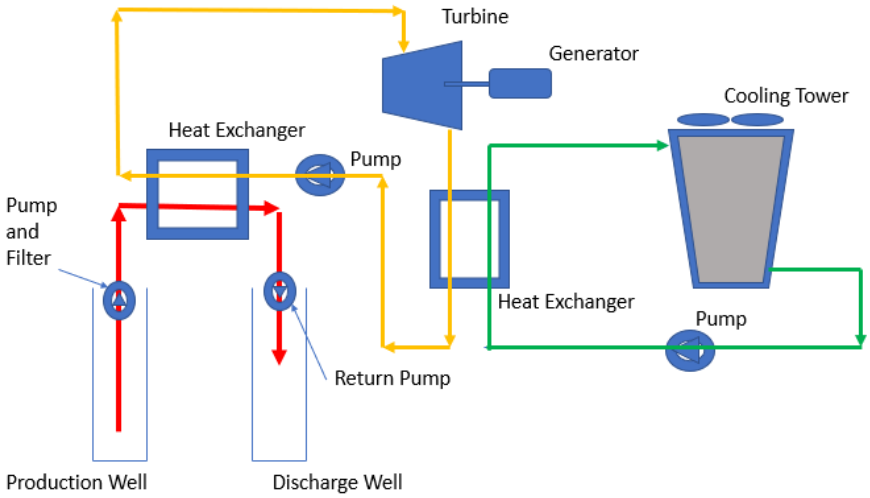

Figure 4.2: Binary Geothermal Power Generation System

Example 3.1: A flash steam geothermal system is used to create electricity. Production well produces high pressure hot water at 1.5 MPa, and 180 °C (with enthalpy of h1=763.05 kJ/kg). This hot water then is flashed in a flash tank to reduce the pressure to 400 kPa and creates a mixture of vapor and liquid with quality of 7.4%). The exiting low pressure saturated vapor is then suitable for running the

steam turbine. Saturated steam at 400 kPa (with enthalpy of h2=2738.1 kJ/kg) then feeds the turbine, where generates power, and discharges from turbine at 10 kPa and 90% quality (with enthalpy of h3=2344.7 kJ/kg). For producing 1 MW power calculate the required mass of the high-pressure steam required from the production well. Assume no losses throughout the processes.

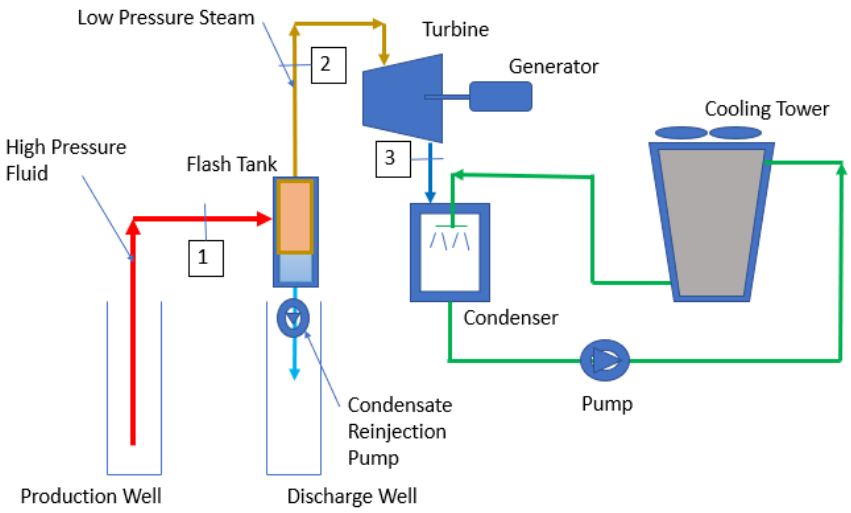

Figure 4.3: Flash Steam System (Example 3.1)

Solution: From energy equation for steady state open system when there is a mixture of vapor and liquid exists in any given pressure/ temperature, we can calculate the quality of the mixture by dividing the mass flow rate of the vapor to total mass flow rate of vapor and liquid. Therefore, in flash tank we have:

$$x = quality\ of\ mixture\ in\ flash\ tank = 0.074 = \dot{m}_2/\dot{m}_1$$

Therefore,

$$\dot{m}_2 = 0.074\,\dot{m}_1$$

Also, based on energy law for steady state, open system, with negligible change in kinetic and potential energies, and an adiabatic turbine (no what loss) then we can write:

$$\dot{W} = Power\ generated\ by\ Turbine = \dot{m}_2 \times (h_2 - h_3)$$

Therefore,

$$\dot{m}_2 = mass\ rate\ of\ steam\ entering\ the\ turbine = \frac{1000}{2738.1 - 2344.7} = 2.542\,\frac{kg}{s}$$

And therefore,

$$\dot{m}_1 = mass\ rate\ of\ steam\ entering\ the\ flash\ tank = 2.543/0.074 = 34.19\ kg/s$$

Example 3.2: A supply of geothermal hot water and a heat exchanger is used as a source of energy in a binary geothermal cycle that uses R-134a as the working fluid. Saturated vapor R-134a leaves the boiler at a temperature of 85°C, and the condenser temperature is 40°C. Calculate the thermal efficiency of the Rankine cycle. The followings are known:

Enthalpy of R-134a liquid leaving the pump = h2 = 112 kJ/kg

Enthalpy of the R-134a at entrance to the pump = h1= 108.26 kJ/kg

Enthalpy of the saturated vapor leaving the boiler = h3 = 279.5 kJ/kg

Enthalpy of the mixture of vapor and liquid leaving the turbine = h4 = 259 kJ/kg

Assume no losses throughout the processes.

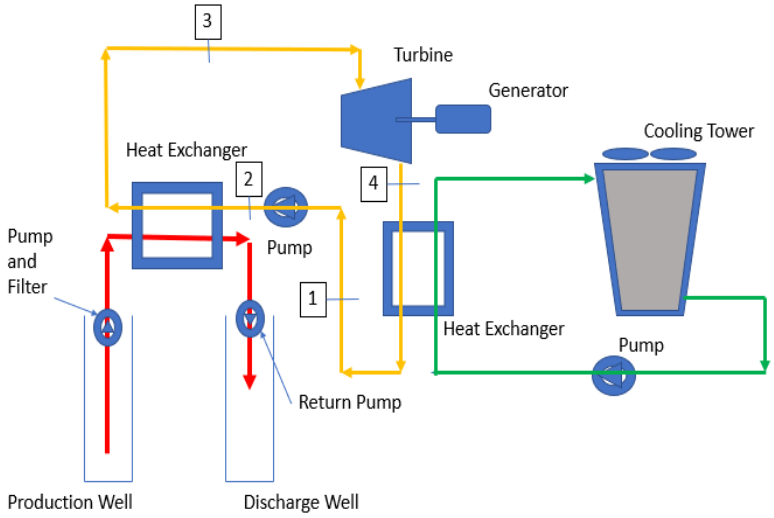

Figure 4.4: Binary System (Problem 2)

Solution: Using three steady state open system with negligible kinetic and potential energy for boiler, turbine, and pump and considering adiabatic turbine and pump the following energy equations can be written for these elements:

$$w_p = worked\ utilized\ for\ running\ the\ pump = \ h_2 - h_1$$

$$w_p = 112 - 108.26 = 3.74\ kJ/kg$$

$$q_h = heat\ transferred\ from\ geothermal\ source\ to\ the\ boiler = h_3 - h_2$$

q_h = 279.5−112 = 167.5 kJ/kg

$$w_t = worked\ generated\ at\ turbine = \ h_3 - h_4$$

$$w_t = 279.5 - 259 = 20.5\ kJ/kg$$

$$w_{net} = net\ work = w_t - w_p = 20.5 - 3.74 = 16.76\ kJ/kg$$

$$\eta_{th} = Thermal\ efficiency of\ Rankine\ cycle = w_{net}/q_h = \frac{16.76}{167.5} = 0.1 = 10\%$$

4.3 Ground-Source Heat Pumps

Ground-source (GSHP) also known as geothermal heat pumps (GHP) are being used in both residential and commercial applications. Such systems use ground, groundwater, or surface water as the means of heat source and sink. Generally, these systems are also named ground coupled (GCHP), groundwater (GWHP) and surface water (SWHP) heat pump respectively.

Before getting to description of each of the above systems, it is necessary to have an understanding about a vapor-compression refrigeration cycle, which is in the heart of many cooling systems, as well as the ground-source heat pump systems. We have discussed this concept in section of energy and energy efficiency in more depth, but due to the important place of refrigeration cycles/ heat pumps in ground-source heat pumps, it is necessary to shortly review this concept again.

A vapor-compression refrigeration cycle is made of four main components.

(a) A compressor that increase the pressure and temperature of the refrigerant from a state near dry vapor to a super heat vapor state,

(b) a condenser that provides means of heat exchange with an environment with high temperature to allow the super heat refrigerant vapor to cool down to a state near saturated liquid,

(c) an expansion valve that causes a drop of temperature and pressure to allow the refrigerant to be in state of mixture of liquid and vapor, and finally

(d) an evaporator in which the heat is absorbed from the cold environment.

The absorbed heat makes the mixture of refrigerant liquid and vapor in evaporator boils to a near saturated (dry) vapor state. Refrigerant cycles inside this system and helps to remove the heat from a colder space and discharge it to an environment with higher temperature. Of course, this process is possible because of the work that is input to the compressor. It is possible to add a three-way switching valve, an extra expansion valve and two check valves parallel to each expansion valve and convert this same cooling generating refrigeration cycle into a heating generation refrigerant cycle as well. This cycle is known as a heat pump and can produce cooling and heating with the same structure. Therefore, this same refrigeration cycle can produce cooling in summer by removing the heat from the area that is required to be cooled (at evaporator) and produce heating in wintertime by discharging

the heat that was removed from the colder environment and will be introduced to the space that is required to be heated (at condenser). It is important to note that both evaporator and condenser are two simple coils that do different duties when operating in cooling and heating mode. Of course, this is possible due to the change of the direction of the movement of the refrigerant in the cycle as it switches from cooling to heating or vice versa.

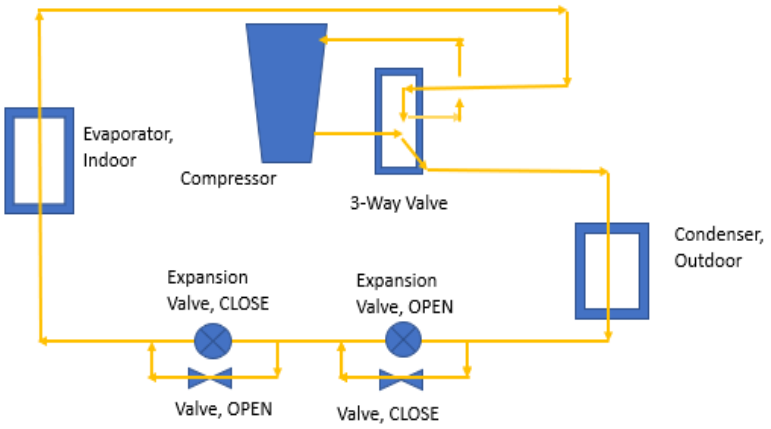

Figure 4.5 - Heat pump cooling cycle

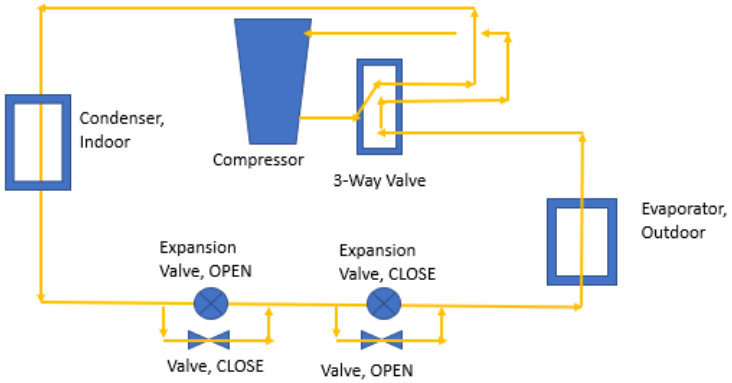

Figure 4.6 - Heat pump heating cycle

After recalling the basics of vapor-compression cycles, let's now discuss different ground source heat pump systems in a little more depth, which have this cycle in its core.

4.4 Ground-Coupled Heat Pump Systems (GCHP)

The most common form of the ground-coupled heat pump systems is made of one vapor-compression refrigerant cycle at the core, and two heat exchangers, one at each refrigerant system coil's (evaporator, and condenser) side. On one side (depending on the heating or

cooling mode) the refrigerant exchanges heat (gives away heat or absorbs heat) with another closed loop of liquid mix of water/ anti-freeze. A pumping system circulates this water/ antifreeze liquid through a designed piping system into the ground. The water/ antifreeze liquid is pumped into the pipes that are buried under the ground. These pipes can be installed either vertically or horizontally depending on the location of the site and design intents. The buried pipes and the water/ antifreeze liquid in it, then use the Earth either as a sink or a source for absorbing or discharging heat into the earth. On the other side of the original vapor-compression refrigerant cycle there is another heat exchanger. The duty of this heat exchanger is to allow exchange of heat at the refrigerant (evaporator, or condenser) coils with a secondary source for cooling or heating applications inside the space intended to be cooled or heated. Each separate loop of the water requires its own circulating pump.

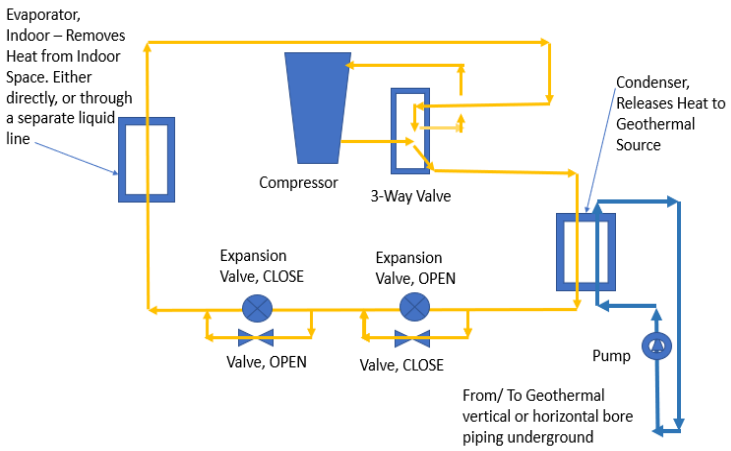

Figure 4.7: Ground-coupled heat pump cooling cycle

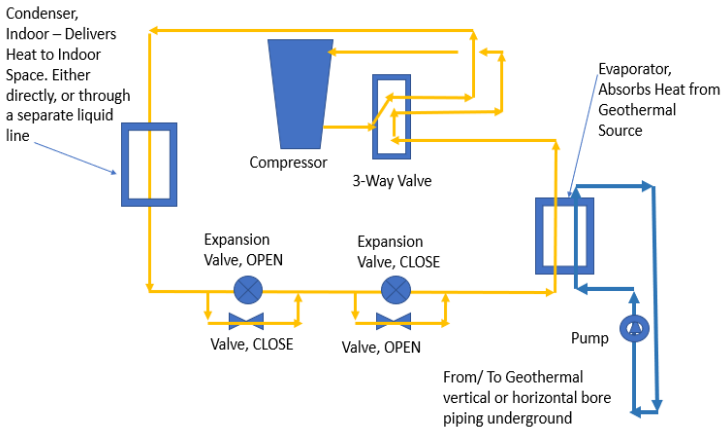

Figure 4.8 Ground -coupled heat pump heating cycle.

In vertical configuration, high-density polyethylene (HDPE) pipes (bores) with 0.75 to 1.5 in. diameter are installed with a u-bend at the bottom. The depth of the pipes generally is between 50 to 600 ft. To reduce the interfere between adjacent pipes a minimum separation 20 ft is recommended when multiple loops are placed.[4] The most advantage of the vertical systems is the fact that the pipes are

in contact with the ground with almost constant temperature that increases the efficiency of the system. The disadvantage of the vertical systems is its higher cost due to special equipment needed for drilling. In horizontal arrangement design can be of single-pipe, multiple-pipe, and spiral types, that generally are made of stretched small diameter polyethylene tubes. The most important advantage of the horizontal ground coupled heat pumps is its lower cost due to the less need for specialized equipment and contractors. The disadvantage of this type is the fluctuation of the ground heat due to its low depth installation that contributes to lower efficiency. [4]

4.5 Ground-water Heat Pump Systems (GWHP)

In the commercial sector, groundwater heat pumps can be extremely attractive, since they only need two relatively inexpensive wells (production well and injection well), and therefore, very little land area is required for such systems. The important aspect of this system is the net zero water usage, since the water coming out of production well, will be returned to the injection well almost without any loss in quantity. The most common type of groundwater heat pump system is supplemented by a water-to-water heat exchanger in which, a second loop of water exchanges heat with the groundwater loop, and then exchanges heat with a water-to-air heat pump serving the conditioned space. There is also a circulation pump needed on each separated water loop. Where production well water temperature of 60 F or less is available, this water can be used directly in heat pump coiling systems. The advantages of ground water heat pumps are lower cost, lower space required, and simple technology. The disadvantages of the groundwater heat pumps are limited availability of the water, possible higher water regulations are some areas, and need for water treatment where the water is used directly in the heat pump. [4]

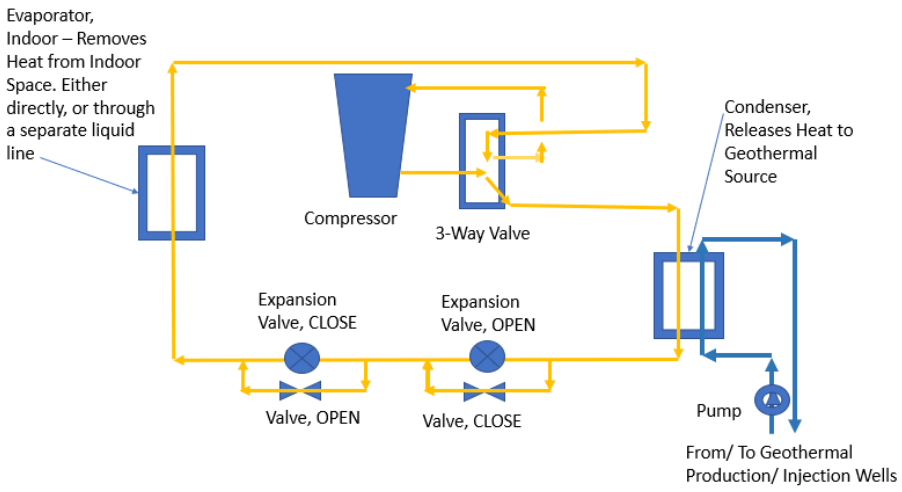

Figure 4.9 Groundwater heat pump cooling configurations

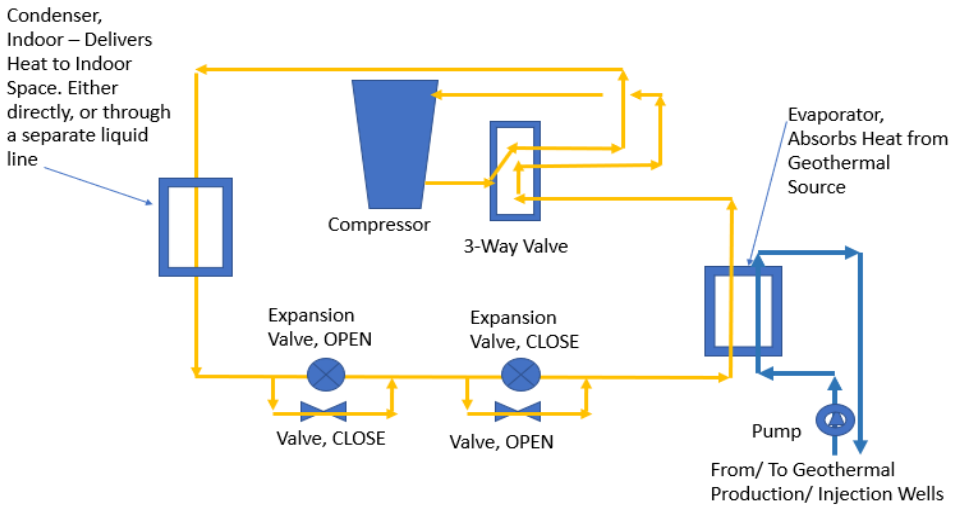

Figure 4.10 Groundwater heat pump heating configurations

4.6 Surface Water Heat Pump Systems (SWHP)

Even though the surface water heat pumps are not the same as groundwater heat pumps due to a different thermal characteristic and different mechanism of water heat exchange with the ground heat, but due to very similar installation methods, it is a good place here to have a few words about these systems here as well. In these systems, either a closed-loop or an open-loop configuration is used. Water pipes are either drowned in a nearby lake, river, or other open bodies of water in a separate water loop, or are used to convey the lake, river, or open water body water directly. In both cases there is a need for utilizing a heat exchanger and a pump on the open or closed loops. ASHRAE [4] recommends submerged piping material to be thermally fused HDPE tubing with ultraviolet (UV) radiation protection. The advantages of the surface water heat pump systems are low cost, low energy consumption and low maintenance, and its disadvantages are piping exposure to damage and wide variation of water temperature, contributing to lower efficiency. With water temperature available at 50 F or below complete cooling can be achieved, and with higher water temperatures pre-cooling is possible with these systems. In warm weather it is possible to do the heating as well.[4]

In the following paragraphs we will review ground couple heat pump design as it is recommended by ASHRAE Application Handbook [4]. This will be useful for the reader to become familiar with the terms and equations for solving problems of such contents. For a detailed design guideline, it is recommended to refer to the ASHRAE Applications Handbook [4].

4.7 Design of Vertical Ground Coupled Heat Pumps

A

SHRAE [4] recommends the Ingersoll and Zobel [5] method for calculating the required length of bore. The general steady state heat transfer equation then is given as:

$$q = L \times (t_g - t_w)/R \qquad equ\ (1a)$$

Where,

q = heat transfer rate, Btu/h or W

L = required bore length, ft or m

t_g= ground temperature, °F or °C

t_W = liquid temperature, °F or °C

R = effective thermal resistance of the ground, h. ft. °F/Btu or m °C/W

Braud et al [8][9] rewrote this equation as equation 1b.

$$q = L \times (U \times \Delta T) \qquad equ\ (1b)$$

Where,

U = geothermal fluid heat transfer conductance rate to earth, Btu/ h. ft. °F or W/m °C

$\Delta T = \frac{T_{wi}+T_{wo}}{2} - T_g$, °F or °C

"The steady state equation then is modified to represent the variable rate of a ground heat exchanger by using series of constant-heat-rate "pulses". Therefore, thermal resistance of the ground per unit length is calculated as a function of time corresponding to the time span over which a particular heat pulse occurs. A term is also included to account for thermal resistance of the pipe wall and interfaces between the pipe and fluid and the pipe and the ground." [4] The following equations are the results of these corrections for cooling equ-2 and heating equ-3 respectively. The required bore is the larger of two lengths calculated by these two equations.

$$L_C = \frac{q_a \times R_{ga} + (q_{lc} - 3.41 \times W_C) \times \left(R_b + PLF_m \times R_{gm} + R_{gd} \times F_{SC}\right)}{t_g - \frac{t_{wi} + t_{wo}}{2} - t_P} \qquad equ\ (2)$$

$$L_h = \frac{q_a \times R_{ga} + (q_{lh} - 3.41 \times W_h) \times \left(R_b + PLF_m \times R_{gm} + R_{gd} \times F_{SC}\right)}{t_g - \frac{t_{wi} + t_{wo}}{2} - t_P} \qquad equ\ (3)$$

Where,

F_{SC} = short circuit heat loss factor

L_C = required bore length for cooling, ft

L_h = required bore length for heating, ft

PLF_m = part load factor during design month

q_a = net annual average heat transfer to the ground, Btu/h

q_{lc} = building design cooling block load, Btu/h

q_{lh} = building design heating block load, Btu/h

R_{ga} = effective thermal resistance of ground (annual pulse), h.ft.°F/Btu

R_{gd} = effective thermal resistance of ground (daily pulse), h.ft.°F/Btu

R_{gm} = effective thermal resistance of ground (monthly pulse), h.ft.°F/Btu

R_b = thermal resistance of pipe, h.ft.°F/Btu

t_g = undisturbed ground temperature, °F

t_P = temperature penalty for interference of adjacent bores, °F

t_{wi} = liquid temperature at heat pump inlet, °F

t_{wo} = liquid temperature at heat pump outlet, °F

W_c = power input at design cooling load, W

W_h = power input at design heating load, W

Heat transfer rate, building loads, and temperature penalties are positive for heating and negative for cooling. Also, Fourier number (F_O) presented by Carslaw and Jager [6] and the process recommended by them need to be used as follows to calculate R_{ga}, R_{gm}, and R_{gd} in equations 2 and 3. Based on this method the time of operation, outside pipe diameter, and thermal diffusivity of the ground are related based on equation 4.

$$F_O = 4 \times \alpha_g \times \frac{\tau}{d_b^2} \qquad equ\ (4)$$

where,

α_g = thermal diffusivity of the ground, ft^2/day

τ = time of operation, days

d = outside pipe diameter, ft^2

In this proposed method the 10-year (3650 day), one month (30 days), and 6-hour (0.25 day) equivalent should be used to calculate the equivalent thermal resistance for varying heat pulses, for using to calculate associated Fourier numbers as follows.

$\tau_1 = 3650\ days$ equ (5)

$$\tau_2 = 3650 + 30 = 3680\ days \qquad equ\ (6)$$

$$\tau_f = 3650 + 30 + 0.25 = 3680.25\ days \qquad equ\ (7)$$

The Fourier numbers then are:

$$Fo_f = 4 \times \alpha \times \frac{\tau_f}{d_b^2} \qquad equ\ (8)$$

$$Fo_1 = 4 \times \alpha \times (\tau_f - \tau_1)/d_b^2 \qquad equ\ (9)$$

$Fo_2 = 4 \times \alpha \times (\tau_f - \tau_2)/d_b^2$ equ (10)

The next step is to use the calculated Fourier numbers to calculate associated G values from the following experimentally developed table, either directly or via interpolations:

G	Fo
0.128	1

0.263	10
0.433	10^2
0.614	10^3
0.797	10^4
0.978	10^5
1.1595	10^6

$$R_{ga} = \frac{G_f - G_1}{k_g} \quad equ\ (11)$$

$R_{gm} = (G_1 - G_2)/k_g$ equ (12)

$$R_{gd} = \frac{G_2}{k_g} \quad equ\ (13)$$

Where k_g is the ground thermal conductivity in Btu/ h. ft. °F.

References [9][10] offer a way for calculating "q_a" as follows:

$$q_a = (C_{fc} \times q_{lc} \times EFL\ hours_C + C_{fh} \times q_{lh} \times EFL\ hours_h)/8760\ hours \quad equ\ (14)$$

C_{fc} and C_{fh} are cooling and heating correction factors respectively, whish are given as factors based on the average cooling EER and average heating COP of all the units used in the specific building, where the geothermal ground source heat pump is designed for. Typical values of C_{fc} for cooling EER of 11,13,15, and 17 are given as 1.31, 1.26, 1.23, and 1.20 respectively. Also, typical values of C_{fh} for heating COP of 3, 3.5, 4, and 4.5 are given as 0.75,0.77, 0.8, and 0.82 respectively. It is good to remember that the COP or coefficient of performance for heating is the heating effect produced by the unit (Btu/h or W) divided by the energy equivalent of the electrical input (Btu/h or W) and therefore a dimensionless value. While the cooling EER is the cooing effect produced by the unit (Btu/h) divided by the electrical input (W), and therefore, its dimensions are equal to Btu/W. h.

Two other factors in equation 14 are EFLH for cooling and heating, which are the ratio of annual cooling/ heating energy requirements to rated capacity of the cooling/ heating equipment. It depends on certain location, building function, and type. For a typical list of EFLH for cooling and heating can be found in reference [11]. For example, in this list one can find EFLH for cooling and heating value for Atlanta, for a typical 8 to 5 office one 5 days a week are between 950 to 1360 and between 480 to

690 respectively. The reference [11] represents a modified form of "Development of Equivalent Full Load Heating and Cooling Hours for GCHPs Applied to Various Building Types and Locations", ASHRAE 1120-TRP, Final Report, CDH Energy Corp., Cazenovia, NY, Sept. 2000". In this reference the values on the low end of range assume units off during unoccupied hours in cooling season and 10 F setback in heating. Values on high end assume no set-back control.

Example 2.3: A small vertical GCHP system is built of 400 feet long tube (2-200 feet pipes with a U-bend at the bottom). If the ground temperature at this location is 55 °F, and the average temperature of the liquid in pipes is 42 F, and the ground thermal conductivity is 0.5 Btu/ h. ft. °F, what is the amount of heat transferred through this system? Use the Ingersoll and Zobel steady-state equation.

Solution: Ingersoll and Zobel steady-state equation is:

$$q = L \times \frac{(t_g - t_w)}{R}$$

Using the values given in the problem, the total steady-state heat transfer through this system is:

$$q = 400\ ft \times \frac{(55°F - 42°F)}{0.5\frac{Btu}{h.ft.°F}} \quad = 10{,}400\ Btu/h$$

Example 2.4: Use Carslaw and Jager method to calculate the effective thermal resistance of ground (annual pulse), effective thermal resistance of ground (monthly pulse), and effective thermal resistance of ground (daily pulse), for a location in which thermal diffusivity of the ground is 0.5 ft^2/day and thermal conductivity of the ground is 0.8 Btu/ h. ft. °F. Use a tube with external diameter of 1.2".

Solution: Based on Carslaw and Jager method we first need to calculate the Fourier number for 10 years, 1 month, and 6-hour time of operation first.

$\tau_1 = 3650\ days$

$$\tau_2 = 3650 + 30 = 3680\ days$$

$$\tau_f = 3650 + 30 + 0.25 = 3680.25\ days$$

The associated Fourier numbers then are:

$$Fo_f = 4 \times \alpha \times \frac{\tau_f}{d_b^2}$$

$$Fo_f = 4 \times 0.5 \frac{ft^2}{day} \times \frac{3680.25\ days}{\left(\frac{1.2}{12}\right)^2\ ft^2} = 736{,}050$$

$$Fo_1 = 4 \times \alpha \times (\tau_f - \tau_1)/d_b^2$$

$$Fo_1 = 4 \times 0.5 \frac{ft^2}{day} \times \frac{3680.25 - 3650}{\left(\frac{1.2}{12}\right)^2\ ft^2} = 6050$$

$$Fo_2 = 4 \times \alpha \times (\tau_f - \tau_2)/d_b^2$$

$$Fo_2 = 4 \times 0.5 \frac{ft^2}{day} \times \frac{3680.25 - 3680}{\left(\frac{1.2}{12}\right)^2\ ft^2} = 50$$

Using the calculated Fourier numbers and some interpolations, we can calculate the associated G values from the Table-1 as follows, G_f=1.1, G_1=0.75, and G_2=0.4.

Finally, by using ground thermal conductivity and calculated values for different G's, we can calculate the different effective thermal resistance of ground for annual, monthly, and daily pulses as follows:

$$R_{ga} = \frac{G_f - G_1}{k_g} = \frac{1.1 - 0.75}{0.8} = 0.4375\ h.ft.F/Btu$$

$$R_{gm} = (G_1 - G_2)/k_g = \frac{0.75-0.4}{0.8} = 0.4375\ h.ft.F/Btu$$

$$R_{gd} = \frac{G_2}{k_g} = \frac{0.4}{0.8} = 0.5\ h.ft.F/Btu$$

Example 2.5: Use the effective thermal resistances calculated in problem-3 above, to calculate the required length of vertical tubes for an office building using vertical tubing arrangement for a ground coupled heat pump system. The following information are known:

F_{SC} = short circuit heat loss factor = 1.04

PLF_m = part load factor during design month = 0.8

q_a = net annual average heat transfer to the ground = 150,000 Btu/h

q_{lc} = building design cooling block load = 355,000 Btu/h

q_{lh} = building design heating block load = 189,300 Btu/h

R_b = thermal resistance of pipe = 0.1 h. ft. °F/Btu

t_g = undisturbed ground temperature, = 55°F

t_P = temperature penalty for interference of adjacent bores = 4.3 °F

t_{wi} = liquid temperature at heat pump inlet = 85 °F (cooling); 45 °F (heating)

t_{wo} = liquid temperature at heat pump outlet = 96.4 °F (cooling); 39 °F (heating)

W_c = power input at design cooling load = 3,300 W

W_h = power input at design heating load = 2,500 W

Solution:

Input the given data in corrected Ingersoll and Zobel equations for cooling and heating will result in the followings:

$$L_C = \frac{q_a \times R_{ga} + (q_{lc} - 3.41 \times W_C) \times \left(R_b + PLF_m \times R_{gm} + R_{gd} \times F_{SC}\right)}{t_g - \frac{t_{wi} + t_{wo}}{2} - t_P}$$

$$L_C = \frac{-150{,}000\,\frac{Btu}{h} \times 0.4375\ \ h.ft.\frac{F}{Btu} + \left(-355{,}000\,\frac{Btu}{h} - \frac{\frac{3.41 Btu}{h}}{W} \times 3{,}300\ W\right) \times (0.1\ \text{h. ft. °F/Btu} + 0.8 \times 0.4375\ h.ft.F/Btu\ \ + 0.5\ h.ft.F/Btu\ \ \times 1.04)}{55 - \frac{85 + 96.4}{2} - (-4.3)}$$

$$= \ 10{,}830\ ft$$

$$L_h = \frac{q_a \times R_{ga} + (q_{lh} - 3.41 \times W_h) \times \left(R_b + PLF_m \times R_{gm} + R_{gd} \times F_{SC}\right)}{t_g - \frac{t_{wi} + t_{wo}}{2} - t_P}$$

$$L_h = \frac{150{,}000\,\frac{Btu}{h} \times 0.4375\ \ h.ft.\frac{F}{Btu} + \left(189{,}300\,\frac{Btu}{h} - \frac{3.41 Btu}{h} \times 2{,}500\ W\right) \times}{(0.1\ \text{h. ft. °F/Btu} + 0.8 \times 0.4375\ h.ft.F/Btu\ \ + 0.5\ h.ft.F/Btu\ \ \times 1.04)}$$
$$55 - \frac{39 + 45}{2} - (4.3)$$
$$= \ \ 20{,}910\ ft$$

The heating length is longer and therefore the deciding factor.

Example 3.6: For a large office building operating 5 days a week between 8 to 5 in Atlanta a ground coupled heat pump system is designed for providing building cooling and heating requirements. Cooling block load and heating block load of the building are 2,400,000 Btu/h and 2,800,000 Btu/h respectively, and the average cooling EER and average heating COP of heat pumps serving the building are 13 and 3.5 respectively. Calculate the net annual average heat transfer to the ground by this system. Use average low and high values for EFLH for cooling and heating.

Solution: By using equation 14 we have:

$$q_a = (C_{fc} \times q_{lc} \times EFL\ hours_C + C_{fh} \times q_{lh} \times EFL\ hours_h)/8760\ hours$$

or,

$$q_a = (1.26 \times 2{,}400{,}000 \times (950 + 1360)/2 + 0.77 \times 2{,}800{,}000 \times (480 + 690)/2)/8760\ hours\ = 542{,}691\ Btu/h$$

ASHRAE Application Handbook [4] specifies the advantages and disadvantages of horizontal design versus vertical design as being less expensive, no need for special contractors, no need for large drilling rigs, no contamination of aquifers, and low residual temperature effect, and larger land requirement, and more chance for damaging of other utilities.

ASHRAE Application Handbook [4] offers a simple pipe design for residential buildings. ASHRAE has tabulated some approximated length of trench (horizontal) or bore (vertical) per ton for residential buildings.

The in-depth engineering calculations for piping and associated pumping for different types of bore installation are beyond the scope of this book. For a detailed discussion for designing both vertical bore and horizontal trench network refer to 2007 ASHRAE Application Handbook [4].

4.8 Intermediate and Low Temperature Direct Use Applications

In the areas where geothermal water with minimum of 70 F is available, such resources can be used directly for heating homes or offices. They also can be used for domestic water heating, growing plants, and warming water, or for other industrial uses. One of the direct uses of these resources is utilizing under roads piping in cold environments to melt ice and snow. They also can be utilized for district heating applications. Cooling using geothermal direct-use systems can be done with the help of absorption chillers. [1]

One important target when designing direct-use systems is to capture the maximum heat possible for every gallon of water pumped to keep the cost reasonable, since the pumping cost is one of the main operating costs of the system. Keeping the pumping cost low requires achieving better temperature differences, and higher efficiency pumps and of course the rest of the systems and equipment throughout the production to disposal of the operating water. A complete direct-use system contains four major sub-systems, each with its special needs and design considerations. The first sub-system is the production system. This system includes production wellbore and the associated wellhead equipment. Since there might be significant distance between the point of use and the point of production of direct-use geothermal energy, the distribution part may or may not be complex. The second sub-system of a direct-used geothermal system is, therefore, the transmission and distribution system from point of production in the site, to the point of use. The third system is the user sub-system. The user equipment must be compatible with the product of the direct-use system as well. The final sub-system of direct-used geothermal systems is the disposal system. The disposal sub-system can be either injection back to the wells, or release of the surface depending on the distance between the production site and end-use customers. It can be seen now that important factors affect the cost of the total direct-use geothermal systems. Factors such as well depth, flow rate, available geothermal fluid temperature, distance between the point of production and point of use, ease of disposal, etc. [4]

Along with the pumping that is the most expensive part of the operation cost, the cost of the well itself is also one of the most expensive portions of the overall system, and it increases as the accessible fluids are located deeper under the ground. One of the other important issues that needs to be considered for designing direct-use systems is the composition of geothermal fluid. The composition of the geothermal fluid affects the material used throughout the system. The direct-use fluids generally contain many chemical elements such as oxygen, hydrogen ion, chloride ion, carbon dioxide, etc. that contribute to corrosion of the regularly used material in construction. Therefore, it requires testing and improvement which is costly as well. The composition of geothermal fluid also affects the disposal of geothermal fluid. [4]

4.9 Enhanced (Engineered) Geothermal Systems

A naturally available geothermal system, generally known as hydrothermal system, requires three basic elements to let humans generate electricity from these resources. The elements are heat, fluid, and permeability. Permeability is the fact that there is pathway for the liquid to move freely between the underground hot rocks and absorb heat from these resources. Enhanced (Engineered) geothermal systems (EGS) are human assist geothermal energy. In other words, there is a need for some engineering to let the available energy under the ground be accessible. In locations that hot rocks are available under the ground, but they are so solid and large that would not allow easy movement of liquid through these rocks, engineers use EGS. In this system, high pressure water is injected deep underground under controlled conditions to help the existing cracks in the rocks to open, and allow permeability and therefore, free movement of water between the hot rocks. Pumps are used to bring hot water from these newly generated reservoirs and are used to generate electricity. [1]

Introduction to Bioenergy

4.10 Biomass

Consumption of renewable energy in the United States is the highest in history, contributing to energy security, greenhouse gas reductions, and other social, economic, and environmental benefits. The largest single source of renewable energy is biomass, representing 3.9 quadrillion of 9.6 quadrillion British thermal units (Btu) in 2015 (EIA 2016). Biomass includes agricultural and forestry resources, municipal solid waste (MSW), and algae. [20] The source of biomass energy is living organisms, such as plants, wood, and waste, which all got their original energy from the sun. "Biomass-based energy as a composite category of wood (23%), waste (5%), and biofuels (21%) contributes 50% of 2014 consumption." [20]

$CH_{1.4}O_{0.6}$ is the chemical formula for the combustible portion of biomass. Common feedstocks of biomass are trees, forest residues, grasses, agricultural crops, agricultural residues, animal waste, and municipal solid waste. "Biomass energy currently costs $0.09/KWh but could eventually be as low as $0.05/KWh" [19]. With the help of the sun's energy, plants perform the process of photosynthesis in which carbon dioxide and water will be converted to carbohydrates. The energy that is stored in carbohydrates later can be released by burning them. The process of burning carbohydrates delivers heat that can be used in industry, for generating electricity, or for other purposes. "Industry is the biggest user of biomass. 61% of biomass energy is used by industry, 17% goes to the production of electricity, and 13% is used in homes and the rest going to other applications" [19]. Carbohydrates can be processed to generate biofuel. To produce biofuels the rigid structure of the plant cell wall needs to be broken down first. This can be accomplished either through high temperature deconstruction or low temperature deconstruction. High temperature deconstruction uses high heat and pressure to break down solid biomass into liquid or gas intermediates. During low temperature deconstruction biological catalysts such as enzymes are used to break down biomass into intermediates. This opens the structure of biomass and lets the polymers become exposed and then broken down into simple sugar building blocks during hydrolysis process. [18] After deconstruction, produced crude bio-oils, syngas, sugar, and other structures through biological or chemical processes will be upgraded to

produce final products. "Microorganisms, such as bacteria, yeast, and cyanobacteria, can ferment sugar or gaseous intermediates into fuel blend-stocks and chemicals. Alternatively, sugars and other intermediate streams, such as bio-oil and syngas, may be processed using a catalyst to remove any unwanted or reactive compounds in order to improve storage and handling properties." [18]

Thermal conversion process is commonly used to burn, dehydrate, and stabilize biomass stocks, such as scraps from paper or lumber mills. Other methods such as direct-firing, co-firing, and anaerobic decomposition are also common methods.

Lewandowski et al. [12] categorizes the different methods of thermal biomass conversion to the following processes based on the temperature and amount of oxygen involved in thermal decomposition of biomass.

Hydrothermal carbonization (HTC) (180-250 °C) + hot pressurized water

$$CH_{1.4}O_{0.6} + H_2O \rightarrow hydrocarbon\ (solid\ fuel) + gaseous\ and\ liquid\ residues$$

Torrefaction: Biomass (200-300 °C) →30% (gases + volatiles) +70% torrefied biomass

$$CH_{1.4}O_{0.6} \rightarrow C_{0.7}\ H_{1.0}O_{0.4}\ (solid) + C_{0.3}\ H_{0.4}O_{0.2}\ (gasses)$$

Slow pyrolysis (carbonization): Biomass + O_2 (a small amount at the beginning) (280-550 °C) →biochar

$$CH_{1.4}O_{0.6} \rightarrow C + tar + 0.6\ H_2O + 0.1\ H_2\ and\ other\ gas\ products$$

Fast pyrolysis: Biomass (500-800 °C) →biochar + oil + flammable gas

$$CH_{1.4}O_{0.6} \rightarrow about\ 200\ different\ volatile\ compounds\ (oil, tar) + C + CO_2 + other\ flammable\ gases$$

Gasification: Biomass + O_2 (limited amount) (800-1000 °C) →flammable gas

$$CH_{1.4}O_{0.6} + 0.2\ O_2 \rightarrow CO + 0.7\ H_2\ (theoretically),$$

$$CH_{1.4}O_{0.6} + 0.4\ O_2 \rightarrow 0.7\ CO + 0.3\ CO_2 + 0.1\ H_2O + 0.6\ H_2\ (technically)$$

Supercritical steam gasification: Biomass + $H_2O \rightarrow CO_2 + H_2$

$$CH_{1.4}O_{0.6} + 1.4\ H_2O \rightarrow CO_2 + 2.1\ H_2$$

High temperature steam gasification: Biomass + H_2O (>1000°C) → $CO_2 + H_2$

$$C_mH_n + 2m\ H_2O \rightarrow m\ CO_2 + (2m + n/2)H_2$$

Combustion: Biomass + $O_2(stoichiometric\ amount) \rightarrow thermal\ energy + flue\ gas$

$$CH_{1.4}O_{0.6} + 1.05\ O_2 + (3.95\ N_2) \rightarrow CO_2 + 0.7\ H_2O + (3.95\ N_2)$$

One important picture that can be seen from the above chemical equations is the fact that as we move from HTC, and torrefaction method to pyrolysis, to gasification and finally to complete combustion, the required quantity of air (oxygen) to perform the process increases. "From an ecological standpoint, the least favorable process is the combustion of biomass, and therefore only devalued waste biomass originating, e.g., from municipal waste (RDF-Refuse-Derived Fuel) or from sewage treatment plants (screenings, activated sludge) should be utilized using this method. All other types of biomasses, both full-valued and waste, should be subjected to initial thermal conversion (torrefaction, pyrolysis, or gasification) before final combustion. As a result of this material or chemical recycling, many valuable products, semi-products, and chemical compounds are recovered, otherwise obtained through industrial syntheses, which are time- and work- consuming, more expensive, and negatively impact the environment" [12][13]

The idea behind torrefaction is to heat the biomass stock to a high enough temperature (200 to 300 °C) so the biomass would not be able to absorb any humidity and loses its capability of rotting. Through this process briquettes are developed that still contain about 90% of the original energy and are high energy density sources with very good storing capability. Briquettes are used in both direct and co-firing applications. Either they are burned directly to generate steam to run steam turbines and generate electricity or being used as a supplement fuel to a coal burning electricity generation system, they can help reducing the overall pollution associated with electricity generation processes. An important fact about biomass is that ":it contains little sulfur and nitrogen, so it does not produce the pollutants that cause acid rain." [19] Based on reference [12] torrefaction reactors can operate mechanically (auger (helix screw), rotary drum, ablative), gravitationally (multiple hearth furnace, turbo-dryer, moving compact bed), and pneumatically (torbed, fluidized bed).

In the pyrolysis method, biomass is burned without presence of oxygen (only a negligible amount at the beginning is required) to a temperature between 280 to 800° C, that changes the chemical structure of the biomass. "Pyrolysis thermal decomposition of biomass is a complex process in which the following reactions overlap; dehydration, isomerization, dehydrogenation, aromatization, charring, oxidation and others. These are accompanied by secondary reactions, e.g., thermal decomposition of water into water gas, cracking, syngas synthesis, condensation reactions etc." [12] The final products of this process are three different products that all can be used as a source of energy. The final products of pyrolysis process are pyrolysis oil (also known as bio-oil or biocrude), synthetic gas (syngas), and a solid residue called biochar. Both pyrolysis oil and syngas can be burnt to generate energy, and biochar can be used as a form of additive to enrich the soil. According to reference [12] pyrolysis reactors can operate pneumatically (fluidized bed, fixed bed), mechanically (auger, stirrer, rotary, ablative, rake conveyor), or gravitationally.

During gasification process, biomass stock is heated up to more than 800 °C. This extreme heat breaks down the molecules of the biomass to syngas and slag. During gasification process syngas become cleaned of pollution and can be used for electricity generation, and the slag that is a molten liquid can be used for making asphalt, and cement. "There are two types of biomass gasification: indirect (pyrolytic) gasification, which accompanies pyrolysis and is associated with secondary reactions of biomass thermal decomposition, and direct (specific) gasification, occurring due to steam reacting with the biochar." [12][13][14][15][16][7]. Reactors in which the gasification process occurs are either closed co-current or counter-current types.

Transportation of biomass due to its large volume is not profitable, therefore converting it by thermal conversion method that reduces its volume while keeping its energy is highly valuable as well.

4.11 Bioenergy

Biomass can be used for different bioenergy applications such as transportation and heat and power generation industries. Probably the most important application of biomass in bioenergy can be found in the transportation industry, because to the contrary of other renewable energy sources, biomass can be converted directly into liquid fuels "biofuels" to help meet transportation fuel needs. "The two most common types of biofuels in use today are ethanol and biodiesel, both of which represent the first generation of biofuel technology" [18]. Other bioenergy sources used in the transportation industry are biogases, and renewable gasoline blend-stocks and naphthas. "The current primary biomass sources for liquid transportation fuels are predominantly corn grain for ethanol and soybean oil for biodiesel. In general, technologies that convert accessible sugars via fermentation for corn grain and transesterification for soybean oil to transportation fuel for blending are referred to as "first generation."" [20]

Ethanol (CH_3CH_2OH) is a renewable fuel that can be produced from biomass. Ethanol can be used as a blending agent with gasoline. This can increase octane of the fuel. As a result, it can reduce carbon monoxide and other emissions. The most common type is E10 (10% ethanol, 90% gasoline) and is approved for use in gasoline powered vehicles up to E15 (15% ethanol, 85% gasoline). Most ethanol is made from plant starches and sugars such as corn starch. The common method for converting biomass into ethanol is fermentation, that during this process microorganisms such as bacteria metabolize plant sugars and produce ethanol. [18] The steps taken in conversion of biomass to ethanol are feedstock preparation, gasification, cleanup and conditioning the produced syngas, bioconversion, separation to produce ethanol.

Biodiesel is a liquid fuel produced from combining alcohol with vegetable oil and animal fat or recycled cooking grease. It can be blended with petroleum diesel in any percentage. Most common blend is B20 (20% biodiesel 80% petroleum diesel. [18] "The second-largest type of liquid transportation fuels is biodiesel from vegetable oils, fats, and greases. Soybean oil makes up a little more than 50% of the feedstock for biodiesel. At present, about 25% of U.S. soybean oil production is used for biodiesel." [20]

Based on a 2015 report [20] the current (in 2014) biobased fuel production from biomass resources (corn grain, vegetable oil, other fats, oils, and greases, feed for gasoline blend stock, naphtha, and landfill gas) is about 16,095.44 million gallons, with the largest amount (14,106.81 million gallons) is contributed by corn grain. Also based on the same report biomass consumed for fuel production from all those same resources is 127.17 million bioenergy equivalent dry tons, with the largest amount (119.55 million bioenergy equivalent dry tons) contributed by corn grain as well. The energy produced and resource consumption in this report is based on use of these resources for production of ethanol, gasoline blend-stock/ naphthing, jet/ aviation fuels, diesel/ heating oil, and biogas, CNG, and LNG.

Besides transportation industry, bioenergy contributes to heat and power generation industry as well. "The current primary biomass sources for heat and power are predominantly woody biomass and wood waste for home heating and for industrial use as fuel. Woody biomass/wood waste, the biogenic portion of MSW, and landfill gas also make contributions to the electricity sector. Animal manure can also be collected and converted to biogas via anaerobic digestion. This gas is recovered, treated, and used to generate energy for farm and wastewater treatment applications." [20] Based on 2015 report [20] total inherent energy of biomass resources (wood/ wood waste, animal manure, biogenic MSW, other waste biomass, and landfill) consumed for heat and power from were 1,580.2 TBtu and 695.8

TBtu for heating and electricity generation respectively, with the largest contribution given from wood and wood waste for both heat and electricity generation.

Another source of biomass used for electricity generation and heating is through landfills. "Landfill gas is generated by decomposition of organic material at landfill disposal sites. The average composition of landfill gas is approximately 50% methane and 50% carbon dioxide and water vapor by volume. The methane percentage, however, can vary from 40% to 60%, depending on several factors, including waste composition (e.g., carbohydrate and cellulose content). The methane in landfill gas may be vented, flared, or combusted to generate electricity or useful thermal energy on-site, or injected into a pipeline for combustion off-site. Landfill gas is primarily consumed in the electric sector. Estimates from the 2015 EIA Electric Power Annual indicate that in 2013, 239.5 bcf of landfill gas produced 10.5 billion kWh of electricity in the electric sector." [20]

Biogenic MSW can be used for electricity generation and heating as well. "Biogenic MSW consists of organic non fossil material of biological origin that is a byproduct or a discarded product. Biomass waste includes MSW from biogenic sources, landfill gas, sludge waste, agricultural crop byproducts, straw, and other biomass solids, liquids, and gases. It excludes wood and wood-derived fuels (including black liquor), biofuels feedstocks, biodiesel, and fuel ethanol. Biogenic MSW is primarily used in the electrical and industrial sectors. Estimates from the 2015 EIA Electric Power Annual indicate that in 2013, the electricity sector consumed more than 15.0 million dry tons of biogenic municipal waste to produce 8.5 billion kWh of electricity and 1.9 TBtu of thermal energy. The industrial sector was the largest consumer of waste biomass for thermal energy in 2013, using more than 8.0 million dry tons of various types of waste biomass to produce 25.2 TBtu of thermal energy." [20]

Finally, biomass can be used for electricity generation and heating by anaerobic decomposition. Anaerobic decomposition is a process where microorganisms, such as bacteria, break down material in the absence of oxygen. Anaerobic decomposition usually happens in landfills. In landfills biomass is crushed and decompressed and creates an anaerobic (oxygen poor) environment. An anaerobic environment helps biomass decay. This results in the production of methane, that is an excellent source of energy. In addition to landfills, decomposition can also be implemented on farms. Manure and other animal waste can be converted to sources of energy. "Anaerobic decomposition is a biological process that occurs when organic matter (in liquid or slurry form) is decomposed by bacteria in the absence of oxygen (i.e., anaerobically). The decomposition process releases biogas consisting of approximately 60% methane and 40% carbon dioxide. This gas can be recovered, treated, and used to generate energy, replacing traditional fossil fuels. Anaerobic digester systems can be installed successfully at operations that collect manure as a liquid, slurry, or semi-solid. Existing farms use a variety of different types of digester designs—such as anaerobic sequencing batch, complete mix, covered lagoon, fixed film, induced blanket, and plug flow reactors, and energy use technologies—such as boiler or furnace fuel, cogeneration, electricity generation, or flaring." [20]

Beyond transportation, and power and heat generation, other notable bioenergy applications are biobased chemicals, that can replace petroleum-derived chemicals, and wood pellets.

End of Chapter Problems:

1. A flash steam geothermal system is used to create electricity. Production well produces high pressure dry steam at 2.0 MPa, and 200°C (with enthalpy of h=852.26 kJ/kg). This steam then is flashed in a flash tank to reduce the steam pressure to 500 kPa and creates a mixture of vapor and liquid with quality of 10%). The exiting low pressure saturated vapor is then suitable for running the steam turbine. Saturated steam at 500 kPa (with enthalpy of h=2748.1 kJ/kg) then feeds the turbine, where generates power, and discharges from turbine at 15 kPa and 85% quality (with enthalpy of h=2,242.4 kJ/kg). For producing 1.2 MW power calculate the required mass of the high-pressure steam required from the production well. Assume no losses throughout the processes.
2. A supply of geothermal hot water and a heat exchanger is used as a source of energy in a binary geothermal cycle that uses R-134a as the working fluid. Saturated vapor R-134a leaves the boiler at a temperature of 90°C, and the condenser temperature is 44°C. Calculate the thermal efficiency of the Rankine cycle. The followings are known:
   Enthalpy of R-134a liquid leaving the pump = h2 = 117.32 kJ/kg
   Enthalpy of the R-134a at entrance to the pump = h1= 114.28 kJ/kg
   Enthalpy of the saturated vapor leaving the boiler = h3 = 277.11 kJ/kg
   Enthalpy of the mixture of vapor and liquid leaving the turbine = h4 = 255 kJ/kg
   Assume no losses throughout the processes.
3. A small vertical GCHP system is built of 600 feet long tube (4-150 feet pipes with a U-bend at the bottom). If the ground temperature at this location is 55 °F, and the average temperature of the liquid in pipes is 44 F, and the ground thermal conductivity is 0.5 Btu/ h. ft. °F, what is the amount of heat transferred through this system? Use the Ingersoll and Zobel steady-state equation.
4. Use Carslaw and Jager method to calculate the effective thermal resistance of ground (annual pulse), effective thermal resistance of ground (monthly pulse), and effective thermal resistance of ground (daily pulse), for a location in which thermal diffusivity of the ground is 0.5 ft^2/day and thermal conductivity of the ground is 0.75 Btu/ h. ft. °F. Use a tube with external diameter of 1.0".
5. Use the effective thermal resistances calculated in problem-3 above, to calculate the required length of vertical tubes for an office building using vertical tubing arrangement for a ground coupled heat pump system. The following information are known:
   F_{SC} = short circuit heat loss factor = 1.04
   PLF_m = part load factor during design month = 0.8
   q_a = net annual average heat transfer to the ground = 180,000 Btu/h
   q_{lc} = building design cooling block load = 385,000 Btu/h
   q_{lh} = building design heating block load = 219,300 Btu/h
   R_b = thermal resistance of pipe = 0.1 h. ft. °F/Btu
   t_g = undisturbed ground temperature, = 55°F
   t_P = temperature penalty for interference of adjacent bores = 4.3 °F
   t_{wi} = liquid temperature at heat pump inlet = 85 °F (cooling); 45 °F (heating)
   t_{wo} = liquid temperature at heat pump outlet = 96.4 °F (cooling); 39 °F (heating)
   W_c = power input at design cooling load = 3,400 W
   W_h = power input at design heating load = 2,600 W
6. For a large office building operating 5 days a week between 8 to 5 in Atlanta a ground coupled heat pump system is designed for providing building cooling and heating requirements.

Cooling block load and heating block load of the building are 2,600,000 Btu/h and 2,850,000 Btu/h respectively, and the average cooling EER and average heating COP of heat pumps serving the building are 11 and 4.0 respectively. Calculate the net annual average heat transfer to the ground by this system. Use average low and high values for EFLH for cooling and heating.

References:

[1] https://www.energy.gov/eere/geothermal/geothermal-basics

[2] https://en.wikipedia.org/wiki/Geothermal_gradient

[3] Rybach, Ladislaus (September 2007). "Geothermal Sustainability" Geo-Heat Centre Quarterly Bulletin Vol. 28, no. 3; Klamath Falls, Oregon: Oregon Institute of Technology pp. 2-7. ISSN 0276-1084. Achieved from the original on 2018-03-08, Retrieved 2018-03007.

[4] ASHRAE HVAC Applications Handbook, 2007. American Society of Heating, Refrigerating and Air Conditioning Engineers, Atlanta, Ga.

[5] Ingersoll, L. R. and A. C. Zoble, 1954, Heat conduction with engineering and geological application, 2nd ed., McGraw-Hill, New York.

[6] Carslaw, H.S. and J. C. Jaeger, 1947. Heat conduction in solids. Claremore Press, Oxford.

[7] Moon, H., and S.J. Zarrouk; "Efficiency of geothermal power plants: a worldwide review"; New Zealand Geothermal Workshop 2012 Proceedings; 2012; Auckland, New Zealand.

[8] Braud, H.J., Oliver,J., and H. Klimkowski, 1988. Earth Source Heat Exchanger for Heat Pumps, Geo-Heat Center Quarterly Bulletin, Vol. 11, No.1, (Summer), pp. 12-15.

[9] https://www.geothermal-energy.org/pdf/IGAstandard/ISS/2003Germany/II/5_1.lun.pdf

[10] Kavanaugh, S.P., and K. Rafferty, 1997. Ground-Source Heat Pumps, ASHRAE, Atlanta, Georgia, 167 p.

[11] https://help.looplinkpro.com/en/latest/examples/Equivalent_Full_Load_Cooling_and_Heating_Hours.pdf

[12] Lewandowski, W.M.; Ryms, M.; Kosakowski, W. Thermal Biomass Conversion: A Review. Processes **2020**, 8, 516. https://doi.org/10.3390/pr8050516. © 2020 by the authors. Licensee MDPI, Basel, Switzerland. This article is an open access article distributed under the terms and conditions of the Creative Commons Attribution (CC BY) license (**http://creativecommons.org/licenses/by/4.0/**)

[13] Hua, X.; Gholizadeh, M. Biomass pyrolysis: A review of the process development and challenges from initial researches up to the commercialization stage. *J. Energy Chem.* **2019**, *39*, 109–143. [**Google Scholar**] [**CrossRef**][**Green Version**]

[14] Reed, T.B.; Das, A. Handbook of Biomass Downdraft Gasifier Engine Systems. In *Solar Energy Research Institute under the U.S., Department of Energy Solar Technical Information Program*; The Biomass Foundation Press: Golden, CO, USA, 1988. [**Google Scholar**]

[15] Bain, R.L. Biomass Gasification Overview. In Proceedings of the Presentation in National Renewable Energy Laboratory, Golden, CO, USA, 28 January 2004. [**Google Scholar**]

[16] Geurds, M. Biomass gasification technologies status and applications. In Proceedings of the CTIT Conference, Hanoi, Vietnam, 18–20 September 2006. [**Google Scholar**]

[17] Bukar, A.A.; Oumarou, M.B.; Tela, B.M.; Eljummah, A.M. Assessment of Biomass Gasification: A Review of Basic Design Considerations. *Am. J. Energy Res.* **2019**, *7*, 1–14. [**Google Scholar**] [**CrossRef**]

[18] https://www.energy.gov/eere/bioenergy/biofuel-basics

[19] https://www.teachengineering.org/content/cla_/activities/cla_activity2_energy_sources_research/energy_source_fact_sheets.pdf

[20] U.S. Department of Energy. 2016. 2016 Billion-Ton Report: Advancing Domestic Resources for a Thriving Bioeconomy, Volume 1: Economic Availability of Feedstocks. M. H. Langholtz, B. J. Stokes, and L. M. Eaton (Leads), ORNL/TM-2016/160. Oak Ridge National Laboratory, Oak Ridge, TN. 448p. doi: 10.2172/1271651. http://energy.gov/eere/bioenergy/2016-billion-ton-report.

Chapter 5

Emerging Alternative Energy Harvesting Technologies

Valmiki Sooklal

5.1 Introduction to Emerging Alternative Energy Harvesting Technologies

Previously we discussed energy and considered some of the more established harvesting technologies such as wind and solar. In this chapter we will explore some of the emerging technologies that are being developed for energy harvesting. These include devices based on piezoelectric, thermoelectric and triboelectric energy generation.

Piezoelectric Energy

Certain crystalline materials are capable of generating an electric when subjected to mechanical deformation referred to as the direct piezoelectric effect. The converse is also true in that physical deformation will occur if the same material is exposed to an electric field (inverse piezoelectric effect). Piezoelectric energy harvesting devices typically feature low profile, flexible structures with long life spans, that use external forces such as wind or wave motion to generate energy. Depending on the size and configuration of the harvester, power levels can range from nW to W [1]. Table 6.1 compares some common piezoelectric materials that can be used in the construction of these devices.

Materials	Advantages	Disadvantages	Applications
Ceramics	Good piezoelectric, mechanical and thermal properties, ease of manufacturing	Toxic lead	General applications
Polymers	Good mechanical flexibility, fatigue life, higher chemical resistance	Lower piezoelectric coefficients than ceramics, smaller working temperature range	Wearable, biocompatible

Lead-free	Lead free, comparable piezoelectric properties with ceramics	Lower piezoelectric coefficients than ceramics, lower thermal stability, more difficult to fabricate	Environmentally compatible
Nanomaterials	Easy to form, biologically safe, low cost	Lower piezoelectric properties	Nanogenerators
Single crystals	Very good piezoelectric performance	Toxic lead, lower mechanical properties, higher cost	General applications

Table 5.1. Comparisons of common types of piezoelectric materials [2].

Polymers such as polyvinylidene fluoride and ceramics like lead zirconate titanate are among the most popular materials used in piezoelectric harvesting devices due to their performance and ease of manufacturing.

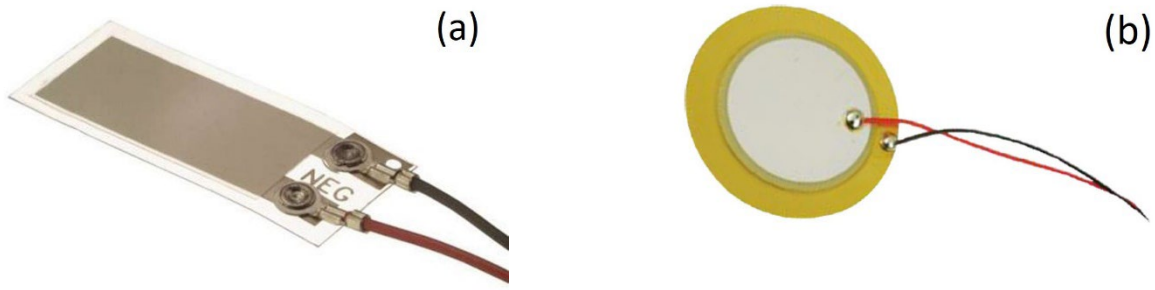

Figure 5.1: (a) Flexible piezoelectric transducer (image courtesy TE Connectivity) (b) Diaphragm piezoelectric transducer (image courtesy MulticompPro)

An example of a flexible and diaphragm piezoelectric transducer is shown in Figure 5.1.

5.1.1 Piezoelectric Modes of Operation

Some piezoelectric materials such as aluminum nitride and zinc oxide exhibit a direct piezoelectric response as dipoles exist without an electric field being present. If these dipoles are well aligned in a particular orientation referred to as a polar axis, the material produces a larger power output when deformed. For other materials, the dipoles are oriented randomly in the crystal and require reorientation using high electric fields at elevated temperatures to obtain an effective piezoelectric response. This process is known as poling. In the absence of an external force, the piezoelectric material exists in an equilibrium state between positive and negative electric charges or neutral state. When subjected to mechanical deformation, the crystals become electrically polarized as shown in Figure 6.2.

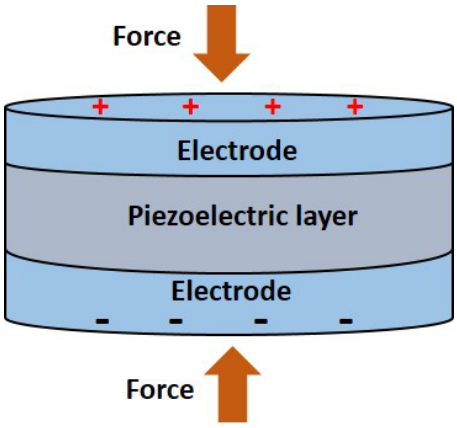

Figure 5.2: Sketch showing polarization of a piezoelectric transducer with external loading.

The direct and inverse piezoelectric effects [3] can be expressed as follows:

$$\text{Direct: } D = d\,\sigma + \varepsilon\,E \tag{5.1}$$

$$\text{Inverse: } \delta = s\,\sigma + d\,E \tag{5.2}$$

where δ is the strain, σ is the stress, E is the electric field intensity, D is the electric displacement, d is the piezoelectric coefficient, ε is the permittivity and s is the elastic compliance.

The most common modes of operation for a piezoelectric material are the 33-mode and 31-mode which are defined by the direction of the polar axis and force application. These will be subsequently described here.

33-Mode

In 33-mode, the polar axis of the piezoelectric device is oriented along the 3- direction. The applied stress is applied in a direction parallel to the 3-direction and at right angles to the polar axis as shown in Figure 6.3. This results in voltage being generated along the 3-direction.

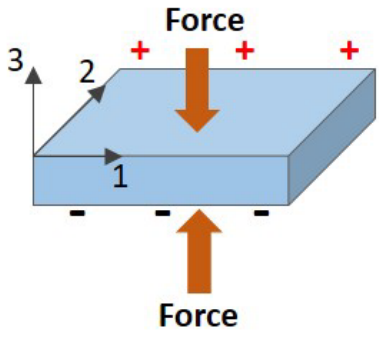

Figure 5.3: Piezoelectric material operating in 33-mode with external loading.

31-Mode

As with the previous mode, the polar axis of the piezoelectric device in 31 mode is also along the 3-direction. However, the applied stress in this case occurs along the 1-direction or perpendicular to the polar axis as shown in Figure 6.4. In 31-mode, the voltage is generate perpendicular to the applied force.

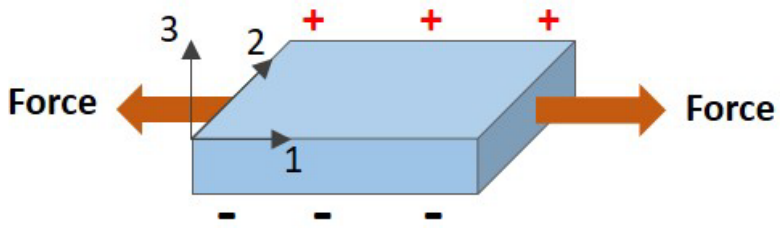

Figure 6.4: Piezoelectric material operating in 31-mode with external loading.

Mechanical-Electrical Energy Conversion

The open circuit voltage, V produced in 33 or 31-mode is given by

$$V = \frac{d_{ij}}{\varepsilon_r \varepsilon_0} \sigma_{ij} t \tag{5.3}$$

where $d_{ij}$is the piezoelectric coefficient

σ_{ij} is the applied stress

$\varepsilon_r, \varepsilon_0$ are the relative dielectric constant and permittivity of a vacuum respectively

t is the gap distance between electrodes

The subscripts ij, refer to the operating mode of the piezoelectric device. For example, in 33-mode the piezoelectric coefficient is d_{33} and the applied stress will be σ_{33}. Piezoelectric energy harvesters operating in 33-mode have higher piezoelectric coefficients (d_{33}) than those of comparable d_{31} devices and produce higher output voltages. However, harvesters operating in 31-mode have a smaller electrode distance (t), allowing them to produce a larger current output compared to 33-mode devices. Equation *** can be written in the form:

$$V = g_{ij} \sigma_{ij} t \tag{5.4}$$

where $g_{ij} = \frac{d_{ij}}{\varepsilon_r \varepsilon_0}$ and is known as the piezoelectric voltage constant.

The output electric power P, can be calculated as follows [4]:

$$P = \frac{1}{2} C V^2 \cdot f \tag{5.5a}$$

$$= \frac{1}{2} \cdot g_{33} \cdot d_{33} \cdot F^2 \cdot \frac{t}{A} \cdot f \quad (5.5b)$$

where C is the capacitance given by $\varepsilon_r \varepsilon_0 A/t$ and

f is the frequency of vibration

Example 5.1: A ceramic piezoelectric transducer measuring 30 mm long × 20mm wide with a thickness of 10 mm is subjected to an axial load F as shown in Figure 6.5.

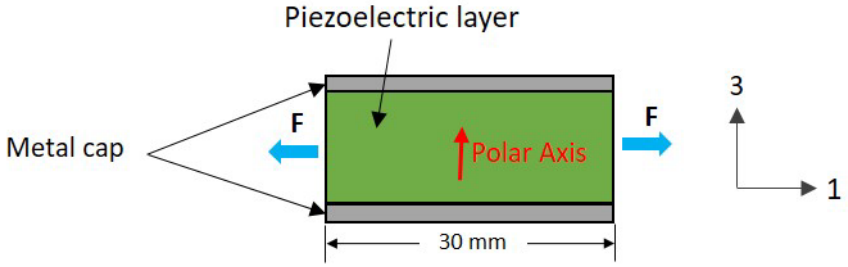

Figure 5.5: Sketch of a ceramic piezoelectric transducer.

Estimate the open circuit voltage produced if $F = 10N$. The transducer specifications are provided in Table 6.2 below

d_{33}(10^{-12} C/N)	d_{31}(10^{-12} C/N)	g_{33}(10^{-3} V m/N)	g_{31}(10^{-3} V m/N)
352	108	25	11

Table 5.2. Ceramic Piezoelectric transducer specifications

Solution:

Since the applied loading is in 1-direction, the device is operation in 31-mode. The stress can be found from:

$$\sigma_{31} = \frac{F}{A} = \frac{10N}{(0.02m)(0.01m)} = 50{,}000N/m^2$$

Using Eq. 5.4 the open circuit voltage is:

$$V = g_{ij}\sigma_{ij}t = g_{31}\sigma_{31}t = (0.011\,Vm/N)(50{,}000\,N/m^2)(0.01m)$$

$$= 5.5 \text{ Volts}$$

Example 5.2: The cylindrical piezoelectric transducer is used to harvest energy when subjected to a compressive load. The piezoelectric layer has a diameter of $20mm$ and a thickness of $1.2\ mm$. The polar axis oriented as shown in Figure 6.6.

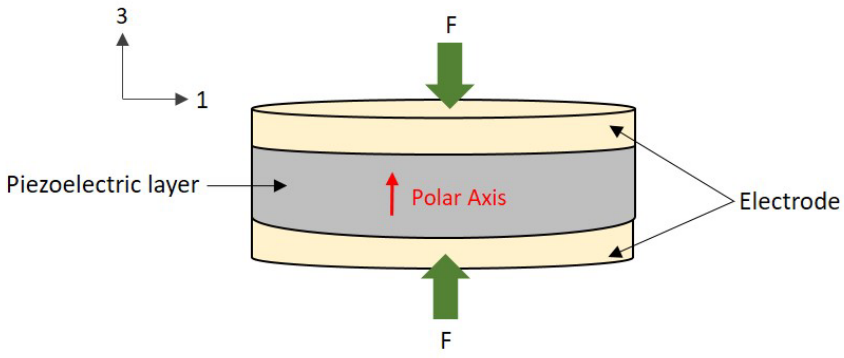

Figure 5.6: Sketch of a cylindrical piezoelectric transducer.

The operating load is 325 N applied uniformly to the upper electrode surface at a frequency of 2 Hertz. Determine the power output using Table 5.2 for the transducer specifications.

Solution:

The applied loading is in 3-direction, which means the device is operating in 33-mode. Using Eq. 5.5b

$$P = \frac{1}{2} \cdot g_{33} \cdot d_{33} \cdot F^2 \cdot \frac{t}{A} \cdot f$$

$$= \frac{1}{2} (0.025\, Vm/N)(352 \times 10^{-12} C/N)(325\ N)^2 \left(\frac{0.0012m}{\pi(0.01m)^2}\right) (2)$$

$$= 7.1\ \mu V$$

The stress is given by:

$$\sigma_{33} = \frac{F}{A} = \frac{325N}{\pi(0.025m)^2} = 165{,}521.14 N/m^2$$

The open circuit voltage is:

$$V = g_{ij}\sigma_{ij}t = g_{33}\sigma_{33}t = (0.025\, Vm/N)(165{,}521.14\, N/m^2)(0.0012m)$$

$$= 4.97 \text{ Volts}$$

5.1.2 Application Examples

The use of piezoelectric energy harvesting devices have continued to draw attention in recent times as an alternate means of power generation compared to conventional technologies such as wind and solar. Piezoelectric harvesting is a good solution for applications requiring high voltage, high energy density, high

capacitance and minimal mechanical damping. Power levels can range from mW to W when scaled for use in larger arrays such as in wave energy harvesting applications. There are four basic configurations [5] that can be used for energy harvesting applications namely the cantilever beam, circular diaphragm, cymbal and stack type.

The cantilever beam transducer can consist of one or two piezoelectric layers attached to a conductive non-piezoelectric layer as shown in Figure 6.7. with one end fixed to create a flexural mode of operation. They have been successfully used in wind energy harvesting, biomechanical applications to harvest energy from human motion such as walking, breathing and heartbeat and also wearable devices such clothing, gloves etc. They can also be used in oscillating structures such as buildings and bridges, automotive applications to harvest vibrational energy and aerospace applications such as wing deformation during flight.

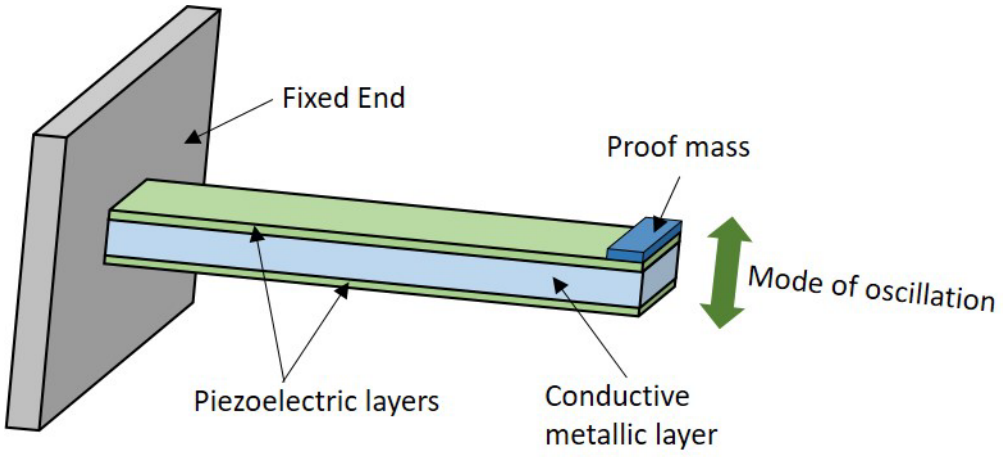

Figure 5.7: Sketch of a cantilever type piezoelectric transducer.

The circular diaphragm type of transducer consists of a thin disk-shaped piezoelectric layer that is attached to metal shims as shown in Figure 6.8. A proof mass can be attached to the diaphragm core to improve power output.

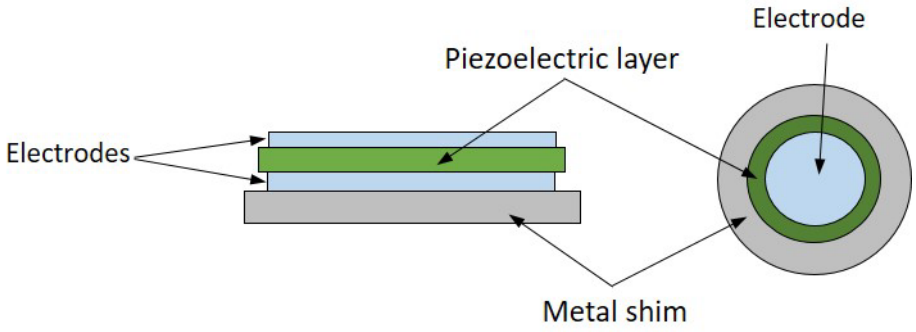

Figure 5.8: Sketch showing a circular diaphragm piezoelectric transducer.

Circular diaphragm transducers are stiffer than cantilever type and applications include use in pressure loaded systems such as the dynamic car pressure in car tires that can be used to power tire monitoring sensors and breathing apparatus for scuba equipment or firefighters to convert the fluctuating pressure to electrical energy to power a variety of instruments or sensors. They can also be used to harvest mechanical vibrational energy for example in high speed rail systems.

Cymbal type transducers have a piezoelectric layer placed between two metal caps that are coupled together as shown in Figure 5.9. When the metal caps are subjected to axial load, it is converted to a radial stress and amplified in the piezoelectric layer resulting in higher charge generation.

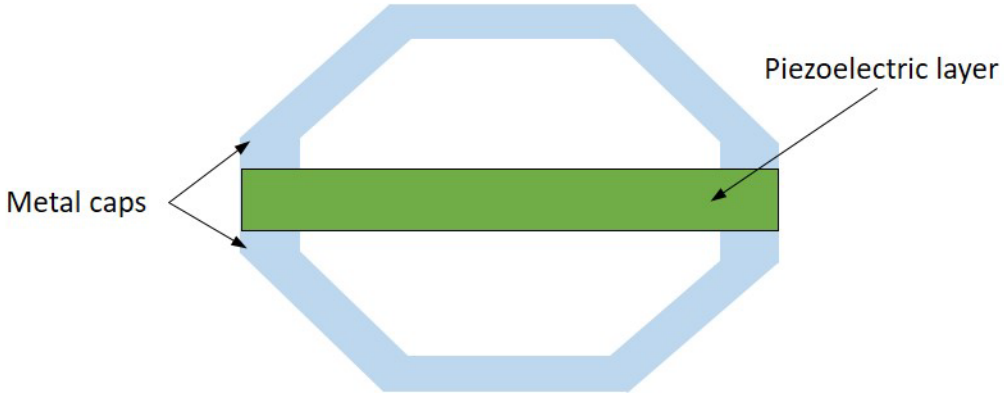

Figure 5.9: Sketch showing a cymbal piezoelectric transducer.

Cymbal transducers are preferable in high force/power output applications such as tiles on walkway and road surfaces [6].

The stack type piezoelectric transducer consists of multiple layers of piezoelectric material stacked on top of each other with electrode layers separating them as shown in Figure 5.10. The piezoelectric material is arranged such that the poling direction aligns with the applied load.

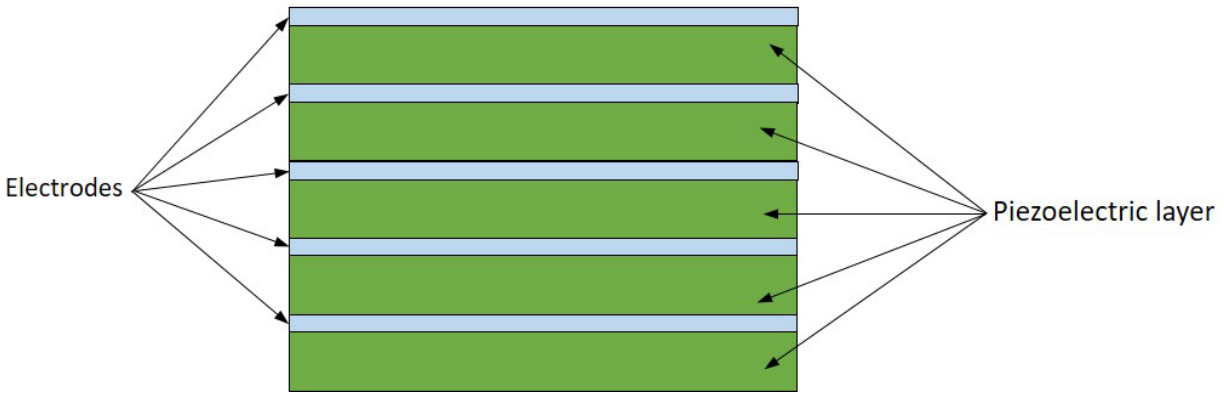

Figure 5.10: Sketch showing a stack piezoelectric transducer.

These types of transducers are used in high pressure/stress applications such as gun-fired munitions, vibratory motion from flight, underfloor energy harvesting from human and traffic motion and automotive suspension systems.

5.2 Thermoelectric Energy

When two dissimilar materials are joined together to create a loop and each junction is maintained at a different temperature, an electromagnetic force is generated around the loop. This is known as the Seebeck effect, and is the principle on which thermocouples operate. Thermoelectric energy harvesters use the same principle to convert heat into an electrical output. They are usually composed of semiconductors that allow the motion of charge carriers between two points that exhibit a temperature gradient. In n-type semiconductors, the charge carriers result from free electrons while in the p-type, the charge carriers are in the form of "free holes" due to missing electrons in the valence band. The basic structure of a TEG consists of both n-type and p-type semiconductors connected in series by a metal strip.

TEGs typically have outputs on the μW to mW ranges but can be scaled to kW values by combining multiple pairs of n-type and p-type semiconductors to generate the desired electrical output. Since they are solid state devices with no moving parts the offer several advantages such as being compact, zero greenhouse gas emission and can be mounted in any orientation. They also provide reliable and quiet operation.

5.2.1 Principle of Operation of Thermoelectric Generators

A thermocouple provides the basic constituents for a thermoelectric generator (TEG) and contains both n-type and p-type semiconductors that are connected by a metal conductor as shown in Figure 6.11.

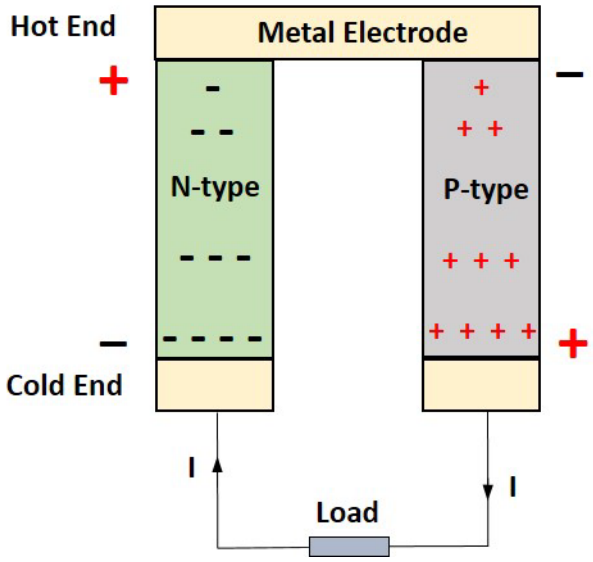

Figure 5.11. Sketch showing basic constituents of a thermoelectric generator.

Carriers on the hot end of the device have higher kinetic energy and consequently diffuse towards the cold end. Over time, the cold end with the p-type semiconductor becomes positively charged while the n-type cold end becomes negatively charged. At the hot end, the p-type semiconductor becomes positively charged and the n-type becomes negatively charged. The charge build up at the cold end results in an electromotive force ΔV, known as the Seebeck voltage, which is directly proportional to the temperature difference ΔT, existing between the hot and cold ends of the semiconductors. These can be related through introduction of the Seebeck coefficient S as follows [7]:

$$S = -\frac{\Delta V}{\Delta T} = -\frac{(V_{hot} - V_{cold})}{(T_{hot} - T_{cold})} \tag{5.6}$$

The Seebeck coefficient is a measure of the magnitude of the induced thermoelectric voltage due to the temperature difference between the two materials. The voltage is typically very low for most semiconductors (tens to hundreds of $\mu V/K$). To characterize the output of the TEG, we make use of the dimensionless figure of merit Z_T which is defined as follows:

$$Z_T = \frac{S^2 T}{\rho \kappa} \tag{5.7}$$

where $T = (T_{hot} + T_{cold})/2$ is the average temperature, ρ is the electrical resistivity and κ is the thermal conductivity. For a one-dimensional steady state heat transfer process with no heat losses through the device walls, the maximum thermo-electrical conversion efficiency of the TEG, $\eta_{TEG,max}$ can be estimated using:

$$\eta_{TEG,max} = \frac{T_{hot} - T_{cold}}{T_{hot}} \times \frac{(1+Z_T)^{1/2} - 1}{(1+Z_T)^{1/2} + \frac{T_{cold}}{T_{hot}}} \tag{5.8}$$

where $(T_{hot} - T_{cold})/T_{hot}$ is the Carnot efficiency. It should be noted that Eq *** works effectively for small temperature differences and assumes Z_T to be relatively constant over the range. The power generated by a TEG can be calculated using:

$$P_{TEG} = P_{transfer} \times \eta_{TEG} \tag{5.9}$$

where $P_{transfer}$ in Watts is the rate of heat transfer between the hot and cold sides of the TEG and is given by

$$P_{transfer} = \frac{T_{hot} - T_{cold}}{R_{TEG}} \tag{5.10}$$

where R_{TEG} [^{0}C/W] is the thermal resistance of the TEG.

Example 5.3: A bismuth-telluride TEG operates with the cold end at an ambient temperature of 24 ^{0}C with the hot end maintained at 59.6 ^{0}C and the cold end at 49.2 ^{0}C. The Seebeck coefficient is $-177\mu V/K$ for the n-type and $160\mu V/K$ for the p-type material. The electrical resistivity is $12.4\mu\Omega m$ for both materials and the thermal conductivity of the n-type is $1.4\ W/mK$ and $1.7\ W/mK$ for the p-type respectively. Determine the figure of merit.

Solution:

To find Z_T we can make use of Eq. 5.7 as follows

$$Z_T = \left(\frac{(S_n - S_p)^2}{(\rho_n \kappa_n + \rho_p \kappa_p)}\right) \times T$$

We first find T by converting the hot and cold end temperatures to Kelvin and using:

$$T = \frac{T_{hot} + T_{cold}}{2} = \frac{(332.75 + 322.45)K}{2} = 327.6\ K$$

On substitution of $S_n = -177\mu V/K$; $S_p = 160\mu V/K$; $\rho_n = \rho_p = 12.4\mu\Omega m$; $\kappa_n = 1.4\ W/mK$; $\kappa_p = 1.7\ W/mK$ in Eq. 5.7 we have:

$$Z_T = \left(\frac{((-177 - 160)\mu V/K)^2}{((12.4\mu\Omega m \times 1.4\ W/mK) + (12.4\mu\Omega m \times 1.7\ W/mK))}\right) \times (327.6\ K)$$

$=0.98$

Example 5.4: Determine maximum thermo-electrical conversion efficiency and estimate the power generated by the TEG in Example 6.3, given the thermal resistance is 3.95 ^{0}C/W.

Solution:

Using Eq. 6.8 and substituting for Z_T yields:

$$\eta_{TEG,max} = \frac{(59.2 - 49.2)°C}{59.2°C} \times \frac{(1 + 0.98)^{1/2} - 1}{(1 + 0.98)^{1/2} + \frac{49.2°C}{59.2°C}}$$

$$= 0.06$$

From Eq. 5.10

$$P_{transfer} = \frac{T_{hot} - T_{cold}}{R_{TEG}} = \frac{(59.6 - 49.2)°C}{3.95°C/W} = 2.63\ W$$

Substituting for $P_{transfer}$ in Eq. 6.9 we have

$$P_{TEG} = 2.63\ W \times 0.06 = 0.16\ W$$

5.2.2 Application Examples

TEGs have been gaining interest as a convenient method of recycling waste energy from heat sources and converting them to an electrical output. Their size and simplicity also make them attractive as a power source for wireless sensor networks. There are several possible applications for TEGs, and these can be divided into three categories based on the type of heat source namely (1) radioisotope, (2) natural and (3) waste heat sources. In this section we will consider natural and waste heat source examples [8].

Some natural heat sources that have employed TEGs for harvesting energy include natural gas, solar and the human body. TEGs have been used in the natural gas industry on offshore platforms, along pipelines, and gas wells and on the consumer side in devices such as propane camping stoves. Solar thermoelectric generators (STEGs) are designed to recover hear from solar radiation and convert it into electricity and can utilize optical concentration to focus sun rays or be of the non-concentrated type. Optical concentration sensors include cylindrical lenses, Fresnel lenses, parabolic mirrors and flat mirrors. Non-concentrated STEGS are limited to flat plate collectors and vacuum tubes. Some hybrid systems combine photovoltaic and thermoelectric systems to convert solar energy into electrical energy. The human body is a natural and stable heat source and wearable TEGs (WTEGs) have been incorporated into clothing, watch wrist bands, bracelets etc. These are good options for charging and powering small electronics like watches using the heat supplied by the body.

Waste energy heat sources provides many opportunities for energy harvesting using TEGs as large amounts of low grade waste energy is released into the environment. TEGs can be used for large scale industrial applications such as municipal wastewater and in plants that produce hot gases such as stone wool and cement manufacturing plants. They can also been used on the smaller scale in residential applications to

harvest waste heat energy from sources such as air conditioning systems and wood burning stoves/fireplaces. Automobiles are another area in which TEGs can be used to recover energy mainly from exhaust gases. TEGs have also been used in aircraft when integrated between the hot part of a propeller and the bypass flow of the cooler. They are also suitable for use on ships in high heat locations such as the main engine exhaust gas outlet line. It is estimated that a 2% gain in energy efficiency per year can be achieved from the installation of TEGs [9].

5.3 Triboelectric Energy

Have you ever taken off a fleece jacket, reached for a metal door knob and received a small jolt of static electricity? This phenomenon is known as the triboelectric effect in which a material becomes electrically charged after being in contact with a different material through friction. Although, the effect has been known for thousands of years, the mechanism behind triboelectrification is still being investigated. Generally, it is believed that when two different materials come into contact, a chemical bond is formed between some parts of the two surfaces (adhesion). Charges then move from one material to the other in order to equalize their electrochemical potential. These transferred charges can be either electrons or ions/molecules. When the materials are separated, some of the bonded atoms have a tendency to keep extra electrons, and some a tendency to give them away, possibly producing triboelectric charges on the surfaces. The presence of excess charges on the insulator surface can extracted in the form of electrical energy through the electrostatic induction effect. This is accomplished introducing an external circuit between the two surfaces to equalize the electric potential. Such devices, known as triboelectric nanogenerators (TENGs), have been used in the last decade in a variety of energy harvesting applications involving mechanical vibrations, human motion, ocean waves and wind flow [10].

5.3.1 Principle of Operation of TENGS

The operation of TENGs is based on a combination of triboelectric and electrostatic induction effects. There are four different modes in which an electrical output can be generated [11] which be discussed in the section.

Vertical contact-separation mode

The vertical contact-separation TENG is the most basic of the designs. It comprises two dissimilar dielectric materials in a parallel configuration, that make contact with each other. These dielectric surfaces each have a conductive electrode layer deposited on the top and the bottom of the stacked structure as shown in Figure 6.12. A physical contact between the two dielectric films creates oppositely charged surfaces. Once the two surfaces are separated by a small gap by the lifting of an external force, a potential drop is created. If the two electrodes are electrically connected by a load, free electrons in one electrode would flow to the other electrode to build an opposite potential in order to balance the electrostatic field. Once the gap is closed, the triboelectric charge-created potential disappears and the electrons flow back.

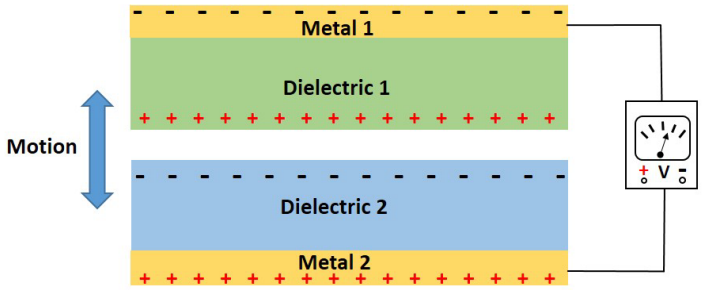

Figure 5.12: Vertical contact-separation TENG.

The typical working cycle for a TENG in the vertical contact-separation mode is shown in Figure 6.13. In the datum position (I) both dielectric materials are separated by a distance of $x(t)$. An external force is applied to press both surfaces together (II), resulting in the dielectic materials acquiring an opposite net surface charge σ. As the external force is reduced, the surfaces begin to separate by a distance d^* causing an electric potential difference to be created on the upper and lower surfaces (III). If the electrodes are connected an external load such as a voltmeter, free charges will flow between conductors to balance the electrostatic potential resulting in a current flow $\delta \mathrm{I}$ and a build up of opposite net free charges Q on the electrodes. From the fully released state (IV), as the surfaces begin to be pressed together again, an electric potential is again developed on the upper and lower electrodes with charges flowing in the opposite direction with an external load connected (V). The external force continues to be applied until the surfaces become pressed together again (II) and the process is repeated.

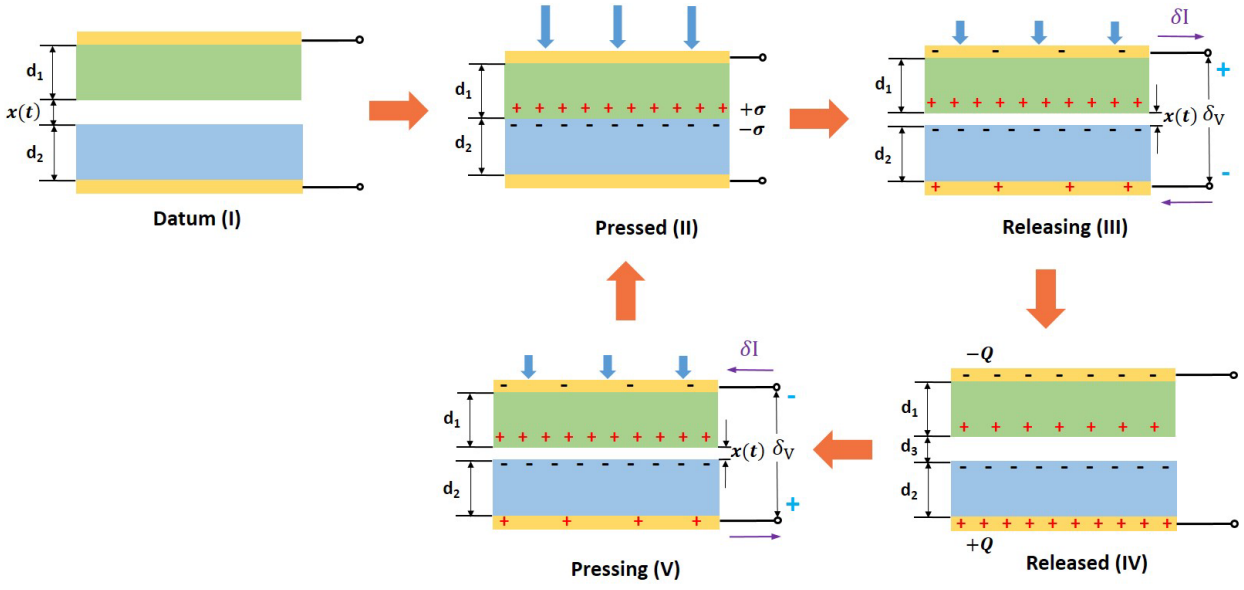

Figure 5.13: Principle of operation of a TENG in contact separation mode.

The vertical contact-separation is known for its design simplicity and easy of manufacture while being robust and providing high output power density [12].

We will consider the two-dimensional model considers shown in Figure 6.13. The two uniform and parallel dielectric layers have a surface area S, thicknesses d_1 and d_2 and dielectric constants ε_1 and ε_2 respectively and a separation distance $x(t)$, which varies depending on the magnitude of the externally applied force. The voltage generated in the contact separation TENG is given by

$$V = -\frac{Q}{S\varepsilon_0}\left(\frac{d_1}{\varepsilon_1} + \frac{d_2}{\varepsilon_2} + x(t)\right) + \frac{\sigma x(t)}{\varepsilon_0} \tag{5.11}$$

where Q is the amount of transferred charge between the electrodes, σ is the triboelectric surface charge density and ε_0 is the relative permittivity of a vacuum [13]. For the open circuit condition, $Q = 0$ and V_{OC} is given by:

$$V_{OC} = \frac{\sigma\varepsilon_0}{x(t)} \tag{5.12}$$

In the short circuit case $V = 0$ and the charge Q_{SC} is given by:

$$Q_{SC} = \frac{S\sigma x(t)}{(d_0 + x(t))} \tag{5.13}$$

where $d_0 = \frac{d_1}{\varepsilon_1} + \frac{d_2}{\varepsilon_2}$

Typical open circuit voltage and short circuit current graphs are shown in Figure 6.14, for a complete contact cycle.

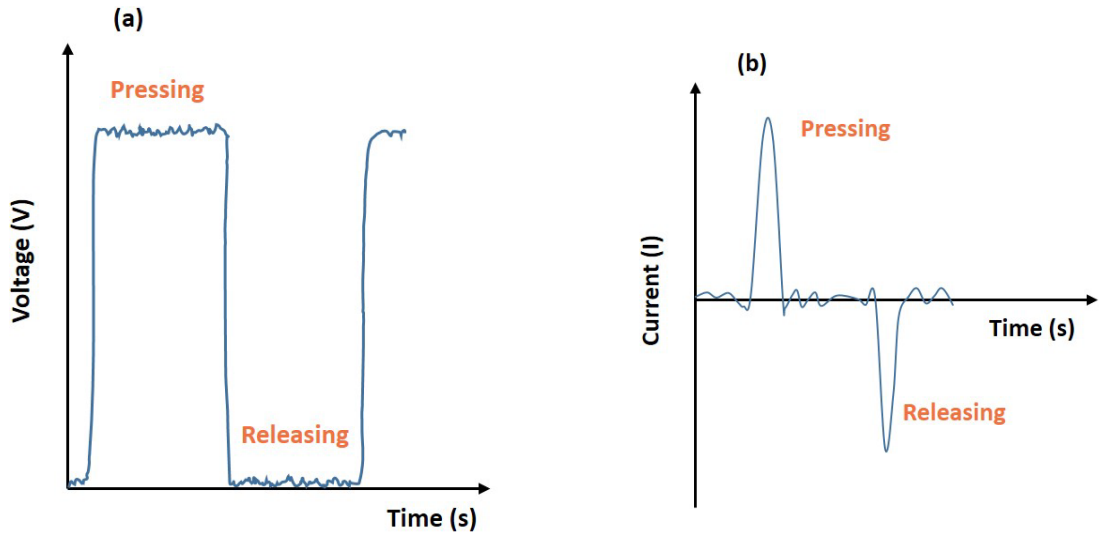

Figure 5.14: Graphs showing typical open circuit voltage and short circuit current for a complete contact cycle of operation for a vertical contact-separation TENG .

The output voltage varies linearly with displacement x and triboelectric surface charge density σ with the latter being the most important material parameter in terms of device performance.

Example 5.5: A triboelectric generator operating in vertical contact mode has a surface charge density of $33.6\mu C/m^2$ and a dielectric surface contact area of $4 \times 10^{-3}m^2$. Determine the short circuit charge as the distance of separation between plates approaches $6 \times 10^{-3}m$, given the following:

$\varepsilon_0 = 8.854 \times \frac{10^{-12}C^2}{Nm^2}$; $\varepsilon_{r1} = 7.1$; $\varepsilon_{r2} = 3.8$;

$d_1 = 0.2 \times 10^{-4}m$; $d_1 = 0.3 \times 10^{-4}m$

Solution:

Substituting to find d_0 from

$$d_0 = \frac{d_1}{\varepsilon_1} + \frac{d_2}{\varepsilon_2} = \frac{0.2 \times 10^{-4}m}{7.1} + \frac{0.3 \times 10^{-4}m}{3.8}$$

$$= 1.071 \times 10^{-5}m$$

From Eq. 5.13 we have

$$Q_{SC} = \frac{S\sigma x(t)}{(d_0 + x(t))} = \frac{(4 \times 10^{-3} m^2)(33.6 \times 10^{-6} C/m^2)(6 \times 10^{-3} m)}{(1.071 \times 10^{-5} m + 3 \times 10^{-3} m)}$$

$$= 2.67 \times 10^{-7} C$$

Contact-Sliding Mode

The components of this TENG are identical to those described in the vertical contact-separation mode. However, in this case the motion is characterized by relative sliding of the two dielectric films while they are in contact with each other as shown in Figure 6.15. This sliding motion results in a lateral polarization which drives electrons on the top and bottom electrodes to flow in order to completely balance the field created that was created by the triboelectric charges. An AC output is generated from the periodic sliding apart and return of the two dielectric films while contact is maintained. Although planar motion is depicted here, sliding can also occur from cylindrical rotation, or disc rotation.

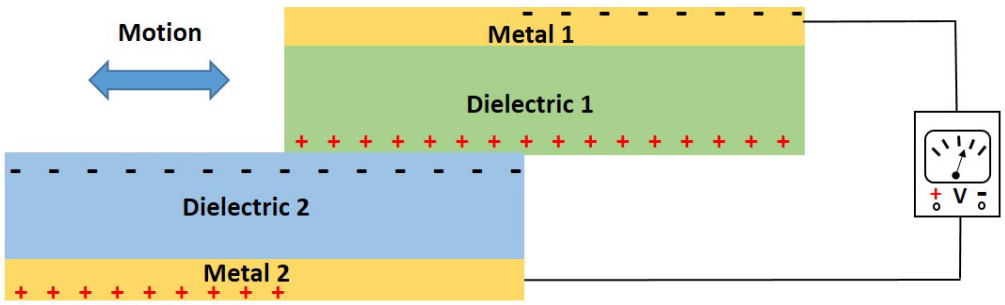

Figure 5.15: TENG operating in contact-sliding mode.

Single-electrode mode

In contrast to vertical contact separation and contact sliding modes that employ two electrodes connected by wires to an electrical load, single-electrode mode TENGs are composed of one primary electrode and a single free dielectric layer as shown in Figure 6.16. These devices are useful in applications where a moving surface is part of the TENG and cannot be connected by a wire or lead such as a person walking on a floor. In such cases, single-electrode mode TENGs, where the electrode on the bottom part of the TENG is grounded are a good option. As an object approaches or departs the fixed bottom TENG surface, electron exchange occurs between the bottom electrode and the ground to maintain the potential change of the electrode. In this mode energy harvesting can result from both contact-separation mode and contact-sliding mode.

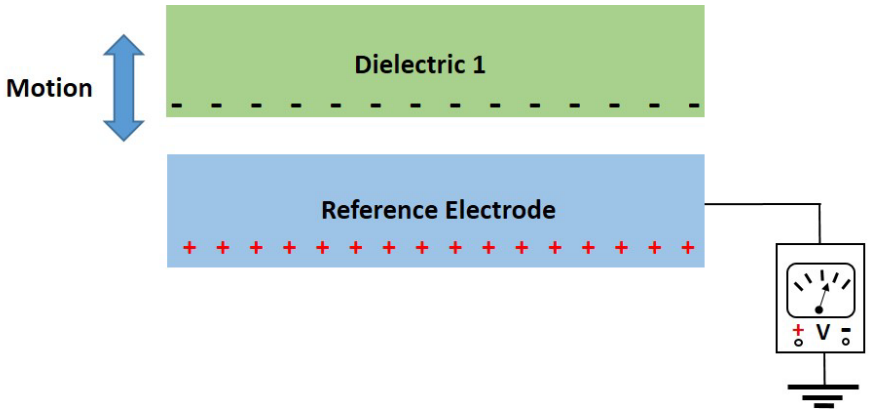

Figure 5.16: TENG operating in single-electron mode.

Freestanding triboelectric-layer mode

These devices are similar to the single electrode TENGs but consist of two electrodes separated by an air gap b, with a free standing dielectric layer located a distance d^* from the lower electrodes, as shown in Figure 5.17. A moving object becomes naturally charged due to contact with air or another object, such as our shoes being charged after coming in contact with the floors. The charges may remain on the surface for hours without any further contact or friction since the charge density has already reached a maximum. If the gap distance b,between the two electrodes are of the same order as the size of the moving object, the object's approach to and/or departure from the electrodes creates an asymmetric charge distribution in the media, which causes the electrons to flow between the two electrodes to balance the local potential distribution. The oscillation of the electrons between the paired electrodes produces power. The moving object does not have to touch directly the top dielectric layer of the electrodes so that, in rotation mode, free rotation is possible without direct mechanical contact; wear of the surfaces can be drastically reduced. This type of TENG is useful in harvesting energy in cases such as human walking or a moving automobile.

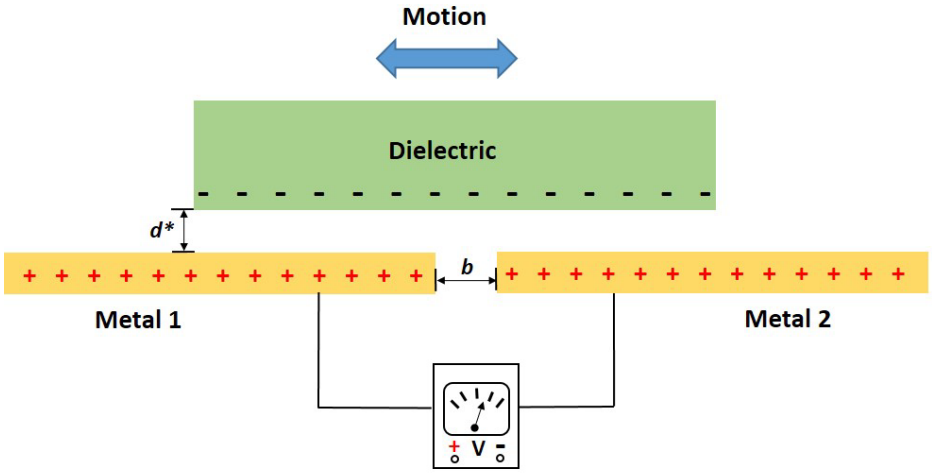

Figure 5.17: TENG operating in freestanding mode.

5.3.2 Application Examples

Within the last decade, TENGs have been used in several novel energy harvesting devices involving motion or mechanical vibration. It is useful to classify their generating capacity as micro or macro depending on power output. Figure 6.18 gives some examples of TENGs operating in vertical contact-separation mode. In these applications, two dielectric films are placed on opposing surfaces that are become pressed together when load is applied.

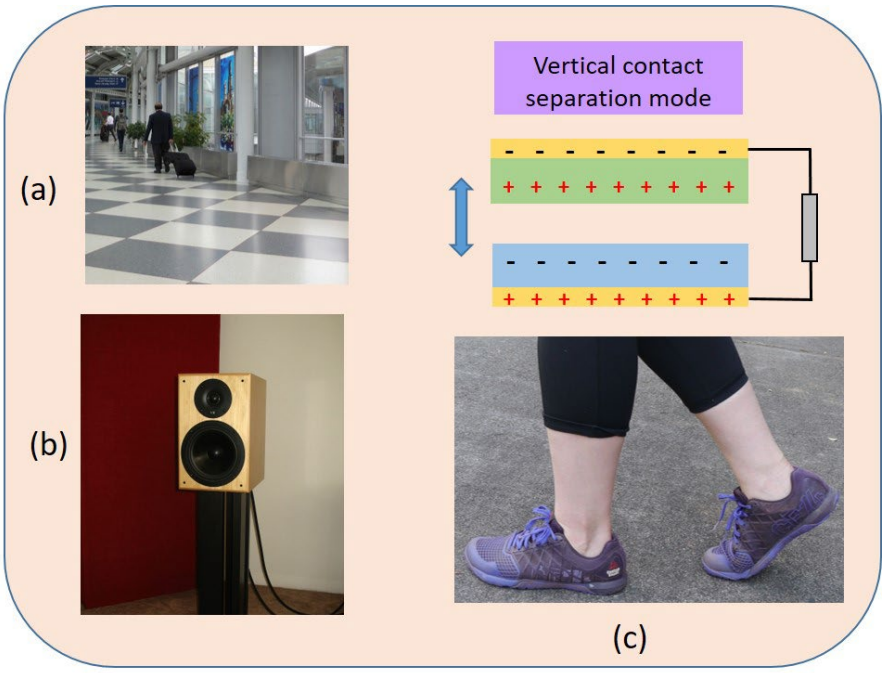

Figure 5.18: Examples of vertical contact-separation TENGs used in (a) Floor tiles (b) loudspeaker drivers and (c) within the soles of walking shoes.

Figure 5.19 gives some examples of the freestanding triboelectric mode applications. The shoe sole shown in Figure 5.19 (a) is made of a dielectric material becomes naturally charged from contact with the air and other objects. As the shoes contacts electrode patches which are embedded in the floor surface a current is produced. In Figures 5.19 (b) and (c) illustrates another example of the freestanding triboelectric mode where a dielectric such as the rotating car tire or train does not have to make mechanical contact with the road surface or track reducing potential wear of the surfaces. The dielectric may be part of the car tire or attached to the underside of the train and the electrodes are positioned at a set distance away such as on the track. Charge is produced as the dielectric approaches and leaves the electrodes.

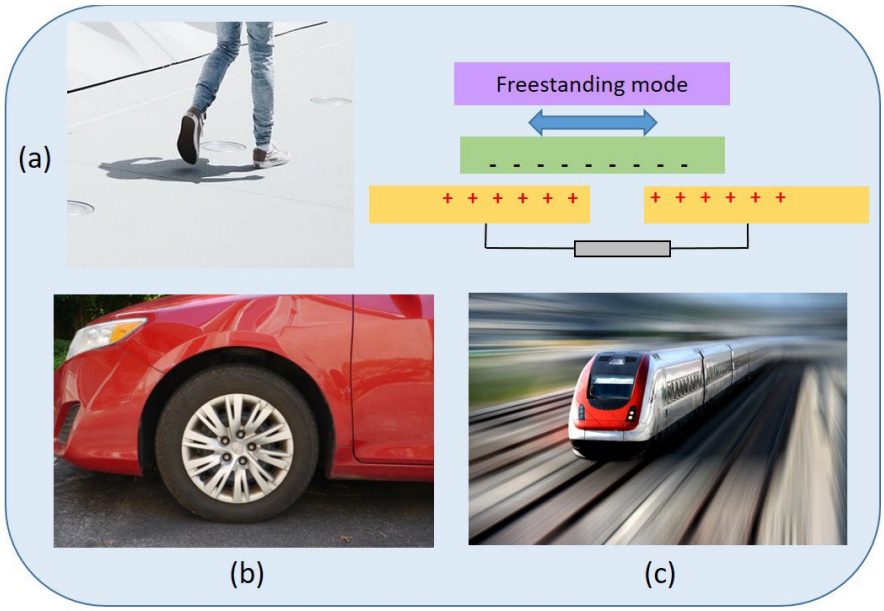

Figure 5.19: Examples of free standing TENGs used in (a) Shoe soles (b) Car tires and (c) Train underside.

More recent applications include wearable devices such as clothing in which the electrodes are in the form of fibers that are braided together with common fabrics such as yarn as shown in Figure 6.20. Both dielectric and conductive fibers are combined to produce the yarn from which clothing can be knitted. Micro power sources are capable of generating output power densities as much as 1200 Wm^1 for sliding and rotation based TENGs in applications such as vibrations from machines and structures and cell phone screens. Such applications are particularly useful for powering small electronic devices and sensors.

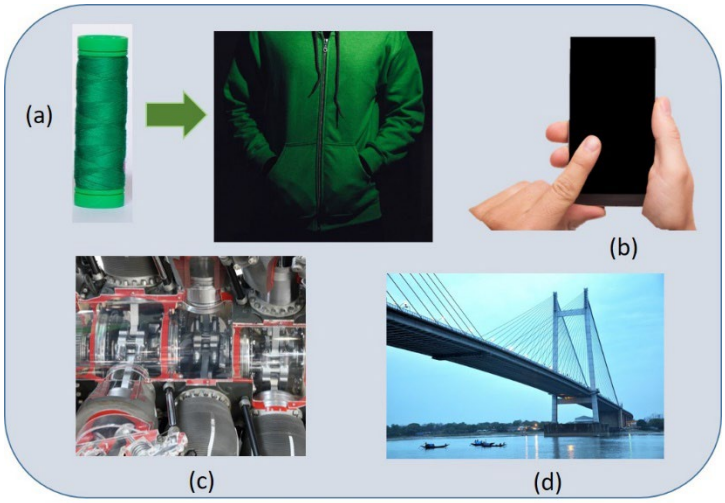

Figure 5.20: Energy harvesting applications for TENGs in (a) Composite yarn fibers used to produce clothing (b) single electron mode on cell phone touchscreen (c) machine vibrations (d) bridge structures.

On the macro scale contact-electrifications between liquid and solid surfaces and the packaged TENGs [14] can be used for energy harvesting from flowing water sources such as rivers and ocean waves. Although the energy produced be individual TENGs may be in the mW range , combining them in large arrays allows them to be scaled theoretically to produce kW power outputs [15].

References

[1] L. Zuo and X. Tang, "Large-scale vibration energy harvesting," *J. Intell. Mater. Syst. Struct,* vol. 24, no. 11, 2013.

[2] T. Li and P. S. Lee, "Piezoelectric Energy Harvesting Technology: From Materials, Structures, to Applications," Small Structures, vol. 3, 2022.

[3] I. Chopra, "Review of state of art of smart structures and integrated systems," AIAA, vol. 40, pp. 2145-2187, 2002.

[4] K. Uchino, "Piezoelectric Energy Harvesting Systems-Essentials to Successful Developments," Energy Technology, pp. 829-848, 2018.

[5] C. Covaci and A. Gontean, "Piezoelectric Energy Harvesting Solutions: A Review," Sensors, vol. 20, no. 12, 2020.

[6] J. Adhikari, R. Kumar and S. Jain, "Angular poling efect on cymbal piezoelectric structure using rhombohedral and tetragonal PMN-0.33PT for energy harvesting applications," Applied Physics A, vol. 128, no. 384, 2022.

[7] J. Cai and G. Mahan, "Effective Seebeck coefficient for semiconductors," Physics Rev. B-Condens Matter Mater. Phys., vol. 74, 2006.

[8] M. A. Zoui, S. Bentouba, J. G. Stocholm and M. Bourouis, "A Review on Thermoelectric Generators:Progress and Applications," Energies, vol. 13, 2020.

[9] T. Uyanık, E. Ejder, Y. Arslano˘glu, Y. Yalman, Y. Terriche, C.-L. Su and J. M. Guerrero, "Thermoelectric Generators as an Alternative Energy Source in Shipboard Microgrids," Energies, vol. 15, 2022.

[10] J. V. Vidal, V. Slabov, A. L. Kholkin and M. P. Soares dos Santos, "Hybrid Triboelectric-Electromagnetic Nanogenerators for Mechanical Energy Harvesting:A Review," Nano-Micro Letters, p. 13:199, 2021.

[11] Z. L. Wang, "Triboelectric nanogenerators as new energy technology and self-powered sensors – Principles, problems and perspectives," Faraday Discussions, p. 12, 2014.

[12] Z. L. Wang, J. Chen and L. Lin, "Progress in triboelectric nanogenerators as a new energy technology and self-powered sensors," Energy Environ. Sci., vol. 8, no. 8, p. 2250, 2015.

[13] M. Lasagni, P. Pavan, A. Bertacchini and L. Larcher, "Force Impact Effect in Contact-Mode Triboelectric Energy Harvesters: Characterization and Modeling," in IECON 2018 - 44th Annual Conference of the IEEE Industrial Electronics Society, Washington, 2018.

[14] Z.-H. Lin, G. Cheng, L. Lin, S. Lee and Z. L. Wang, "Water–Solid Surface Contact Electrification and its Use for Harvesting Liquid-Wave Energy," Angewandte Chemie International Edition, vol. 52, no. 48, pp. 12545-12549, 2013.

[15] H. Zhang, Y. Yang, Y. Su, J. Chen, K. Adams, S. Lee, C. Hu and W. L. Zhong, "Triboelectric Nanogenerator for Harvesting Vibration Energy in Full Space and as Self-Powered Acceleration Sensor," Advanced Functional Materials, vol. 24, no. 10, pp. 1401-1407, 2013.

[16] Y. Liu, J.-R. Riba, M. Moreno-Eguilaz and J. Sanllehi, "Application of Thermoelectric Generators for Low-Temperature-Gradient Energy Harvesting," Applied Sciences, vol. 13, no. 2603, 2023.

Chapter 6

Contemporary Power Systems and Distributed Generation

Yousef Mahmoud

6.1 Introduction to Contemporary Power Systems and Distributed Generation

The electric power system has been the largest available system in the last century. The U.S. power grid consists of over 7,300 power plants, over 200,000 miles of power lines transmitting power at high-voltage, and millions of low-voltage power lines, supplying power to 145 million customers throughout the country. Designing, controlling, and operating the electric power system is not an easy task and requires careful consideration and coordination among its various parts. For example, a constant struggle exists to balance the generated power with the delivered power, which varies with customer needs. Without maintaining this balance, the voltage and frequency of the supplied power can fluctuate, exceeding the allowable thresholds and posing a danger to customer equipment and apparatus connected to the grid.

Another challenge in operating any power system is ensuring that the power flowing through any transmission line does not exceed its capacity. With the expansion and diversification of power systems, designers must consistently verify that under all operating conditions and required loads, the power flowing through any line will not surpass the rating of the available line. This is referred to as the Power Flow Problem.

Electric power systems, like any other system, are susceptible to maloperation and faults. The majority of these faults are caused by the unintentional connection of any part of the system to the ground, resulting in large currents flowing from the grid to the ground before the protection system operates to isolate the faulted part. To ensure the effective operation of the protection system, designers should perform accurate calculations of the short-circuit current levels that could flow through the system in a process known as Short-Circuit Currents Calculation.

Beyond the existing challenges inherent in contemporary power systems, new complexities have arisen with the integration of emerging renewable energy resources like solar and wind power into the electric grid, a concept referred to as distributed generation. Renewable energy sources not only complicate power flow and short-circuit current calculations but also introduce challenges in power balancing, necessitating the resolution of complex situations for the efficient and safe operation of the power system. The protection of the system needs to be restructured with more complex considerations to account for the variable nature of renewable energy resources, which fluctuate with meteorological conditions. Similarly, maintaining stable

operation and a constant frequency becomes cumbersome due to the unpredictability of wind and solar resources, which can change rapidly.

This chapter will present and discuss a range of challenges and introduce the principles and foundations necessary to comprehend, analyze, and study electric power systems. It will encompass the fundamental components of power systems, the structure of modern power systems, basics of alternating current (AC) circuit analysis, three-phase systems, power flow analysis, and faults. The chapter will also delve into renewable energy systems and the challenges linked to their integration with the grid. Furthermore, it will provide a comprehensive discussion of energy storage systems as a promising ***Solution*** for the various challenges posed by distributed generation.

6.2 Contemporary Power Systems

Electric power systems are broadly comprised of three main components: generation, transmission, and distribution, as depicted in Figure 5.1. Generation stations play a crucial role by supplying electric power to be transmitted and distributed to customers. Typically situated far from urban areas close to fuel resources, these generation stations necessitate the transmission of the generated power through long-distance transmission lines. These transmission lines carry power at extremely high voltages, which can pose risks to human safety. As a result, transmission lines are not responsible for delivering power directly to end customers. Instead, distribution lines play the role of connecting the transmission lines to the end customers, operating at lower voltage levels and transmitting power from the transmission lines to customer loads. Figure 5.1 illustrates the three components of a power system: generation is represented in red, transmission lines in blue, and distribution lines in green.

As seen, the voltage levels are different at the generation, transmission, and distribution levels where transformers are used to change the voltages at each level. The voltage at the generation stations does not usually exceed 20 KV in large power stations for economic and efficient operation of the generators. Step-up transformers are used to increase the generation voltage to higher voltages (132 KV, 230 KV, 345 KV, 500 KV, or 765 KV). Higher voltages are the transmission level means lower power losses and more efficient transmission of electric power as will be illustrated in Example 5.1. Because the voltage of transmission lines is extremely high above 132 KV, it poses safety threats to human living in neighborhoods around the power lines. Therefore, the voltage of the transmission lines is reduced through step-down transformers to a lower level suitable for distribution inside neighborhoods. The voltage of the distribution system is usually 120 V or 240 V for residential customers but can be higher for large industrial loads. Sometimes, the distribution system consists of two or three stages where the voltage is reduced further in each step getting closer to residential loads.

Similar to any electrical system, the electric power system is not without its imperfections, leading to power losses that can compromise efficiency. Transmission and distribution lines encompass ohmic resistance, causing a portion of transmitted power to be converted into heat. This dissipated power can contribute to substantial losses in long-distance transmission lines, resulting in inefficient power transmission. To address this issue and enhance the efficiency of electric power transmission, transmission lines operate at significantly high voltages.

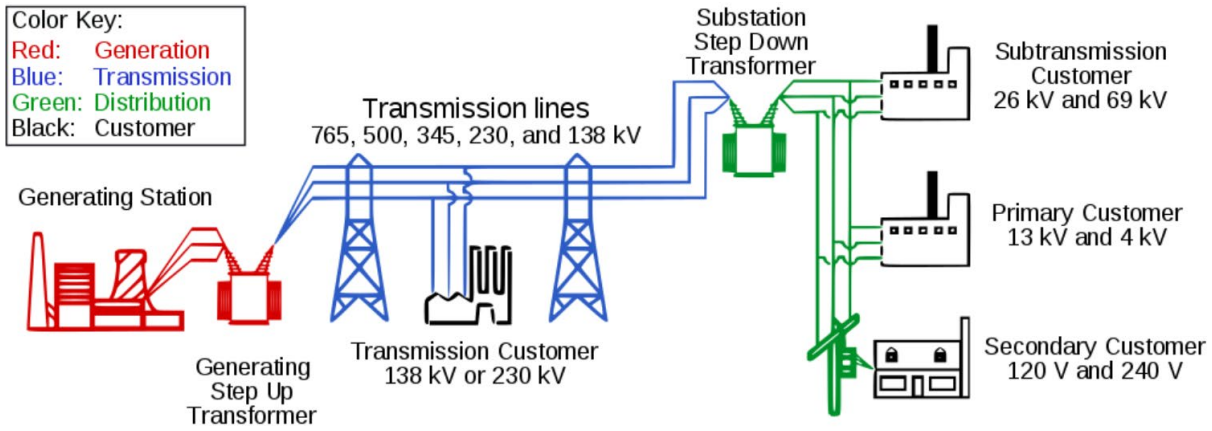

Figure 6.1: The Three Stages Of Transmitting And Distributing Electric Power

To illustrate this concept, consider a transmission line transmitting a power value denoted as *P*. As electric power, *P*, is the product of current, *I*, and voltage, *V*, higher transmission line voltages correspond to lower currents required to transfer the same amount of power, *P*. Given that power losses are directly proportional to the current, as indicated in equation (5.1), it becomes evident that transmission lines with higher voltage levels encounter reduced power losses. The following equation establishes the relationship between power losses in a transmission line and the current flowing through that line.

$$P_{loss} = I^2 * R_{line} \qquad (6.1)$$

where R_{line} symbolizes the ohmic resistance of the transmission lines. In conclusion, transmission line voltage is optimized to minimize power losses during transmission. Lower current levels associated with higher voltage settings, as illustrated in equation (1), lead to reduced power losses.

Another significant factor to consider is that distribution lines are generally much shorter than transmission lines, which cover vast distances, sometimes reaching hundreds of thousands of kilometers. Due to this disparity in length, the utilization of lower voltages in distribution lines does not lead to substantial power losses as it would in the case of transmission lines. As a result, the use of lower voltages in transmission lines does not necessarily result in significant power losses, in contrast to the situation with transmission lines.

Example 6.1:

Consider a transmission line linking a power generation unit situated in Austin, Texas to a distribution system located in Marietta, Georgia. This transmission line spans a length of 1,480 kilometers and possesses an ohmic resistance of 0.31 Ω per kilometer.

A – Calculate the power losses and the efficiency of the transmission line.

B- Repeat (A) if a step-up transformer is employed to raise the voltage of the transmission line to 765 KV.

Solution:

A- If 5 MW of power is being transmitted through the transmission lines at a voltage level of 120 kV, we can determine both the power losses in kilowatts (KW) and the efficiency of the transmission. Power losses can be calculated using the formula (5.1):

$$P_{loss} = I^2 * R_{line}$$

where I is the current and R_{line} is the resistance. Given that power (P) equals current (I) times voltage (V):

$$P = I * V$$

We can solve for I:

$$I = \frac{P}{V} = \frac{5\ MW}{120\ KV} = 41.6\ A$$

Substituting this value of I back into the power loss formula:

$$P_{loss} = I^2 * R_{line}$$

$$P_{loss} = 41.6^2 * 0.41 * 1480$$

$$P_{loss} = 1.050\ MW$$

The efficiency (η) of the transmission line can be calculated using the formula:

$$\eta = \frac{P - P_{loss}}{P} * 100\%$$

$$\eta = \frac{5 - 1.0501}{5} * 100\%$$

$$\eta = 78.9\%$$

B- Since the voltage V of the transmission line changed, the current transferred in the transmission line to transfer the same amount of power P will change accordingly. The new current I can be calculate as follows:

$$I = \frac{P}{V} = \frac{5\ MW}{765\ KV} = 6.5\ A$$

Substituting this value of I back into the power loss formula:

$$P_{loss} = I^2 * R_{line}$$

$$P_{loss} = 6.5^2 * 0.41 * 1480$$

$$P_{loss} = 25.6\ KW$$

Again, the efficiency (η) of the transmission line can be calculated using the formula:

$$\eta = \frac{P - P_{loss}}{P} * 100\%$$

$$\eta = \frac{5M - 25.6K}{5M} * 100\%$$

$$\eta = 99.4\%$$

Significantly noticeable is the substantial reduction in power losses that occurs as the voltage of the transmission lines is elevated through the transformer, increasing from 120 kV to 765 kV. The power underwent a remarkable decrease of 40-fold, plummeting from over 1 MW to under 26 kW. Consequently, this shift contributes to a substantial efficiency increase for the transmission lines, surging from 78.9% to an impressive 99.4%.

6.3 Components of Contemporary Power Systems

The primary objective of an electric power system is to guarantee the consistent delivery of electric power that caters to fluctuating customer demands. To fulfill this aim of generating dependable electric power, transmitting it across regions, and distributing it to end-users, an array of components is essential. Among the various components, the pivotal constituents of an electric power system encompass generators, transformers, transmission lines, and loads.

6.3.1 Power Generators

Power generators stand at the heart of electric power systems, taking on the responsibility of generating the necessary electric power and infusing it into the electric grid to meet fluctuating demands. Given the principle of power conservation—where power cannot be spontaneously generated anew—generators serve to convert power from various forms into its electric form. In contemporary electric power systems, the predominant method of this conversion involves transforming mechanical power into electric power through the use of electric power generators, as illustrated in Figure 5.2.

The process becomes more obvious when examined in a more detailed diagram, showcased in Figure 5.3. Here, the steps of electric power conversion via steam turbines are illustrated. The generation of mechanical energy frequently relies on steam turbines, which leverage heat to produce mechanical energy by boiling water and generating high-pressure steam. This steam, in turn, propels the rotation of turbine blades. Heat can be supplied to these steam turbines through the combustion of fossil fuels like gas, petroleum, or coal. Alternatively, heat can be generated through nuclear reactions in nuclear power generation.

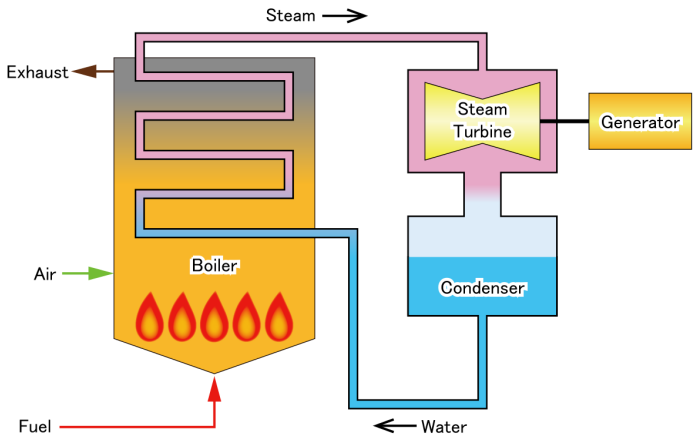

Figure 6.2: HLGH-EVEL diagram showing a steam power plant

"Illustration of Steam power generation" by Σ64 is licensed under CC BY 4.0

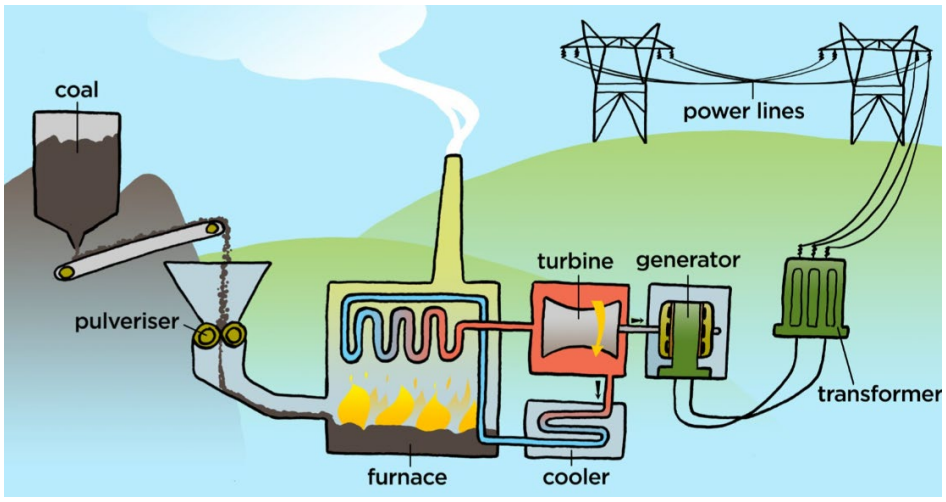

Figure 6.3: The components of a steam power plant

"Coal powerstation" by Siyavula Education is licensed under CC BY 2.0

Electric generators are available in a variety of types and constructions, yet the most frequently utilized type in power systems is synchronous generators. Other types, such as permanent magnet generators and induction generators, also exist. This section delves into the construction and operation of synchronous generators, which, like other electric generators, is a key element of power generation.

Synchronous generators are generally composed of two major parts: the stationary stator and the rotating rotor, as depicted in Figure 5.4. The rotor is equipped with a magnet featuring constant magnitude and rotating direction. When the rotor shaft is set into motion through the steam turbine, it generates a rotating magnetic field characterized by a consistent magnitude.

The stator is equipped with wound coils that facilitate the conversion of the rotating magnetic field produced by the rotor into currents, in accordance with Faraday's principle. As per Faraday's law, the presence of a varying magnetic field within a coil induces a current. Given that the magnetic field is both rotating and altering in direction, it leads to the induction of currents within the stator coils, as exemplified in Figure 5.5. This figure illustrates the voltage waveform and the principle of the rotating magnetic field alongside the three coils of the stator. Notably, this process results in the generation of a three-phase voltage waveform.

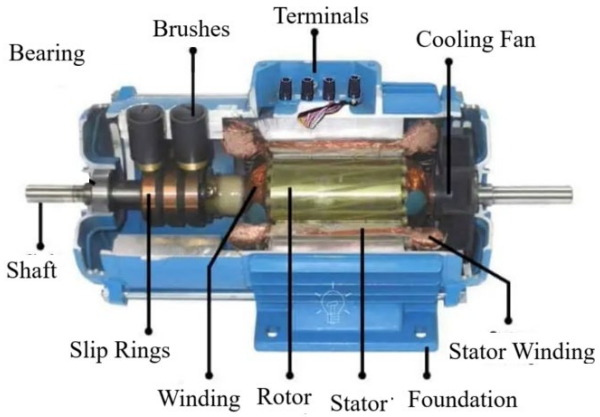

Figure 6.4: The construction of synchronous generators

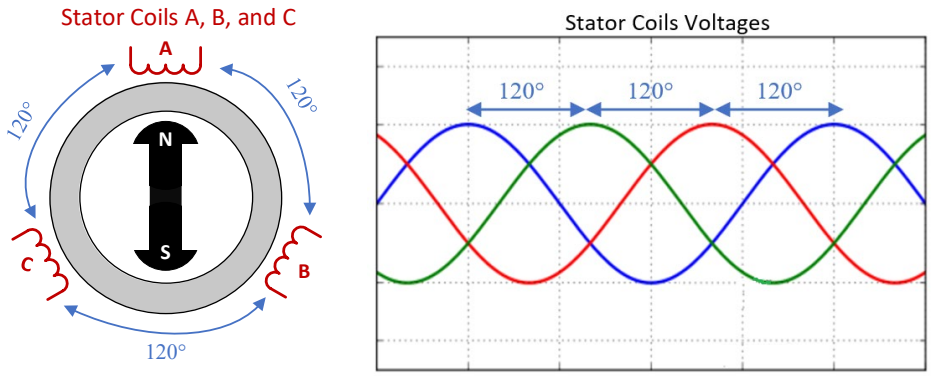

Figure 6.5: generation of voltage waveforms in synchronous generators

It is worth noting that while steam turbine-based power stations driven by steam turbines are the prevailing choice in modern power systems for supplying power, there are emerging alternatives such as solar systems and wind turbines. Wind turbines employ electric generators, which are rotated by wind energy. On the other hand, solar modules generate electricity by directly converting sunlight into useful energy, bypassing the need for electric generators, as discussed in previous chapters.

6.3.2 Transformers

Transformers stand as one of the pivotal devices that form the backbone of electric power systems. These devices play a crucial role in power systems by facilitating the conversion of voltage levels, as previously elucidated. They possess the capability to either amplify or attenuate voltage, functioning as either step-up or step-down transformers based on the specific application.

Typically, a transformer consists of a magnetic core and two coils wound around this core, as depicted in Figure 5.6. The ratio between the number of turns in the primary coil and the secondary coil determines the relationship between the input and output voltage. This relationship is governed by the following formula:

$$\frac{V_{primary}}{V_{secondary}} = \frac{N_{Primary}}{N_{Secondary}} \tag{6.2}$$

Here, $V_{primary}$ and $V_{secondary}$ denote the input and output voltages, respectively, while $N_{primary}$ and $N_{secondary}$ represent the number of turns in the primary and secondary coils, respectively. As shown in equation (5.2), when the number of turns in the secondary coil surpasses that in the primary coil, the transformer functions as a step-up transformer. Conversely, if the number of turns in the secondary coil is fewer than that in the primary coil, the transformer operates as a step-down transformer.

Transformers play an essential role in the transmission and distribution of electric power. Their primary function revolves around elevating the voltage for transmission between different regions. This elevation of voltage is tantamount to transmitting power at lower current levels, considering that power results from the multiplication of current and voltage, as previously discussed. Transmitting power at reduced current levels substantially curtails power losses resulting from the resistance of transmission lines, given that power losses are contingent on current as was illustrated in previous sections.

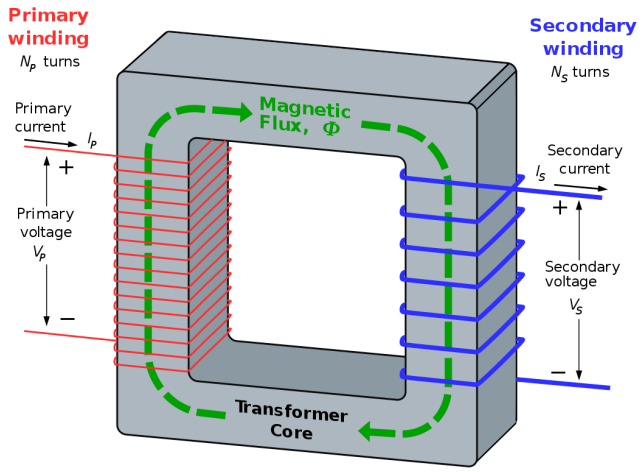

Figure 6.6: The Main Compoenets Of Transformersa

"Idealised single-phase transformer also showing the path of magnetic flux through the core" by BillC is licensed under CC BY-SA 3.0

The operation principle of transformers can be elucidated through Faraday's law. The flow of current within the primary coil generates a magnetic field in the core, thereby inducing current within the secondary coil. This electric current is conveyed through the magnetic field from the primary coil to the secondary coil via the core, devoid of any direct electrical connection. Given that the coils may possess varying numbers of turns, differing voltages are induced. This disparity in induced voltages enables the primary and secondary coils to operate at distinct voltage levels.

6.3.3 Transmission Lines

In power plants, generators are strategically situated beyond urban areas and inhabited regions, aiming to prevent pollution and toxic emissions from adversely affecting nearby populations. Furthermore, the efficiency of electricity generation is enhanced by utilizing large central generators located close to fuel sources, in contrast to employing smaller generators within city limits. Consequently, extensive transmission lines are typically required to convey electric power from electricity-producing zones to power-consuming regions.

Transmission lines, as depicted in Figure 6.7, encompass lengthy current-carrying conductors that are upheld by towers serving as structural supports for the conductor's weight. These conductors, often constructed from materials such as copper or aluminum, shown in Figure 5.8, exhibit high conductivity. This high conductivity results in lower resistivity, thereby mitigating power losses within the lines.

Figure 6.7: Transmission Lines Transmitting Power Over Long Distances

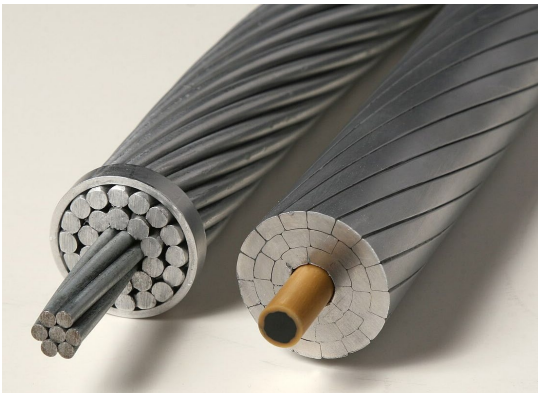

Figure 6.8: Conductors Used in Overhead Lines

"Overhead power line conductor comparison: a conventional steel-reinforced round-wire ACSR conductor (left) and a high-capacity, low sag ACCC conductor with light-weight composite core and compact trapezoidal aluminum strands (right)" by Dave Bryant is licensed under CC BY-SA 3.0

6.3.4 Loads

Loads encompass the devices that consume electric power across residential, commercial, and industrial structures. Within electric power systems, three main categories of loads are typically connected: resistive, inductive, and capacitive loads. Among these, resistive loads are the most prevalent and consume real power, as described by the relationship. Conversely, capacitive and inductive loads do not directly consume real power; instead, they store power and subsequently release it back into the grid in cycles. The oscillating power from capacitive and inductive loads, reverberating between the loads and the grid, is referred to as reactive power.

6.4 Fundamentals of AC power

Electric power systems revolve around the generation, transmission, and distribution of electric power in the form of alternating current (AC). The primary rationale for employing AC currents in these systems lies in the efficiency of transforming AC power between different levels through the utilization of transformers. Conversely, the conversion of direct current (DC) from one voltage level to another necessitates more intricate power electronics converters, making the process more cumbersome. Moreover, the efficiency of DC conversion might not match that achieved by AC transformers.

This section reviews AC circuits. Any AC circuit can feature three fundamental elements: resistors, capacitors, and inductors. In contrast to DC circuits, capacitors and inductors within AC circuits possess equivalent impedances. These impedances are contingent upon the circuit's frequency and can be computed through the following formulas:

$$Z_c = \frac{1}{jwC} \tag{6.3}$$

$$Z_L = jwL \tag{6.4}$$

where w is the angular frequency of the power source. The presence of the imaginary number 'j' within the aforementioned impedances indicates that the ratio between the current's phase angle and the voltage is 90 degrees. This angle is positive for inductors "+90" and negative for capacitors "-90" as shown in Figure 5.9 below.

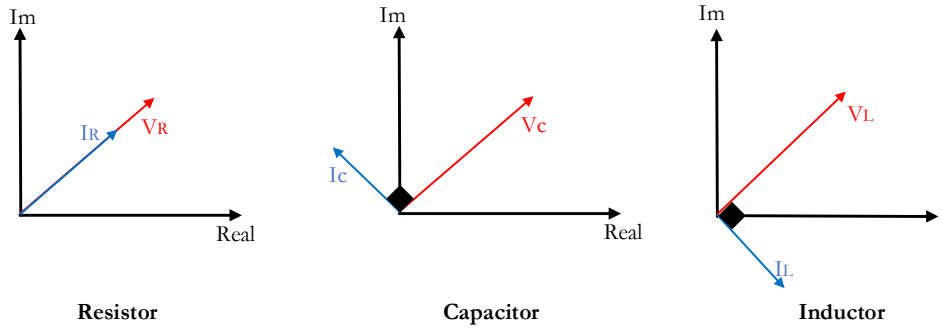

Figure 5.9: Phasor Diagrams For The Ac Circuit Elements

As such, capacitive and inductive components within an AC circuit can be considered analogous to resistors in a DC circuit. In simpler terms, Ohm's law remains applicable for the three elements as in (5.5) – (5.7) similar to Kirchoff's voltage and currents laws represented in (8) and (9):

$$V_L = I * Z_L \tag{6.5}$$

$$V_C = I * Z_C \tag{6.6}$$

$$V_R = I * R \tag{6.7}$$

$$0 = V_1 + V_2 + V_3 + \cdots + V_n \tag{6.8}$$

$$0 = I_1 + I_2 + I_3 + \cdots + I_n \tag{6.9}$$

The real power of an element in AC circuits can be expressed as:

$$P = I * V * cos(\theta) \tag{6.10}$$

Here, θ represents the angle between the voltage and current. The term cos(θ) is denoted as the power factor of an element. As there is no phase angle between the current and voltage of a resistor, the angle θ is equal to zero. In contrast, due to the phase angle between current and voltage in both capacitors and inductors, the real power P in both components is consistently zero. In other words, capacitors and inductors do not actively consume power. Nonetheless, they momentarily store power, releasing it back over one cycle. This phenomenon is referred to as power oscillation and is quantified through reactive power Q, as defined by the following equation:

$$Q = V * I * sin(\theta) \tag{6.11}$$

The majority of loads connected to power systems comprise a blend of resistive, capacitive, and/or inductive elements. Consequently, these loads can consume both active and reactive power, causing the angle θ to lie within the range of 0 to ±90 degrees. When a load exhibits a greater proportion of capacitive components compared to inductive components, the angle falls between 0 to −90 degrees. This scenario results in what is known as a leading power factor where the current angle leads the angle of the voltage. Conversely, when a load is weighted more towards inductive components, the angle falls within 0 to +90 degrees, leading to a lagging power factor where the angle of the current lags that of the voltage. The collective power of a load is typically denoted as apparent power (S) and can be computed using any of the subsequent formulas:

$$S = V * I^* \tag{6.12}$$

$$S = P + jQ \tag{6.13}$$

Where I^* is the conjugate of the current I. A diagram illustrating the relationship between the apparent power and both active and reactive power can be seen in Figure 5.10.

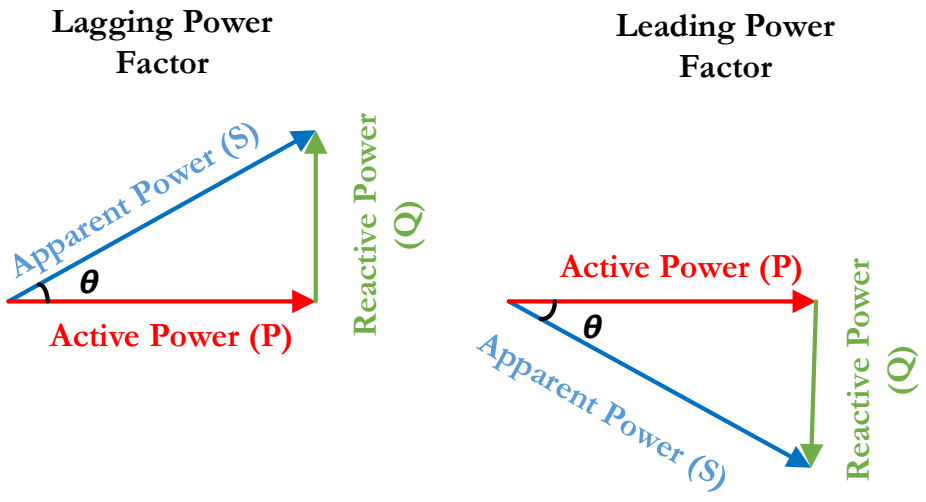

Figure 6.10: Power Factor Diagram

Example 6.2: The following circuit is powered by an AC voltage source Vs = $40\sqrt{2}\sin(4t + 20°)$. Calculate the impedances of the three elements in the circuit if R = 6 Ω, L = 2 H, and C = 1/16 F.

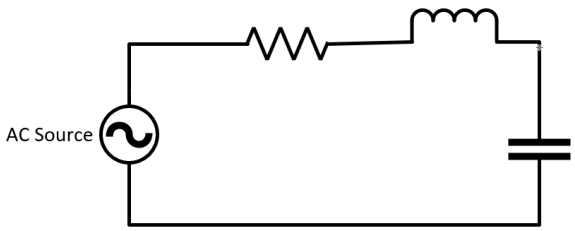

Solution:

The impedance of the resistor equals to the resistor value as follows:

$$Z_r = R$$

$$Z_r = 6\,\Omega$$

Equation (5.3) can be used for calculating the impedance of the capacitor:

$$Z_c = \frac{1}{jwc}$$

$$Z_c = \frac{1}{j4*\frac{1}{16}}$$

$$Z_c = -j4\,\Omega$$

Finally, the inductor impedance can be calculated using (5.4) as follows:

$$Z_L = jwL$$

$$Z_L = j4 * 2 = j8$$

$$Z_L = j8\,\Omega$$

Example 6.3: Calculate the value of the AC current passing through the three series elements in the same circuit above if the values of inductor and capacitor change as follow: Z_L = j8, and Z_C =-j4.

Solution:

The value of the current in the circuit can be calculated through KVL.

$$v_s = v_r + v_L + v_c$$

$$40\angle 20 = 6 * i + j8 * i - J4 * i$$

Manipulating the above equation in term of the current I result in:

$$i = \frac{40\angle 20}{6+J4}$$

$$i = 5.457\angle\text{-}13.7 \quad A$$

Representing the current in sinusoidal form produces:

i=5.457$\sqrt{2}$sin(4t - 13.7)

Example 6.4: Find the AC voltages of the elements in the circuit if Vs = 12$\angle 0\ V$, R=12 Ω, and Z_L = j16.

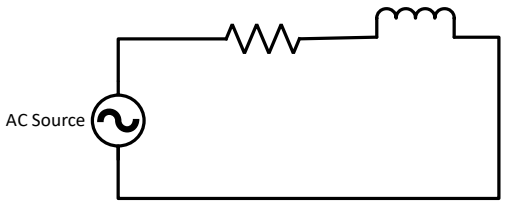

Solution:

To calculate the voltage of an element in this circuit, the voltage divider rule can be used:

$$V_R = \frac{v_S * R}{R + Z_L}$$

$$V_R = \frac{12\angle 0 * 12}{12 + j16} = 72 < -53.1$$

$$V_R = 72 < -53.1\ \text{V}$$

Similarly, the voltage divider rule can be used to find the voltage of the inductor:

$$V_L = \frac{v_S * Z_L}{R + Z_L}$$

$$V_L = \frac{12\angle 0 * j16}{12 + j16}$$

$$V_L = 72 < -53.1\ \text{V}$$

6.5 Three phase Circuits

The AC circuits outlined in the preceding section are commonly referred to as single-phase circuits, with each power source corresponding to a single generator as in Figure 6.11 (A). However, real-world AC systems often feature generators composed of three phases. In these systems, each generator incorporates three voltage sources of equal magnitude, yet spaced 120 degrees apart, as depicted in Figure 6.11 (B). As three-phase systems consist of three distinct phases, the generator output generates three voltage waveforms of equal magnitude, each spaced 120 degrees apart. These waveforms are depicted in Figure 6.12.

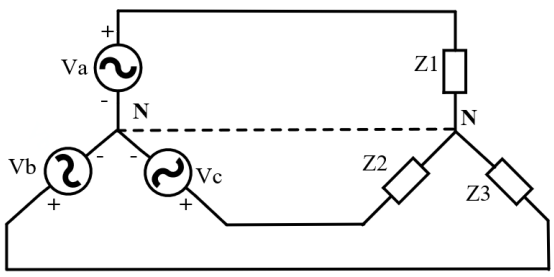

Figure 6.11: Single Phase Circuit Compared to Three Phase Circuit

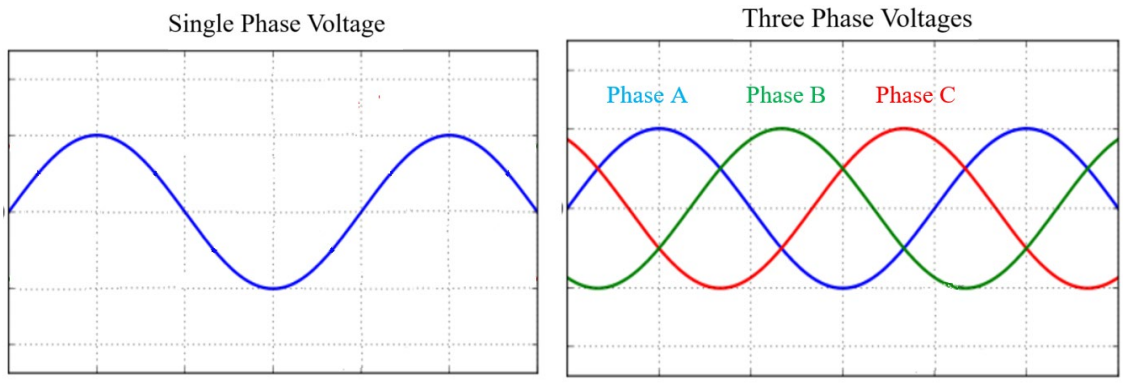

Figure 6.12: Voltage Waveforms Comparisons Between Single And Three Phase.

Employing a three-phase configuration in electric power systems offers several advantages over a single-phase setup. One significant benefit is the reduction in the number of required conductors. In contrast to the use of two conductors (positive and negative) for each power source in a single-phase system, merely three wires are necessary for three power sources within a three-phase system. Consequently, a three-phase system requires fewer conductors to transfer the same amount of power when compared to a single-phase system.

It is worth noting that in balanced three-phase systems, the neutral line can often be eliminated due to the absence of current in it. This occurs because the neutral current, derived from the summation of the three phase currents, becomes null. In a balanced system, the currents possess equal magnitudes but differ in phase by 120 degrees, culminating in a neutral current of zero, as illustrated in the forthcoming example.

Example 6.5: Consider three-phase currents I_A, I_B, and I_C with a phase angle difference of 120 degrees between them. Demonstrate the concept of neutral current being zero in a balanced three-phase system.

Solution:

The neutral current in a three-phase system can be calculated by summing the currents in the three phases:

$$I_N = I_A + I_B\angle 120 + I_C\angle -120$$

Since all the magnitudes of all the currents are equal, the currents IB and IA can be replaced by IA.

$$I_N = I_A + I_A(cos(120) + j\,sin(120)) + I_A\,(cos(-120) + j * sin(-120))$$

$$I_N = I_A + I_A \cdot (-0.5 - j3/2) + I_A \cdot (-0.5 + j3/2)$$

Simplifying the expression:

$$I_N = I_A - 0.5I_A - 0.5I_A + 0j - j3/2I_A + j3/2I_A = 0$$

This result confirms that the neutral current (I_N) in a balanced three-phase system is indeed equal to zero.

A final consideration in understanding three-phase systems pertains to their representation in power system diagrams. Three-phase circuits are commonly depicted using single-line diagrams. Given that the three lines possess identical magnitudes and are spaced 120 degrees apart, having knowledge of the current and angle of one line enables the determination of the current in the other lines. As a result, for simplicity, single-line diagrams often showcase only one of the phases, as exemplified in Figure 5.13.

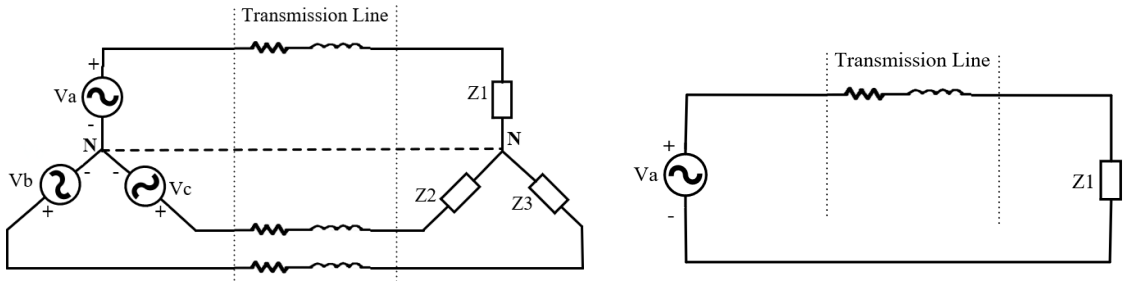

Figure 6.13: Three Phase System Represented By A Single Line Diagram.

6.6 Power Flow Analysis

Modern power systems encompass expansive networks of generators and loads spanning extensive geographical regions, interlinked through transmission lines. A simplified illustration of such a power system is presented in Figure 5.14. It comprises three generators (G_2, G_3, G_4), two loads (S_{D1}, S_{D4}), and five transmission lines serving to transmit power between generators and loads while establishing connections between these system components. Within this network, the four designated nodes "1" – "4" are termed 'buses,' functioning as shared connection points for transmission lines, generators, and loads.

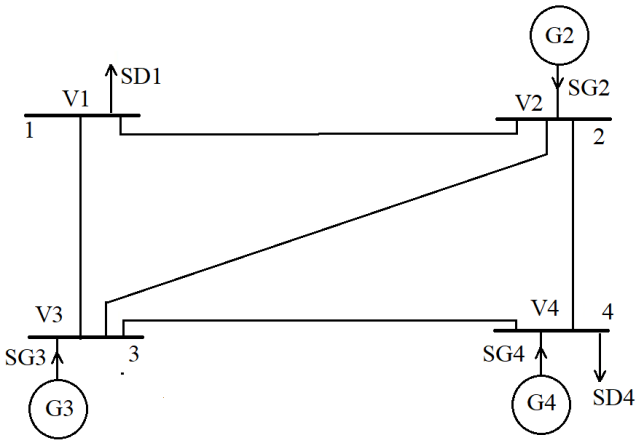

FIGURE 6.14 A SIMPLIEFIED EXAMPLE OF POWER SYSTEM

Among the pivotal objectives for power system designers and operators is the determination of bus voltages and the calculation of power flow—both active and reactive—across transmission lines. This vital task is commonly known as the power flow problem, where these intricate computations are performed. Power system designers systematically repeat these calculations across various anticipated

loading and generation scenarios to ensure that voltage levels remain within prescribed limits and power flow remains within the transmission lines' capacity.

6.6.1 Y-Matrix Calculation

The power flow equations for a simplified power system, depicted in Figure 6.15, can be formulated using Kirchhoff's Voltage Law (KVL). The ensuing equations describe the interrelations between the voltages and currents within the power system and can be expressed as follows:

$$I_1 = V_1 * y_{10} + (V_1 - V_2) * y_{12} + (V_1 - V_3) * y_{13} \quad (6.14)$$

$$I_2 = V_2 * y_{20} + (V_2 - V_1) * y_{12} + (V_2 - V_3) * y_{23} + (V_2 - V_4) * y_{24} \quad (6.15)$$

$$I_3 = V_3 * y_{30} + (V_3 - V_1) * y_{13} + (V_3 - V_2) * y_{23} + (V_3 - V_4) * y_{34} \quad (6.16)$$

$$I_4 = V_4 * y_{40} + (V_4 - V_2) * y_{24} + (V_4 - V_3) * y_{34} \quad (6.17)$$

Here, the variable y_{xy} signifies the admittance of the transmission line that links bus x with bus y. The equations (5.14) through (5.17) can be conveniently organized in a matrix representation in (6.18)

$$\begin{bmatrix} I_1 \\ I_2 \\ I_3 \\ I_4 \end{bmatrix} = \begin{bmatrix} Y_{11} & Y_{12} & Y_{13} & Y_{14} \\ Y_{21} & Y_{22} & Y_{23} & Y_{24} \\ Y_{31} & Y_{32} & Y_{33} & Y_{34} \\ Y_{41} & Y_{42} & Y_{43} & Y_{44} \end{bmatrix} \quad (6.18)$$

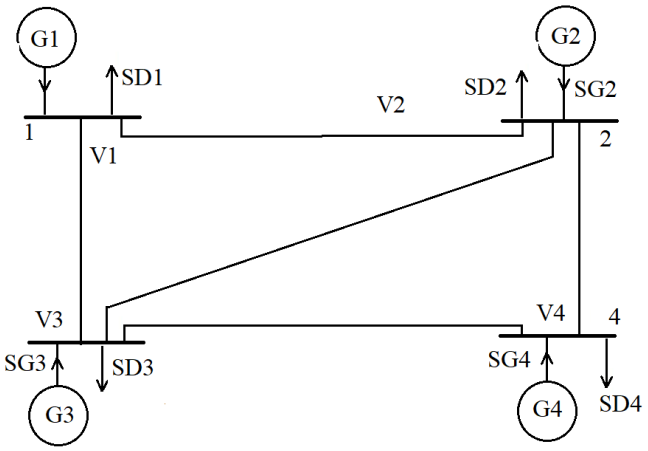

Figure 6.15: A Power System with Four Busses And Five Transmission Lines

Where the variables Y_{xy} can be defined as follows:

$$Y_{11} = y_{10} + y_{12} + y_{13} \quad (6.19)$$

$$Y_{22} = y_{20} + y_{12} + y_{23} + y_{24} \quad (6.20)$$

$$Y_{33} = y_{30} + y_{13} + y_{23} + y_{34} \quad (6.21)$$

$$Y_{44} = y_{40} + y_{24} + y_{34} \tag{6.22}$$

$$Y_{12} = Y_{21} = -y_{12} \tag{6.23}$$

$$Y_{23} = Y_{32} = -y_{23} \tag{6.24}$$

The matrix depicted in equation (5.18) is commonly referred to as the Y-matrix. Calculating the Y-matrix marks the foundational step for initiating any study or analysis within a power system. To exemplify this process, let us consider the following example where we calculate the Y-matrix for a straightforward power system comprising four buses.

Example 5.6: The figure shows the one-line diagram of a simple four-bus system. The Table gives the line impedances identified by the buses on which these terminate. The shunt admittance (y_{10}, y_{20}, y_{30}, and y_{40}) at all the buses is assumed negligible. Find the admittance matrix Y_{bus} for the shown power system.

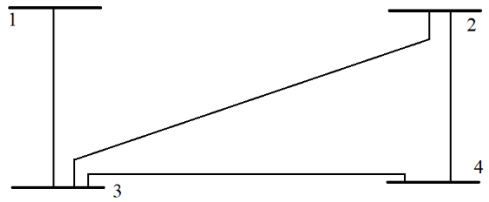

Figure 6.16: The Power System for Example 5.6

Line, bus to bus	R	X
1 - 2	0.05	0.15
1 - 3	0.1	0.3
2 - 3	0.15	0.45
2 - 4	0.1	0.3
3 - 4	0.05	0.15

Solution:

First, all the line impedances will be converted to admittances as follows:

$$y_{12} = \frac{1}{0.05 + j\ 0.15} = 2 - j6$$

$$y_{13} = \frac{1}{0.1 + j\ 0.3} = 1 - j3$$

$$y_{23} = \frac{1}{0.15 + j\ 0.45} = 0.667 - j2$$

$$y_{24} = \frac{1}{0.1 + j\ 0.3} = 1 - j3$$

$$y_{34} = \frac{1}{0.05 + j\ 0.15} = 1 - j6$$

The equation for Y_{bus} in (5.18) can be used to find the matrix as follows:

$$Y_{bus} = \begin{bmatrix} Y_{11} & Y_{12} & Y_{13} & Y_{14} \\ Y_{21} & Y_{22} & Y_{23} & Y_{24} \\ Y_{31} & Y_{32} & Y_{33} & Y_{34} \\ Y_{41} & Y_{42} & Y_{43} & Y_{44} \end{bmatrix}$$

Following the definitions of the Y_{xy} in the matrix from (6.19) – (6.24), the matrix becomes:

$$Y_{bus} = \begin{bmatrix} y_{13} & 0 & -y_{13} & 0 \\ 0 & y_{23}+y_{24} & -y_{23} & -y_{24} \\ -y_{31} & -y_{23} & y_{31}+y_{32}+y_{34} & -y_{34} \\ 0 & -y_{24} & -y_{34} & y_{43}+y_{42} \end{bmatrix}$$

The admittances of the transmission lines can be calculated using the impedances in the table. Substituting these values in the matrix results in:

$$Y_{bus} = \begin{bmatrix} 1-j3 & 0 & -1+j3 & 0 \\ 0 & 1.666-j5 & -0.666+j2 & -1+j3 \\ -1+j3 & -0.666+j2 & 3.666-j11 & -2+j6 \\ 0 & -1+j3 & -2+j6 & 3-j9 \end{bmatrix}$$

6.6.2 Power Flow Problem

Using the Y-Matrix introduced earlier, this section derives the power flow equations commonly employed in the industry to solve power flow problems. The derived equations govern the relationships between voltages, currents, and power flow within the system. The apparent power injected into bus *i* by a power source is equivalent to the power transmitted through the transmission lines connected to that bus. This relationship can be expressed by utilizing equations (6.12) and (6.13) as follows:

$$S_i = P_i + j\,Q_i = V_i I_i^* \quad , i = 1,2, \ldots, n \tag{6.25}$$

Here, *V* represents the voltage at the bus in relation to the ground, and *I* signifies the current departing from the bus. Solving the load flow problem is more convenient when utilizing the current *I* as opposed to its conjugate I^*. Consequently, by applying the complex conjugate to both sides of the equation, we obtain:

$$P_i - j\,Q_i = V_i^* I_i \quad , i = 1,2, \ldots, n \tag{6.26}$$

The current leaving a bus, denoted as I, results from the summation of all currents injected into the transmission lines connected to it. By employing the Y-matrix, this outgoing current from the bus can be represented as follows:

$$I_i = \sum_{k=1}^{n} Y_{ik} V_k \tag{6.27}$$

Substituting (5.27) in (5.26) yields:

$$P_i - j\,Q_i = V_i^* \sum_{k=1}^{n} Y_{ik} V_k \quad , i = 1,2, \ldots, n \tag{6.28}$$

The following can be written using (5.28):

$$P_i(real\ power) = |V_i| \sum_{k=1}^{n} |Y_{ik}|\,|V_k| \cos(\theta_{ik} + \boldsymbol{\delta_k} - \boldsymbol{\delta_i})\,;\ i = 1,2, \ldots, n \tag{6.29}$$

$$Q_i(reactive\ power) = -|V_i| \sum_{k=1}^{n} |Y_{ik}|\,|V_k| \sin(\theta_{ik} + \boldsymbol{\delta_k} - \boldsymbol{\delta_i})\,;i = 1,2, \ldots, n \tag{6.30}$$

Since both equations can be formulated for each bus in a power system network, the total number of equations describing such a network is twice the number of buses, resulting in 2n power flow equations. Observing the equations, it becomes evident that every bus is defined by four variables: P_i, Q_i, V_i, and δ_i. This accounts for a total of 4n variables. Fortunately, practical considerations enable power system analysts to predetermine and set two variables at each bus. Consequently, the remaining 2n variables can be calculated using the set of 2n equations.

Solving for the remaining 2n bus variables presents a challenge due to the non-linear nature of the algebraic equations. These equations involve bus voltages in product form and incorporate sine and cosine terms, making an explicit ***Solution*** unattainable. As a result, the ***Solution*** can only be achieved through iterative numerical techniques.

6.7 Short Circuit Analysis

Power system networks are vulnerable to abnormal behavior during fault. In power systems, faults refer to the unintentional connection of a current-carrying conductor to the ground. These conditions occur due to equipment insulation failures or accidental faulty operations within the system. If not promptly addressed, these situations can lead to the simultaneous collapse of the power system, resulting in a blackout. Moreover, they can cause significant damage to power system components due to the large short-circuit currents that flow through the system when a fault connects a portion of the system to the ground.

In power systems, two types of short circuit faults can occur: symmetrical faults and unsymmetrical faults as categorized in Figure 6.16 Symmetrical faults arise from a short circuit involving all three phases of the system connected to the ground as in Figure 6.17. While symmetrical faults are uncommon, a three-phase short circuit analysis is essential due to the severity of the resulting short-circuit currents, against which the system must be safeguarded.

Unsymmetrical faults, on the other hand, encompass faults where either one phase is connected to the ground or, in some cases, two phases are involved with or without ground connection, as illustrated in Figure 6.18. Analyzing unsymmetrical faults is more complex, requiring sophisticated tools such as the symmetrical components of the system.

To ensure the safety and stability of power systems, comprehensive protection measures are implemented to interrupt the significant short-circuit currents that may occur within the system. Circuit breakers are strategically placed to isolate faulty sections from the rest of the system. Modern power systems are equipped with advanced protection systems that incorporate distributed circuit breakers across all segments of the network. The primary goal is to swiftly isolate any faulty portion of the power system without triggering destabilization.

The selection of appropriate ratings for circuit breakers necessitates meticulous analysis, involving the determination of short-circuit currents resulting from faults in various parts of the system. This process, known as short-circuit studies, is vital during the construction of a new power system, aiding in determining the necessary circuit breaker ratings. Furthermore, short-circuit studies are conducted whenever modifications are made to the power system, such as integrating solar power sources or

wind energy systems. These studies facilitate the calculation of updated short-circuit currents resulting from the newly introduced elements. In certain instances, even minor adjustments or additions to the power system may mandate a re-design of the protection systems.

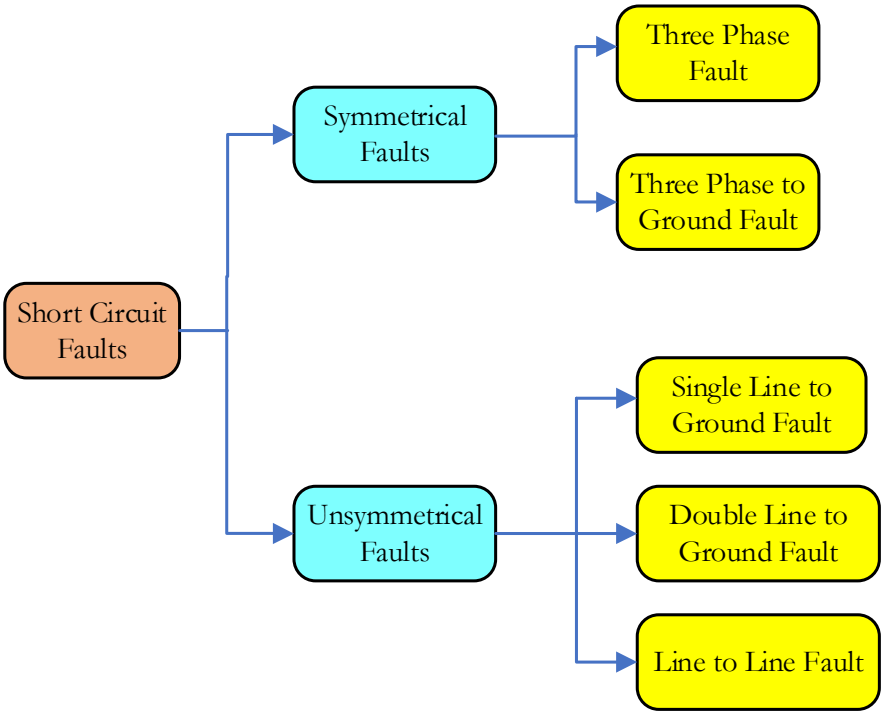

Figure 6.16: Classification Of Short Circuit Faults in Power Systems

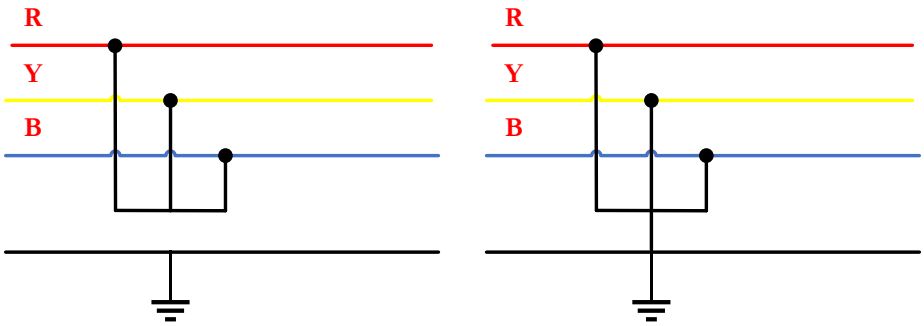

Figure 6.17: Symmitrical Fault In Electric Power Systems

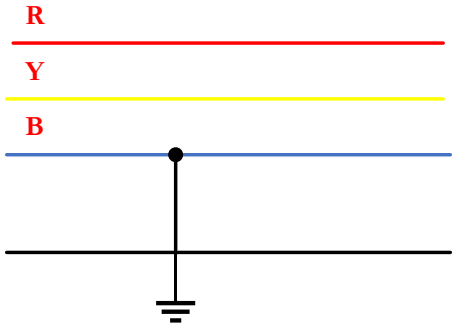

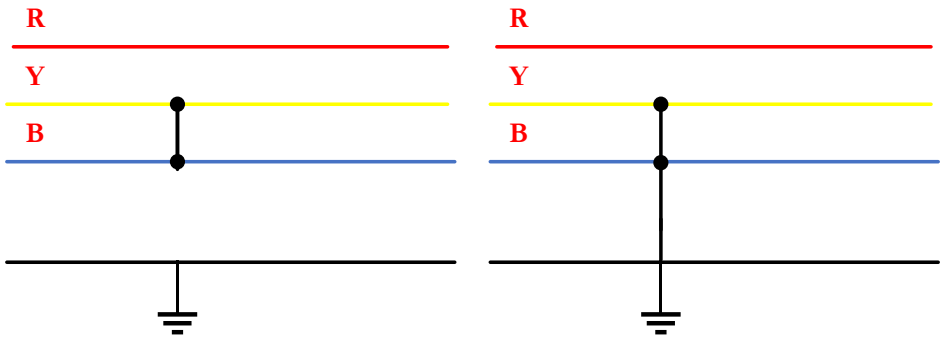

Figure 6.18: Unsymmitrical Faults In Electric Power Systems

6.8 Solar PV systems

Solar photovoltaic (PV) systems are designed to harness sunlight and convert it into electrical power. This section delves into their implementation at the system level, highlighting three frequently employed configurations. These configurations include:

1. **Grid-Connected Systems**

These systems feed generated power directly into the utility grid. The electricity produced is integrated seamlessly into the broader grid infrastructure as shown in Figure 6.19. The figure shows a grid-connected setup in which solar PV panels supply power to a building while maintaining a connection to the utility grid. Solar PV modules are intended to provide power to the building's electrical demands. However, due to variations in solar generation, the generated power might not consistently match the building's current load. In such cases, the utility grid steps in to supplement the required power.

Likewise, during times when the PV modules produce an excess of power beyond the building's needs, this surplus energy is fed back into the grid. In grid-connected systems, the PV array can be mounted on poles, installed on the building's roof, or integrated into the building's structure itself, known as building-integrated photovoltaics (BIPV).

2. **Stand-Alone Systems**

These setups incorporate batteries in conjunction with solar modules. The batteries store excess energy for use when sunlight is not available, ensuring a continuous power supply as shown in Figure 5.20. Stand-alone PV systems prove to be highly cost-effective, particularly in remote locations devoid of grid connections. Extending utility grids to such areas can incur substantial expenses, often reaching thousands of dollars per mile. In these isolated regions, conventional alternatives are limited to noisy and maintenance-intensive generators.

3. **Off-Grid Systems**

These systems are connected directly to specific loads and do not rely on the utility grid or batteries for power storage. They provide localized energy generation tailored to the designated loads. It involves connecting PV modules directly to specific loads, without the need for storage units or grid connectivity. Such systems are typically found in rural areas where their primary function is to pump

water for agricultural purposes. In pursuit of cost-effectiveness, these systems prioritize affordability over high efficiency, often foregoing power conditioning units. A prominent example is PV water pumping, where the array's wiring is directly connected to a motor that drives a pump.

Nearly all PV systems, except for those falling within the third category, necessitate power conditioning units, commonly known as inverters as shown in Figure 5.19. These inverters serve the crucial role of converting the DC solar power generated by the panels into AC power, which is compatible with grid connections and household appliances. Additionally, power conditioning units play a pivotal role in optimizing system efficiency by enabling the extraction of the maximum power point from the solar PV system. This is achieved through adjustments to the operating voltage, ultimately resulting in the generation of maximum power.

These power conditioning systems also serve a critical purpose in systems featuring energy storage. They facilitate the charging and discharging of batteries integrated with solar PV systems, effectively managing the energy flow to and from the storage systems.

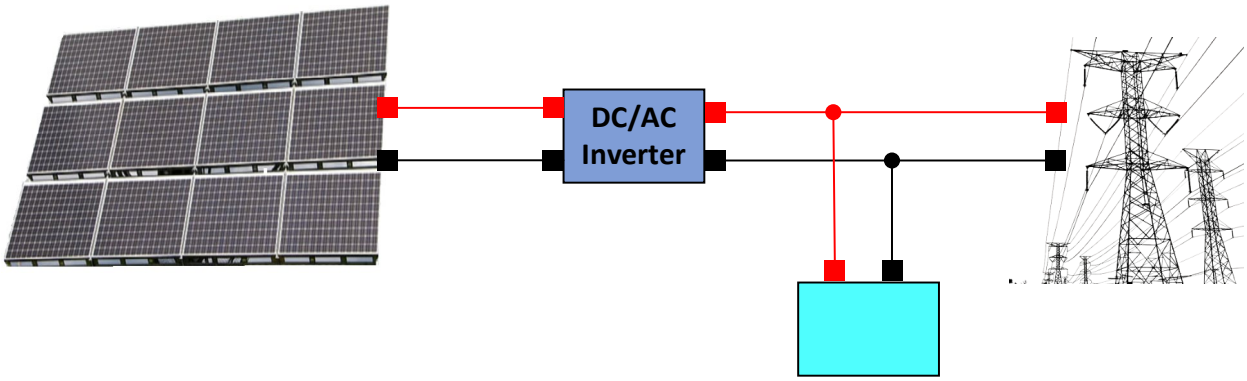

Figure 6.19: Grid-Connected Solar Pv System

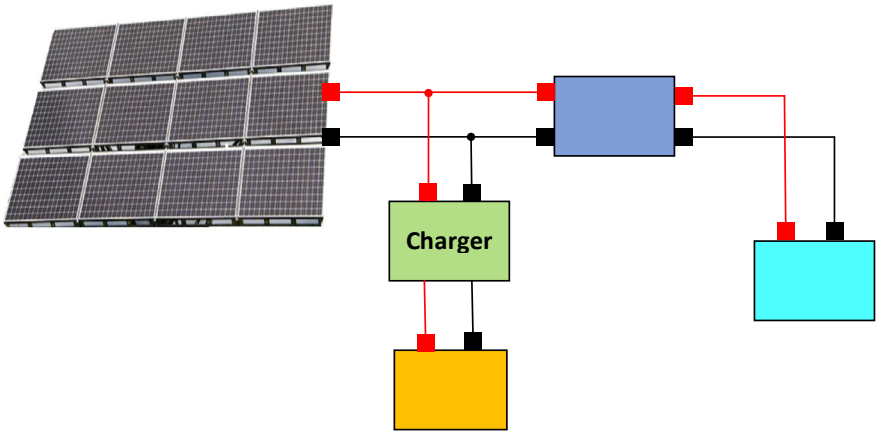

Figure 6.20: Stand-Alone Solar PV System With Energy Storage

6.9 An Alternative Solar Energy System

Over 70% of the world's electrical power is currently generated from fossil fuels, including coal, petroleum, and natural gas. Regrettably, these resources are finite, and their depletion is inevitable. Furthermore, power generation from fossil fuels contributes to environmental degradation, primarily through the emission of greenhouse gases. These emissions, as depicted in Figure 21, are detrimental to the environment and significantly contribute to global warming.

Figure 6.21: Power Plants Demonstrating Geen House Gasses Produced by Burning Fossil Fuels

Figure 6.22: Solar Thermal Concentrating Power Plant

Among the promising alternatives to replace fossil fuels and meet global energy demands, solar energy stands out. In addition to solar PV systems, this abundant resource can be harnessed for electricity generation through thermal power systems.

Thermal solar systems, depicted in Fig. 6.22, capitalize on the sun's heat to generate electricity. A multitude of mirrors are strategically positioned to concentrate sunlight onto a tower. This concentrated sunlight heats water, producing steam that drives turbines for electricity generation. In contrast, solar photovoltaic (PV) systems rely on sunlight, not heat, to generate electricity. Solar PV modules are semiconductor devices engineered to produce DC power when exposed to sunlight.

6.10 Energy Storage Systems

In the last decade, energy storage systems have played a vital role in advancing electrical power systems. These systems have the potential to address ongoing issues stemming from the high penetration of renewable energy resources within the power grid.

The electric current within the grid exists in alternating current (AC) form and cannot be directly stored in the form of electrical energy. Therefore, energy is stored in diverse ways: electrochemically through batteries, magnetically via superconducting magnetic energy storage, kinetically through flywheels, as potential energy in hydroelectric power plants, or as compressed air in compressed air energy storage.

6.10.1 Battery Storage Systems

While being the first introduced energy storage systems, batteries continue to be the most cost-effective and widely utilized technology for energy storage. The operational principles of batteries were initially investigated by Benjamin Franklin in 1748, and significant studies on batteries emerged in 1873. However, it was not until the 20th century that batteries saw their first important practical applications.

Battery operation is characterized by two phases: charging and discharging. Charging takes place through internal chemical reactions prompted by a voltage applied to the battery terminals. The reverse process occurs during discharging when the internal reactions are reversed.

1. **Lead Acid batteries:**

It is the oldest type of battery, invented in 1859 by the French physicist Gaston Planté. These batteries are commonly employed in low-cost applications that do not demand high energy density. Lead-acid batteries find utility in a range of applications, spanning from 1 kW for uninterruptible power sources to 10 MW for transport distribution systems.

Although lead-acid batteries are cost-effective, they have gradually been supplanted by nickel-metal hydride or lithium-ion batteries, despite their higher costs. This shift is due to the enhanced energy density (resulting in lighter weight) and higher specific energy offered by nickel-metal hydride and lithium-ion batteries.

2. **NiCd/NiMH Batteries**

NiCd (nickel-cadmium) batteries were invented by the Swedish engineer Waldemar Jungner in 1899, following the invention of lead-acid batteries. NiCd batteries possess a lower energy density and are typically employed in applications ranging from 1 kW to 0.5 MW. Additionally, NiCd batteries have raised environmental concerns due to their cadmium content, necessitating complex recycling procedures. As a result, they have been supplanted by NiMH (nickel-metal hydride) batteries.

NiMH batteries offer a higher energy density and find use in applications spanning from 1 kW to approximately 1 MW. However, a notable drawback of NiMH batteries is their elevated self-discharge rate.

3. Li-Ion Batteries

Li-ion (lithium-ion) batteries were introduced in 1970 by the American chemist Michael Whittingham. In recent times, these batteries have gained significant popularity due to their remarkable energy density. Nonetheless, a notable drawback lies in their internal resistance, which can result in overheating and potential battery failure. Li-ion batteries are utilized in high-power applications ranging from 1 kW to 1 MW. They stand as the most frequently employed battery technology in grid applications within the USA.

4. Sodium Sulfur Batteries

Lithium-ion batteries were first introduced in 1970 and have remained well-suited for grid storage. However, these batteries do come with certain drawbacks, including the presence of hazardous elements such as metallic lithium, which can catch fire upon contact with water. An incident occurred in September 2011 at a Japanese plant in Tsukuba, leading one of the manufacturers to temporarily halt production until October 2012 and implement new precautionary measures. Sodium-Sulfur batteries are well-suited for applications spanning approximately from 0.8 to 10 MW.

6.10.2 Supercapacitor Storage Systems (SSSs)

While research in the field of electrochemical capacitors began in the 1950s, it was not until 1978 that the technology was commercialized and introduced as the supercapacitor. The most significant advantage of supercapacitors lies in their capability for rapid charging and discharging, often referred to as a higher power rating, owing to their low internal resistance.

6.10.3 Flywheel Storage Systems

While the principle of operation had been understood for some time, the first practical application of flywheel technology appeared in Austria and Switzerland around 1950. During this period, the gyrobus was introduced, utilizing electricity stored in flywheels instead of drawing power from overhead lines. Flywheels operate by storing kinetic mechanical energy within a rotating wheel, discharging when a load is connected and charging when torque is applied to the wheel.

Contemporary flywheels possess capacities ranging from 0.5 kWh to 10 kWh, with the aim of achieving 25 kWh in the future. The majority of flywheels utilized in energy storage applications exhibit a round-trip efficiency of 70-80%, with around 100,000 full charge/discharge cycles. Moreover, the power density of flywheels is approximately ten times that of batteries.

6.10.4 Superconducting Magnetic Energy Storage (SMES)

Fundamentally, a Superconducting Magnetic Energy Storage (SMES) system comprises three main components: a current source system, the superconducting coil, and the refrigerator system. The energy is stored within the system in the form of a direct current (DC) circulating within a coil. This coil operates at superconducting temperatures, achieved by employing either liquid helium or liquid nitrogen.

6.10.5 Pumped Hydro-storage

Pumped hydro storage is employed to store electric energy in the form of potential energy. During periods of surplus electric power, this excess energy is used to operate a pumping system that transfers water from a lower-level lake or river to a higher-altitude artificial pool, as depicted in Figure 5.23. Subsequently, when energy demand arises, the elevated water is released, flowing through a hydroelectric generation process to convert the stored potential energy back into electric power. The efficiency of pumped hydro storage can reach up to 80%.

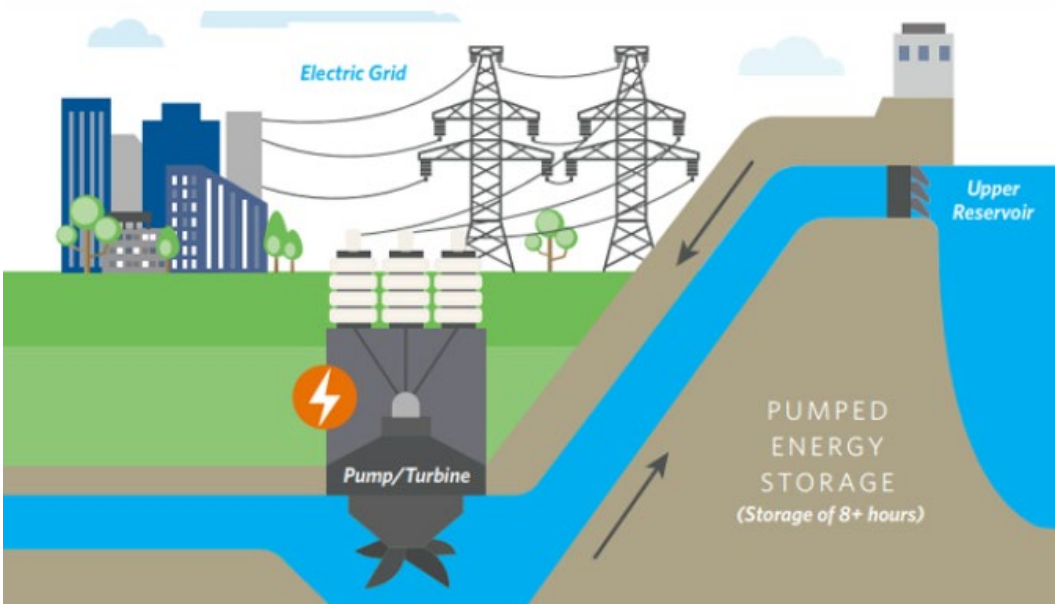

FIGURE 5.23 PUMP HYDRO STORAGE SYSTEM

6.10.6 Compressed Air Energy Storage (CAES)

Compressed Air Energy Storage (CAES) is commonly utilized for large-scale energy storage purposes. In this system, surplus power within the grid is harnessed to compress air into a reservoir. When electricity demand rises, the compressed air is heated and expanded through a gas turbogenerator, generating electricity in the process.

Globally, there are only two notable CAES systems: one in Germany with a capacity of 290 MW and another in Alabama, USA, with a capacity of 60 MW.

6.11 Services of Energy Storage Systems

6.11.1 Conventional Services

1. **Energy Arbitrage**

This practice is commonly known as "peak shaving" or "demand shifting." It involves purchasing electricity from the grid during periods of lower prices and storing it in energy storage systems. Then, when electricity prices rise, the stored energy can be sold back to the grid, allowing consumers to capitalize on price fluctuations and potentially save on energy costs. This approach helps to balance electricity demand and supply while maximizing the benefits of energy storage.

2. **Peak Shaving**

This is similar to energy arbitrage, where energy is stored during periods of low demand and discharged when demand is high. However, the objective here is not primarily economic; rather, it focuses on mitigating load peaks and circumventing the need to activate additional generation units.

3. **Load Leveling:**

Load leveling involves storing energy when demand is low and releasing it back into the grid when electrical load is high. What sets load leveling apart is its emphasis on not only mitigating load peaks but also achieving a more consistent distribution of load, effectively flattening out fluctuations in demand.

4. **Generator Bridging**

This concept refers to using energy storage systems to provide energy to the grid during the process of transitioning from one power generator to another.

5. **Generator Ramping and Load Following**

Energy storage systems often respond more swiftly to load changes compared to traditional generator units. This service leverages energy storage to track load fluctuations and promptly react to rapid load variations. This, in turn, enables generators to adjust their supplied power in alignment with their recommended capacities. This practice not only enhances the longevity of the generators but also enhances overall power quality.

6. **Transmission Investment Deferral**

Energy Storage Systems (ESSs) can be utilized to postpone the need for upgrading the transmission system, thereby addressing congestion problems. Instead of installing new transmission lines to increase the capacity, energy storage systems can supply the peak electric power without having it to be transmitted through fully loaded transmission lines.

7. **Black-Start**

This pertains to the act of energizing and providing power to specific loads during a blackout, before the grid's generators are brought back online and restored to service.

6.11.2 Renewable Generation Services

In this context, energy storage systems offer flexibility to manage the fluctuations inherent in renewable energy resources that are integrated into the grid.

1. **Curtailment Minimization**

This practice involves absorbing the surplus power generated by renewable energy resources and injected into the grid. Instead of allowing the excess power to go to waste during periods of peak generation, energy storage systems store this surplus energy for later use.

2. **Ancillary Services Support**

Renewable generation systems integrated with Energy Storage Systems (ESSs) can achieve novel ancillary services, including but not limited to inertia emulation, rapid frequency response, and voltage control. Energy storage systems can mitigate grid fluctuations in frequency and voltage caused by the intermittent renewable energy resources.

6.12 Distributed Energy Resources

In conventional power systems, electricity is generated in large-scale centralized power plants and then transmitted over long-distance transmission lines to reach consumer loads. In contrast, Distributed Energy Resources (DERs) are smaller-scale energy sources situated close to customer loads, enabling localized electricity supply. DERs offer the additional advantage of supplying power to remote loads in areas lacking transmission line infrastructure or where such infrastructure would be expensive to establish. Moreover, DERs boast lower construction costs and shorter implementation times compared to large generators and transmission line facilities.

Distributed Energy Resources (DERs) encompass a diverse range of technologies. Among the most commonly employed DER technologies are renewable Distributed Generators (DGs) and Energy Storage Systems (ESSs). In recent times, there has been a notable surge in the adoption of renewable DGs, particularly wind and solar energy resources. These renewable DGs are favored for their environmental friendliness and sustainability.

However, it's crucial to note that renewable DGs are influenced by meteorological conditions, rendering their generation variable and challenging to predict accurately. This variability poses a significant operational challenge for microgrids, which must be effectively addressed to facilitate the extensive integration of DERs.

Despite the numerous advantages of renewable Distributed Generators (DGs), the higher upfront costs they entail can create obstacles for potential investors. To encourage investments in renewable energy, the United States has implemented a variety of policies and regulations, including:

1. **Renewable Portfolio Standards (RPS)**

These standards require electricity providers to supply a certain portion of their energy using renewable DGs.

2. Public Benefit Funds

Funds are collected by imposing small taxes on electricity rates and are utilized to support renewable energy projects.

3. Output-Based Environmental Regulations

These regulations set limits on emissions to incentivize electric companies to improve efficiency and adopt renewable DGs.

4. Interconnection Standards

Technical standards that must be met by providers before connecting renewable energy systems to the grid.

5. Net Metering

This policy encourages customers, including residential ones, to install independent renewable DGs. Customers are compensated for surplus power they generate, and they can also draw power from the grid when needed.

6. Feed-in Tariffs

Increasingly used for renewable energy development, this policy requires utilities to establish long-term contracts for purchasing power from renewable energy sources.

7. Property Assessed Clean Energy (PACE)

Under this policy, costs for renewable energy projects or energy efficiency improvements are added to residential property assessments, motivating property owners to invest in such improvements.

8. Financial Incentives

Many states offer loans, grants, tax credits, and rebates to stimulate the expansion of renewable energy.

These policies collectively aim to create a supportive environment for renewable energy investment, promote sustainability, and reduce reliance on traditional energy sources.

6.13 Microgrids

Among several definition of microgrid, almost the most commonly used one is that defined by the U.S. Department of Energy ``a group of interconnected loads and distributed energy resources (DERs) with clearly defined electrical boundaries that acts as a single controllable entity with respect to the grid and can connect and disconnect from the grid to enable it to operate in both grid-connected or island modes".

According to this definition, a microgrid is characterized by three distinct attributes: clear electrical boundaries, a controlling mechanism that oversees and manages generation units and loads as a controllable entity, and an installed generation capacity that exceeds the maximum load, enabling it to disconnect from the main utility grid and operate in islanded mode.

In simpler terms, microgrids can be seen as compact power systems capable of supplying reliable energy and functioning in isolated mode. They have the capacity to generate, distribute, and manage electricity supply to local consumers. Given the necessity to maintain a balance between generation and loads, microgrids might choose to limit or postpone some of their loads, referred to as flexible loads. Alternatively, the installation of energy storage systems can help reduce or avoid load curtailment and postponement.

Microgrids offer several benefits for both customers and the utility grid, including:

1. **Improved Reliability**

Microgrids enhance reliability by implementing self-healing capabilities within the local distribution network, ensuring quicker recovery from outages and disruptions.

2. **Higher Power Quality**

Microgrids manage local loads more effectively, resulting in a more consistent and stable power quality for connected customers.

3. **Reduced Carbon Emissions**

The incorporation of diverse energy sources within microgrids contributes to a reduction in carbon emissions, promoting cleaner energy generation.

4. **Economic Operation**

Microgrids can lead to economic benefits by reducing costs associated with transmission and distribution (T&D) infrastructure, as they rely on localized energy sources.

5. **Renewable Distributed Generation (DGs)**

Microgrids enable the integration of less expensive renewable distributed generation sources, offering more sustainable and cost-effective energy options.

6. **Energy Efficiency**

Microgrids can respond to real-time market prices, optimizing energy consumption and usage patterns, thus enhancing overall energy efficiency.

In summary, microgrids bring advantages that encompass improved reliability, better power quality, environmental benefits, economic efficiency, renewable energy utilization, and enhanced energy management.

The capability to isolate a microgrid and disconnect it from the main grid is a standout feature, signifying a key advantage of microgrid systems. This attribute becomes particularly valuable during unforeseen disruptions or voltage fluctuations.

In instances of disturbances or voltage variations, the microgrid seamlessly transitions from its grid-connected mode to an islanded mode. This shift allows the microgrid to sustain a dependable and uninterrupted power supply to connected loads by utilizing Distributed Energy Resources (DERs).

References:

V. A. Boicea, "Energy Storage Technologies: The Past and the Present," in Proceedings of the IEEE, vol. 102, no. 11, pp. 1777-1794, Nov. 2014, doi: 10.1109/JPROC.2014.2359545.

G. G. Farivar et al., "Grid-Connected Energy Storage Systems: State-of-the-Art and Emerging Technologies," in Proceedings of the IEEE, vol. 111, no. 4, pp. 397-420, April 2023, doi: 10.1109/JPROC.2022.3183289.

S. Parhizi, H. Lotfi, A. Khodaei and S. Bahramirad, "State of the Art in Research on Microgrids: A Review," in IEEE Access, vol. 3, pp. 890-925, 2015, doi: 10.1109/ACCESS.2015.2443119.

R. Dai, R. Esmaeilbeigi and H. Charkhgard, "The Utilization of Shared Energy Storage in Energy Systems: A Comprehensive Review," in IEEE Transactions on Smart Grid, vol. 12, no. 4, pp. 3163-3174, July 2021, doi: 10.1109/TSG.2021.3061619.

D P Kothari, I J Nagrath, Modern Power System Analysis, third edition, McGraw-Hill Company, ISBN-13: 978-0-07-049489-3

Nick Jenkins, Embedded Generation (Energy Engineering), IET Power and Energy Series, Volume 31, ISBN-13: 9780852967744

United States Department of Energy, "Final Report on the August 14, 2003 Blackout in the United States and Canada", April 2004.

Σ64, "Illustration of Steam power generation", June 2020, https://commons.wikimedia.org/wiki/File:Steam_Power_Generation_01.svg

Siyavula Education, "Coal powerstation", April 2014, https://www.flickr.com/photos/121935927@N06/13580665473

Electrical Technology, "Synchronous Motor: Construction, Working, Types & Applications", https://wp.me/p4O3ZJ-eRT

BillC, "Idealised single-phase transformer also showing the path of magnetic flux through the core", January 2006, https://commons.wikimedia.org/wiki/File:Steam_Power_Generation_01.svg

WallpaperFlare, "HD wallpaper: cable, power lines, electric transmission tower, utility pole", https://www.wallpaperflare.com/cable-power-lines-electric-transmission-tower-utility-pole-wallpaper-exygh

Dave Bryant,"Overhead power line conductor comparison: a conventional steel-reinforced round-wire ACSR conductor (left) and a high-capacity, low sag ACCC conductor with light-weight composite core and compact trapezoidal aluminum strands (right)" February 2008, https://commons.wikimedia.org/wiki/File:ACSR_and_ACCC.JPG

PXFUEL, "Smoke, Ecology, The Environment, Chimney, Combined Heat and Power Plant, Pollution, Smoke Stack, Environmental Issues, Factory, Air Pollution", HTTPS://WWW.PXFUEL.COM/EN/FREE-PHOTO-OGACR

JAMES GUETSCHOW, "An Aerial Shot of the IVANPAH Solar Electric Generation System", HTTPS://WWW.PEXELS.COM/PHOTO/AN-AERIAL-SHOT-OF-THE-IVANPAH-SOLAR-ELECTRIC-GENERATING-SYSTEM-14096756/

BLACK &VEATCH, "Pumped Energy Storage", HTTPS://WWW.BV.COM/INDUSTRIES/HYDROPOWER-HYDRAULIC-STRUCTURES/PUMPED-STORAGE-HYDROPOWER